"THE INFLUENCE OF POWDER BED POROSITY VARIATIONS ON THE FILLING OF HARD GELATIN CAPSULES BY A DOSATOR SYSTEM"

Philip John Woodhead, B.Pharm. (Hons.)

Thesis submitted to the
University of Nottingham
for the degree of
Doctor of Philosophy, October, 1980.

Acknowledgements

I am particularly grateful to Professor J.M. Newton, whose advice and encouragement have helped enormously during the last three years.

The use of the gamma counting equipment was made possible by the generosity of the Department of Medical Physics, Queens Medical Centre, Nottingham. Technical and theoretical guidance was supplied throughout by Dr. J.G. Hardy, while Dr. S.A. Jackson was largely responsible for the production of the grey-scale images of porosity distributions.

Dr. E.J. Williams, of the Department of Mechanical Engineering, Nottingham University, was of assistance in the selection and use of vibration systems, while staff of the Department of Civil Engineering, in particular Mr. M.J. Bettison, were very helpful in connection with the instrumentation of the capsule filling machine.

The section of work concerning crystal growth owes much to the efforts of Mr. W. Roys, of the Department of Physics, Nottingham University, who also contributed some useful ideas generally.

Some of the statistical and mathematical aspects of the work were explained with great patience by Mr. P.H. Riley, of the Cripps Computing Centre, Nottingham University.

Numerous items of apparatus were produced by the

engineers of the Applied Science Faculty Workshop, Nottingham University, and the Mechanics Shop, Crossley Carpets, Halifax.

Mr. A. Laughton, of Eli Lilly & Co. Ltd., Basingstoke, kindly demonstrated the operation of the capsule filling machine.

Finally, my thanks go to the staff of the Department of Pharmacy, Nottingham University, without whom this work would not have been possible, and to all friends and colleagues whose good humour has created an enjoyable working atmosphere.

Contents

Abstract

The weight variation of hard gelatin capsules filled by a dosator-type machine has several possible causes, one of which, the presence of density variations within the powder feed bed, has been evaluated, using a number of particle size fractions of lactose as a model powder material.

Existing theories suggested that the bulk density, or porosity of a powder bed depends on the velocity and intensity of deposition of the particles, together with the properties of the powder. Experiments with lactose confirmed this, indicating in particular that low velocity deposition encourages the formation of regions of relatively high porosity. The application of vibration, especially in a vertical direction, proved effective in reducing the porosity of powder packings, and optimum frequency and acceleration appeared to be largely independent of particle size.

A system was developed for detecting porosity variations within powder beds, using the technique of gamma-ray attenuation, the principle being that the reduction in intensity of a gamma-ray beam traversing a powder bed is a function of local porosity. The observed linear attenuation coefficient of lactose was found to be a function of porosity, for reasons not fully established, hence a calibration expression for the attenuation

coefficient was proposed, and was used in subsequent local porosity determinations.

The radial distribution of porosity within cylindrical samples of lactose, prepared under various conditions, was studied, and a means of presenting such distributions pictorially was developed. The influence of deposition method, and applied vibration,on the uniformity of such packings, was clearly demonstrated.

A semi-automatic dosator-type capsule filling machine was used to evaluate the relationship between powder feed bed porosity variations and capsule fill weight variation. The results indicated that in the case of lactose, the influence of porosity variations, of the order of magnitude encountered, tends to be masked by other phenomena affecting the filling process.

List of Tables

List of Figures

Chapter 1

Introduction

1.1 Hard gelatin capsule technology

1.1.1 The use of hard gelatin capsules

Gelatin has been used to encapsulate drugs since the early 19th century, a few years before tablets were introduced, but manufacture of hard gelatin capsules on a commercial scale did not begin until about 1875 (Jones and Turner, 1974). Before the turn of the century, both Parke-Davis & Co. and Eli Lilly & Co. were marketing empty capsules, and these two firms remain the world's leading producers of hard gelatin capsule shells today. The manufacturing method has changed little in principle over the years, although of course, automation and improvements in machine design have meant that output has risen enormously. Metal rods of the required shape are dipped into an aqueous gelatin solution, removed, and after drying, the capsule shells are cut to the desired length and stripped from the rods. Most hard gelatin capsules consist of two cylindrical components with hemispherical ends, the cap being shorter and slightly wider than the body for ease of closing, and they also have in-built self-locking devices, consisting of small indentations on both cap and body, which lock together on closing.

It is only comparatively recently that hard gelatin capsules have found widespread use in

drug administration. Solid oral dosage forms started to become very popular in the 1930s, and since that time, tablets have dominated the market in terms of technology and production volume. In the last 20-25 years, however, there has been a considerable increase in hard gelatin capsule production, coinciding with the development of high-speed automatic filling machines.

There are several advantages in administering drugs in hard gelatin capsules (Anon, 1977). Gelatin is universally acceptable in terms of toxicology, and its solubility in the GI tract allows rapid release of the contents. It is a useful dosage form for masking unpleasant tastes, and can be employed for drugs which are difficult or impossible to tablet. It lends itself well to high speed production, and is relatively inexpensive.

One major drawback is the moisture sensitivity of gelatin. Hygroscopic materials may absorb water from the gelatin, leaving it brittle, but such problems are not insurmountable.

Traditionally, hard gelatin capsules are filled with powders, granules or pellets, but pastes and oils have recently been presented in this form. Tablets are also sometimes enclosed in capsules, particularly in clinical trial batches. Recently, low dose preparations for inhalation therapy have been formulated in hard gelatin capsules. A mechanical device is used by the patient to puncture the capsule shell and disperse the powder, which

can then be drawn into the lungs (Carmichael et al, 1978).

The vast majority of hard gelatin capsules, however, are for oral use, and are filled with a mixture of powders, comprising one or more drug substances, together with, in most cases, a number of excipient materials. Typical additives include lubricants, which prevent the build up of excessive frictional forces between powders and metal surfaces encountered in the filling process; disintegrants, which help to disperse the capsule contents after ingestion; surfactants, which aid penetration of gastric acid into the capsule contents, and diluents, which serve merely to make the fill weight up to a suitable level, and allow for changes in drug bulk density. The role of excipients in the formulation of solid dosage forms is discussed by Jones (1979).

1.1.2 Capsule-filling machinery

The filling of hard gelatin capsules has been developed to such a point that it is now a highly automated process employing precision-built machinery which will generate high output with very little operator involvement. There are, however, a number of lower capacity filling machines in use, ranging from the hand-operated, low output models like the Tevopharm through the semi-automatic Lilly, Parke-Davis or Colton machines, to the small versions of current automatic production machines (Ridgway and Callow, 1973). Naturally, the choice of filling machine will be

influenced greatly by the scale of operation for which it is intended.

Of the high-output automatic production machines, there are three main manufacturers, employing two distinct filling mechanisms. Hofliger and Karg produce machines which employ a "dosing disc" filling method. Powder is fed onto a disc and into a series of cylindrical dies. The powder in these dies is formed into compressed plugs by alternate compression by cylindrical punches and topping-up with further powder. The plugs are then transferred to a position above empty capsule bodies into which they are ejected.

The mG2 company manufactures capsule filling machines which operate on the dosator nozzle principle. A series of stainless steel tubes, or dosators, are mounted in a horizontally rotating turret which carries the dosators along a cam track. Below this turret is an annular feed tray containing powder, which rotates around a different centre to the turret. In this way, there is a position at which the dosators move directly above the feed tray, and their respective speeds are matched; at this point, the cam track causes each dosator to dip into the feed tray, pick up a powder plug and rise up out of the feed bed. At a different position on the cam track, each dosator is lowered again, but now, the dosators are aligned not with the feed tray but with a chain carrying empty capsule bodies. It is at this position that the powder plugs are ejected.

To ensure that a powder plug is retained in the dosator nozzle, compression is usually necessary, and this is provided through the depression by the cam profile of a plunger located inside the nozzle. Successful ejection of the plug requires the plunger to be depressed again at the appropriate time.

mG2 machines are said to be of the continuous type, since the dosators, are continuously moving around the cam track. The third major manufacturer, Zanasi Nigris, produces machines of the dosator type also, but until relatively recently, all Zanasi models were of the intermittent rather than the continuous type. Dosators are mounted in multiples of two on reciprocating arms which rotate backwards and forwards through 180^{o}, pausing briefly to lower and raise the dosators. Thus, while one set of dosators picks up powder plugs from the feed bed, ejection into empty capsule bodies is taking place from the other set. During pick-up and ejection, the feed bed and the empty capsule bodies are stationary, but while the dosators are reciprocating, the capsules move on to the next station and the feed tray rotates, bringing a fresh part of the powder bed into position. As with the mG2, compression and ejection of the plugs are effected by depression of a plunger within the dosator nozzle.

Under typical production conditions, involving any of these three makes of capsule filling machine, the operator loads bulk powder into one hopper and empty, closed

capsule shells into another. Powder is conveyed from the hopper to the dosing disc or feed tray, and the capsules are "rectified" (leaving them the required way up), separated, and the bodies transferred to the ejection stations. The caps rejoin the bodies after filling, and the closed, filled capsules are ejected from the machine into a suitable receptacle.

These and other types of capsule filling machinery are described in some detail by Marquardt and Pfeiffer (1977), Faust et al (1976) and Hostetler and Bellard (1976).

1.1.3 The dosator

The work of this thesis is primarily concerned with the source of fill weight variation in the filling process as performed by dosator-type systems, and hence a closer examination of the design and operation of such systems is required.

Fig. 1.1 compares the design of the mG2 and Zanasi dosators, and it can be seen that they have a number of common features. The lower part of the nozzle, which is the part that comes into contact with the powder, has a machined cylindrical bore extending several centimetres upwards from the outlet. The plunger rests on a return spring, and in its rest position, the plunger tip must lie far enough up the nozzle to allow the desired quantity of powder to enter. As can be seen in Fig. 1.1, the tip of the plunger is generally a little wider than the shaft

Fig. 1.1 Zanasi and mG2 dosators

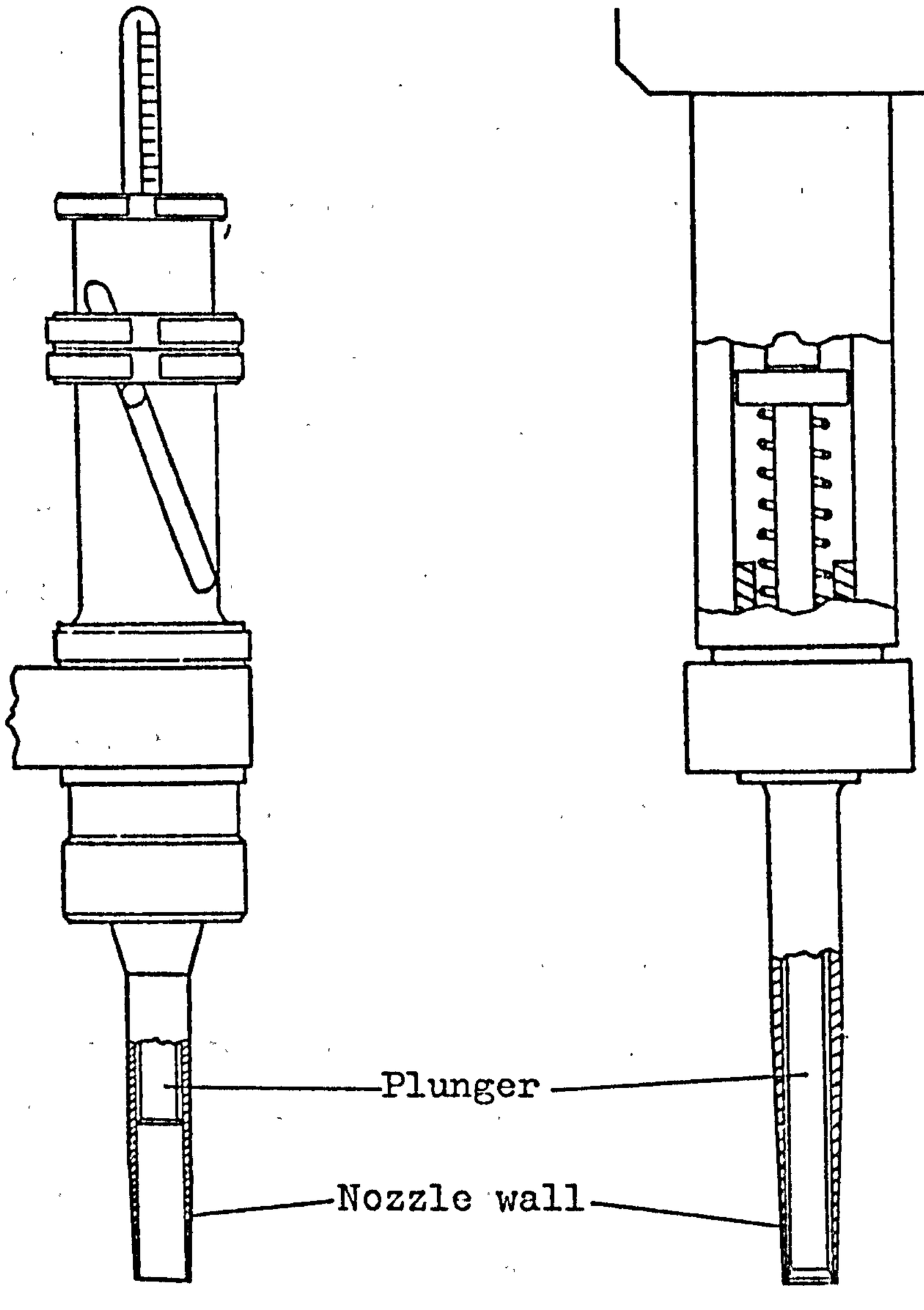

Zanasi

mG2

above it. When the dosator enters a powder bed, air is necessarily displaced from inside the nozzle, and for this reason, a small hole is drilled in the nozzle wall to aid venting. The nozzle and plunger are precision made, from stainless steel, and are available in eight sizes, ranging from 000 (the largest) through 00,0,1,2,3,4 to 5 (the smallest). They are designed so that there is enough clearance between nozzle and plunger to allow free travel of the plunger, but little information is available with regard to exact dimensions.

Details of the filling process, by which powder is transferred from a feed bed to a capsule shell by means of a dosator,are as follows. The dosator nozzle is lowered into the powder bed such that there is no relative lateral movement between dosator and bed. When the nozzle outlet has almost reached the base of the bed, the dosator comes to a halt. There is now a defined bulk volume of powder within the nozzle. By depressing the plunger, this powder is compressed, and the vertical compressive stress applied gives rise to increased frictional interaction between the powder and the nozzle bore. If sufficient stress is transferred to the nozzle outlet, a stable arch will form there, supporting the powder and enabling it to be retained in the nozzle. The plunger is withdrawn and the nozzle raised out of the powder bed. The dosator is then transferred to a position above an empty capsule body, and again, there must be no relative lateral movement

between dosator and capsule body. The plunger is depressed again, and providing there is sufficient force available to overcome the frictional forces developed between powder and nozzle bore, the plug will be successfully ejected. The depression of the plunger is carried out mechanically, such that the plunger undergoes a fixed pre-selected displacement. In the compression stage, this displacement is chosen to give the desired reduction of bulk volume of powder in the nozzle. For ejection, the plunger is depressed so that the tip reaches the nozzle outlet.

This apparently simple process can,however, be subject to a number of difficulties in practice. Failure to eliminate relative lateral movement between dosator nozzle and powder bed has been observed on high speed film (Newton, 1978) on an mG2 machine. The consequences of this are difficult to define, but the bulk volume of powder entering the nozzle is likely to be affected.

The retention of powder within the dosator nozzle is dependent on several factors. Jolliffe (1980) has made a detailed study of this aspect of capsule filling and has related properties such as Jenike Flow Factors, and the frictional properties of powders and nozzle surfaces, to retention ability. His theoretical approach is based on the problems encountered in the storage of particulate materials in tall cylindrical vessels, and has led to the possibility of predicting (a) the optimum nozzle surface

characteristics for powders of known flow and shear properties, and (b) the minimum compressive stress required to ensure retention of these powders.

Assuming that powder retention is achieved, transfer to the capsule body must be carried out without loss of any powder from inside the nozzle. Machine vibration may cause such loss to occur, and Newton's high speed film shows that this is,not only possible, but can occur to a widely varying degree.

Under normal operating conditions, when the dosators are repeatedly picking up and ejecting powder plugs, the nozzle bore may become coated with powder. This will alter the magnitude of the frictional interaction between the plug and the bore, since part of the powder-wall friction will be replaced by powder-powder friction. The effective capacity of the nozzle may also be reduced, and if the coating becomes excessive, free travel of the plunger may be hindered (Jolliffe, 1980).

Few papers have been published concerning the variation of capsule fill weight on dosator-type machines. Irwin et al (1970) filled capsules with powder blends containing clomacran phosphate as active ingredient, together with lactose or free-flowing starch. The machine they used was a Zanasi LZ64. They found that powder flowability, as assessed by the flowometer of Gold et al (1970), correlated very strongly with the coefficient of variation of fill weight, and was affected by the particle size and the

concentration of the active ingredient. Marquardt and Clement (1970) studied fill weight variation on a Zanasi 25-R machine, and had no difficulty achieving coefficients of variation of fill weight as low as 1%. However, they used spherical coated granules rather than powders.

Work carried out on other types of capsule filling machine has put forward powder flowability as the primary influence on fill weight variation (Ito et al, 1969; Reier et al, 1969; Kurihara and Ichikawa, 1977).

When using dosator-type filling systems, the filling process is essentially a volumetric one. For this reason, if there are any large fluctuations in the bulk density of the powder in the feed bed, excessive fill weight variation will be the result. Not only will an unpredictable amount of powder enter the dosator nozzle, but erratic retention may also occur. The use of free-flowing powder can help to ensure that the powder bed is of reasonably uniform bulk density (Jones, 1979), but very free flowing materials cannot easily be retained within the dosator nozzle (Ridgway and Callow, 1973). Cohesive powders are retained with no difficulty, but they present handling problems; production of a uniform feed bed may be difficult, since regions of high porosity can be supported within such materials. A further source of difficulty which applies particularly to cohesive powders lies in the regeneration or replenishment of the feed bed after plugs are removed. Capsule filling machines carry devices for dispersing

these high porosity regions, but the effectiveness of such devices has received little attention.

1.2 The packing of powders

A knowledge of the factors determining the packing behaviour of particulate systems is of importance in many areas of science and technology. The subject was reviewed by Gray in 1968.

The reproducible filling of hard gelatin capsules by dosator systems demands the production and maintenance of a uniform powder bed. Hence, the theoretical and practical aspects of powder packing will be considered.

1.2.1 Characterisation of packings

A powder packing may be regarded as an assembly of solid particles in which each particle is in contact with other particles, and the whole forms a stable mass while supported by a solid boundary.

A fundamental property of the packing which is of interest is its closeness of packing, and this can be expressed in a number of ways:

(a) Bulk density $= \frac{\text{weight of powder}}{\text{total volume of packing}}$

This is usually expressed in g cm^{-3} and is a function of the particle density of the solid material.

(b) Porosity = $\frac{\text{volume of voids}}{\text{total volume of packing}}$

(c) Voids ratio = $\frac{\text{volume of voids}}{\text{volume of solids}}$

(d) Packing fraction = $\frac{\text{volume of solids}}{\text{total volume of packing}}$ = 1 - porosity

These last three quantities are dimensionless. Overall bulk density can be calculated by determining the weight and volume of a packing, and knowledge of the particle density then permits calculation of porosity, voids ratio and packing fraction.

Knowledge of the porosity of a powder packing in isolation may not be enough to predict its stability. It is desirable if possible to be able to relate the measured porosity to one of two experimentally reproducible states, those of "loose" and "close" packing. Unfortunately, the porosity achieved in attempting to obtain either of these extremes is likely to vary with the method used to produce the packing. This problem will be discussed later.

The structure within an assembly of particles is extremely complex in the case of typical powdered materials, as are likely to be encountered in a pharmaceutical environment. For this reason, most of the predictive work carried out on packing structure has been confined to the study of mono-sized spheres. Spheres may pack systematically in a number of ways, giving rise to

coordination numbers ranging from 6 to 12, and levels of porosity ranging from 0.26 to 0.48 (Graton and Fraser, 1935). Introduction of more than one size of sphere makes the prediction of coordination number and porosity considerably more complicated, although a recent paper (Powell, 1980) describes a computer simulation for the random packing of spheres of any given size distribution.

1.2.2 Particle properties

The density to which a powder will pack is influenced by several properties of the constituent particles.

Particle shape is one such property, and has met with several attempts at definition; these are discussed by Ridgway and Scotton (1973), who also describe a method for sorting particles into different shape classes. Nakajima et al (1978) developed a method for obtaining a shape distribution, using sieves with different shaped apertures, while Standish and McGregor (1977) have calculated an average shape factor based on the pressure drop observed when passing air through a powder bed. Shergold (1953) found that rounded particles pack more closely than angular ones, and using this observation, he took the percentage voids in compacted gravel as a measure of its angularity. He introduced an "angularity number", ranging from 0 at 33% voids (spherical particles) to 12 at 45% voids (highly angular particles). Wakeman (1975), studying log normal size distributions of spherical

and angular particles, was generally in agreement with Shergold's findings, obtaining a lower porosity with spherical particles than with non-spherical particles for loosely packed beds, but both he and Gray (1968) suggest that irregular particles can pack more densely than spherical ones when subjected to compression or vibration. This is explained by the ability of angular particles to interlock and fill,some of the void spaces.

Particle size is a quantity that is fundamental to most aspects of powder technology. Its influence on packing density is such that as the size of particles decreases, the porosity will increase. The reason for this is that small particles have a higher surface area:mass ratio than large particles. A large surface area gives rise to more points of contact and greater adhesion between particles, whilst a low mass means that the effect of gravity is lessened. The formation and maintenance of arches and bridges within a packing is thus facilitated, and high porosity regions can be supported.

Absolute size, as discussed above, is important, but practical systems usually consist of particles of more than one size. The particle size distribution has great influence not only on the packing density of a powder, but on its physical behaviour generally. In a much-cited paper, Furnas (1931) derived mathematical equations predicting the particle size distribution of aggregates necessary to achieve maximum density in the manufacture

of mortar and concrete. Such a system requires that the voids between particles of one size are filled with smaller particles, and that all particle sizes can be mixed completely. Furnas in fact obtained two solutions, one for intermittent grading,and one for continuous grading. Carstensen et al (1978) studied loose packings of binary powder blends, in order to establish the fraction of fines required to produce a maximum packing density. They found this fraction to be approximately 0.5 for three different sizes of the smaller component. Messing and Onada (1978a, 1978b) have also considered the packing density of binary mixtures,and have developed a theoretical procedure which accounts for the fact that practical systems usually deviate somewhat from the Furnas model, due to local inhomogeneities. Bo et al (1965) showed that powders of a wide range of sizes pack more closely than those of a similar distribution but narrower size limits; Wakeman's observations (1975) concur with this, as shown in his plot of packing density as a function of geometric standard deviation from nominal particle size.

The packing of powders is influenced also by the surface characteristics of the particles. Dollimore et al (1973) state that adhesion is favoured when particles are sufficiently close for surface forces to overlap; hence, a rough surface with many asperities would be expected to produce greater adhesion than a smooth surface. For a given powder, they found that adhesion was at a

maximum in vacuo, giving rise to low bulk density. The introduction of water vapour reduced this adhesion by decreasing the surface energy of the particles, and the bulk density was seen to increase. Pilpel (1971) discusses the effect of moisture on the cohesion of soils, plotting moisture content against shear strength. The shear strength was found to exhibit two maxima, corresponding to the pendular and capillary states of moisture content, and a minimum in the funicular state. It would appear that the work of Dollimore et al (1973) refers to much lower moisture levels than that of Pilpel (1971). A theoretical approach to adhesion between particles, and the influence of liquid films, is described by Derjaguin (1961).

1.2.3 Deposition

Kolbuszewski (1950) investigated the influence of velocity of fall and intensity of deposition on the resulting porosity of sand packings. He came to the conclusion that (a) a low velocity of fall leads to a high porosity, irrespective of deposition intensity, and (b) a high velocity of fall produces low porosity at low deposition intensities, but increasing the deposition intensity increases the porosity. Macrae and Gray (1961) confirmed these findings in general, although they observed that minimum porosity is achieved by keeping the intensity of deposition within certain critical limits,

and that very low intensities lead to increased porosity. They went on to propose a mechanism of packing during deposition, after filming steel spheres being deposited from a height of 3 feet. Effectively, they concluded that to achieve optimum packing, there must be a critical level of activity in the upper layers of the growing bed; above or below this critical level, incident particles will be unable to find positions of least potential energy and closest packing. The activity at the surface is determined by the mass, velocity and resilience of the particles and their intensity of deposition.

Eastwood et al (1969) were concerned with producing beds of high porosity, and investigated the effect of several variables, many of which have already been discussed. They evaluated a number of methods of bed deposition and found that rapid inversion and righting of the container (a cylinder) gave a higher porosity than either slow inversion, simple pouring methods, or collapsing a fluidised bed.

1.2.4 Compression

The reduction in bulk volume of a mass of powder can be achieved by applying a compressive force to it. Three mechanisms of compaction during the dry pressing of powdered materials have been distinguished; they are (i) particle rearrangement (ii) elastic and plastic deformation and (iii) cold working and fragmentation.

Much of the volume reduction can be achieved with relatively small forces by the first mechanism. Further volume decrease requires the application of rather higher forces, and in fact Skorokhod and Tuchinskii (1978) suggest that an infinite amount of work is necessary to reduce the porosity of porous materials to zero. As far as the study of capsule filling is concerned, only relatively small forces need to be considered, and one of the most important consequences of such forces is that the powder becomes more uniformly packed. This is because the diminution of inter-particle porosity occurs in an orderly manner, large pores being eliminated first (Stanley-Wood, 1978). However, when a uniaxial stress is applied to a mass of powder, it is not all transmitted in the direction of application. The stress decays through particle-particle friction and particle-wall friction, shear stresses are generated, and there arises a definite stress distribution throughout the mass. The density distribution is similarly non-uniform, as shown by Train (1957).

Stress transmission through a powder causes adjacent particle surfaces to move closer together, resulting in an increase in cohesive forces. The coherence of a packing helps to dictate its stability (Train and Lewis,1962) and is enhanced if the particle surfaces are clean. During compression, any surface contaminants may be breached, enabling clean areas to come into contact.

1.2.5 Vibration

Vibration can be applied to a powder packing to reduce its bulk volume, and its main advantage over compression is that considerable volume reduction can be achieved without deforming or fracturing particles.

The vibration can take the form of tapping, which consists of mechanically lifting and dropping a container of powder through a fixed height repeatedly. British Standard 1460 (1967) describes apparatus for this purpose. However, the use of sinusoidal vibration is preferable in as much as it can be clearly defined, controlled, and reproduced.

In contrast to the effects of compression, vibration has been shown to reduce interparticle friction in metal powders (Fisher and Coleman, 1974), thus aiding flow and settling. Roberts and Scott (1978) applied sinusoidal and random vibrations to bulk solids, and observed a reduction in shear strength, and improved flow properties.

The factors affecting the packing of particles by vibration fall into two main categories: (a) the properties of the powder (size, size distribution, shape, surface characteristics) and (b) the vibration conditions (frequency, amplitude, time) (Evans and Millman, 1964). Ayer and Soppet (1965, 1966) studied the vibratory compaction of spheres and angular particles, and related packing efficiency to the diameters of component particles. They found that packing could be optimised by selecting

different size fractions; as the ratio of sizes increased, so did packing efficiency, up to a maximum value. They also found that packing efficiency increased with sphericity. Evans and Millman (1964) also found size distribution to be an important factor in achieving high density packings, and that spherical particles pack to higher densities than irregular ones, but they pointed out that blends that give high densities with one type of powder do not necessarily produce high densities with another type. McGeary (1967), referring to work with spherical particles, has proposed that there should be at least a seven-fold difference between successive sizes to produce efficient packing. Singhal and Drauchuk (1973) subjected several single component packings (mainly glass beads) to vibratory compaction, and found that large particles pack to a lower porosity than smaller particles. The role of friction is mentioned by Bell (1958), who points out that, other things being equal, the greater the frictional interaction between the particles, the greater the kinetic energy required for consolidation.

On the whole, therefore, particle properties have the same influence on vibratory consolidation as they do on the packing of particles generally.

Vibration conditions have a rather less well-defined role. At a given frequency, increasing the power input causes the acceleration and the amplitude of the vibration to increase, while conversely, increasing the frequency

at a fixed power input causes a reduction in amplitude. The acceleration produced at a fixed power input might be expected to be independent of frequency, but at a system's fundamental or resonant frequencies, acceleration and amplitude are magnified. For this reason, several workers have suggested that resonant frequencies should be chosen to optimise the packing of powders (Bell, 1958; Evans and Millman,,1964; Hauth, 1967, Singhal and Dranchuk, 1973). Such resonant frequencies are dependent on the size and nature of the sample/container system, and must usually be found by trial and error. Shatalova et al (1967) put forward a rough guide for choice of frequency, based on particle size (Table 1.1).

Table 1.1

Frequencies for minimum porosity (Shatalova et al,1967)

Size, microns	Frequency, Hz
> 100	100-200
1-100	200-300
< 1	> 300

Evans and Millman (1964) quote a useful range of 20-5000 Hz, adding that ultrasonic frequencies seem to be less effective than sonic frequencies. Hauth (1967), in packing nuclear fuels, found that rapid cycling of frequency over a range of several kHz, encompassing

several resonant frequencies, was most successful in terms of the packing density achieved.

Having selected a useful frequency, the power input should be kept within a critical range; if it is too low, the existing structure will be undisturbed, while excessive acceleration may cause fluidisation of the mass, resulting in high porosity (Singhal and Dranchuk, 1973). This is particularly likely at low frequencies, where high accelerations give rise to large amplitudes (Evans and Millman, 1964). It has been suggested (Stewart, 1962) that the amplitude of vibration should be of the same order of magnitude as the size of particles being packed. As would be expected, the power input needed to achieve the required vibration conditions will increase with the mass of the system being vibrated.

The duration of vibration is a variable which has received little attention. Most workers quote times of a few minutes to achieve the desired packing densities, although Bell (1958) has suggested that for small samples, the majority of the consolidation occurs in the first five seconds. Longer vibration times will be needed for large and/or cohesive samples.

Gray (1968), has said that in spite of the considerable amount of empirical investigation into the vibratory consolidation of particulate material, it remains difficult to predict the most appropriate vibration conditions for systems that have not already been studied

experimentally. This is still true, although Spasskii (1977) has developed a computer program for predicting suitable vibration conditions from a knowledge of the measurable properties of the particulate material. The principle of the theory relates the required vibrational energy input to the energy characteristics of the particle contact interactions.

When preparing a powder bed for the filling of hard gelatin capsules, the overall bulk density is important since it influences the magnitude of the fill weight. However, as has been mentioned previously, uniformity of bulk density is vital to ensure low fill weight variation. Little work has been done to study the uniformity of bulk density within vibrated powder beds, although one would expect that since particles are being rearranged into positions of low potential energy, regions of anomalous (low) density will be broken down, resulting in increased uniformity. Van Brakel and Heertjes (1974), using a technique described in section 3 of this chapter, confirmed this expectation, and went on to study various combinations of vibration conditions, deposition method and particle characteristics. A more detailed account of their work appears in Chapter 6.

A major disadvantage in using vibration for the densification of powders is the problem of segregation, particularly of different particle sizes. This has been observed experimentally by many workers, including Williams

and Shields (1967), Lawrence and Beddow (1968/1969), Ahmad and Smalley (1973), Ripple et al (1973) and Harwood (1977). There is good agreement generally on the factors controlling segregation. Particle size is by far the most significant particle property; density differences have much less effect, and particle shape appears to have little or no influence. Free flowing powders are more likely to segregate than cohesive ones,due to greater freedom of movement. Increasing the vibration acceleration to levels at which there is great activity in the powder encourages segregation; this can be avoided by using higher frequencies, thus reducing the amplitude and the migratory tendency of the particles.

1.3 Powder bed porosity measurement

There are clearly many factors influencing the packing density of powders, which must be considered in the preparation of feed beds from which to fill hard gelatin capsules. However, a knowledge of overall bulk density or porosity sheds no light on the distribution of voids within an individual powder bed, and the scale of local voidage variation can determine whether fill weight variation falls within acceptable limits.

There are a multitude of techniques available for studying the porosity of particulate systems, and they divulge many different types of information.

1.3.1 Intrusive techniques

Pore size distributions are obtained routinely by mercury porosimetry and nitrogen adsorption methods. The two techniques differ in terms of the pore size range they can measure; for mercury porosimetry, the range is approximately 10nm to 100μm, and hence the technique applies mainly to interparticle voids, while nitrogen adsorption is suitable for intraparticle pores ranging from 0.4 to 30nm (Stanley-Wood, 1978). These methods do not reveal the spatial arrangement of voids.

Ridgway and Tarbuck (1966) observed the local voidage variation near the walls of a cylindrical container containing mono-sized spheres, by adding successive known volumes of water. Rapid rotation of the cylinder forced the liquid to the periphery, and the thickness of the annulus occupied by the liquid enabled the local porosity to be calculated. They found that there was a damped oscillating pattern of porosity over a distance of several particle diameters from the walls. Stanek and Eckert (1979a) studied area porosity profiles in random beds of mono-sized spheres, by injecting known volumes of ethanol into the packings and accurately measuring the liquid level after each addition. In a second paper (1979b), they used the same technique to observe a porosity decrease at the interface between two layers of different sized spheres.

A number of workers report the use of penetrating

liquids which set, transforming the packing into a solid mass which can be sectioned and studied in detail. Scott(1962) used a wax to set steel spheres in a cylindrical container,and made an observation similar to that of Ridgway and Tarbuck (1966) concerning porosity variation near the walls. This wall effect was also detected by Benenati and Brosilow (1962), who poured spherical lead shot into a cylindrical container and fixed the packing with an epoxy resin. They investigated radial voidage variation by machining off known thicknesses and recording the loss in weight of the mass. The theory behind this wall effect is discussed by Gotoh et al (1978). Propster and Szekely (1977) used the setting and sectioning method to study the porosity and particle size variations in different layers of blast furnace charge material.

The above techniques are generally time-consuming and destructive. It is preferable to be able to study the local porosity variations in a powder sample,and leave it physically unaltered and intact. Subsequent processing, for example filling into hard gelatin capsules, is then unaffected.

1.3.2 Non-destructive techniques

In recent years, several non-destructive techniques have been employed to detect voidage variations in solid or particulate materials.

Filipczynski et al (1966) describe an ultrasonic

method for determining the degree of porosity in different types of basalt, by measuring the attenuation of wave intensity caused by scattering and absorption. Stone and Clarke (1975) applied similar principles to study the void content of carbon fibre reinforced plastics.

Petrov et al (1974) used a microwave technique to determine the porous structure of water-saturated dielectric materials, including kaolin, clay, a ceramic and silica gel.

Ewell (1979) discusses numerous traditional and new methods of determining porosity in ceramic devices, and suggests scanning laser acoustic microscopy as a useful non-destructive technique. The attenuation of a transmitted acoustic signal is recorded and is related to porosity.

The scattering of ionising radiation can reveal information regarding porosity. Mackenzie and Armitage (1976) used a charged particle backscattering technique to examine pores down to 1nm in compacted silica and alumina samples. Kennett et al (1976) were able to sense dynamic density changes in flowing water due to the presence of air bubbles, by detecting scattered gamma radiation, and claim precise estimation of void fraction. Krautwasser and Nickel (1977) utilised a small angle X-ray scattering technique to study the presence of microporosity at different points in samples of pyrocarbon, while Casteel et al (1978) used the same technique for investigating the porosity of charcoals. They claim that this method of

examining microstructure gives higher resolution than most electron microscopes.

An alternative to the radiation-scattering methods described above is to record the attenuation of a transmitted radiation beam. The reduction in intensity of the beam is related to the density and thickness of the material through which the beam passes. This phenomenon has been exploited, using neutrons, X-rays and γ-rays; the latter two have found more extensive application, and in fact share many of the same properties, being adjacent on the spectrum of electromagnetic radiation.

In the early 1920's, experiments were performed which illustrated the complete correspondence between X-rays and light in their major features of spectra, polarisation and dispersion. Furthermore, there was reasonable proof that X-ray energy is transmitted in directed quanta. A comprehensive account of the properties of X-rays appeared in the following decade (Compton and Allison, 1935).

The interaction between γ-rays and matter was reviewed by Fano (1953a, 1953b) and Siegbahn (1955). Details of the theoretical aspects of γ-ray attenuation are discussed in Chapter 4.

One field in which the presence and distribution of voids in particulate matter has long been of interest is soil mechanics, and in the 1950's, several workers applied the principles of γ-ray attenuation to this problem.

The attraction of the technique was the fact that density determinations could be carried out in situ. Skopek (1957) describes the use of a Cobalt-60 γ -ray source to measure the effective density of dry and saturated sands, while Homilius and Lorch (1957) used Caesium-137 and Cobalt-60 to study the density of near-surface soil layers. This type of experiment involved pushing a probe containing the radioactive source into the ground, and detecting the transmitted radiation using an ionisation chamber. There are a number of other examples of this type of work (Bernhard and Chasek, 1955, 1956; A.S.T.M. Symposium, 1960; Meigh and Skipp, 1960).

The Soil Mechanics Group at Cambridge University made considerable progress in the 1960's in the use of radiographic techniques to study voidage in particulate materials, and Coumoulos (1967) investigated the suitability of neutrons, X-rays and γ -rays for detecting local variations in voids ratio in various sands and clays. The major part of his work describes the development of a γ-ray attenuation technique to investigate the spatial distribution of voidage or porosity, by making measurements at an ordered network of points. The work at Cambridge has been reviewed by Roscoe (1968) and Bransby (1973).

Arthur and Dunstan (1969, 1969/70) preferred X-rays for their studies of particle packing. They carried out a series of line scans on cubic samples of granular materials and obtained what they called "projected thickness

distributions", which were a measure of packing density variations.

Kurz (1972) considered three γ-emitters, Americium-241, Caesium-137 and Cobalt-60, for measuring local porosity variations in packings of calcium carbonate powder. He suggested that the choice of isotope should be influenced by its energy, and the density and thickness of the sample to be studied. His proposed optimisation, based on statistical considerations, is described in Chapter 6. Kurz and Schwedes (1976) carried out more work of this kind when attempting to produce homogeneous packings of calcium carbonate powder, in order to obtain reproducible shear test data. They devised a method of deposition which gave good uniformity of the cohesive calcium carbonate.

Van Brakel and Heertjes (1974) chose the method of X-ray attenuation to assess the degree of homogeneity of various particle packings, particularly glass beads, and were thus able to compare a number of methods of preparation of such packings. Heertjes et al (1978) reverted to γ-ray attenuation to measure local porosity variations, in the study of failure surfaces in packings of glass beads and sand subjected to different stresses.

Sowka and Schubert (1978), using a Caesium-137 source, describe a procedure for determining porosity and moisture content in calcium carbonate filter cakes.

Radiation attenuation techniques are clearly a useful

tool for assessing voidage distribution in particulate masses, but they find diverse other applications. Nuclear radiation gauges can be used to monitor the level of solids or liquids in vessels, the flow of liquids through pipes, and the transport of material along conveyor belts (Carlson et al, 1977). Pekarskii et al (1978) advocate the use of rapid neutrons rather than γ-radiation for the inspection, of density of materials transported along a supply line. Another field in which radiation attenuation methods have found widespread use, is nuclear medicine; apart from the obvious example of 'X-rays' as understood by the layman, radioactive isotopes have been extensively utilised in the measurement of bone density, as described by Cameron et al (1968). In the last few years, radio-isotopes have been used with the aid of the gamma camera as diagnostic agents for studying organ function in patients.

1.4 Origins and scope

From the foregoing discussion, it is clear that although the filling of hard gelatin capsules is a widespread and successful process throughout the pharmaceutical industry, some of the underlying scientific principles are not well understood. The production and maintenance of a uniform powder feed bed, and its importance in controlling capsule fill weight variation, is one area deserving study.

The objective of this work is to develop a technique for assessing the uniformity of packings by measuring local porosity variations, and to use the technique to examine some of the factors affecting the packing behaviour of powder. It is then intended to investigate the significance of powder bed porosity variations with respect to the weight variation of capsules filled by a dosator nozzle system.

Chapter 2

Lactose As A Model Powder

Crystalline α-lactose monohydrate, which will subsequently be referred to as lactose, was chosen as a model powdered material for this work. It is a chemically stable, non-toxic, non-irritant material which is readily available commercially in various grades. It is a common excipient in many solid dosage forms,and has been thoroughly characterised in terms of physical properties (Fell, 1972). At 25°C, the equilibrium moisture content of lactose is negligible except at very high relative humidity (Shotton and Harb, 1965), hence its behaviour is unlikely to be affected by variations in ambient humidity.

2.1 Separation into particle size fractions

A quantity of DMV 125 mesh lactose (DMV Veghel, Holland, Batch No. 104429/03) had already been classified into eight particle size fractions, using a vibratory sieve (Endecotts Ltd., London), an air-jet sieve (Alpine Model A200LS, Alpine Augsburg, W. Germany) and a zig-zag classifier (Alpine Multiplex 100 MZR, Alpine Augsburg, W. Germany) (Jolliffe, 1980). The mean particle volume diameter was determined for each size fraction using a Coulter Counter (model TA, Coulter Electronics Ltd., Herts.), and the results are listed in Table 2.1.

Table 2.1

Particle size classes of lactose

Size fraction	Nominal particle size (μm)	Separation method	Mean particle volume diameter (μm)	Standard deviation (μm)
A	-18.7	Zig-zag classifier	15.6	11.1
B	+18.7-26.5	"	17.8	9.4
C	+26.5-37.5	"	27.7	10.5
D	+37.5-53	"	37.5	14.3
E	+53 -75	Air jet sieve	41.3	14.8
F	+75 -105	"	80.8	22.0
G	+105 -150	"	99.5	34.7
H	+150	Vibratory sieve	155.2	59.6

A $\sqrt{2}$ progression of class intervals was chosen to give constant resolution for each size fraction.

2.2 Flow properties of the particle size fractions

Jolliffe (1980) performed a number of simple experiments on the eight size fractions of lactose, to compare their flow properties. These included measurements of angles of repose and blocking apertures.

Angles of repose were determined by loosely filling a perspex cylinder with powder,then lowering a base plate away from it, causing powder to fall on to the plate and form a heap. Measurement of the dimensions of the heap enabled the angle of repose to be calculated.

Blocking apertures were determined by loosely filling powder into a rectangular perspex box in the base of which were a succession of circular holes of varying diameter, covered by a sliding shutter. On withdrawing the shutter, the largest hole not allowing flow was recorded.

Table 2.2 shows the results of these experiments.

Table 2.2

Some flow properties of lactose particle size fractions

Size fraction	Angle of repose(^{o})	Blocking aperture(cm)
A	48	2.51
B	41	1.85
C	34	1.23
D	32	0.61
E	35.5	0.61
F	31.5	0.26
G	30	0.16
H	28.5	0.16

Carr (1970) put forward the following classification for angles of repose:

Very free flowing	25-30°
Free flowing	30-38°
Fair to passable flow	38-45°
Cohesive	45-55°
Very cohesive,	55°

On this basis, the lactose size fractions range from cohesive (A) to very free flowing (H). This trend is supported by the blocking aperture results, in which a high value indicates poor flow properties, while free flowing powders flow readily through much smaller orifices.

Several methods of measuring angles of repose have been described (Brown and Richards, 1970), but they tend to be rather unreliable for cohesive powders, giving inconsistent results. Consequently, quoted angles above about 60° are of limited significance.

A new method was devised for measuring angle of repose. A Spinning Riffler (Model SR1, Microscal Ltd., London) was modified as shown in Fig. 2.1. Powder was discharged from the vibrating chute, width 44mm, on to an alloy turntable 57mm in diameter, rotating at 15rpm. A conical heap was gradually formed, which reached a steady state after a short time; powder deposited

Fig. 2.1 Apparatus for turntable method of determining angle of repose

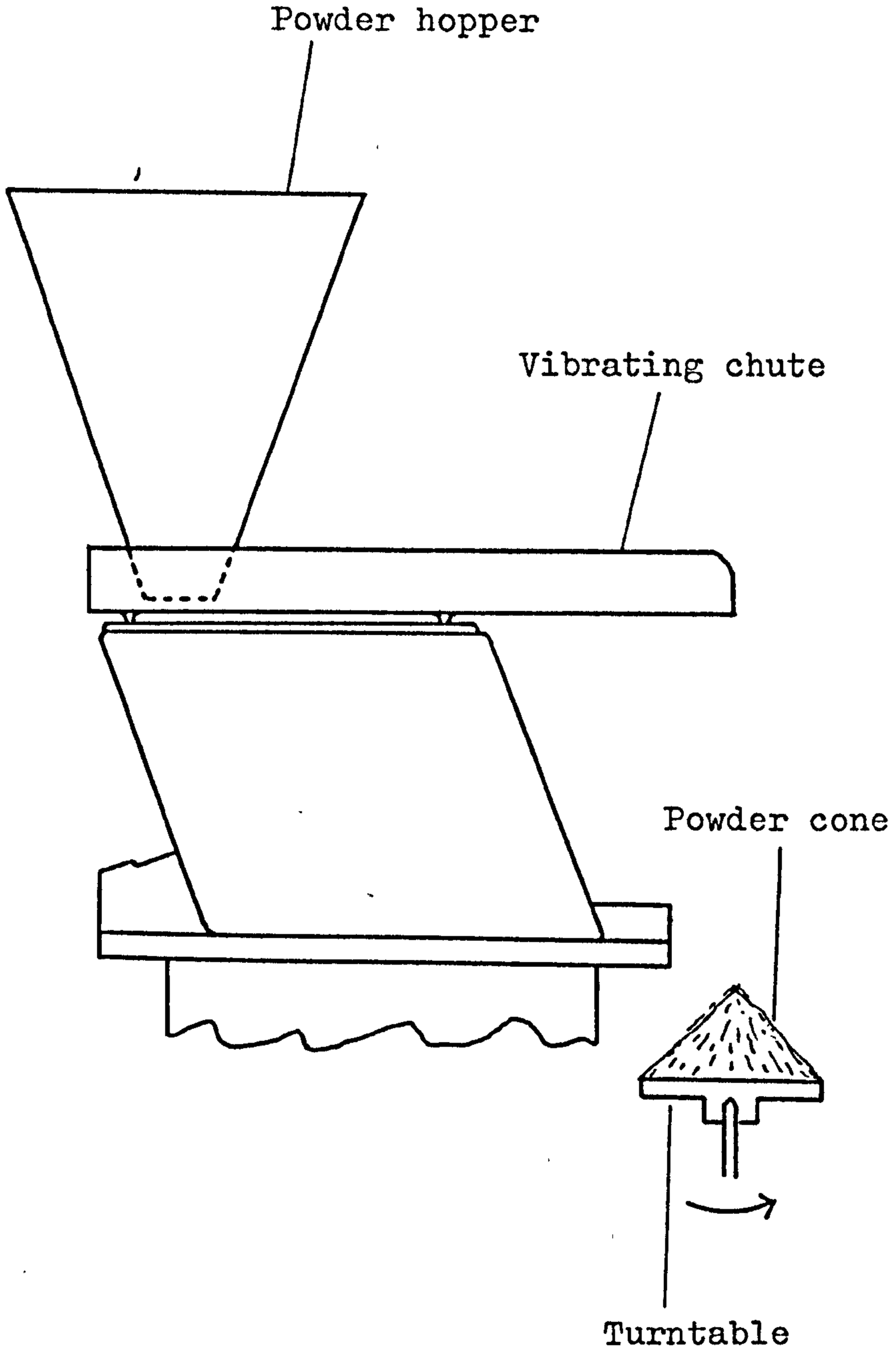

subsequently was not retained on the cone and hence did not alter its shape. The base diameter of the cone was known (57mm), therefore determination of the angle of repose required only the height of the cone to be measured. The results in Table 2.3 are the means of ten determinations for each size fraction.

Table 2.3

Angles of repose: turntable method

Size Fraction	Angle of repose (°)	Coefficient of variation (%)
A	60.6	2.1
B	51.6	2.1
C	44.1	2.2
D	37.1	3.3
E	34.6	2.1
F	32.7	1.6
G	32.6	1.9
H	30.7	2.6

These results provide greater differentiation between the particle size fractions, and are quite reproducible throughout the range, indicating that the method may be suitable for cohesive powders, as well as more free-flowing materials.

2.3 The apparent particle density of lactose

This was determined using an Air Comparison Pycnometer (Model 930, Beckman RIIC, Glenrothes, Scotland), which measures the actual volume of solid present in a known weight of powder.

The determination was repeated several times, and the mean value obtained was 1.55g cm^{-3}. (Particle density is, of course, independent of particle size.)

A knowledge of particle density allows the calculation of porosity from the bulk density of a sample.

$$\text{Porosity} = 1 - \frac{\text{Bulk density}}{\text{Particle density}}$$

2.4 Storage

The particle size fractions of lactose were stored in amber glass jars with screw caps and waterproof liners. Those jars not in everyday use had adhesive tape wrapped around their caps.

2.5 Humidity control

The experiments described in chapters 3 and 8 were carried out in a laboratory in which the relative humidity was maintained at 40% or less, and the temperature rose no higher than 20°C. Due to the location of certain items of equipment, the experiments contained in Chapters 4, 5 and 6 were performed in an air-conditioned laboratory in which humidity and temperature were not monitored.

Chapter 3

The Packing Density Of Lactose

It has already been noted (see Chapter 1) that the density of a packing is influenced by many factors. The effects of two of these factors, deposition method and application of vibration, on the packing density of lactose, have been studied in some detail, to assess the suitability of various methods of bed preparation.

3.1 Influence of deposition method

(A) Experimental

The choice of sample containers was influenced by the fact that these studies were being carried out in connection with the filling of capsules. The filling machine to be used (see Chapter 7) employed aluminium cylinders, approximately 44mm deep and with an internal diameter of about 19mm, for presenting powder beds to the dosator. Therefore, these containers were used in all experiments concerning the packing behaviour of lactose. An aluminium extension collar of the same internal diameter as the containers was attached prior to the deposition of powder, extending the depth of the container by 28mm and allowing the container to be overfilled. After deposition, removal of the collar was followed by levelling of the sample using a spatula blade.

Five deposition methods were investigated, all of

which could be carried out using relatively simple laboratory apparatus.

Calculation of the velocity of deposition of real solid particles in air is complex and may not be very accurate, therefore it was not attempted. Instead, a constant drop height was employed (except in method (i)), this being 100mm from the point of discharge to the top of the aluminium container.

Ten samples were prepared by each method, and their overall porosities were determined and averaged. Size fractions B, D and F were studied.

Method (i)

Powder was poured by hand directly from a jar into the containers. Accurate control of drop height was not attempted, but in all cases it was less than 100mm.

Method (ii)

Powder was allowed to discharge from a vertical cylindrical glass tube, diameter 30mm, fitted with a circular orifice at the base. Deposition into the aluminium containers was only allowed during uninterrupted flow. Several interchangeable orifices of different diameters were available. (See Fig. 3.1).

Method (iii)

Powder was discharged from a vibrating chute (from

Fig. 3.1 Deposition of powder from a vertical cylindrical glass tube

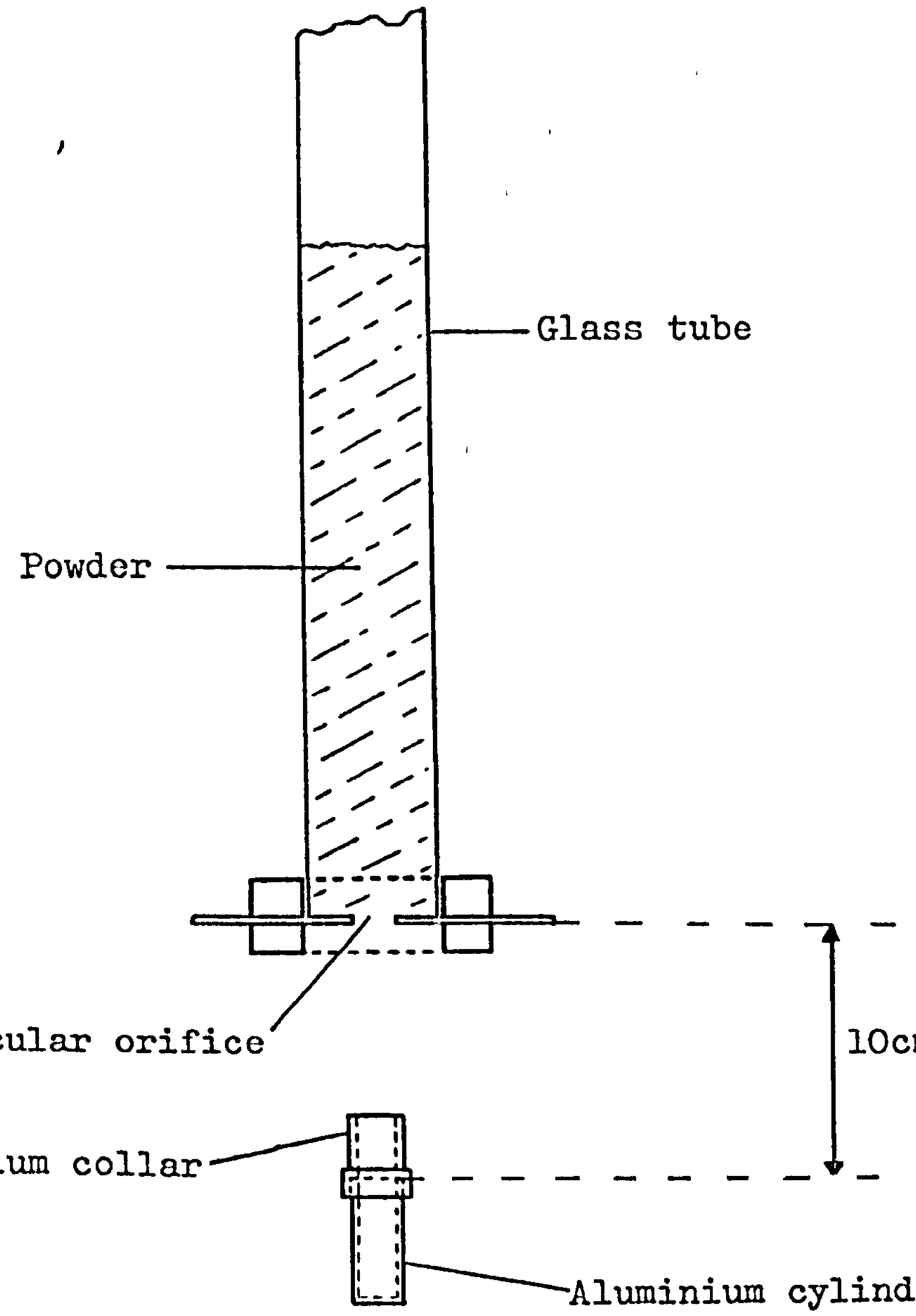

the Spinning Riffler), through an aluminium funnel, and into the sample containers. The outlet of the funnel was of the same diameter as the sample containers. The rate of discharge was variable by adjusting the amplitude of the fixed - frequency (50 Hz) vibration. (See Fig. 3.2)

Method (iv)

A small metal plate of the same width as the vibrating chute (44mm) had a series of 1.5mm diameter holes drilled in it, in such an arrangement that, when clamped to the end of the chute, vibration would cause powder to discharge from these holes, over an area slightly greater than the cross-sectional area of the sample containers. A suitable pattern of holes (see Fig. 3.3) was arrived at by trial and error, with a view to obtaining even deposition and build-up of powder within the container.

Method (v)

A different method of attempting to ensure an even sample build-up was devised. This entailed placing a sample container on the rim of a 230mm diameter turntable, and oscillating it manually backwards and forwards through a "curtain" of powder falling from the vibrating chute. (See Fig. 3.4.)

All experiments were carried out using powder which had been passed through a 150μm sieve to disperse any lumps. In all but method (i), a rough estimate of the rate at

Fig. 3.2 Deposition of powder from a vibrating chute via a funnel

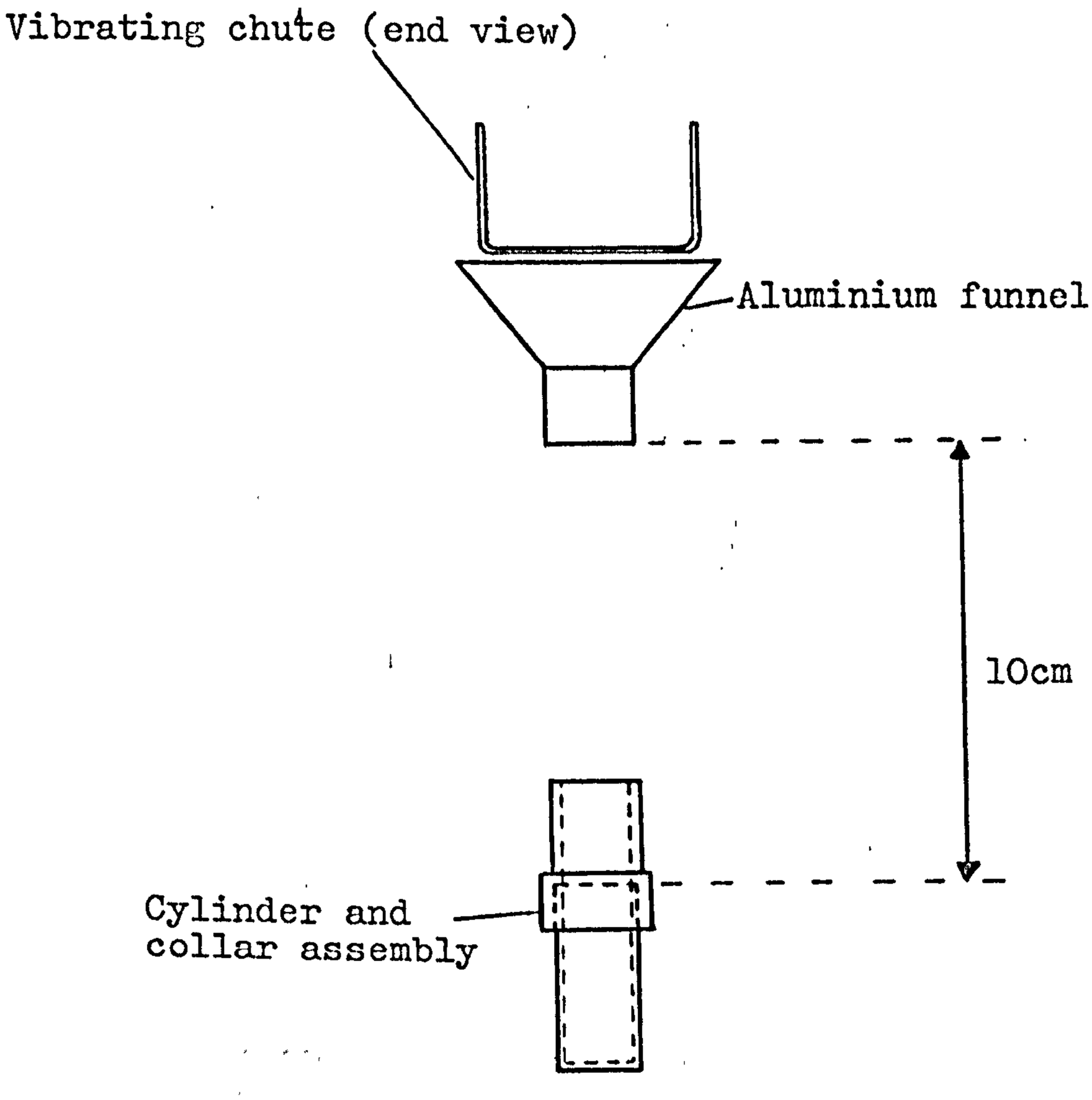

Fig. 3.3 Deposition of powder from a vibrating chute and perforated plate

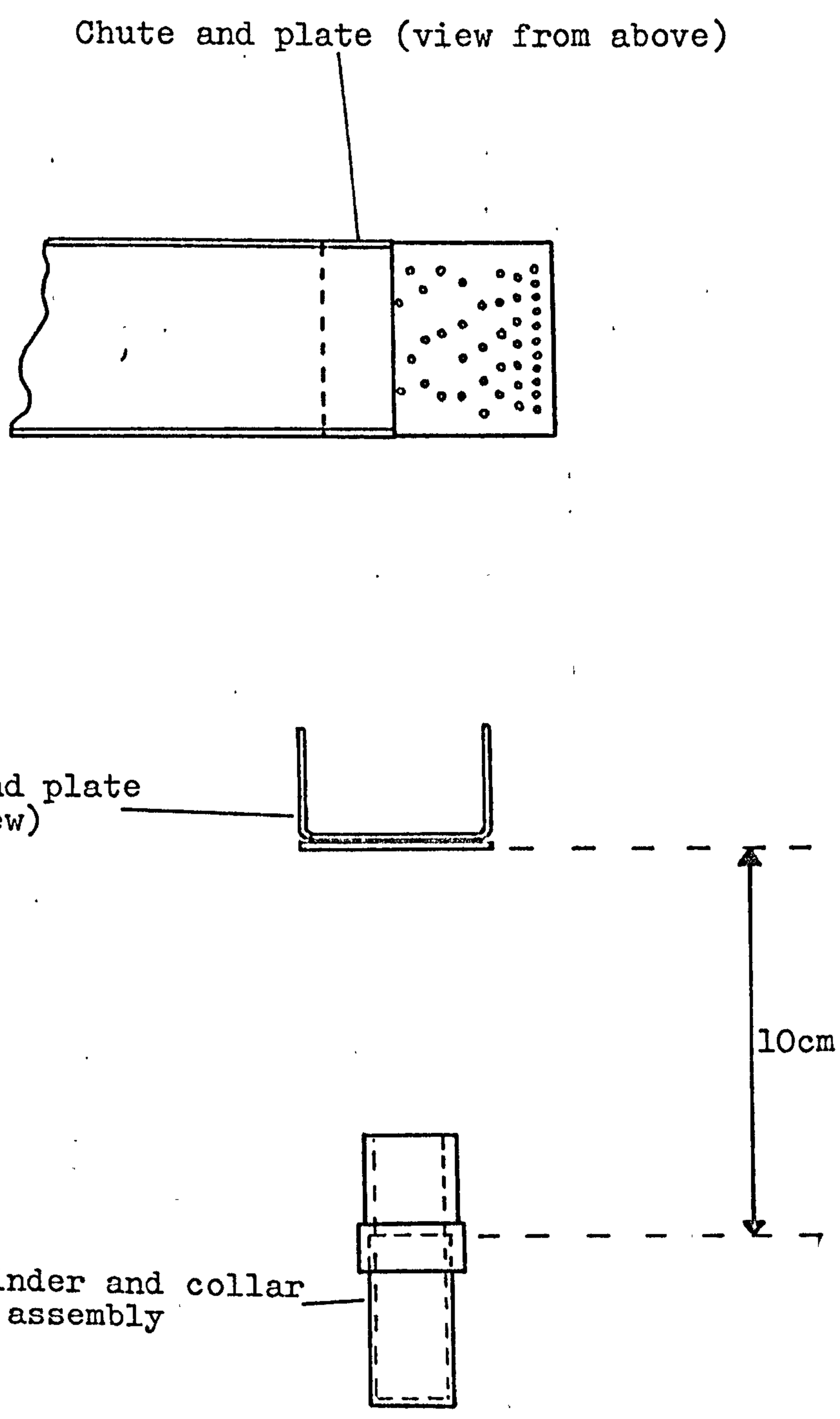

Fig. 3.4 Deposition of powder from a vibrating chute into a slowly oscillating container

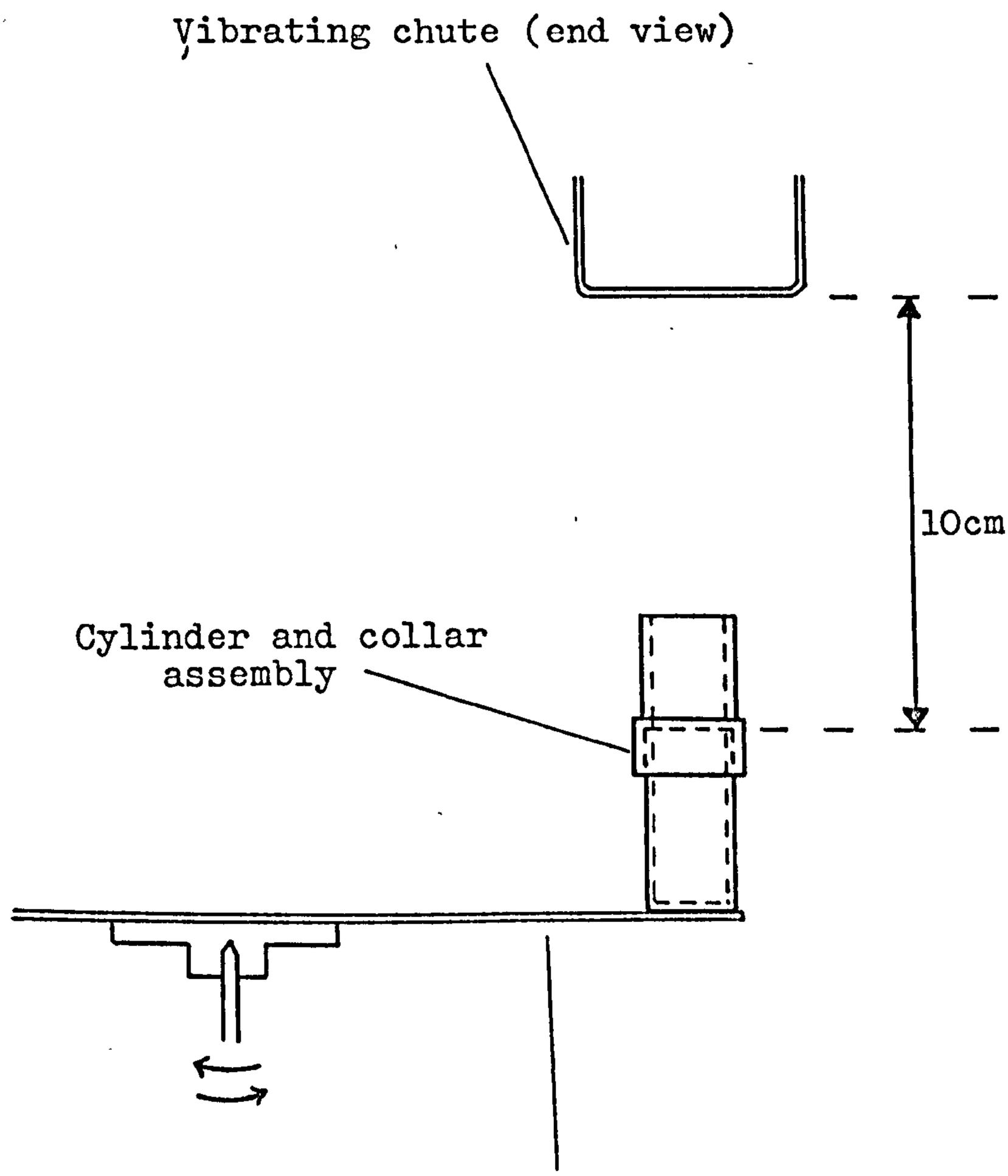

which powder was deposited into the containers was made.

(B) Results

The results are shown in Table 3.1.

(c) Discussion

The theories of Kolbuszewski (1950), and Macrae and Gray (1961) (see Chapter 1) are based on observations of the packing behaviour of free-flowing materials, and hence do not entirely account for the above results.

Fraction F, being relatively free-flowing, behaved largely as expected. High intensity deposition, as in methods (i) and (iia), produced packings of comparatively high porosity, since individual particles were prevented from finding positions of minimum potential energy by the arrival of further particles at an excessive rate. Low intensity deposition, as in methods (iii), (iv), and (v), resulted in samples of lower porosity. The results of (iib) appear at first sight to be anomalous; however, discharge from a 4mm orifice into a container of 19mm diameter resulted in the alternate build-up and collapse of a conical heap. This may be regarded as a kind of secondary deposition, and it causes high porosity because it is of very low velocity.

Fraction B, on the other hand, is quite a cohesive powder, and consequently packs to a high porosity generally. Method (i) produced the highest porosity,

Table 3.1

The effect of particle size and deposition method on sample porosity and its variability

	Deposition method						
	(i)	(iia)*	(iib)*	(iii)	(iv)	(v)	
Deposition rate (g/min)	-			25	5	6	Fraction B +18.7-26.5 μm
Mean porosity	0.649			0.628	0.635	0.621	
Coeff. of variation (%)	1.05			0.91	1.10	1.11	
Deposition rate (g/min)	-	630	350	20	15	10	Fraction D +37.5-53 μm
Mean porosity	0.529	0.520	0.517	0.515	0.522	0.507	
Coeff. of variation (%)	0.78	0.52	0.92	0.49	0.88	0.61	
Deposition rate (g/min)	-	290	40	30	20	10	Fraction F +75-105 μm
Mean porosity	0.536	0.525	0.541	0.497	0.495	0.491	
Coeff. of variation (%)	0.24	0.45	0.49	0.69	1.20	1.28	

*Orifice diameters: Fraction D (iia) 16mm (iib) 12mm
Fraction F (iia) 9mm (iib) 4mm

being an example of high intensity deposition, while method (v) gave samples of somewhat lower porosity. Methods (iii) and (iv) gave porosities a little higher than might be anticipated from a consideration of the deposition rates, but careful observation of the developing samples revealed a tendency for secondary deposition, as described above, to occur. The reason for this is that powder was being deposited in a number of discrete streams in both methods. In method (iii), powder ran down the sloping walls of the funnel, and the emerging powder flux consisted of at least five distinguishable streams. In method (iv), a much larger number of streams were discharged, and although these merged to some extent, the formation of small heaps on the developing sample surface could be seen. The tendency for this secondary deposition to occur appeared to increase with increasing cohesiveness. Fraction B could not be deposited by method (ii).

Fraction D has flow properties intermediate between the preceding two fractions. Method (i) again produced the highest porosity samples, and method (v) the lowest. The samples prepared by deposition from the orifice tube ((iia) and (iib)) were perhaps of slightly lower porosity than expected, bearing in mind their very high deposition intensities. It could be that, since powder was being discharged quite rapidly from the tube, the drop height was effectively greater than 100mm. This would have the effect of lowering the porosity of the samples. Samples

prepared by methods (iii) and (iv) had slightly higher porosities than expected. Some degree of secondary deposition may have been the cause.

Summarising, method (i) is a low velocity, high intensity method of deposition and produces high porosity samples. Method (v) is a low intensity method having a higher deposition velocity and consistently produces low porosity packings., It is not prone to secondary deposition, since the sample is built up in layers. The other methods are rather less well-defined, and do not exhibit consistent trends due to other factors which come into play to a variable extent, depending on the properties of the powder used.

The reproducibility of each method is reflected in the coefficients of variation shown in Table 3.1. There is no single trend applying to all these values, although it would appear that for fraction F, variability increases as deposition rate decreases.

3.2 The effect of vibration

The increase in the bulk density of a powder when controlled vibration is applied is influenced by the properties of the powder, the nature of the container, and the vibration conditions (see Chapter 1). By choosing to use lactose and the cylindrical aluminium containers (described previously), the number of variables was reduced. The effect of vibration on the packing properties

of lactose was studied in three parts:

1. An investigation of the useful frequency range for all particle size fractions.

2. The visible behaviour of selected particle size fractions at a number of frequency/acceleration combinations; amplitude was measured simultaneously in each instance.

3. The effect of increasing the acceleration at selected frequencies on the bulk density of selected size fractions.

In all three types of experiment, both vertical and horizontal vibration modes were evaluated.

3.2.1 Investigation of useful frequency range

(A) Experimental

The vibration system consisted of a 5VA power oscillator and a model 790A vibrator (Goodmans Industries Ltd., Wembley, Middlesex). The latter was mounted on a trunnion such that it could be operated in a horizontal or vertical direction. For vertical vibration, the sample container was held firmly in a steel cup which could be screwed into the vibrator table (Fig. 3.5(a)), and for horizontal vibration, the container was attached to the vibrator by means of a steel ring (Fig. 3.5(b)).

The oscillator was equipped with frequency and power output controls, but no means of measuring acceleration or related quantities was available. The power output scale was in arbitrary units from 0 to 10, and a setting

Fig. 3.5 Attachment of powder sample container to Goodmans vibrator

(a) Vertical mode

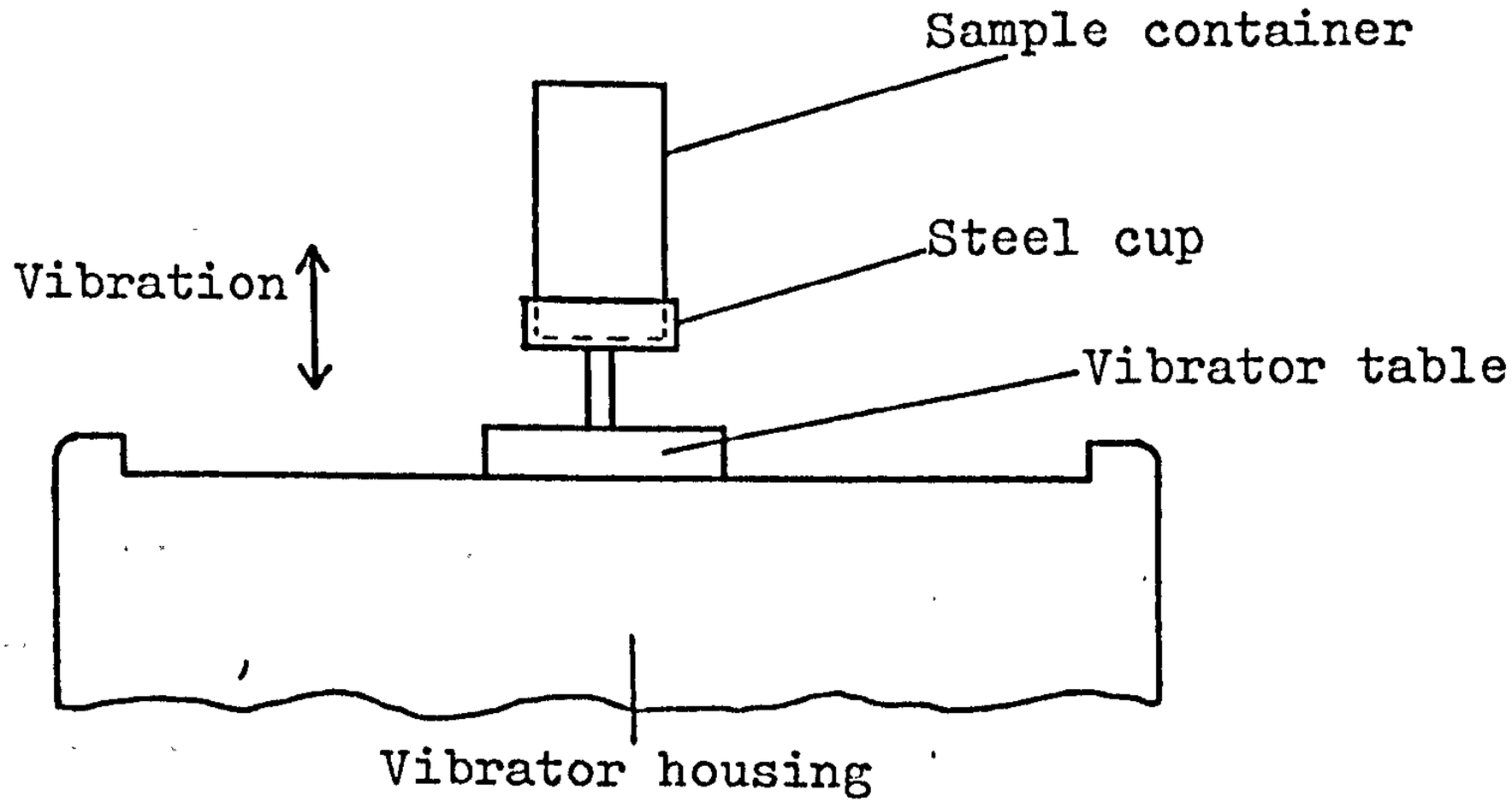

(b) Horizontal mode

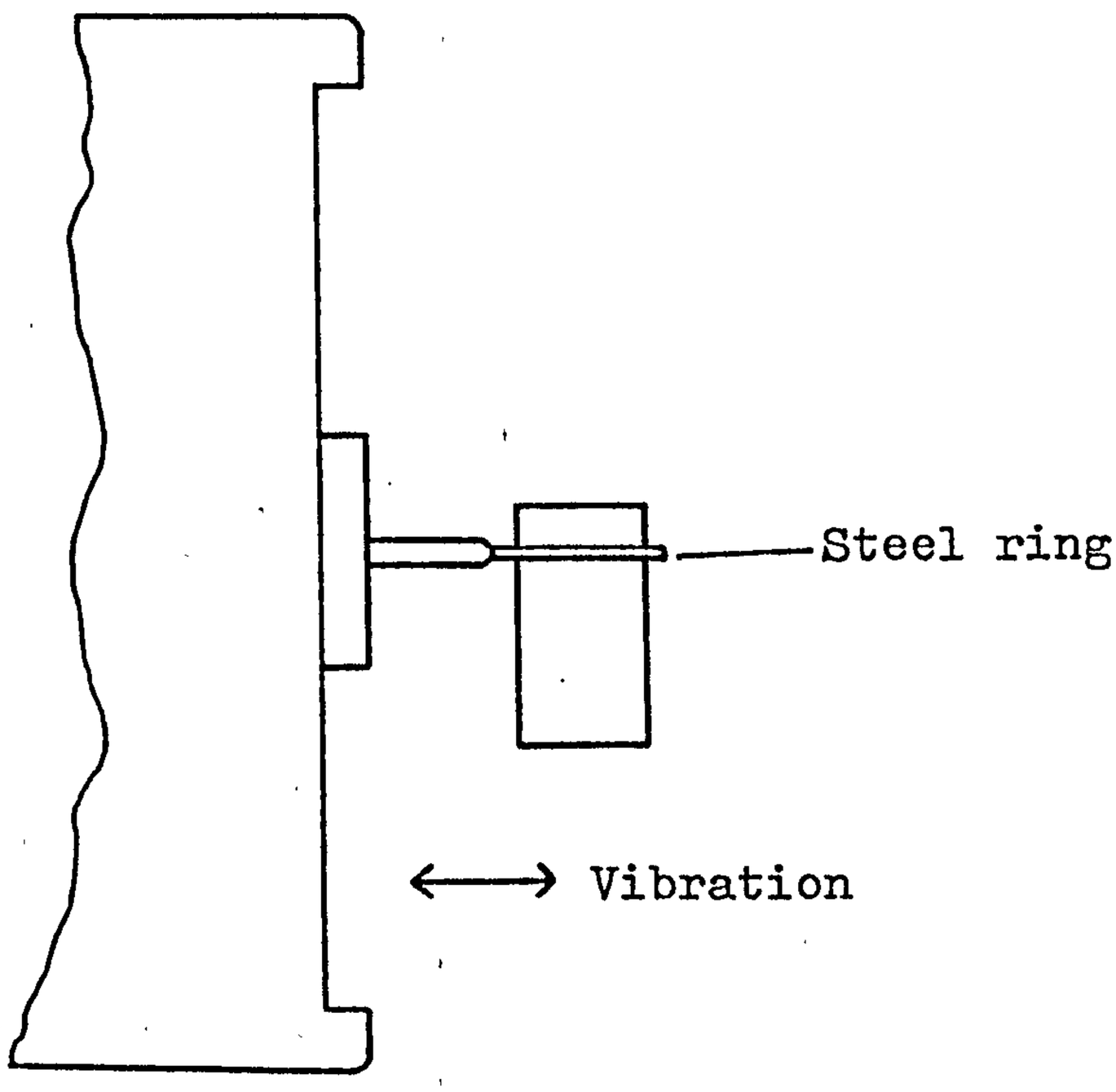

of 5 was chosen for all tests except the horizontal vibration of fraction A. In this latter case, setting 5 proved inadequate, so setting 10 was used.

From preliminary observations, the useful frequency range appeared to be between 30Hz and 600Hz, hence a number of frequencies in this band were tried.

Powder samples were prepared by pouring from a jar into an aluminium cylinder and scraping the upper surface level using a spatula blade. Initial porosity was determined from weight and volume, then the sample was attached to the vibrator. A cylindrical nylon rod, 4cm long and a loose fit in the container, was placed on top of the sample, and the sample was subjected to the chosen vibration for 30 seconds. The rod served two purposes; as well as helping to maintain a flat upper surface, it also provided a means of measuring the consolidation produced. The downward displacement of a spot marked on the top edge of the rod was measured using a travelling microscope, and this was equal to the decrease in sample depth. The final porosity could then be calculated. The rod weighed approximately 12.5g and hence made little or no contribution to the consolidation of the samples.

All eight particle size fractions were studied, in both vertical and horizontal modes.

(B) Results and discussion

The results are presented in the form of graphs of

frequency against final porosity. See Figs. 3.6 to 3.13.

Several points of interest emerge from these graphs. It is evident that for all eight particle size fractions, vertical vibration is more effective in reducing the porosity of the samples than horizontal vibration, over the frequency range studied. In all cases, there is a minimum in the curve indicating an optimum frequency range. These minima vary in breadth, being quite narrow in the case of the cohesive powders (A and B) and becoming broader for more free-flowing materials. The optimum frequency range is similar throughout the particle size range, suggesting that it may be largely container-dependent.

Fractions C to H were packed to roughly the same porosity, while the more cohesive fractions (B, and particularly A) were less responsive, and would require greater power input in order to attain such low porosities. Finally, some size fractions (A,B,C,D) exhibited a second, sharper minimum at approximately 500Hz in the horizontal mode. This was presumably a resonant frequency for the system.

3.2.2 Investigation of visible behaviour of vibrated samples

(A) Experimental

The vibration system described above was replaced by a more comprehensive system consisting of a TA 120

Fig. 3.6 The porosity of vibrated lactose samples as a function of vibration frequency : particle size fraction A

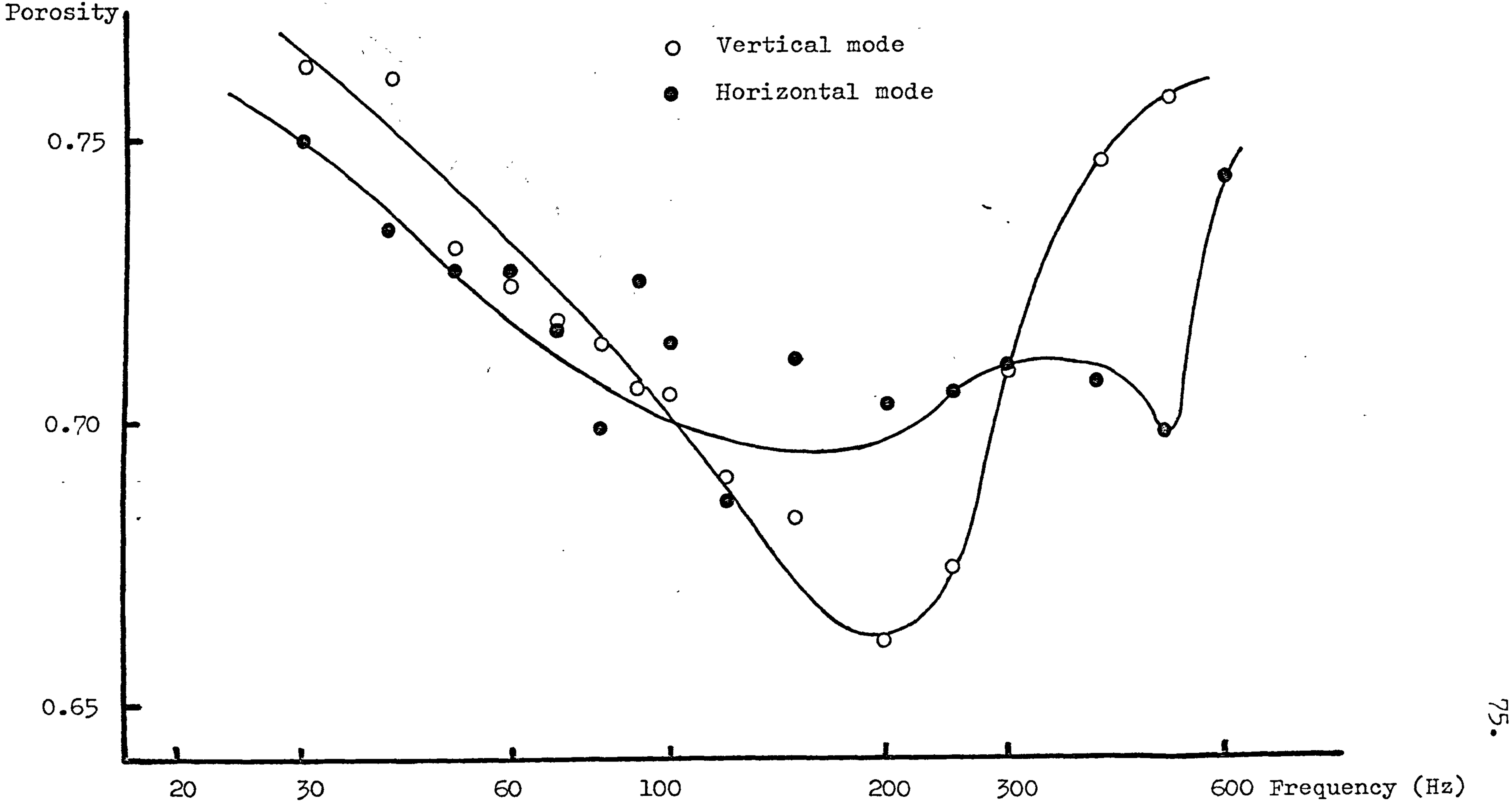

Fig. 3.7 The porosity of vibrated lactose samples as a function of vibration frequency : particle size fraction B

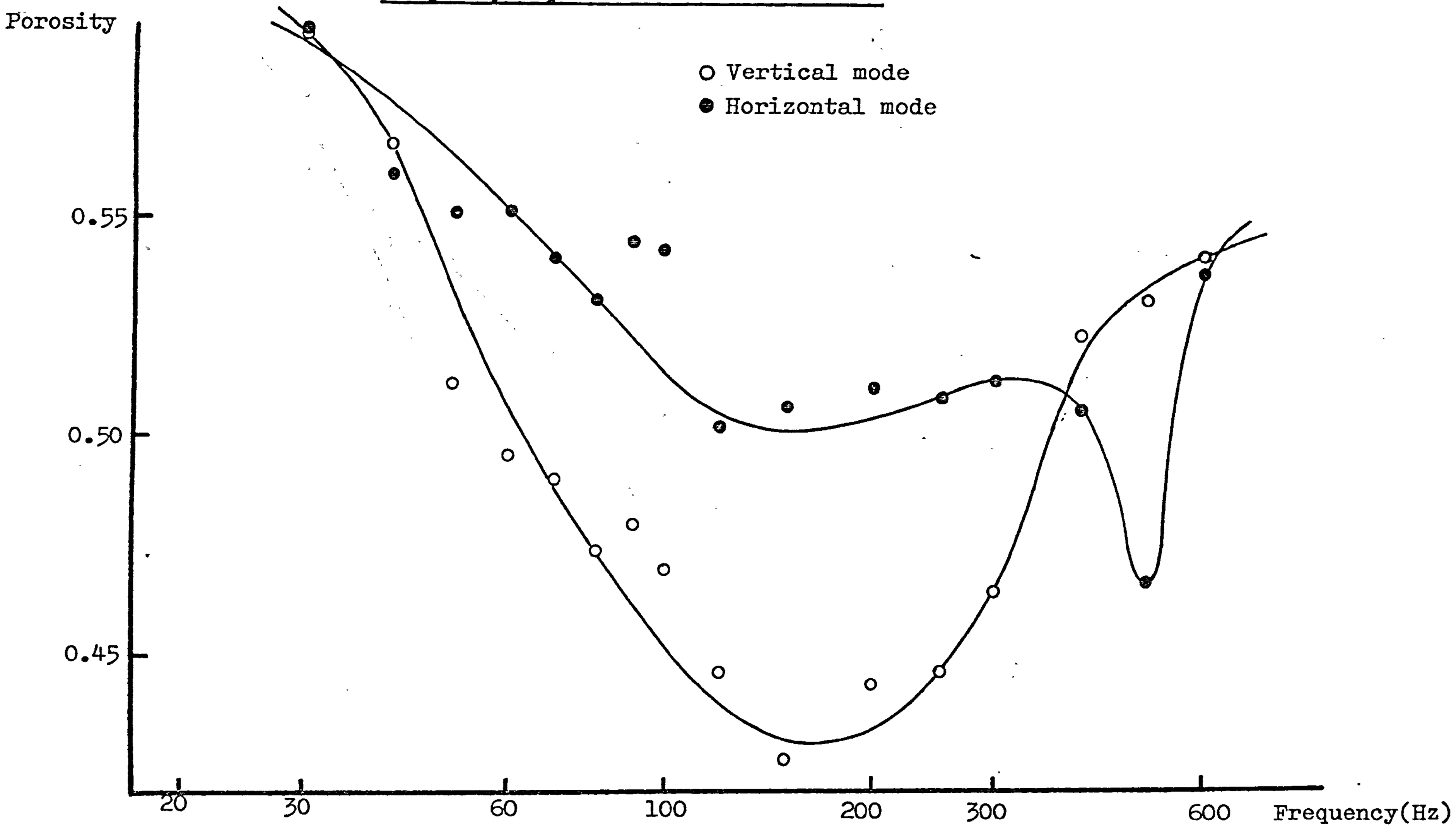

Fig. 3.8 The porosity of vibrated lactose samples as a function of vibration frequency : particle size fraction C

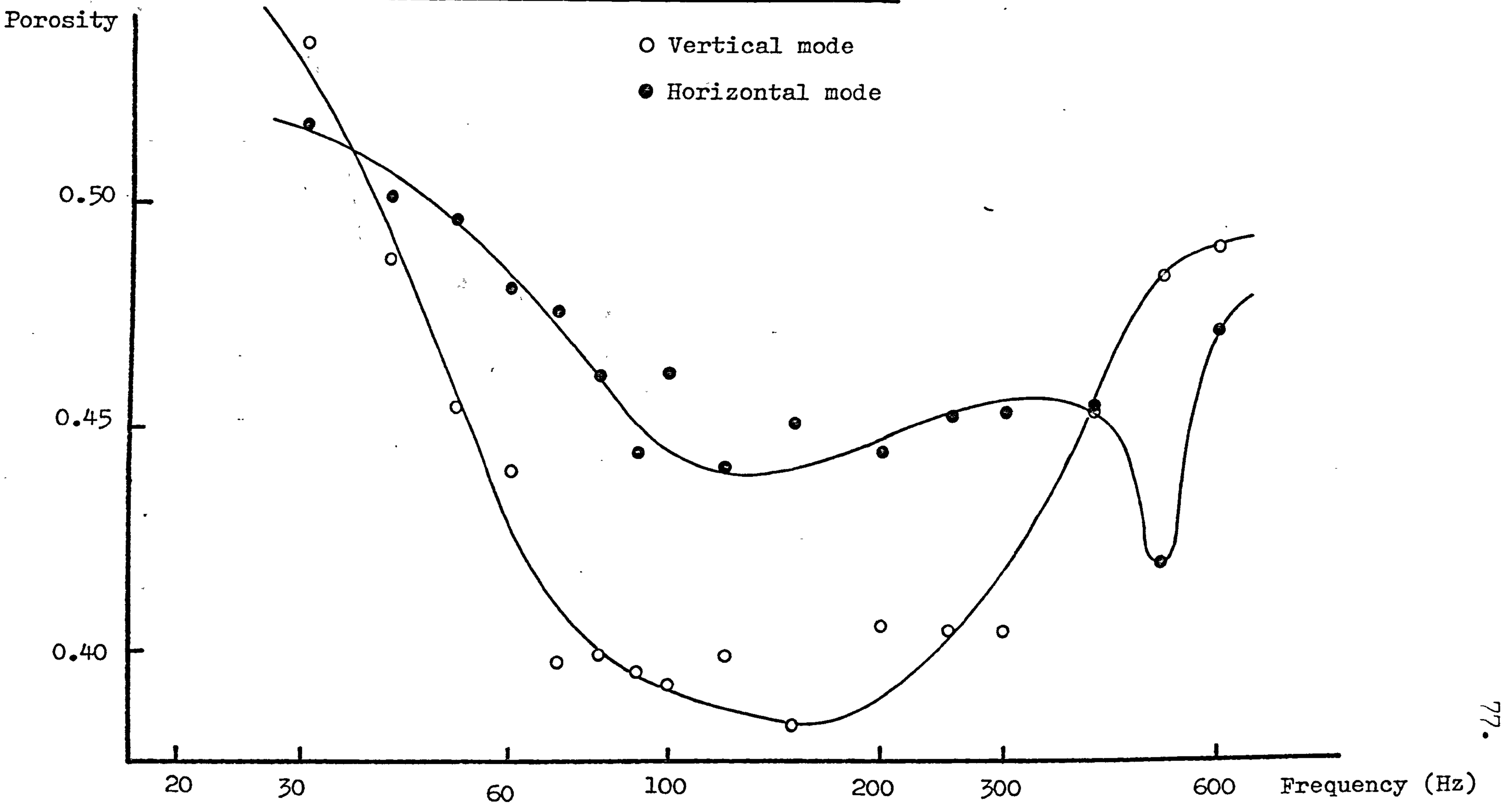

Fig. 3.9 The porosity of vibrated lactose samples as a function of vibration frequency : particle size fraction D

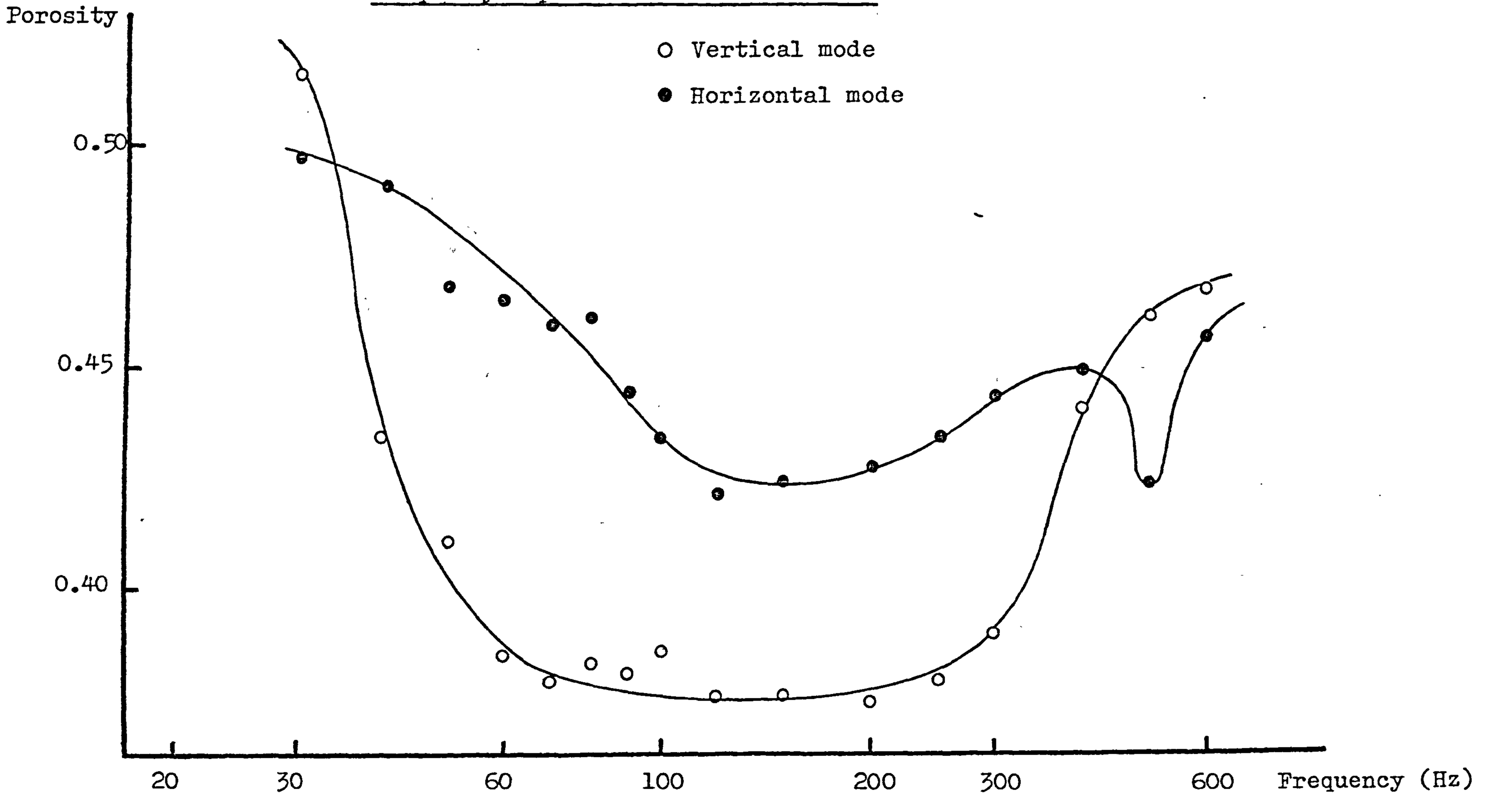

Fig. 3.10 The porosity of vibrated lactose samples as a function of vibration frequency : particle size fraction E

○ Vertical mode
● Horizontal mode

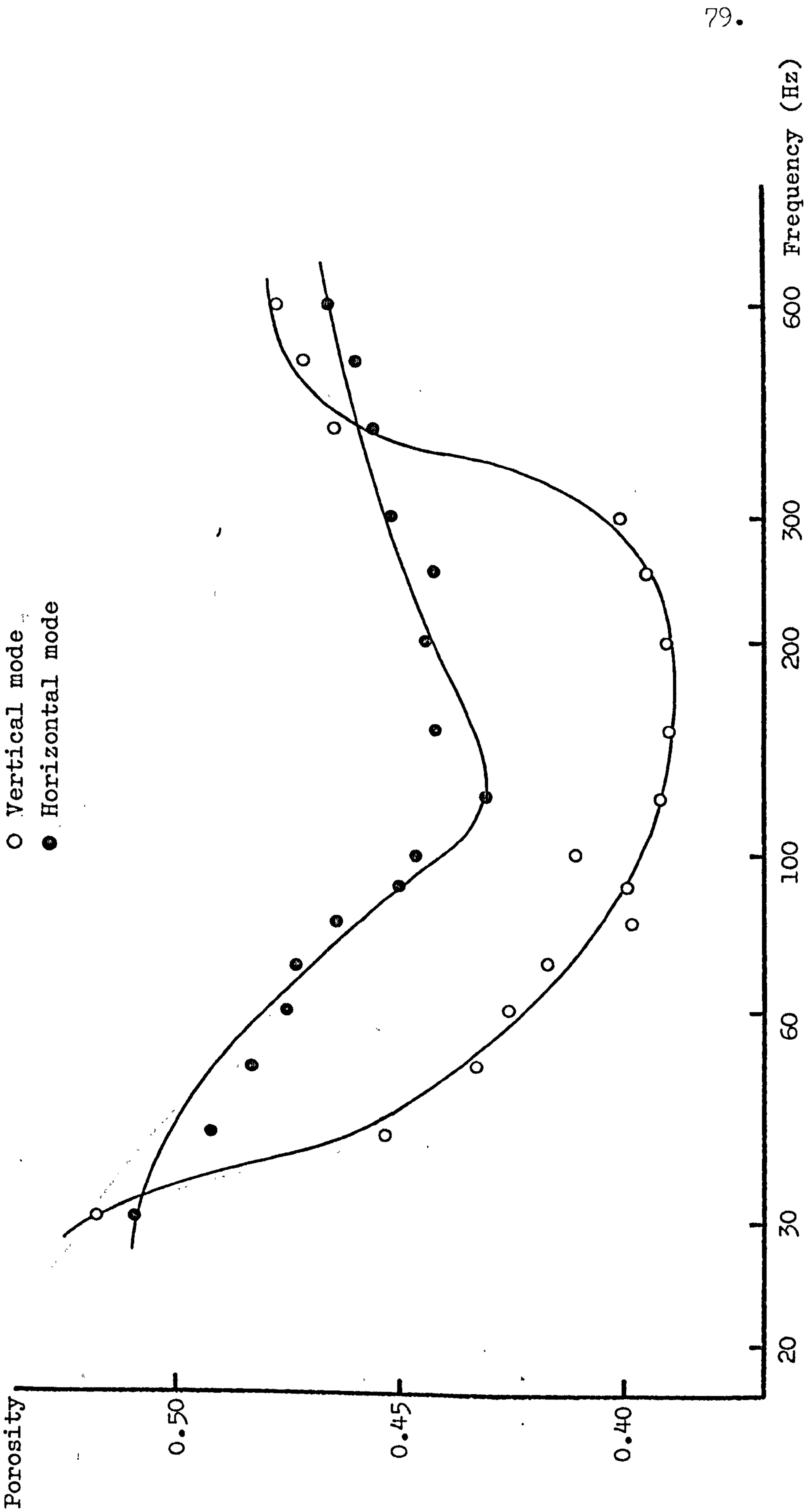

Fig. 3.11 The porosity of vibrated lactose samples as a function of vibration frequency : particle size fraction F

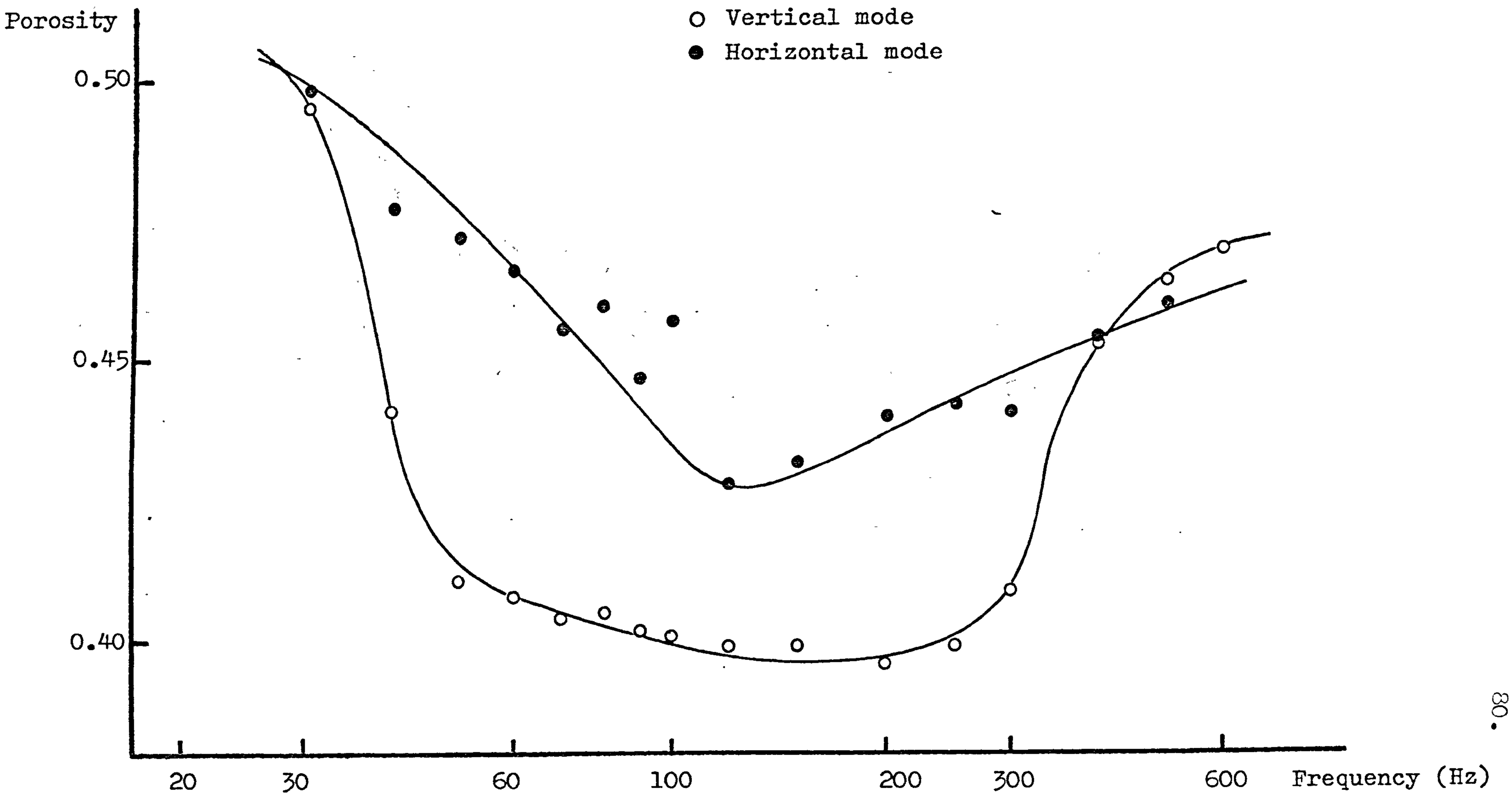

Fig. 3.12 The porosity of vibrated lactose samples as a function of vibration frequency : particle size fraction G

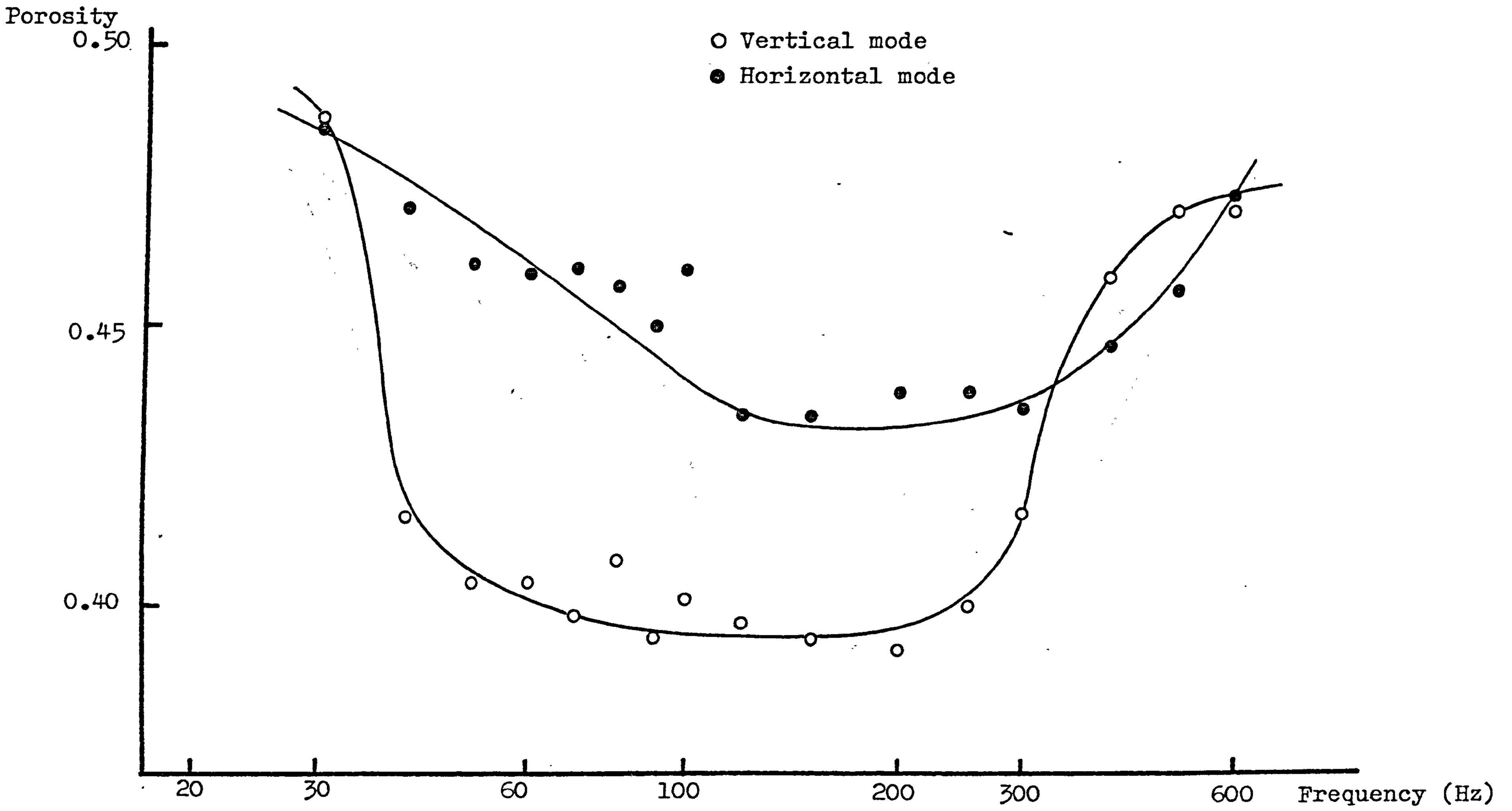

Fig. 3.13 The porosity of vibrated lactose samples as a function of vibration frequency : particle size fraction H

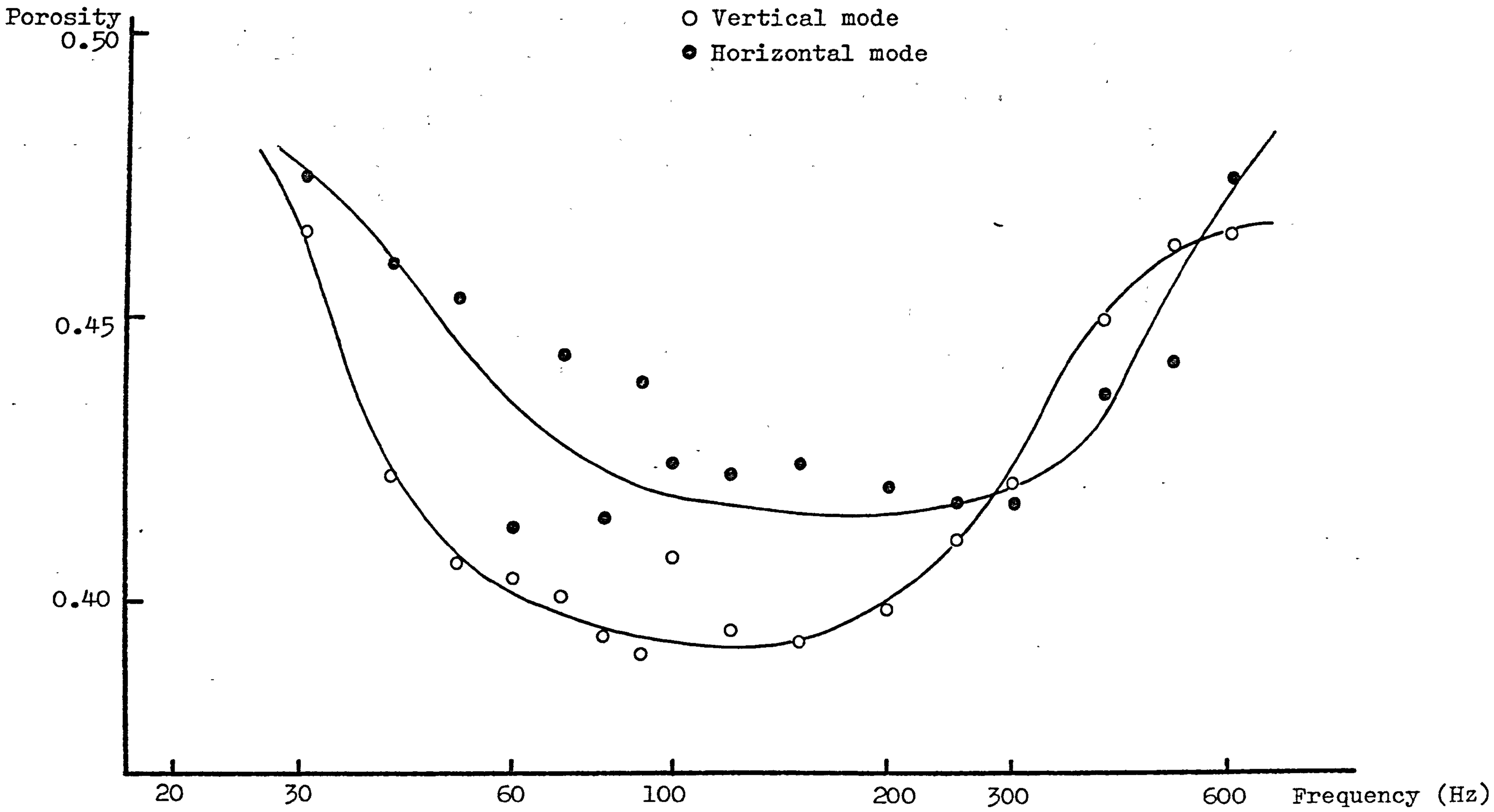

oscillator/amplifier, a VP3 electromagnetic vibrator and trunnion, and a portable vibration analyser, or PVA (all manufactured by Derritron Electronics Ltd., Hastings, Sussex). By mounting a piezo-electric accelerometer (model A/01/T, D.J. Birchall Ltd., Mildenhall, Suffolk) in a suitable place, it was possible to monitor the acceleration, velocity and displacement (amplitude) of an applied vibration. The acçelerometer was connected to the PVA by low-noise co-axial cable.

A circular steel plate was made which could be attached to the vibrator table by means of five countersunk screws. The sample container and accelerometer were mounted on this plate, as shown in Figs. 3.14(a) and 3.14(b).

Powder samples were again prepared by pouring from a jar into an aluminium cylinder, and scraping off the excess powder using a spatula blade. Three particle size fractions (B,D,F) were studied at four acceleration levels (1g, 2g, 4g, 6g) with a number of selected frequencies, in both vertical and horizontal modes. The chosen acceleration levels were set by adjustment of the power output control on the oscillator, and were monitored on the PVA, which also recorded the container displacement in each instance (see Table 3.2). All values of acceleration and displacement quoted are "0 to peak" rather than "peak to peak" or root mean square. A subjective assessment of the visible behaviour of the powders under the various

Fig. 3.14 Attachment of powder sample container to Derritron vibrator

(a) Vertical mode

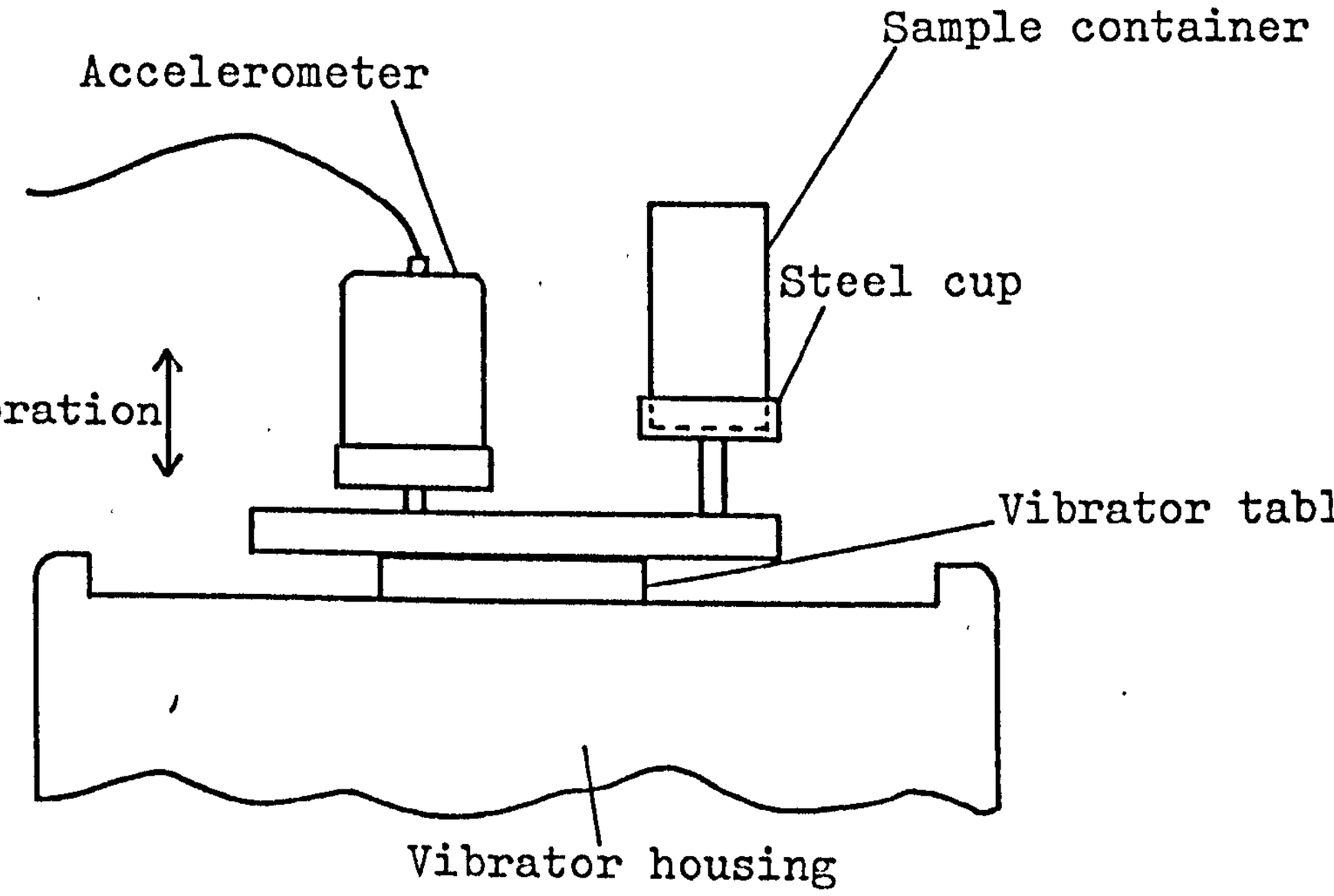

(b) Horizontal mode

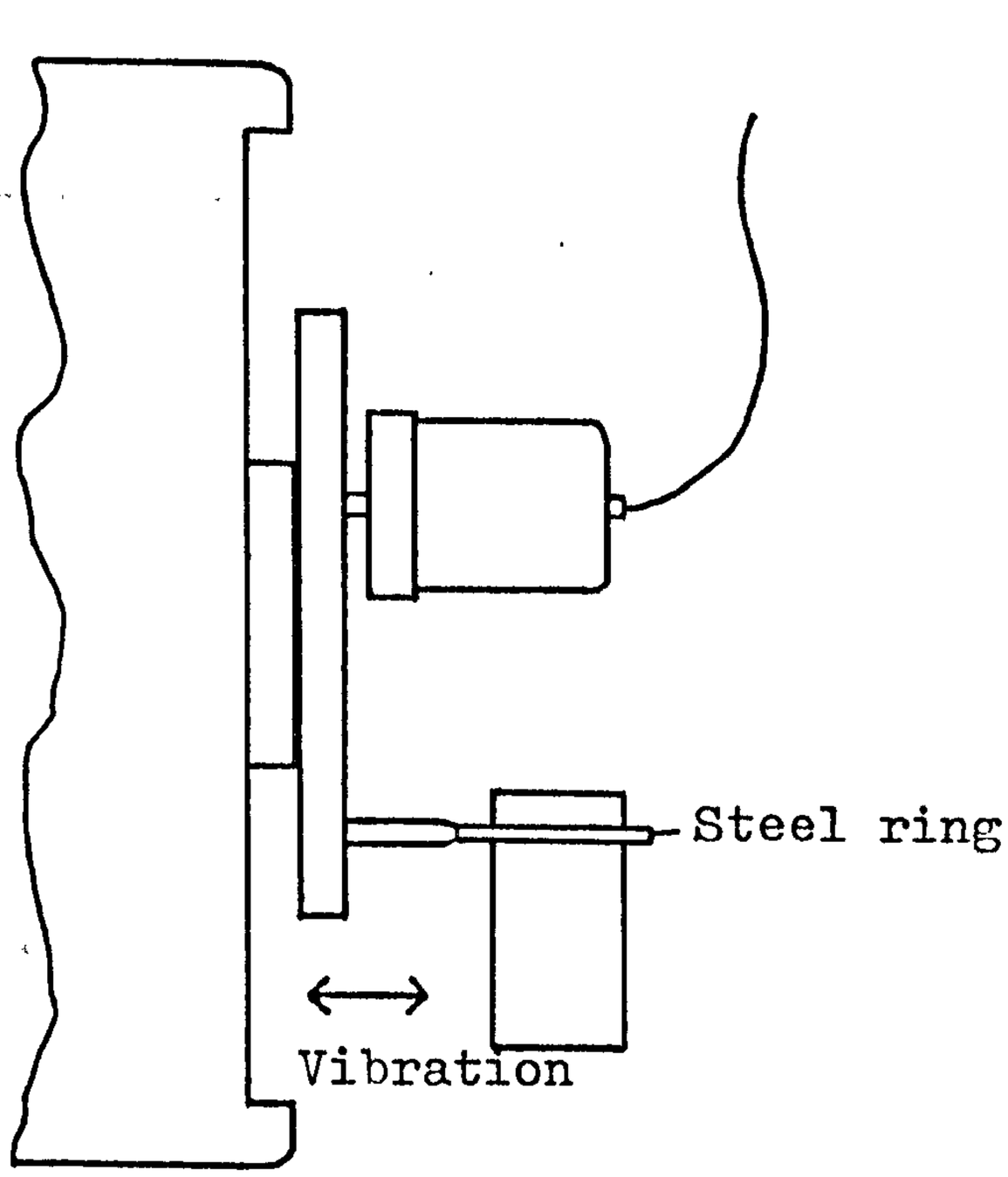

vibration conditions was made, and the results appear in Tables 3.3(a) to 3.3(c).

(B) Results

Displacement proved to be independent of particle size and vibration mode, and therefore, the values in Table 3.2 are all means of six observations.

Table 3.2

Displacement (O-peak) in μm, recorded at various frequencies and accelerations

	Acceleration (O-peak) in 'g'			
Frequency, Hz	1	2	4	6
30	263	540	1083	1592
50	99	196	395	582
70	49	99	195	292
100	24	49	96	143
150	11.4	22	44	66
200	6.3	12.6	25	38
300	2.9	5.7	11.0	16.9
400	1.7	3.1	6.2	9.3
500	1.2	2.1	4.1	6.1
600	0.9	1.5	2.8	4.2

Assessment of the visible behaviour of the vibrated samples was purely qualitative, the following key being used to compare different conditions:

Type of particle movement:

α no visible movement

β microscopic (particles moving independently)

γ macroscopic or bulk movement

δ fluidisation or ejection of powder

ε rotation of whole sample

Description of upper surface:

a level

b sloping

c central ridge

d presence of cracks

e central trough

The use of two letters together e.g. 'ac' indicates a combination, or a condition intermediate between the two. Notation such as '$\gamma \rightarrow \alpha$ ' signifies one condition giving way to another after a period of time.

Table 3.3(a)

The visible behaviour of lactose fraction B when subjected to various vibration conditions

(i) Horizontal vibration

Frequency (Hz)	Acceleration (O-peak) in 'g' 1	2	4	6
30	α/a	ε/ad	δ/e	δ/e
50	α/a	α/ad	βγ/ae	γ/ae
70	α/a	α/bd	βγ/ad	γ/ad
100	α/a	α/ad	α/a	βγ/ad
150	α/a	α/bd	α/a	βγ/cd
200	α/a	α/ad	α/ad	βγ/cd
300	α/a	α/bd	α/bd	γ/c
400	α/ad	α/bd	α/bd	α/bd
500	α/bd	α/bd	ε/bd	γε/bd
600	α/bd	α/bd	α/bd	α/bd

(ii) Vertical vibration

Frequency (Hz)	Acceleration (O-peak) in 'g' 1	2	4	6
30	α/a	α/ad	α/ad	γδ/b
50	α/a	α/ad	α/ad	γ/b
70	α/a	α/ad	α/ad	γ/b
100	α/a	α/ad	α/b	γ→α/b
150	α/a	α/ad	α/b	γ/b
200	α/a	α/ad	α/a	γ/b
300	α/a	α/ad	α/a	α/bd
400	α/ad	α/ad	α/ab	α/bd
500	α/ad	α/ad	α/ab	α/bd
600	α/ad	α/ad	α/ad	α/bd

Table 3.3(b)

The visible behaviour of lactose fraction D when subjected to various vibration conditions

(i) Horizontal vibration

Frequency (Hz)	Acceleration (O-peak) in 'g' 1	2	4	6
30	α/a	β/a	γ/b	γδ/ae
50	α/a	β/a	γ/b	γδ/ae
70	α/a	β/a	γ/ab	γ/c
100	α/a	α/a	β/ac	β/c
150	α/a	α/a	β/ac	β/c
200	α/a	α/ab	αβ/ac	β/c
300	α/ab	α/b	α/c	αδ/c
400	α/ab	α/b	αβ/b	γ/b
500	α/ab	α/b	αβ/bc	γ/bc
600	α/ab	α/b	αβ/b	αγ/bc

(ii) Vertical vibration

Frequency (Hz)	Acceleration (O-peak) in 'g' 1	2	4	6
30	α/a	α/a	δ/b	δ/b
50	α/a	α/ab	γ/b	γ/b
70	α/a	α/ab	γ/b	γ/b
100	α/a	α/ab	α/b	γ/b
150	α/a	α/a	γ→α/b	γ/b
200	α/a	α/a	γ/b	γ/b
300	α/a	α/a	α/b	αγ/b
400	α/a	α/a	α/b	α/b
500	α/a	α/a	α/b	α/b
600	α/a	α/a	α/ab	α/ab

Table 3.3(c)

The visible behaviour of lactose fraction F when subjected to various vibration conditions

(i) Horizontal vibration

Frequency (Hz)	Acceleration (O-peak) in 'g' 1	2	4	6
30	α/ab	β/a	γδ/a	δ/a
50	α/a	β/a	γ/c	γ/c
70	α/ac	β/a	γ/c	γ/c
100	α/a	β/a	γ/c	γ/c
150	α/a	αβ/ac	γ/c	γ/c
200	α/a	αβ/ac	αγ/c	γ/c
300	α/a	α/ab	α/ac	αγ/c
400	α/a	α/ab	α/ac	αγ/bc
500	α/a	α/ab	ε/b	ε/b
600	α/a	α/ab	α/ab	αβ/bc

(ii) Vertical vibration

Frequency (Hz)	Acceleration (O-peak) in 'g' 1	2	4	6
30	α/a	α/a	δ/b	γδ/b
50	α/a	α/a	βγ/b	γ/b
70	α/a	α/a	βγ/b	γ/b
100	α/a	α/a	βγ/b	γ/b
150	α/a	α/a	γ→α/b	γ/b
200	α/a	α/a	β→α/b	γ/b
300	α/a	α/a	αβ/a	β/b
400	α/a	α/a	α/ab	α/b
500	α/a	α/a	α/b	α/b
600	α/a	α/a	α/ab	α/ab

Throughout this experiment, it could be noted that an acceleration of 1g (0 to peak) produced little or no consolidation; the samples generally began to pack down at about 2g.

(C) Discussion

A number of trends emerge from these results. Particle activity increased with increasing acceleration since more kinetic energy was being supplied. This could be detrimental to close packing at low frequencies, since the resulting large amplitude can result in fluidisation of the sample. The effect of frequency is not quite as well-defined, but generally, there was less visible activity at higher frequencies. This is because the amplitude of the vibration was small and large displacement of particles was not encouraged. Powder samples that were subjected to vertical vibration appeared to be more prone to forming a sloping surface. This could possibly be due to the fact that the containers were not mounted centrally on the vibrator table. The rapid subsidence of particle activity, as in '$\gamma \rightarrow \alpha$' for example, was peculiar to vertical vibration, while the formation of a central ridge or trough and the rotation of samples, were restricted to the horizontal mode. The reasons for these last observations are not obvious.

3.2.3. The effect of increasing acceleration on sample porosity

(A) Experimental

The vibration system was as described in 3.2.2, and again, powder samples were prepared by pouring from a jar followed by levelling with a spatula blade.

For each of size fractions B, D and F, four frequencies in both vertical and horizontal modes were selected, which would produce the most consolidation based on the information contained in Figs. 3.7, 3.9, and 3.11. At each frequency, a sample was vibrated for ten minutes at an acceleration of 2g (0 to peak). This was followed by ten minutes at 3g, 4g, 5g etc. until a minimum porosity was reached. The porosity decrease was measured every two minutes by following the descent of the nylon rod using a travelling microscope. The vibration was stopped to facilitate these measurements.

(B) Results and discussion

Graphs were drawn of the decrease in porosity recorded with time at each frequency. See Figs. 3.15 to 3.20.

A summary of the minimum porosity attained at each frequency, together with the acceleration required to achieve it is given in Table 3.4. There is a possibility that in some cases, increasing the acceleration still further would have reduced the porosity of the sample. However, to limit the time span of the experiment, it was

Fig. 3.15 The porosity of vibrated lactose samples as a function of acceleration, increasing stepwise at ten minute intervals. Particle size fraction B, horizontal mode.

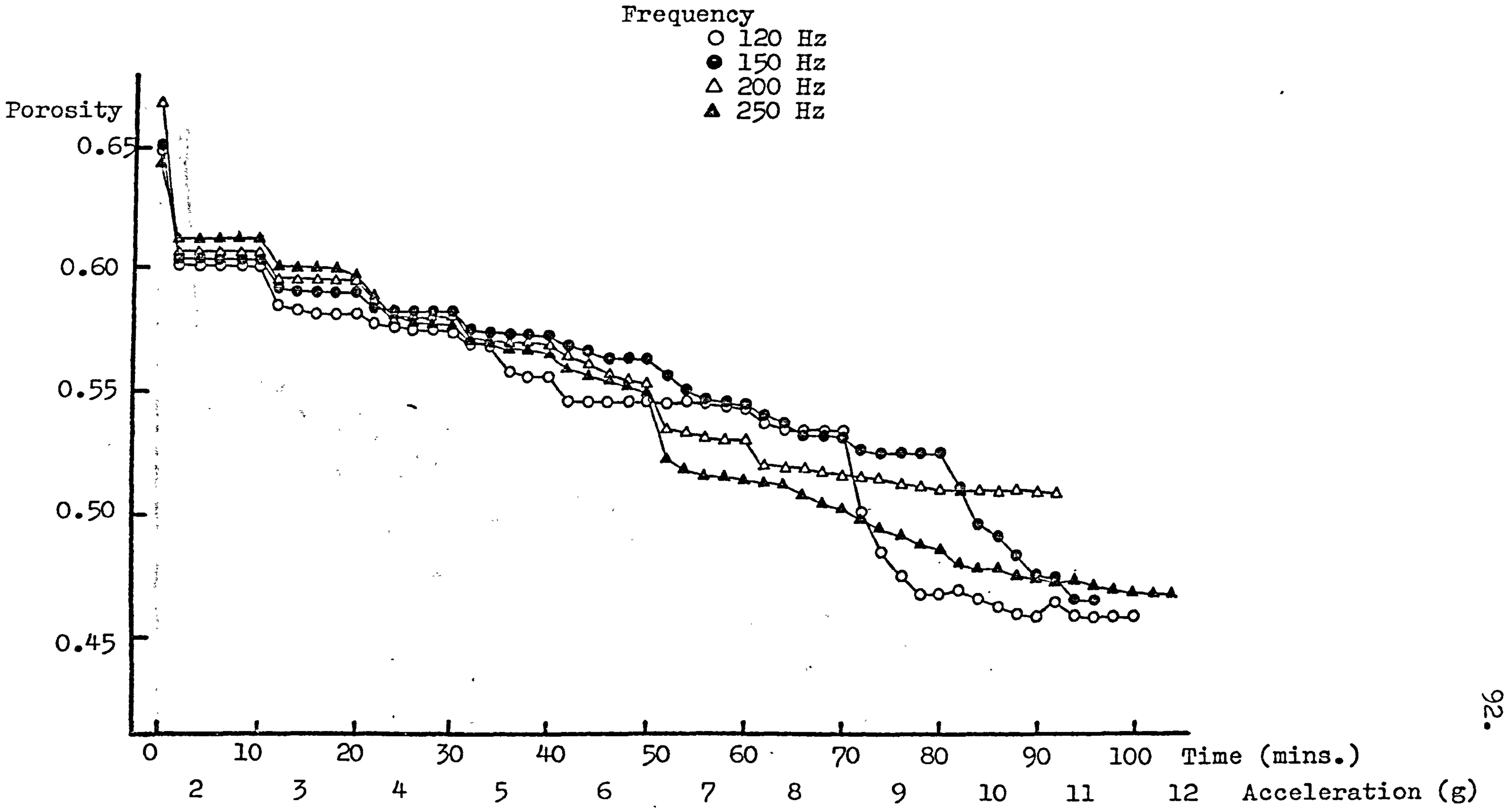

Fig. 3.16 The porosity of vibrated lactose samples as a function of acceleration, increasing stepwise at ten minute intervals. Particle size Fraction B, vertical mode

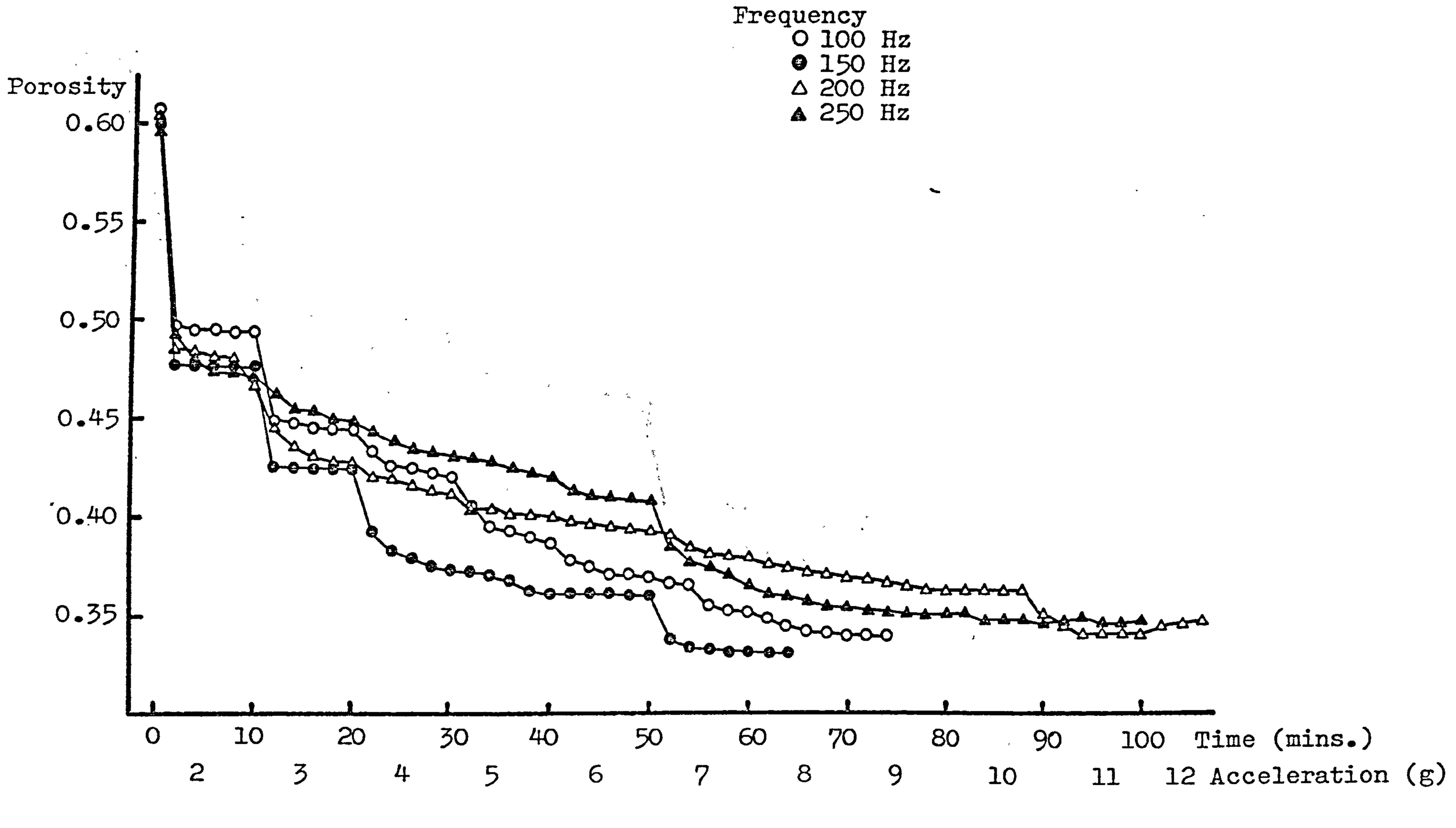

Fig. 3.17 The porosity of vibrated lactose samples as a function of acceleration, increasing stepwise at ten minute intervals. Particle size fraction D, horizontal mode.

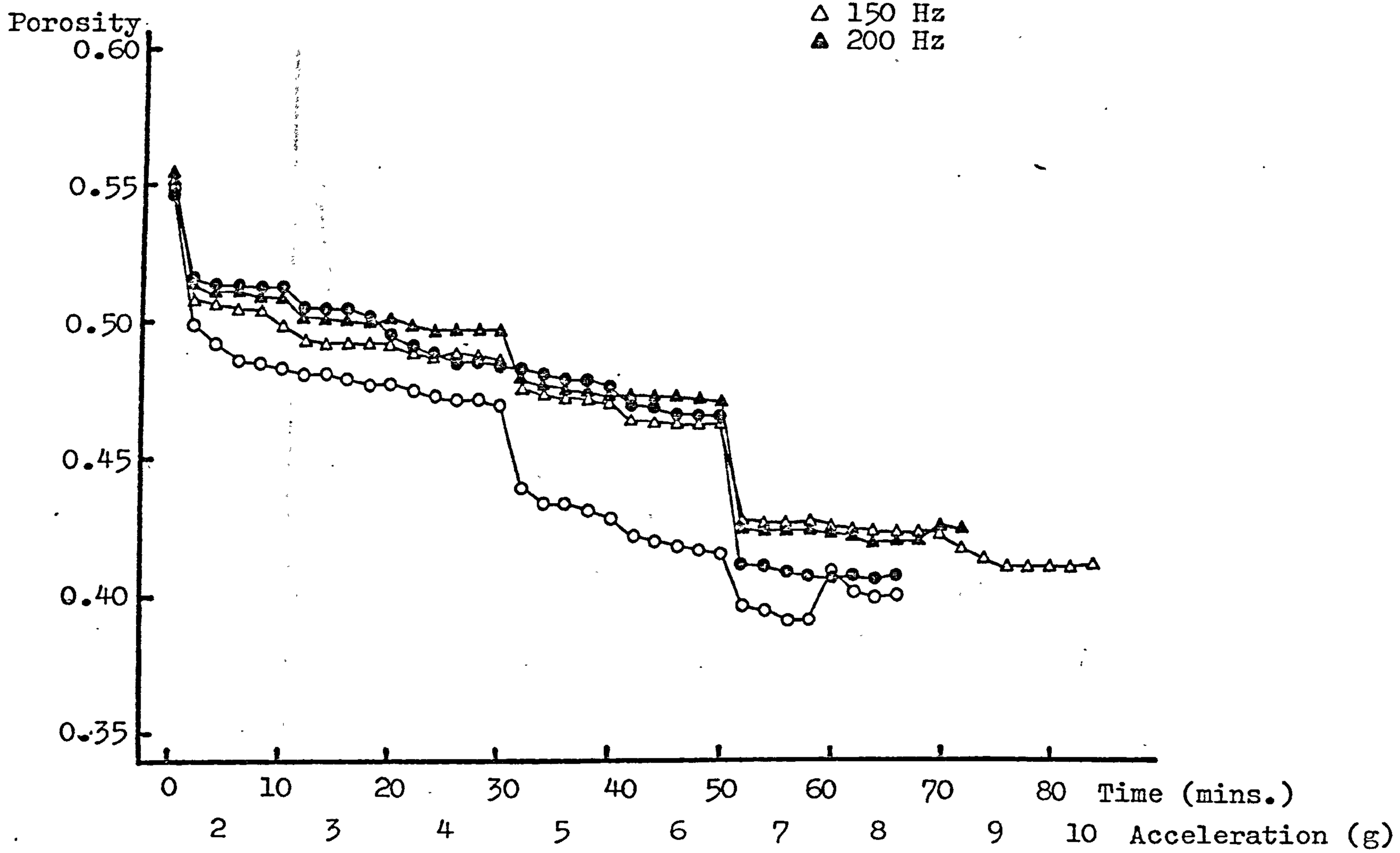

Fig. 3.18 The porosity of vibrated lactose samples as a function of acceleration, increasing stepwise at ten minute intervals. Particle size fraction D, vertical mode.

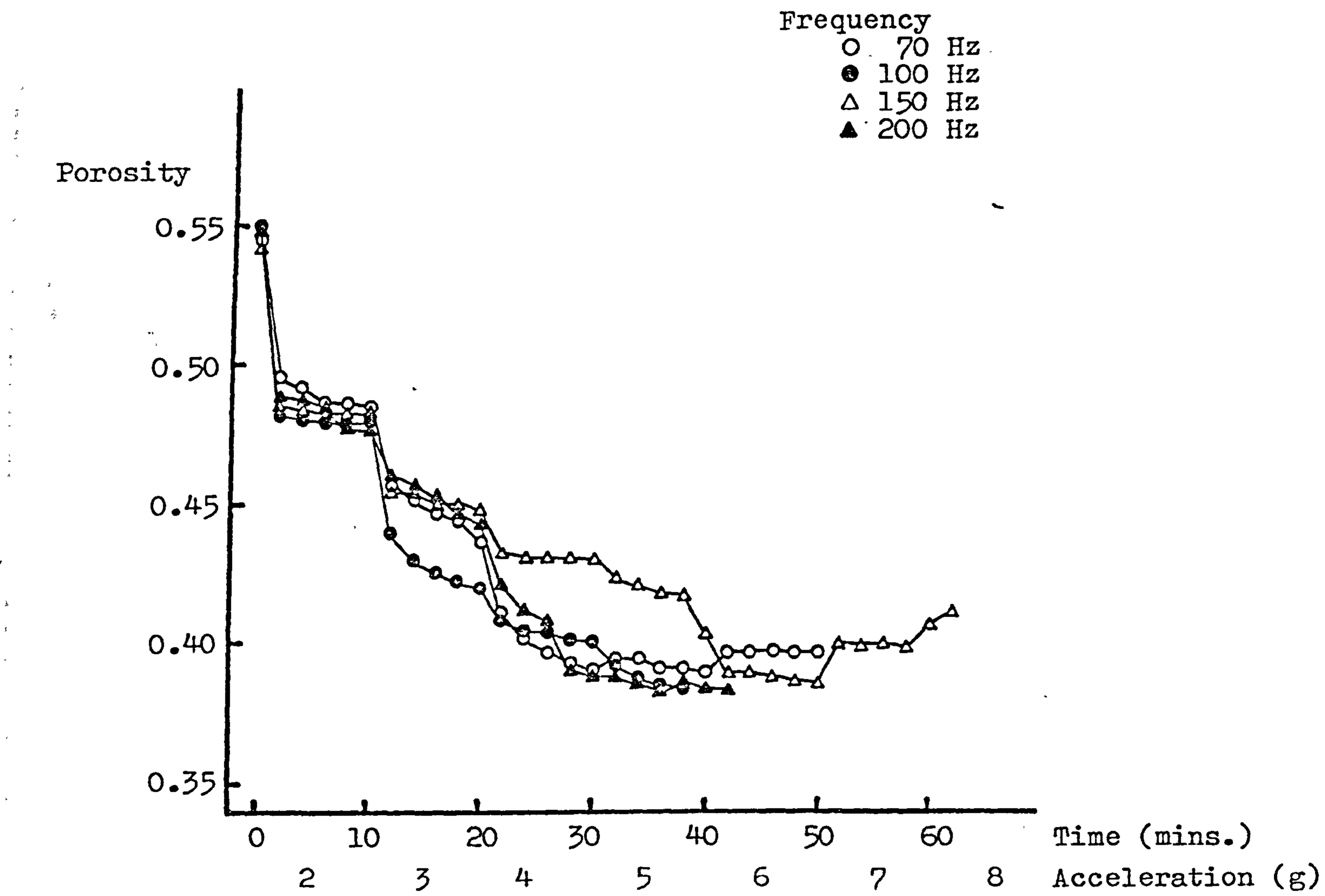

Fig. 3.19 The porosity of vibrated lactose samples as a function of acceleration, increasing stepwise at ten minute intervals. Particle size fraction F, horizontal mode.

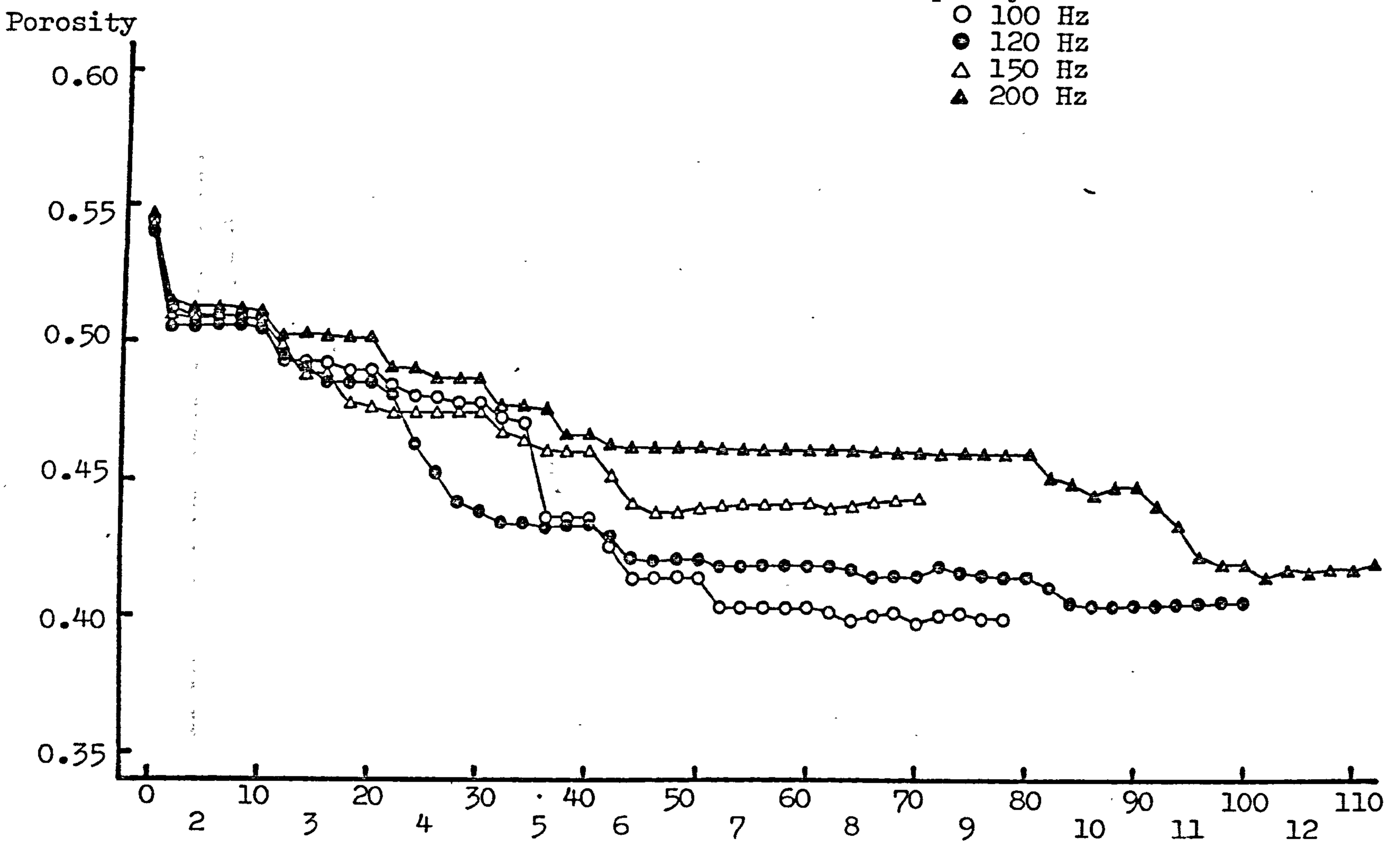

Fig. 3.20 The porosity of vibrated lactose samples as a function of acceleration, increasing stepwise at ten minute intervals. Particle size fraction F, vertical mode.

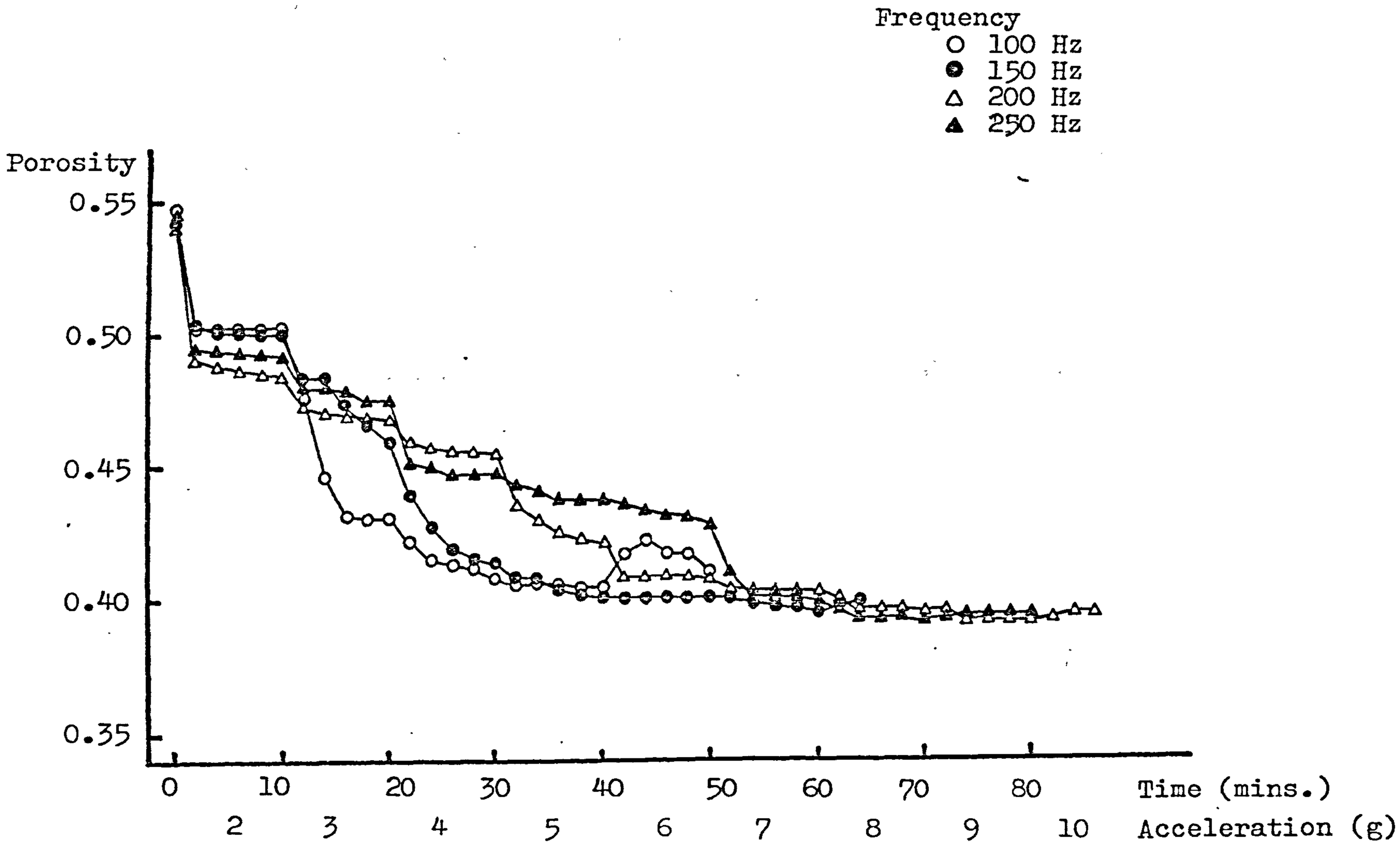

Table 3.4

Minimum porosities attained with lactose fractions B,D and F under various vibration conditions

	Frequency (Hz)	Minimum porosity attained	Acceleration required (g)
Fraction B, horizontal vibration	120	0.459	10
	150	0.466	11
	200,	0.509	9
	250	0.468	11
Fraction B, vertical vibration	100	0.391	8
	150	0.381	7
	200	0.391	11
	250	0.397	10
Fraction D, horizontal vibration	100	0.392	7
	120	0.408	7
	150	0.410	9
	200	0.420	8
Fraction D, vertical vibration	70	0.390	5
	100	0.383	5
	150	0.385	6
	200	0.384	5
Fraction F, horizontal vibration	100	0.397	8
	120	0.404	10
	150	0.439	7
	200	0.415	12
Fraction F, vertical vibration	100	0.404	5
	150	0.395	7
	200	0.392	9
	200	0.392	8

decided to terminate a run on reaching an acceleration that produced no further consolidation.

Figs. 3.15 to 3.20 illustrate the observed effect of increasing the acceleration of an applied vibration. There was a gradual decrease in porosity, punctuated by the periodic increases in acceleration, down to a minimum, beyond which there appeared to be no advantage in raising the acceleration further. At low acceleration levels, most or all of the consolidation appeared to take place within the first two minutes, whilst at higher accelerations, the consolidation was rather more gradual.

Throughout this experiment, the indication obtained earlier that vertical vibration is more effective in reducing porosity than horizontal vibration, was confirmed. In most examples, similar porosities could be achieved, but in the case of horizontal vibration, a higher acceleration was required. One possible explanation for this is that since the particles have to undergo a net downward displacement, agitating them in a vertical mode is more appropriate than a horizontal mode.

If the optimum frequencies for each lactose size fraction and vibration mode are selected on the basis of the results of this experiment, and compared with the optimum frequencies as indicated by experiment 3.2.1, slight discrepancies appear. This is because experiment 3.2.1 compared frequencies at a fixed power output, whereas experiment 3.2.3 was concerned with maintaining

given levels of acceleration. It can be readily observed that the acceleration produced at a fixed power output fluctuates to some extent as the frequency is altered; there is an increase in acceleration at and around the resonant frequencies of the system under test. Therefore, comparisons made at constant power output and those carried out at constant acceleration are not entirely compatible.

3.2.4 Reproducibility of vibratory consolidation

(A) Experimental

For each of the lactose size fractions B, D and F, optimum horizontal and vertical vibration frequencies were selected. Experimental procedure was brought into line with the methods in section 3.1,in so far as the aluminium collar was attached to a container, and powder was poured in from a jar and levelled. The sample was then vibrated at an arbitrarily fixed acceleration of 6g for ten minutes, with the nylon rod resting on the upper surface, after which time the rod and collar were removed. The sample surface was scraped level with a spatula blade, and the overall porosity of the sample was determined. This was repeated ten times, and a mean and coefficient of variation were calculated.

(B) Results and discussion

The results are shown in Table 3.5.

Table 3.5

The porosity and its variability of lactose samples subjected to vibratory consolidation at an acceleration of 6g for 10 minutes

Lactose size fraction	Vibration mode	Vibration frequency (Hz)	Mean porosity	Coefficient of variation (%)
B	Horizontal	120	0.560	2.16
B	Vertical	150	0.478	1.33
D	Horizontal	100	0.441	1.23
D	Vertical	100	0.404	0.67
F	Horizontal	120	0.477	1.65
F	Vertical	150	0.408	1.06

Several points are immediately apparent from these results. In agreement with the findings of previous experiments, vertical vibration produced packings of lower porosity than horizontal vibration. Furthermore, the porosity of vertically vibrated samples was more reproducible than that of horizontally vibrated samples, for each of these three lactose size fractions. The reason for this latter observation is not obvious.

The porosities achieved, particularly with fraction B, were not as low as those obtained at 6g in section3.2.3. The likely cause of this discrepancy is the fact that cohesive powders such as fraction B are relatively sensitive to compression, and even a small load such as the nylon

rod is likely to compress the upper layers of a sample to some extent. In section 3.2.3, these compressed upper layers were an inherent part of the sample whose porosity was being determined, whereas the procedure in section 3.2.4 entailed the removal of that part of the sample located inside the aluminium collar. The compressed region was thus not part of the final sample.

The variability of these results is comparable to that observed in the deposition experiments in section 3.1. It is perhaps partly a measure of the reproducibility of vibratory consolidation, and partly a measure of the variability of the samples before vibration.

3.3 Conclusions

The foregoing experiments have provided information enabling powder samples of a given overall porosity to be prepared, by selecting suitable conditions of deposition, and when required, vibration. An indication of the degree of reproducibility of overall porosity that could be expected, has also been obtained. This type of information would be very useful in a capsule filling process, since the overall porosity of the powder feed bed has a direct bearing on the magnitude of the fill weight.

Chapter 4

The Theory of Gamma Ray Attenuation

Chapter 3 has illustrated that material in the form of powder, such as lactose, can pack to a wide range of porosities, depending on the method of deposition,and on whether it is subjected to mechanical disturbance such as vibration. The magnitude and reproducibility of powder porosity are important considerations in the filling of hard gelatin capsules, but also of importance is the distribution of porosity within individual powder beds. Chapter 1 has indicated that gamma-ray attenuation provides a viable method of detecting local porosity variations in powder samples, and so this technique was studied in detail.

4.1 The interaction of gamma rays with matter

Gamma radiation is emitted by a large number of radioactive isotopes, both naturally occurring and artificial. It is a form of electromagnetic radiation, similar in many respects to light, and is transmitted in directed quanta known as photons. Gamma-emission is characterised by its energy, which may in practice range from a few keV to 10^5 MeV,and each gamma emitter may have one or more photon energies.

Gamma rays traversing matter can interact with it in a number of ways. Fano (1953) mentions twelve different

processes that can occur, of which the following are the most important:-

(i) The photoelectric effect. A photon disappears and an atomic electron, usually from the proximity of the nucleus, leaves its atom at high speed, having absorbed the energy of the photon. This effect predominates at low photon energies and in absorbers of high atomic number.

(ii) Compton scattering. A photon collides with an atomic electron, which recoils, taking up part of the photon energy. The photon goes off in a different direction, its energy depleted and its wavelength longer than before. A photon may undergo several Compton scatters before it is ultimately absorbed by the photoelectric effect. Compton scattering predominates for gamma rays of 1-5 MeV in materials of high atomic number, and even more greatly and over a much wider range in low atomic number materials.

(iii) Pair production. This can only be caused by photons of energy greater than 1 MeV. The photon disappears and its energy is transferred to the creation of an electron-positron pair. This usually occurs in the vicinity of a nucleus. Excess energy over and above 1 MeV is imparted to the electron-positron pair, which is projected predominantly in the direction of the incident photon. This effect predominates at high photon energies, especially in materials of high atomic number.

(iv) Rayleigh scattering. Gamma rays scattered by small angles impart only a small recoil, especially when they are of low energy. If this recoil is absorbed by a whole atom or molecule, then the interaction is termed "coherent", and no energy is transferred from the photon to the atomic system. This type of scattering prevails greatly at low energies, particularly in materials of high atomic number,

There are other minor effects, some of which are barely detectable.

The first three effects are most prevalent, and Fig. 4.1 shows their relative importance at different energies using lead absorbers (reproduced from Faires and Parks, 1973). The combined attenuation coefficient exhibits a minimum; at this photon energy, the radiation has maximum penetration. The most important quantity characterising the penetration and diffusion of gamma quanta in matter is the attenuation coefficient, μ. This depends on the photon energy, and the atomic number(s) of the attenuating medium, and may be defined as the probability per unit path length that a photon will interact with the medium (Hubbell, 1969).

If a slab of material of thickness t is placed between a well-collimated source of mono-energetic photons and a well-collimated detector, then in a layer of thickness dx, a reduction in radiation intensity $-dI/I$ will occur, due to one or other of the interactions mentioned above (see

Fig. 4.1 The attenuation coefficient (μ) of lead as a function of photon energy, showing the contributions of the major interaction processes.

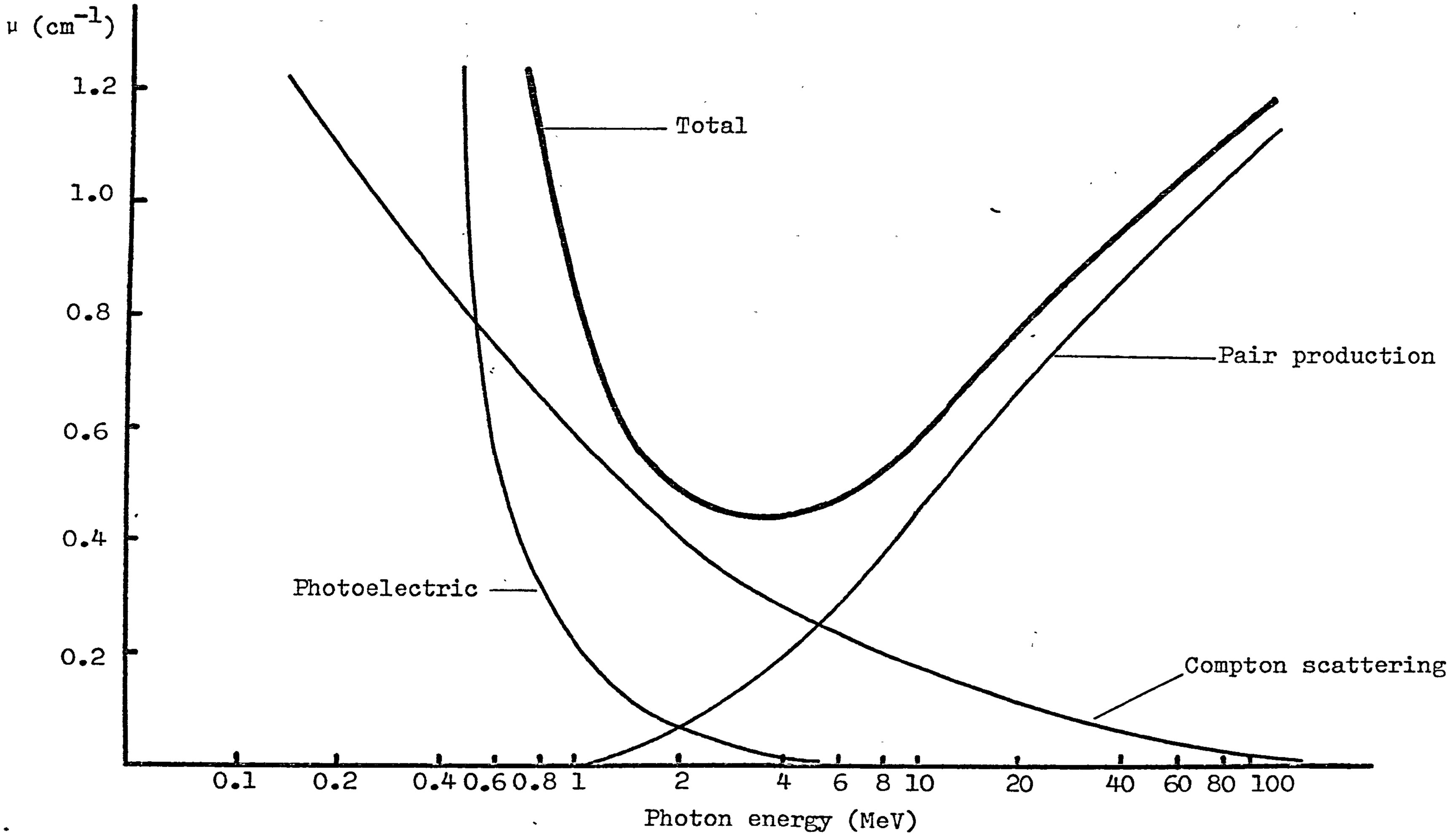

Fig. 4.2). This reduction in intensity is proportional to the attenuation coefficient, μ and the thickness of the layer, dx.

$$-dI/I = \mu\, dx \qquad (4.1)$$

Assuming the medium is homogeneous, this can be integrated to give

$$I = I_o \exp(-\mu t) \qquad (4.2)$$

where I is the transmitted intensity and I_o is the intensity incident on the slab. This exponential equation can also be expressed in terms of numbers of photons incident and transmitted in a given time, N_o and N respectively.

$$N = N_o \exp(-\mu t) \qquad (4.3)$$

The attenuation coefficient, μ, being the total probability that a photon will be removed from the primary beam while traversing unit thickness of absorber, is the sum of the probabilities of occurrence of each kind of interaction.

The above equations apply to "narrow-beam conditions", which is a relative term implying that scattered photons are prevented from reaching the detector by collimators. For situations which do not fall into the narrow-beam

Fig. 4.2 A typical "narrow beam" system

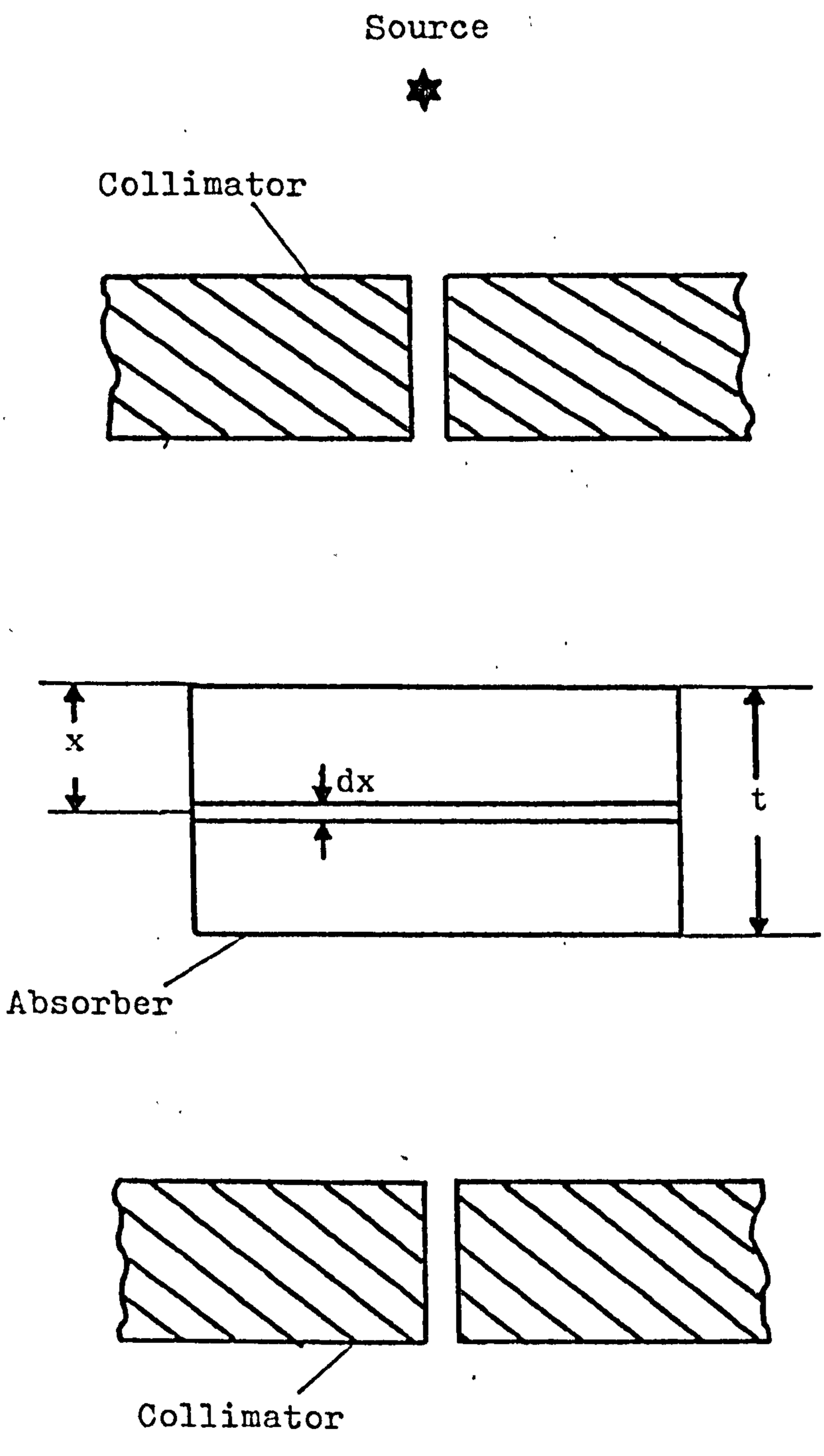

category, the attenuation is still basically exponential, but is modified by the deflection towards the detector of photons initially directed elsewhere. Therefore, there is less attenuation under "broad-beam" than under "narrow-beam" conditions. This effect is more marked for thin absorbers, since as absorber thickness increases, the increased chance of multiple interactions means that scattered photons are unlikely to reach the detector. The detection of secondary photons is accounted for in what is often called the "build-up factor"; under broad-beam conditions, this must be incorporated into the attenuation equation.

The attenuation coefficient, μ , has dimensions of inverse length, hence if t is measured in cm, μ is expressed in cm^{-1}; it is referred to as the "linear attenuation coefficient". This is a convenient term for practical applications, but since it is proportional to the density, ρ, of the absorber, it is common practice, for tabulation purposes, to remove this density dependence and quote the "mass attenuation coefficient", μ/ρ, which, if μ is in cm^{-1} and ρ is in g cm^{-3}, will be in units of cm^2/g. The mass attenuation coefficient of an absorber is the sum of the contributions of all the various interaction processes, and these contributions are tabulated as "photon cross-sections" (Hubbell, 1969), illustrating the relative importance of each type of interaction.

If the absorber is a chemical compound or a mixture,

its mass attenuation coefficient μ/ρ can be calculated approximately from the coefficients μ_i/ρ_i of the constituent elements:

$$\mu/\rho = \sum_i w_i(\mu_i/\rho_i) \qquad (4.4)$$

where w_i is the proportion by weight of the ith constituent. This "mixture rule" does not take into account changes in atomic wave-functions resulting from changes in the molecular, chemical or crystalline environment of atoms, and is therefore subject to error, particularly at very low energies (Hubbell, 1969).

4.2 Application to particulate materials

A mass of powder is a mixture of solid particles and air spaces or voids, and so when it is traversed by a beam of gamma radiation, the photons will interact with the constituent atoms both of the solid material and the air. However, the linear attenuation coefficient of air at a given photon energy is so small compared with solid materials (see Table 4.1), that the effect of air can usually be ignored. Of course, the presence of air between source and detector is not limited to the case of particulate samples. In any experimental arrangement, there will be an air space between source and absorber, and another between absorber and detector, and therefore it is wise to calculate the theoretical contribution of the

Table 4.1

Linear attenuation coefficients of various materials at three photon energies

Material	Density, ρ (g cm^{-3})	Linear attenuation coefficient, μ (cm^{-1}) 1 MeV	3 MeV	6 MeV
Air ($20^{\circ}C$, 76cm Hg)	0.901205	0.0000765	0.0000431	0.0000304
Aluminium	2.7	0.166	0.0953	0.0718
Sand	2.2	0.140	0.0825	0.0587
Water	1.0	0.0706	0.0396	0.0277
Lead	11.34	0.797	0.468	0.505

(reproduced from Hubbell, 1969)

air to the observed attenuation, before deciding whether a correction is necessary.

The basic attenuation equation (4.3) relates the attenuation of a radiation beam to the linear attenuation coefficient and thickness of an absorber. In the case of a particulate material, the attenuating thickness is less than the apparent or measurable thickness, due to the presence of voids. If L is the apparent thickness and ε is the porosity of the sample, then

$$N = N_o \exp\left[-\mu (1-\varepsilon)L\right] \qquad (4.5)$$

(Kurz, 1972). Hence, for a powder sample of apparent thickness, L, and known porosity, ε, its linear attenuation coefficient can be determined by recording N_o and N. As was mentioned previously, N_o and N are, strictly speaking, the numbers of photons incident and transmitted respectively, in a given time. In practice, because the attenuation due to air is negligibe, N_o is taken to be the number of photons detected with the sample out of the beam, and N is the number detected with the sample in the beam, in the same time interval.

The significance of equation (4.5) in the present work, is that given a powder sample of apparent thickness, L, and known linear attenuation coefficient μ, the recording of values of N_o and N provides a means of calculating the porosity, ε, of that part of the sample traversed by the radiation beam. Then, by taking counts at different positions in the sample, local porosity variations can be detected.

Chapter 5

Attenuation of Gamma Rays by Lactose

Having chosen a technique with which to study local porosity variations in powders, a number of preliminary experiments were carried out to investigate the capabilities of the technique. A system was then developed for the purpose of measuring the attenuation coefficient of lactose.

5.1 Counting equipment

A gamma counting system was set up, consisting of the following components (Ortec Ltd., Luton, Bedfordshire):-

	Model
Power supply	402H
High voltage supply	456
Counter (digital)	775
Timer-counter (digital)	771
Ratemeter	441
Single channel analyser	406A
Amplifier	485
Photomultiplier tube (PMT) base with preamplifier	276

Mounted on the PMT base was a 50mm x 50mm sodium iodide detector (Model 2M2/2, Bicron Corporation, Newbury, Ohio, U.S.A.), and this assembly was housed vertically in a lead

castle, thus detecting radiation directed downwards.

Tuning-in to a given energy level or photopeak could be carried out by fine adjustment of the high voltage and the amplifier gain, whilst the width of the energy band or "window" could be set by adjusting the analyser controls. In this way, only photons between an upper and lower energy limit would be counted.

The choice of,gamma source was influenced by several factors. Lactose is a carbohydrate,hence its constituent atoms are all of relatively low atomic number. This, together with the knowledge that samples of only a few centimetres thickness were to be used, meant that a low photon energy would be needed if significant attenuation was to be observed. Two isotopes were available which were considered to be possible candidates, these being Americium-241 and Iodine-125. Americium-241 can be obtained as a directional point source, and has a principal photon energy of 60keV and a half-life of 433 years. Iodine-125 can be incorporated into a resin bead for use as a point source, has a principal photon energy of 27-32 keV and has a half-life of 60 days. The "mixture rule" of equation (4.4) was applied to estimate mass attenuation coefficients for lactose at 60 keV and 30 keV (see Appendix 1) and the following results were obtained:

$$\text{At 60 keV, } \mu/\rho = 0.186 \text{ cm}^2/\text{g}$$

$$\text{At 30 keV, } \mu/\rho = 0.294 \text{ cm}^2/\text{g}$$

The corresponding values of linear attenuation coefficient were obtained by multiplying by the particle density of lactose, which is 1.55 g cm^{-3}.

At 60 keV, μ = 0.288 cm^{-1}

At 30 keV, μ = 0.456 cm^{-1}

Substituting such values into equation (4.5) indicated that for a typical sample of lactose, of apparent thickness L = 4.4cm and porosity ε = 0.5, there would be transmission of 53% of incident 60 keV photons, and 37% of incident 30 keV photons. In other words, there would certainly be a measurable attenuation with either source. Americium-241 was chosen finally because its long half-life meant that no appreciable loss of activity would occur during the course of the work.

5.2 Preliminary experiments

(i) A spectrum was plotted of the 60 keV energy peak by placing an Americium-241 reference source, of nominal activity 10 microcuries (10μCi), directly on the detector, and recording the count rate at various energies between 40 keV and 80 keV. At each energy, a window of $\pm$ 5% was set. The spectrum is shown in Fig. 5.1.

(ii) The fact that the spectrum is not a sharp peak gives some indication that there are limits to the resolution of the detector. To study this further, the effect of

Fig. 5.1 Observed count rate as a function of photon energy, showing the 60keV photopeak of Americium-241

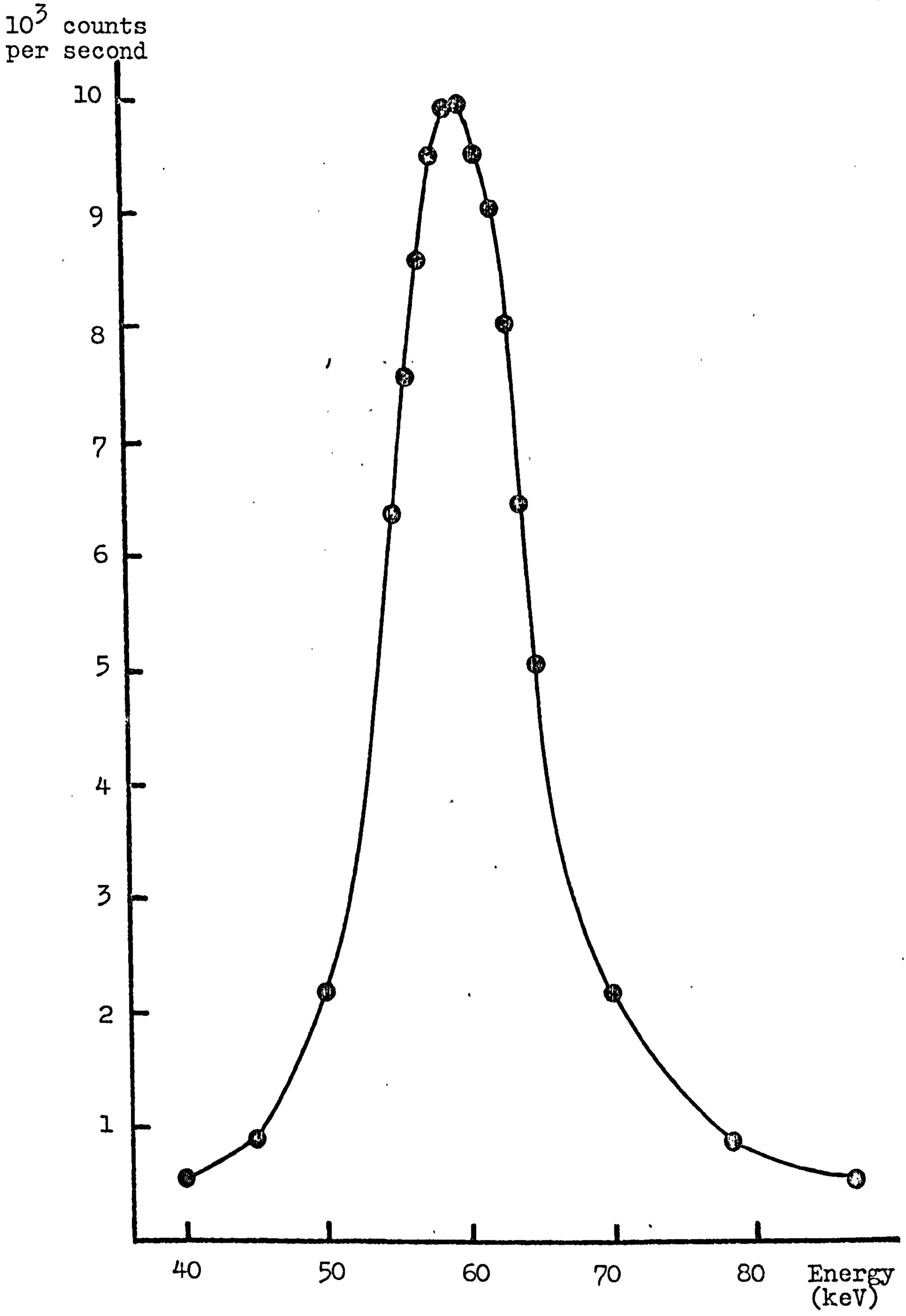

varying the energy window was examined, again using the reference source placed directly on the detector. The count rate was recorded at 60 keV with windows varying from $\pm$ 1% to $\pm$ 25%, and the results are shown in Fig. 5.2. It would appear that quite a wide window is required in order to detect the whole peak; this can be a problem, because the wider the window, the greater the chance of detecting secondary (i.e. scattered) photons. The information in Fig. 5.2 agrees reasonably closely with the shape of the spectrum in Fig. 5.1.

(iii) When a detector crystal registers a pulse, there follows a time interval during which the crystal is incapable of registering another pulse. This recovery time, or "dead time" becomes important at very high count rates, because some of the incident photons are not counted, and in such cases, a correction must be made to the observed count.

An experiment was performed to determine (a) the upper limit of count rate, below which a dead time correction should be unnecessary, and (b) the dead time of the detector. Details of the procedure are given in Appendix 2. The upper limit of count rate was found to be approximately 10^4 counts per second, and the dead time was calculated to be approximately 5.0×10^{-6} seconds.

(iv) Radioactive decay is a random process, and therefore there is no such thing as a "true" count rate; only a mean count rate can be observed. The variability

Fig. 5.2 Observed count rate as a function of the width of the energy "window", for Americium-241

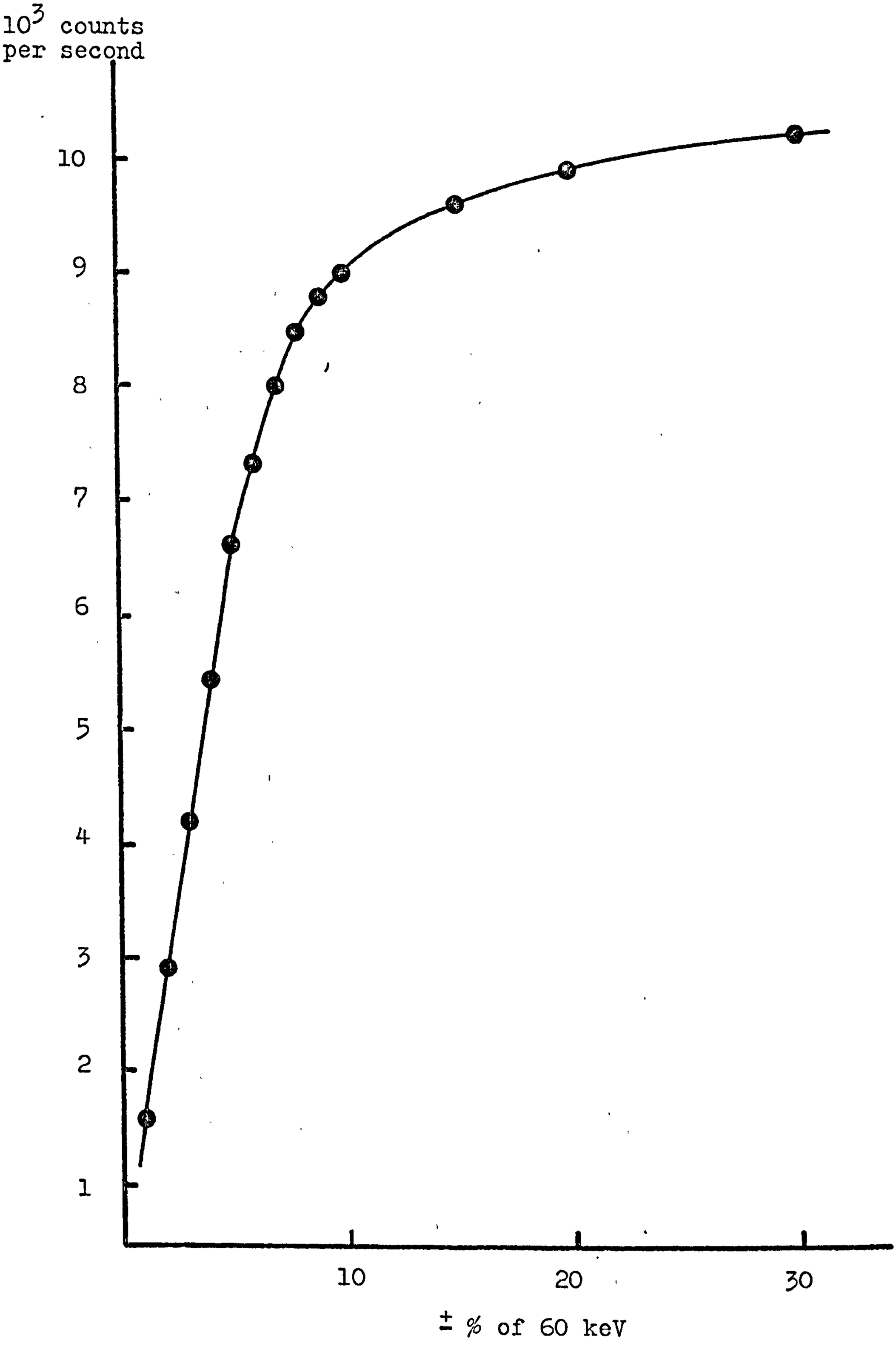

of the observed count rate is governed by the Poisson distribution (Faires and Parks, 1973), which has the property that the variance is equal to the mean. Consequently, the standard deviation is equal to the square root of the mean.

A few simple tests were performed to check that the variability of recorded counts was similar to that predicted by the Poisson distribution. Several absorbers were used, together with three different reference sources, and several counting intervals were tried. Under each set of conditions, ten counts were recorded, and their mean and standard deviation were calculated. In all cases, the standard deviation was of a similar magnitude to the square root of the mean. It was concluded that the nature of the absorber has no effect on count variability.

5.3 Design of a collimator assembly

A system was required with which to determine the attenuation coefficient of lactose, by irradiating samples of the material under narrow-beam conditions. It was felt that the assembly should be as rigid as possible, to prevent relative movement of source, detector or collimators, but allowing easy adjustment of the sample position. The beam width was necessarily a compromise between two opposing requirements; a narrow beam is desirable to minimise the number of secondary (scattered) photons

reaching the detector, but because point sources are of a finite size in practice, very narrow collimators would reduce the count rate and increase the time-span of experiments.

Fig. 5.3 illustrates the design of the collimator assembly, while Figs. 5.4 and 5.5 show the assembly in position on the lead castle, together with the gamma counting equipment.

The outer steel shell consisted of two coaxial cylinders, held a fixed distance apart by a steel bar welded to each cylinder. Each collimator consisted of a length of stainless steel tubing, of internal diameter 2mm, positioned along the axis of the outer cylinder. The space surrounding each steel tube was filled with Woods metal, (BDH Chemicals Ltd., Poole, Dorset), which is an alloy of lead, bismuth, cadmium and tin, melting at about 70°C. It is therefore a very useful shielding material. It was important that the two lengths of stainless steel tubing should be perfectly aligned, in order to obtain satisfactory transmission of gamma rays. This was achieved by holding the two tubes in the desired position with the aid of a long straight steel rod, while molten Woods metal was poured into each cylinder. Hardboard discs were used as temporary base-plates while the shielding material solidified, then the discs and the steel rod were removed (see Fig. 5.6).

A source-holder was made to fit closely over the

Fig. 5.3 The design of the collimator assembly

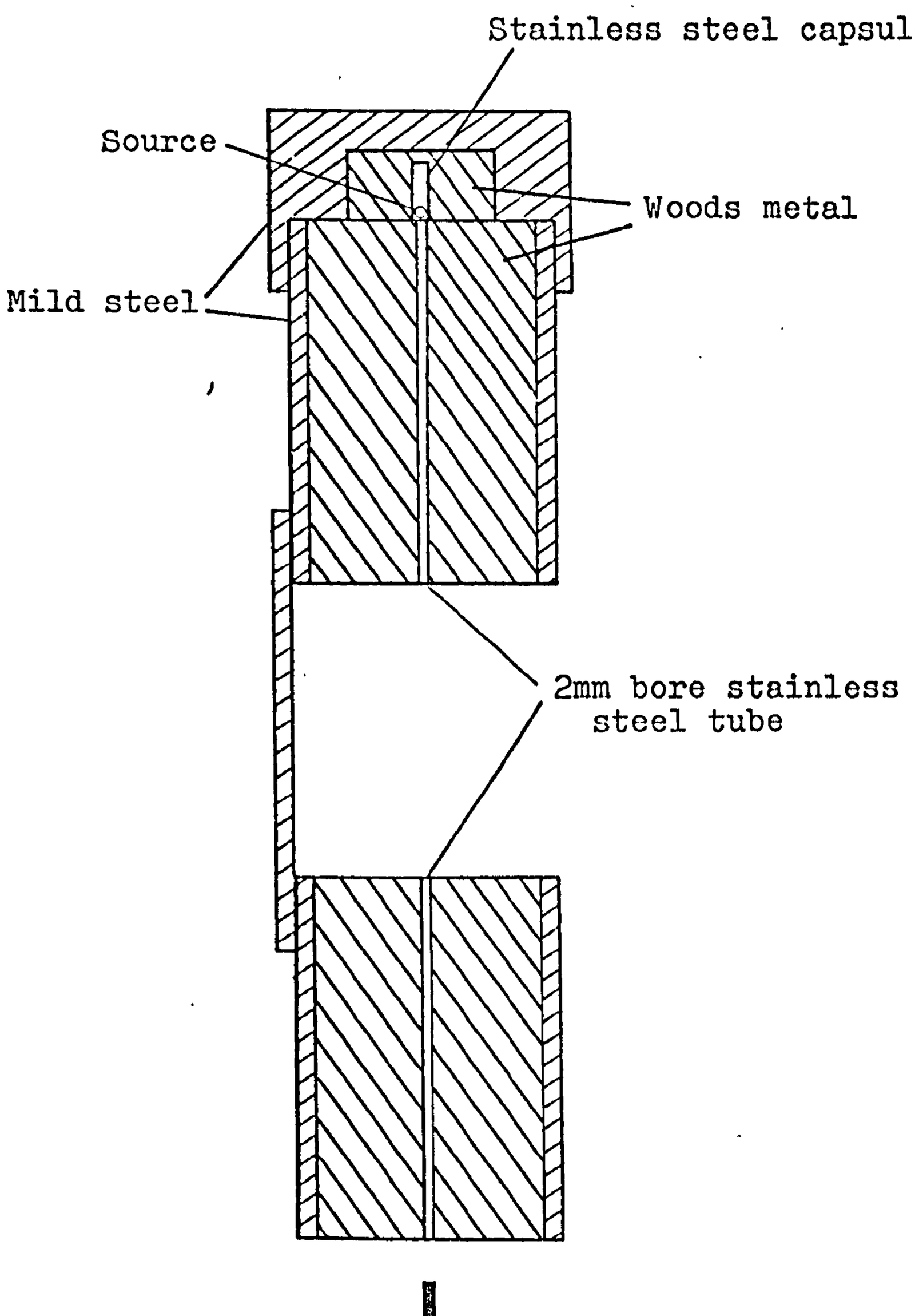

Fig. 5.4 Apparatus for gamma-ray attenuation measurements

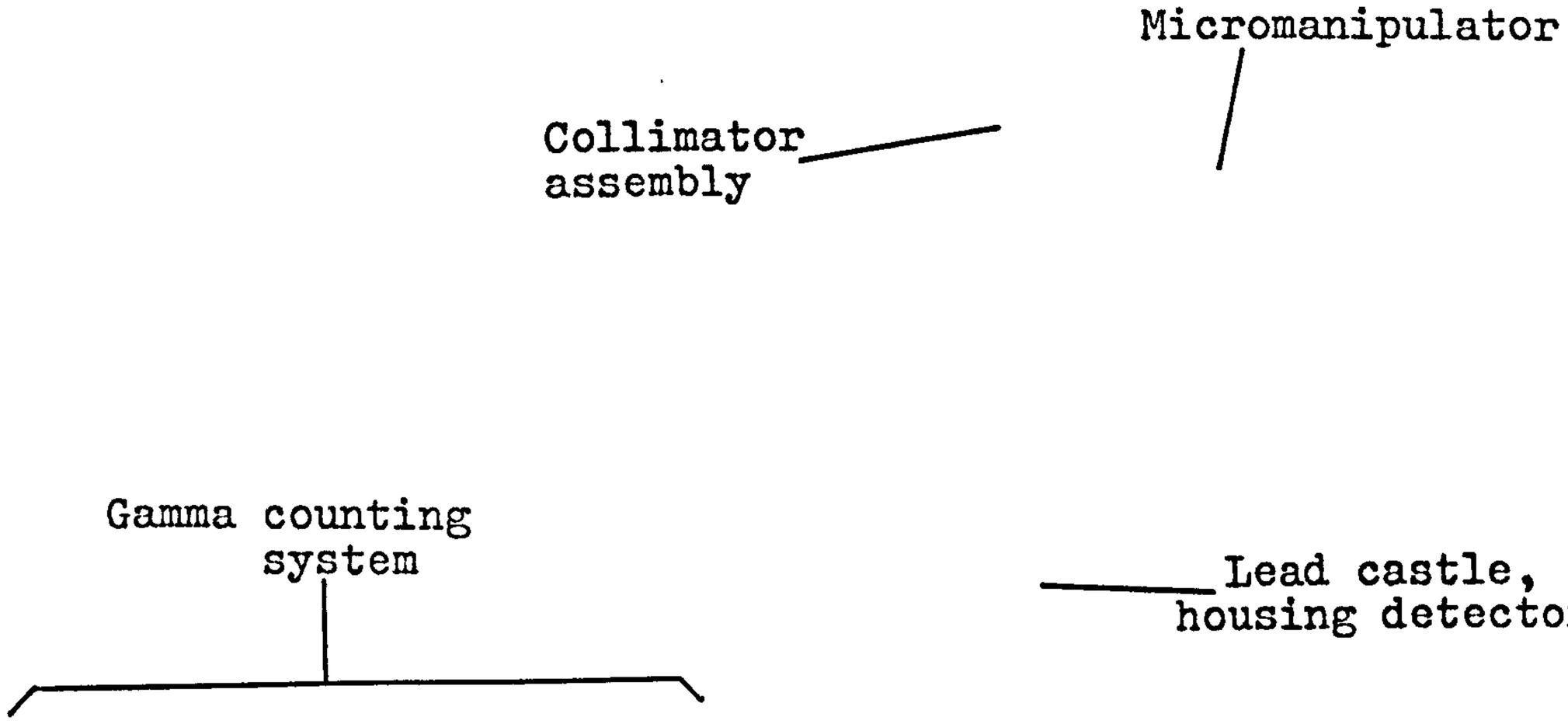

Fig. 5.5 The positioning of a sample in the gamma-ray beam

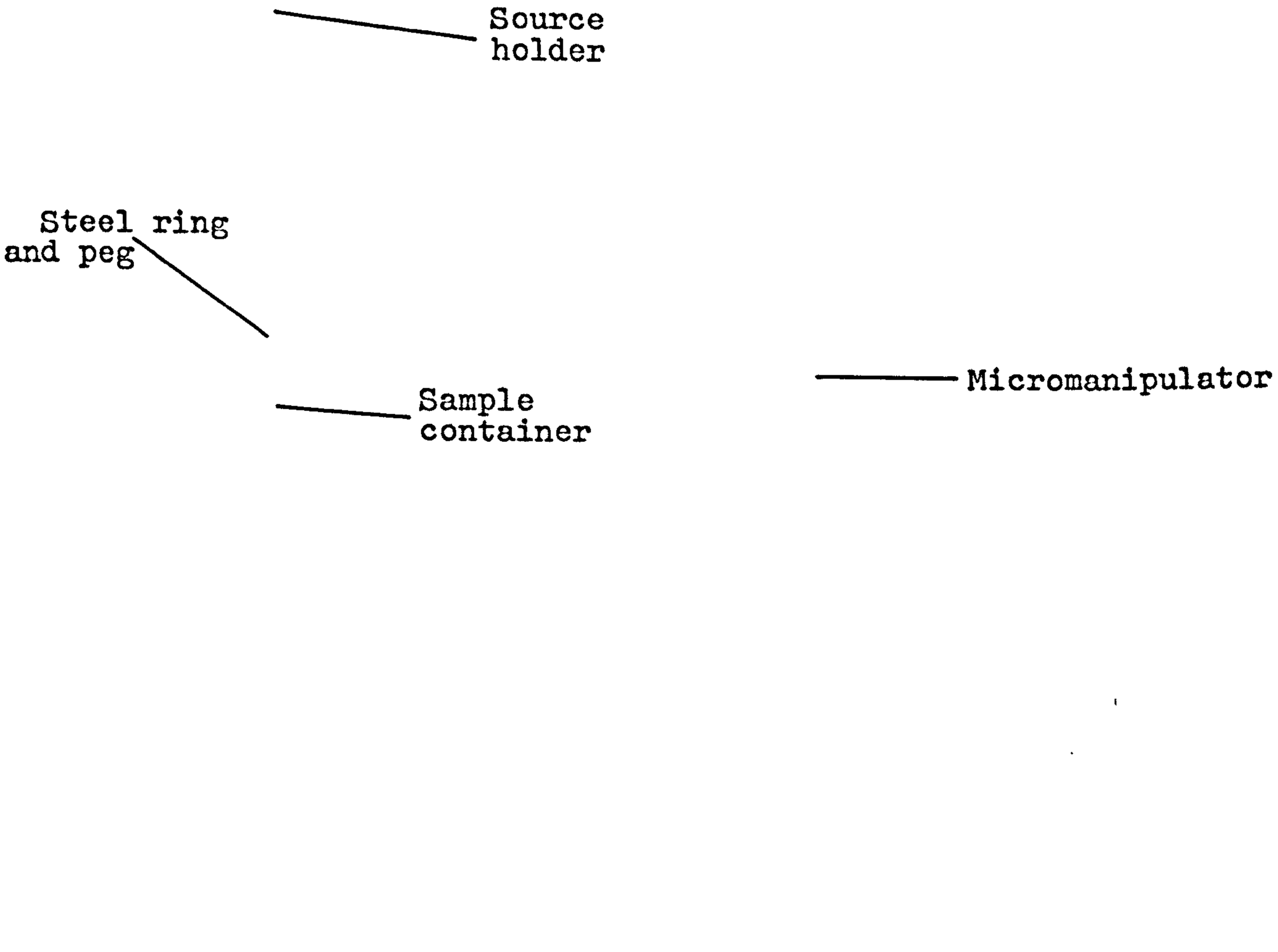

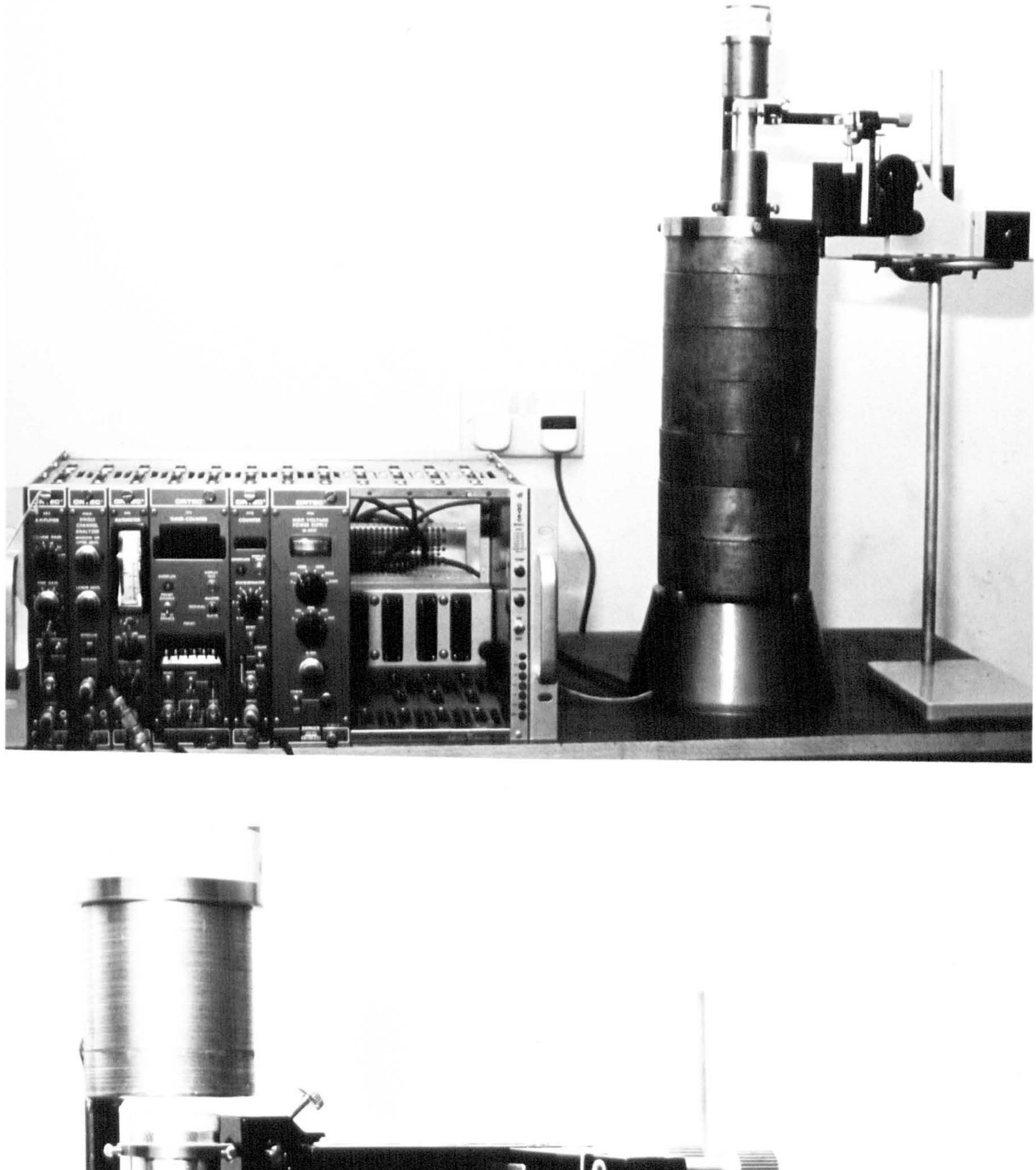

Fig. 5.6 Arrangement ensuring alignment of collimators

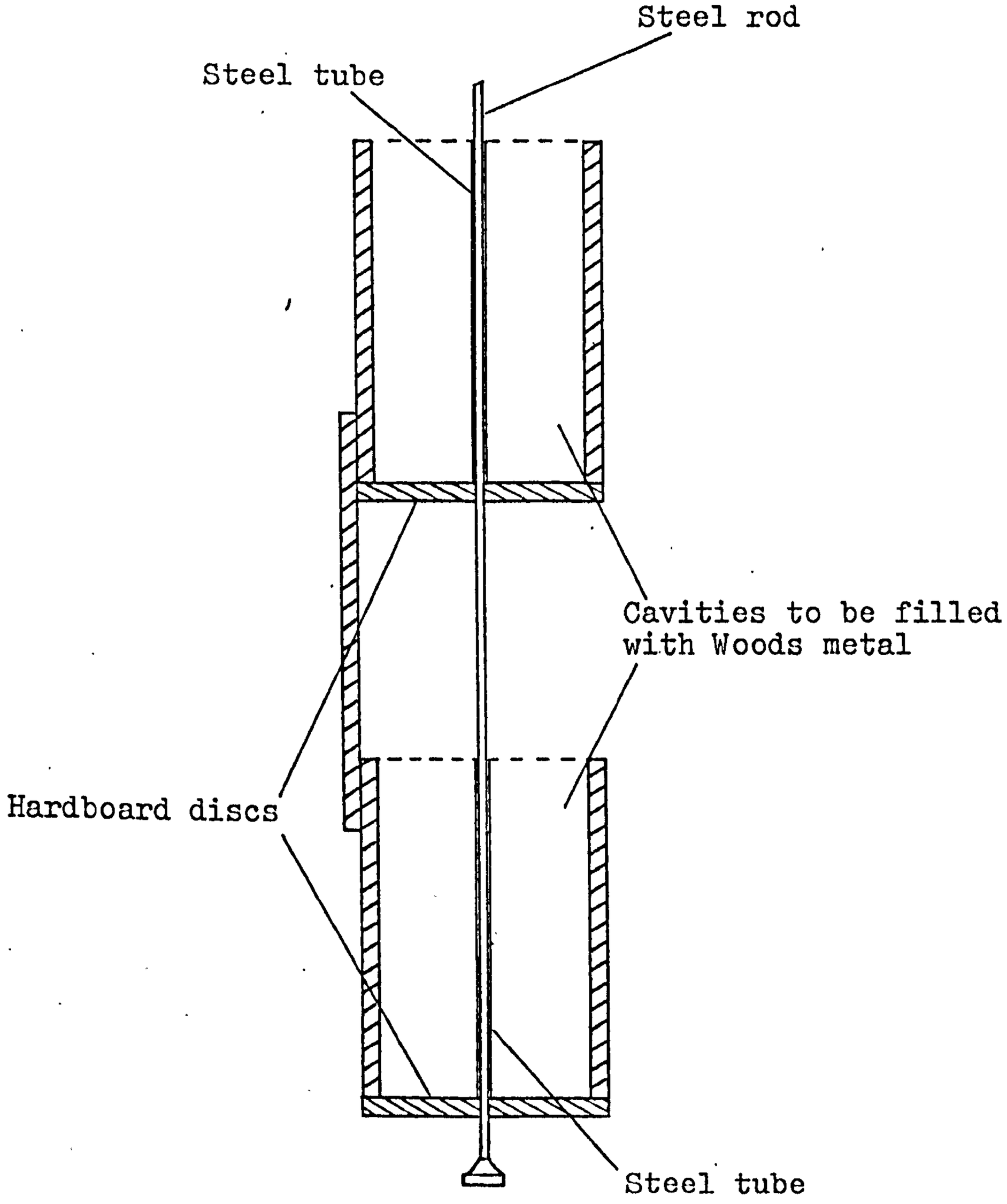

Fig. 5.7 Circular flanged cover for attaching the collimator assembly to the lead castle

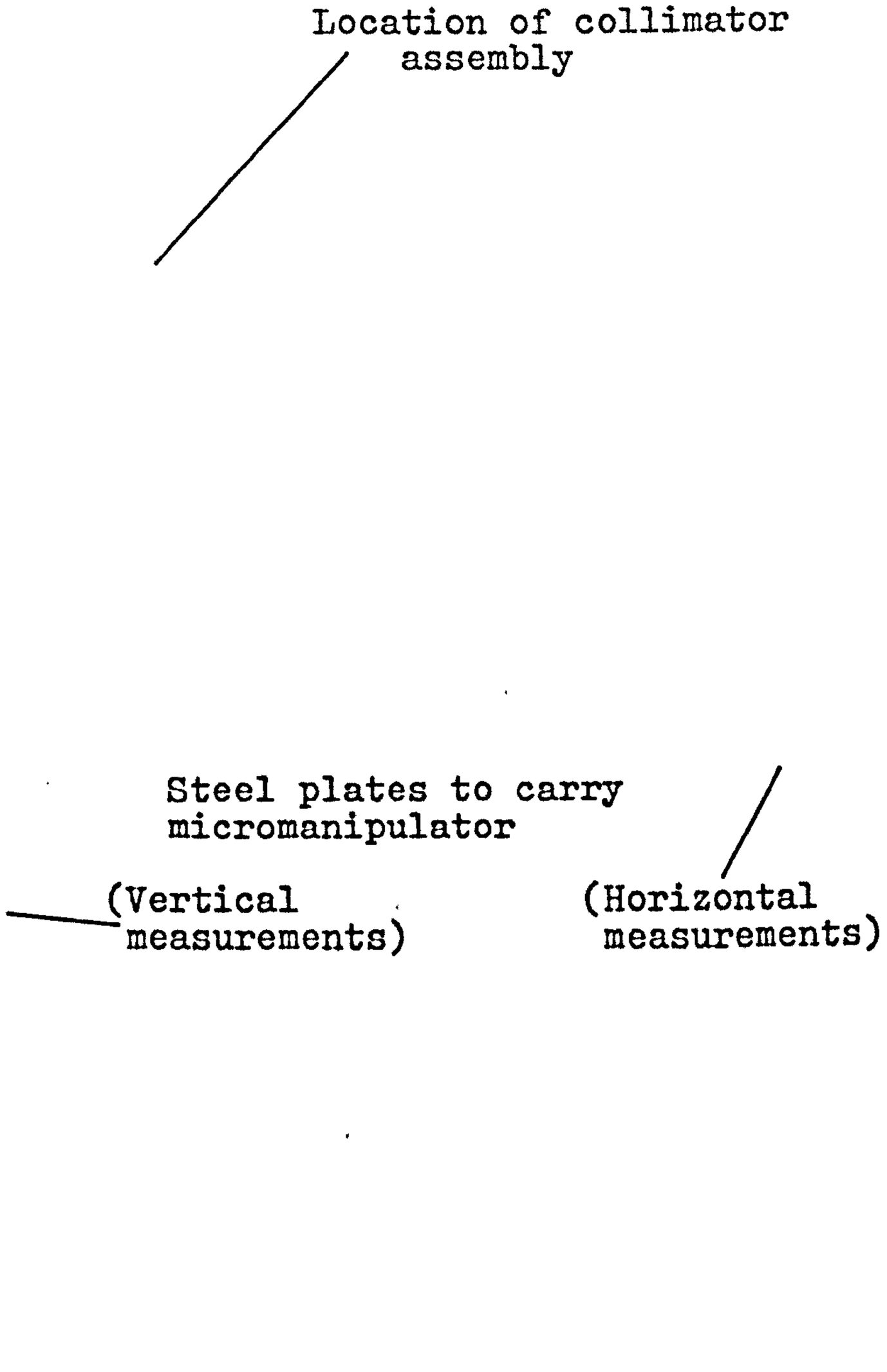

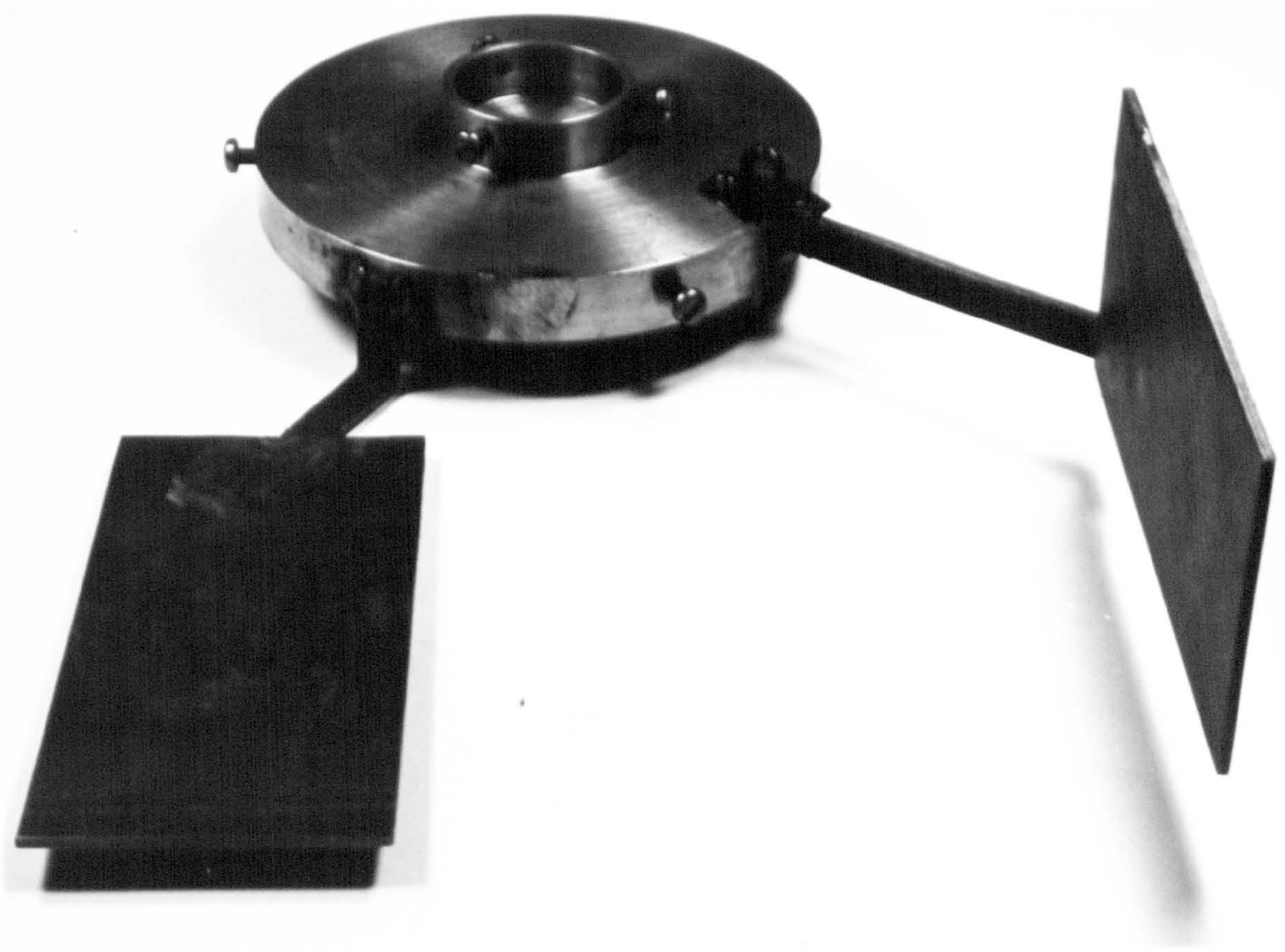

system was set up in such a way that when a sample container was positioned centrally in the radiation beam, its position was denoted by coordinates of (75.0, 25.0). So, for example, an adjustment of 6mm in the x-direction and -6mm in the y-direction would be denoted by coordinates of (81.0, 19.0).

5.4 The attenuation coefficient of lactose

(A) Theory

Equation (4.5) indicates that for a powder sample of known apparent thickness and known porosity, the attenuation coefficient can be determined by recording a sample count (a count with the sample in the beam) and a blank count (a count of the same duration, but with the sample out of the beam).

There are, however, two complications. The first was revealed by Coumoulos (1967), who was able to demonstrate consistently that certain sands and clays exhibited attenuation coefficients that were not constant, but were a function of voids ratio. Coumoulos went as far as to propose that the build-up factor (i.e. the detection of unwanted secondary radiation) varied with the packing density of the samples studied, but did not venture an explanation of why this should happen. However, the convincing nature of the results gives rise to the possibility that particulate materials in general exhibit this type of behaviour.

If significant differences in attenuation coefficient between samples of different overall porosity are to be detected, a statistical treatment of the problem is necessary.

Consider a powder bed of uniform apparent thickness, L_1, and uniform porosity, ϵ_1. The attenuation coefficient, μ_1, can be determined from a sample count N_1, and a blank count N_o, from the, following equation:

$$N_1 = N_o \exp\left[-\mu_1(1-\epsilon_1)L_1\right] \qquad (5.1)$$

If this powder bed is compressed to a lower uniform porosity, ϵ_2, and a lower uniform apparent thickness, L_2, a second sample count, N_2, will now enable a second calculation of attenuation coefficient, μ_2, to be made.

$$N_2 = N_o \exp\left[-\mu_2(1-\epsilon_2)L_2\right] \qquad (5.2)$$

In compressing the bed, however, the attenuating thickness of absorber is unchanged; this may be denoted by t_a, and

$$(1-\epsilon_1)L_1 = (1-\epsilon_2)L_2 = t_a \qquad (5.3)$$

Thus:

$$N_1 = N_o \exp(-\mu_1 t_a) \qquad (5.4)$$

and

$$N_2 = N_o \exp(-\mu_2 t_a) \qquad (5.5)$$

To establish whether there is a significant difference between μ_1 and μ_2, the sample counts N_1 and N_2 must be significantly different, hence the following expression must hold:

$$N_2 - N_1 \geqslant p.\sigma_1 + p.\sigma_2 \qquad (5.6)$$

where σ_1 is the standard deviation of N_1

σ_2 is the standard deviation of N_2

p denotes the probability level (for 95% confidence, at ∞ degrees of freedom, p = 1.96).

Fig. 5.8 illustrates the principle of equation (5.6).

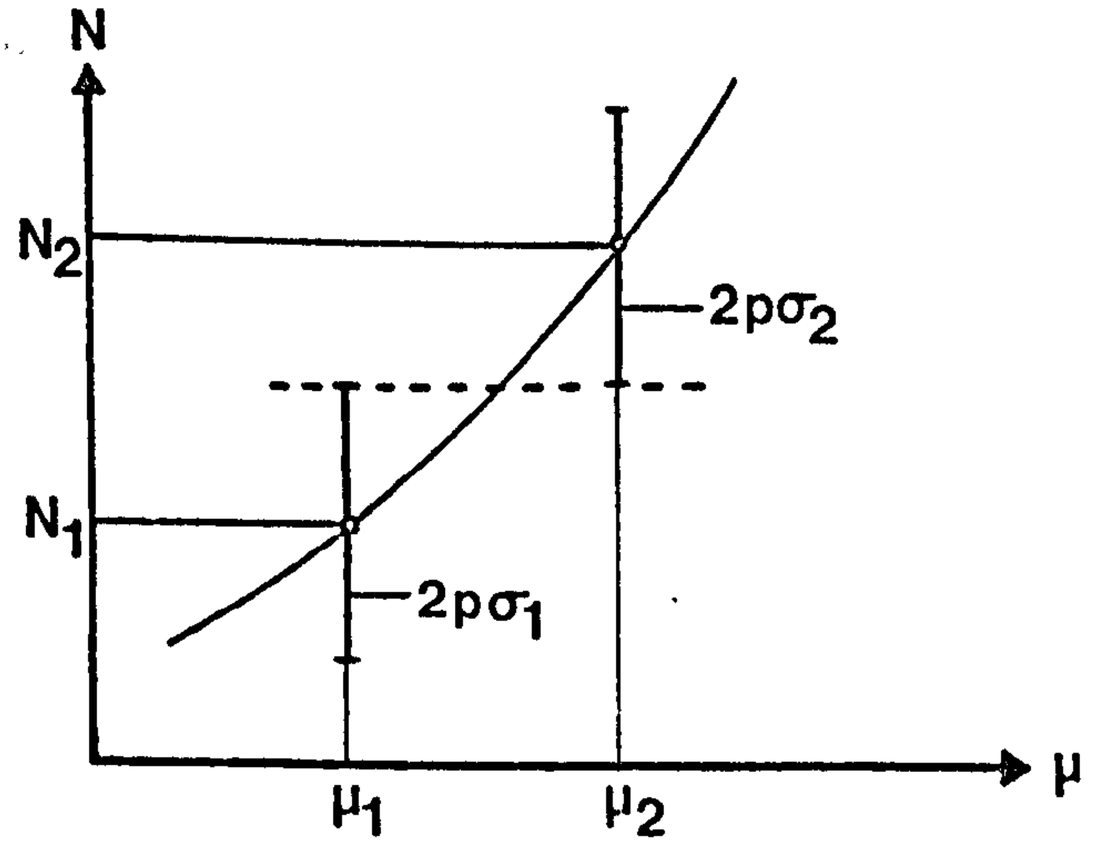

Fig. 5.8 Qualitative representation of equation (5.6)

N_1 and N_2 are individual counts, governed by the Poisson distribution, a property of which is that the standard deviation is equal to the square root of the mean.

Hence $\sigma_1 = \sqrt{N_1}$ and $\sigma_2 = \sqrt{N_2}$

From equations (5.4) and (5.5) it now follows that:

$$\sigma_1 = N_o^{\frac{1}{2}} . \exp\left(-\tfrac{1}{2}\mu_1 t_a\right) \qquad (5.7)$$

$$\text{and } \sigma_2 = N_o^{\frac{1}{2}} . \exp\left(-\tfrac{1}{2}\mu_2 t_a\right) \qquad (5.8)$$

Substituting (5.4), (5.5), (5.7), and (5.8) into (5.6):

$$N_o\left[\exp(-\mu_2 t_a) - \exp(-\mu_1 t_a)\right] \geqslant p.\ N_o^{\frac{1}{2}}\left[\exp(-\tfrac{1}{2}\mu_2 t_a) + \exp(-\tfrac{1}{2}\mu_1 t_a)\right]$$

which rearranges to:

$$\frac{N_{o_{min}}}{p^2} = \left[\frac{\exp(-\tfrac{1}{2}\mu_2 t_a) + \exp(-\tfrac{1}{2}\mu_1 t_a)}{\exp(-\mu_2 t_a) - \exp(-\mu_1 t_a)}\right]^2 \qquad (5.9)$$

The physical meaning of equation (5.9) is that in order to detect a difference between two attenuation coefficients, μ_1 and μ_2, at a level of confidence denoted by p, there is a minimum blank count, $N_{o_{min}}$, which must be attained. The equation thus determines the minimum time interval for recording counts.

By the same token, if an attenuation coefficient, μ is to be determined, and confidence limits of a given magnitude are required, say, $\pm \Delta\mu$, then equation (5.9) can be used in a modified form to calculate the value of $N_{o_{min}}$:

$$\frac{N_{o_{min}}}{p^2} = \left[\frac{\exp\left[-\tfrac{1}{2}(\mu+\Delta\mu)t_a\right] + \exp\left[-\tfrac{1}{2}(\mu-\Delta\mu)t_a\right]}{\exp\left[-(\mu+\Delta\mu)t_a\right] - \exp\left[-(\mu-\Delta\mu)t_a\right]}\right]^2 \qquad (5.10)$$

As would be expected, as $\Delta\mu$ decreases, $N_{o_{min}}$ increases.

If there are two powder beds of the same overall uniform porosity, but different apparent thicknesses, then to determine whether a significant difference exists between their measured values of attenuation coefficient, equation (5.9) cannot be applied, since the beds have different values of attenuating thickness, t_a. However, equation (5.10) may be applied to each bed in turn, yielding two values of $N_{o_{min}}$ which will ensure confidence limits of a chosen magnitude in both cases. Then, if the confidence limits of the two observed values of μ do not overlap, it may be concluded that a significant difference exists.

This statistical treatment has been adapted from a derivation employed by Kurz (1972), for detecting significant differences in local porosity levels in powder samples (see Chapter 6).

The second complication referred to at the beginning of this section is the fact that the theory outlined above applies to powder samples of known uniform porosity. It is a simple task to determine the overall porosity of a sample, providing it is in a container of measurable volume, but nothing is known about the uniformity of the sample, hence a sample count taken at an arbitrary position in the sample may not be particularly representative of the sample as a whole. One way of overcoming this problem would be to choose a material which packs regularly, thus

producing packings of uniform porosity, while being sufficiently compressible for attenuation coefficients to be determined at a range of overall porosities. Such a material was not found, and even if it had have been, the results obtained with it would have had little relevance to the problem in hand, which was to study the attenuation coefficient of lactose. The problem was largely overcome by adopting an experimental procedure which ensured that sample counts were as representative of the whole sample as possible.

(B) Experimental

The lactose particle size fractions chosen for these experiments were fractions A, B, C and F, emphasis being placed on the more cohesive powders, because they afford a greater range of porosity.

A 14 mCi Americium-241 point source was used, (code No. AMC 24., The Radiochemical Centre, Amersham, Bucks.) having an active diameter of 2mm, and giving a count rate (blank) of about 400 counts per second. This was well within the limits imposed by the detector dead-time. The "window" width chosen was $\pm$ 10% of the peak energy.

Fraction C was chosen initially and was loosely overfilled into an aluminium cylinder; excess powder was scraped off, using a spatula blade. The weight and volume of the sample were recorded, and its overall porosity was calculated. The attenuating thickness of the sample, t_a,

was found from the porosity and depth of the sample (see equation (5.3)). Suitable values of p, the probability level, and $\Delta\mu$, the confidence interval, were chosen, and the linear attenuation coefficient, μ, of lactose, as estimated by the "mixture rule" of section 5.1, was substituted, together with t_a and $\Delta\mu$, into equation (5.10). Thus, an approximate value of $N_{o_{min}}$ was obtained. The values used were:

$$\varepsilon = 0.550$$

$$L = 4.458\text{cm}$$

hence $t_a = 2.006\text{cm}$

$$\mu = 0.288\text{cm}^{-1}$$

$$\Delta\mu = 0.00125\text{cm}^{-1}$$

$$p = 1.96$$

$N_{o_{min}}$ was thus calculated to be approximately 1,100,000. At a count rate of 400 cps, this count would take about 46 minutes. Bearing in mind that many samples, of varying t_a, were to be studied, it was decided to adopt a standard counting interval of 60 minutes.

In order to make the 60-minute sample count representative of the sample as a whole, it was split into 60 one-minute counts. Given the internal diameter of the sample container (about 1.9cm) and the diameter of the gamma-ray beam (2mm), a network of 60 counting positions, consisting of hexagonally-packed circles, as shown in Fig. 5.9, was

Fig. 5.9 Array of counting positions for the determination of attenuation coefficient

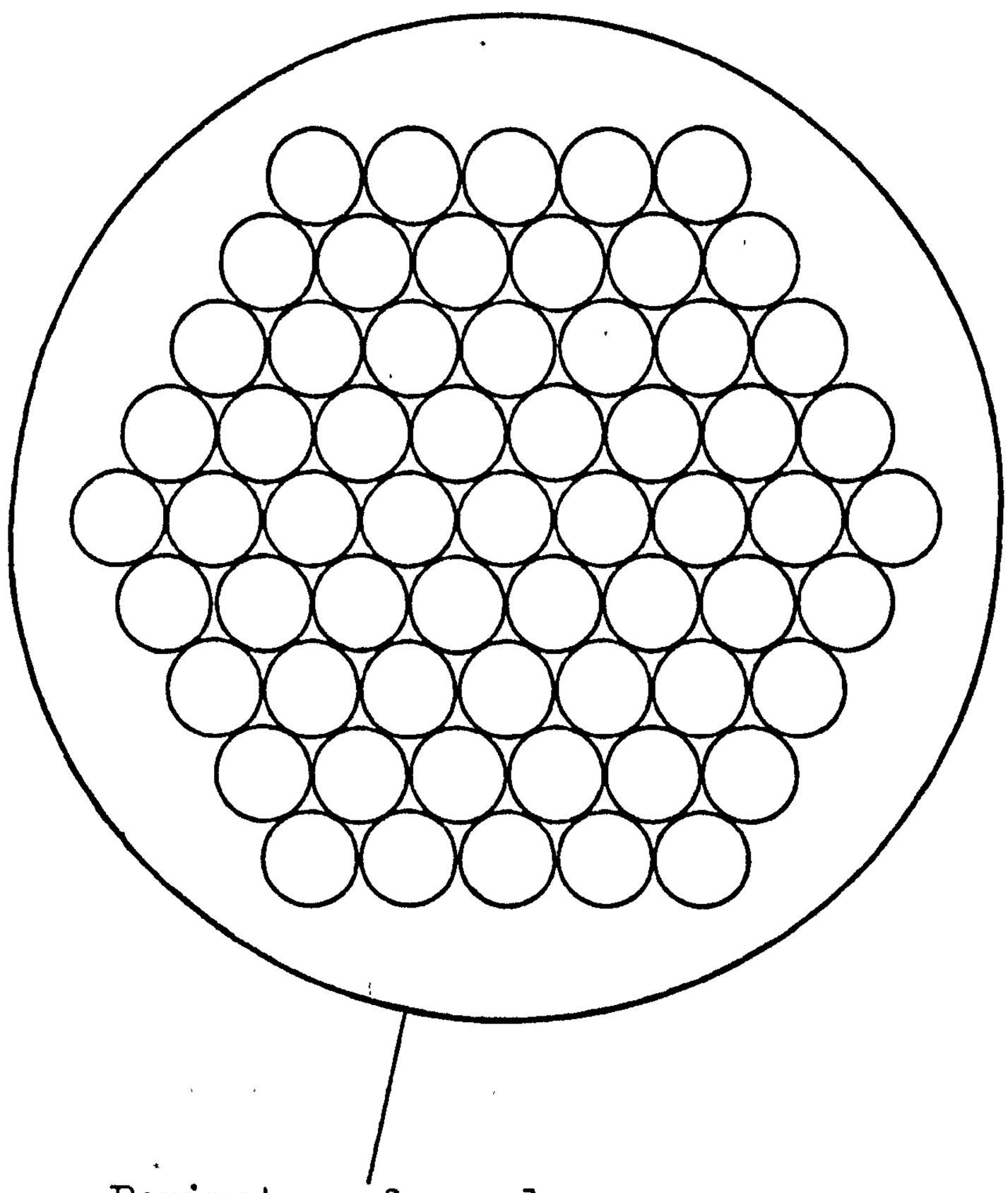

established, and by counting in each position for the same time interval, approximately ¼ of the sample was irradiated equally. Positioning of the sample was carried out using the micromanipulator (see section 5.3).

The sample count and a 60-minute blank count were interspersed in the following manner:

Blank	15 minutes
Sample	20 x 1 minute
Blank	15 minutes
Sample	20 x 1 minute
Blank	15 minutes
Sample	20 x 1 minute
Blank	15 minutes

Blank counts were obtained by passing the beam through an empty container of the same dimensions as the sample container. In this way, attenuation due to the aluminium container base was removed from the calculations.

Two separate experiments were performed:

(i) For each of the four lactose fractions, a value of attenuation coefficient was determined on a loose packing (L = approximately 4.4cm), then the sample was compressed in stages, and a further value of μ was determined at each new porosity; t_a remained constant.

(ii) Instead of compressing a fixed mass of each size fraction, increasing quantities were packed in stages

into the same volume (that of the container), and the effect of decreasing porosity on attenuation coefficient at constant L was studied. In this case, t_a was not constant.

(C) Results

Attenuation by particulate materials is governed by the following equation:

$$N = N_o \exp(-\mu t_a)$$

(See equations (5.4) and 5.5))

This can be re-written as:

$$\mu = \frac{\ln \frac{N_o}{N}}{t_a} \qquad (5.11)$$

Equation (5.11) was used to calculate values of attenuation coefficient, and the results are listed in Tables 5.1 and 5.2.

(D) Treatment of results

Counting times were fixed at 60 minutes throughout these experiments, therefore $\Delta\mu$ for a given result was influenced by the magnitude of t_a, and had to be determined in each case. A computer program was written in which recorded values of μ, p and t_a were substituted into equation 5.10, together with likely values of $\Delta\mu$. When

Table 5.1

The effect of overall porosity, ε, on attenuation coefficient, μ, at constant attenuating thickness, t_a.

Lactose size fraction	Total blank count, N_o (4x15min)	Total sample count, N (60x1min)	L (cm)	t_a (cm)	ε	μ (cm^{-1})
A	1490744	1051264	4.326	1.121	0.751	0.3116
	1493984,	1057216	3.849	1.121	0.709	0.3085
	1475364	1046534	3.522	1.121	0.682	0.3064
	1483417	1055887	3.233	1.121	0.653	0.3033
	1491741	1061683	2.883	1.121	0.611	0.3034
	1490699	1064531	2.508	1.121	0.553	0.3004
	1509330	1081172	2.264	1.121	0.505	0.2976
	1511730	1082177	1.999	1.121	0.439	0.2987
B	1511202	970616	4.326	1.449	0.665	0.3055
	1511871	977399	4.031	1.449	0.641	0.3010
	1514512	978629	3.708	1.449	0.609	0.3014
	1498309	967999	3.391	1.449	0.573	0.3015
	1508189	975696	3.090	1.449	0.531	0.3006
	1477744	959317	2.789	1.449	0.480	0.2982
	1504540	976677	2.588	1.449	0.440	0.2982
C	1481904	820410	4.326	1.959	0.547	0.3018
	1486630	823867	4.017	1.959	0.512	0.3013
	1485264	84977	3.884	1.959	0.496	0.3020
	1501840	833972	3.771	1.959	0.481	0.3003
	1462439	813838	3.564	1.959	0.450	0.2992
	1470068	817661	3.445	1.959	0.431	0.2994
F	1466091	806907	4.326	1.984	0.541	0.3010
	1476557	813381	4.038	1.984	0.509	0.3005
	1417087	779250	3.903	1.984	0.492	0.3014
	1393609	768308	3.744	1.984	0.470	0.3001
	1359579	750620	3.642	1.984	0.455	0.2994
	1484195	821014	3.483	1.984	0.430	0.2984

Table 5.2

The effect of overall porosity, ε, on attenuation coefficient, μ, at constant apparent thickness, L.

Lactose size fraction	Total blank count, N_o (4x15min)	Total sample count, N (60x1min)	L (cm)	t_a (cm)	ε	μ (cm^{-1})
A	1501523,	1059228	4.326	1.130	0.739	0.3088
	1488740	1015090	4.326	1.256	0.710	0.3049
	1483702	949704	4.326	1.468	0.661	0.3039
	1482041	904244	4.326	1.636	0.622	0.3020
	1487128	885250	4.326	1.720	0.602	0.3016
	1482017	835933	4.326	1.900	0.561	0.3014
	1482263	787889	4.326	2.101	0.514	0.3008
	1490662	769255	4.326	2.192	0.493	0.3018
	1485549	954533	4.326	1.455	0.664	0.3040
	1480077	926436	4.326	1.549	0.642	0.3025
	1486710	889484	4.326	1.700	0.607	0.3022
B	1483326	840036	4.326	1.893	0.562	0.3004
	1487746	810759	4.326	2.021	0.533	0.3004
	1476390	771840	4.326	2.153	0.502	0.3012
	1480661	754756	4.326	2.256	0.478	0.2987
	1483152	722275	4.326	2.404	0.444	0.2993
	1481009	818303	4.326	1.958	0.547	0.3030
	1475376	796190	4.326	2.049	0.526	0.3010
	1486455	784572	4.326	2.142	0.505	0.2983
C	1483525	754072	4.326	2.259	0.478	0.2996
	1480642	727734	4.326	2.367	0.453	0.3001
	1480572	706070	4.326	2.482	0.426	0.2983
	1484834	810096	4.326	2.033	0.530	0.2980
	1482248	777712	4.326	2.161	0.500	0.2985
F	1485236	753443	4.326	2.270	0.475	0.2990
	1481259	736017	4.326	2.351	0.457	0.2975
	1481401	716944	4.326	2.447	0.434	0.2966
	1481102	704285	4.326	2.486	0.425	0.2990

the calculated value of $N_{o_{min}}$ agreed closely with the recorded value of N_o, the corresponding $\Delta\mu$ value was accepted. In calculating confidence intervals in this way, the assumption was made that a count, N, was wholly representative of the sample; in practice, only approximately $\frac{2}{3}$ of the sample was represented.

The graphs in Figs. 5.10 and 5.11 show measured attenuation coefficients as a function of overall porosity, at constant t_a and at constant L respectively. The two sets of results, being in close agreement, were combined and a linear regression was performed, yielding the following data for the relationship between μ and ε.

Intercept at zero porosity : $\mu = 0.289\ cm^{-1}$

Gradient = $0.0215\ cm^{-1}$

Correlation coefficient = 0.805 (significant at the 1% level)

(E) Discussion

The results in Figs. 5.10 and 5.11 indicate that, using the experimental arrangement described, the observed value of the linear attenuation coefficient of lactose ($\mu_{lactose}$) is a function of overall porosity. Over the range of porosity studied, a significant linear relationship is suggested, but it would be unwise to conclude that this is necessarily the best fit. However, as a means of providing a calibration equation for subsequent porosity

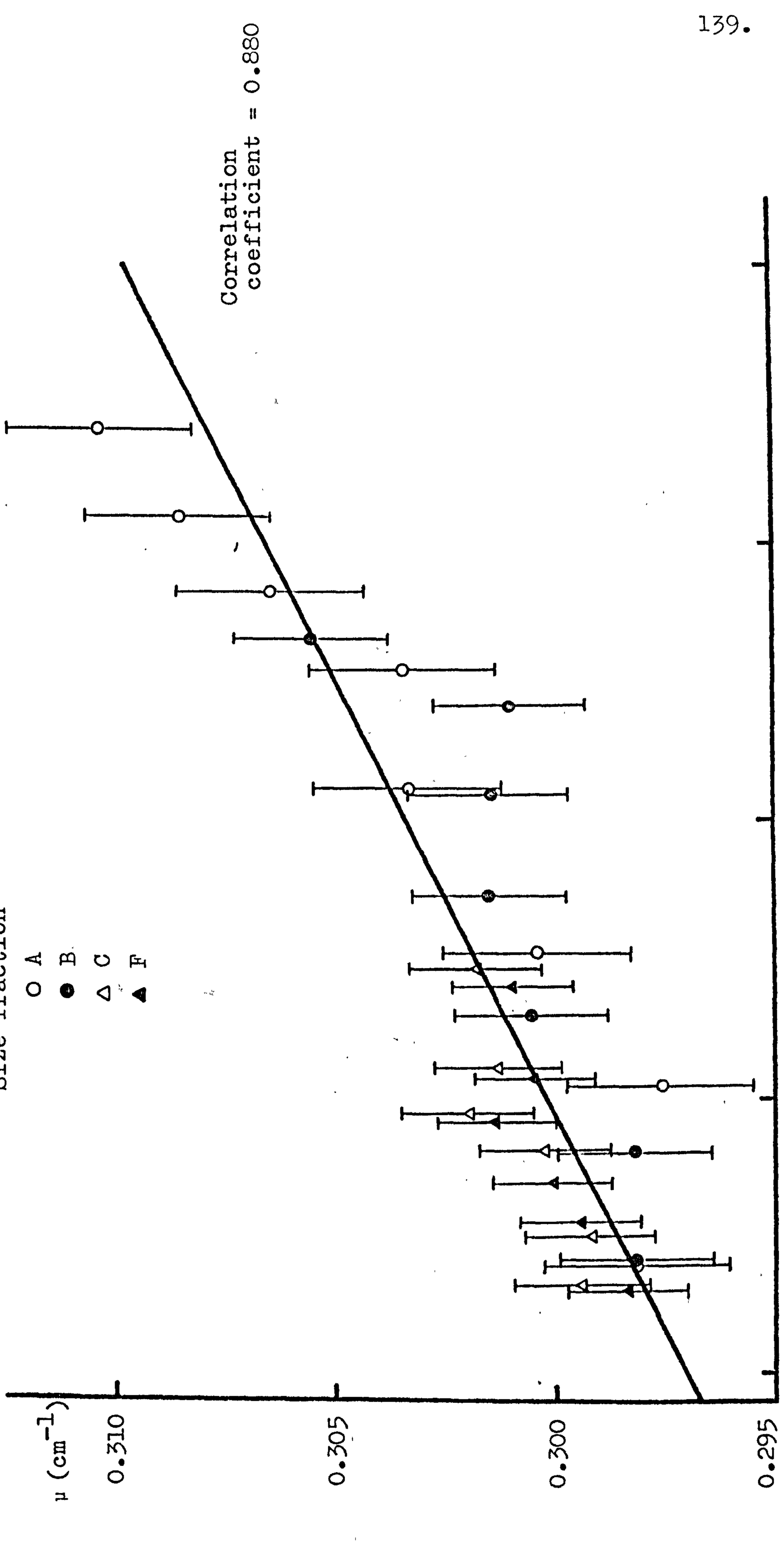

Fig. 5.10 Observed attenuation coefficient, μ , of lactose as a function of porosity, at constant attenuating thickness, t_a

Fig. 5.11 Observed attenuation coefficient, μ, of lactose as a function of porosity, at constant apparent thickness, L.

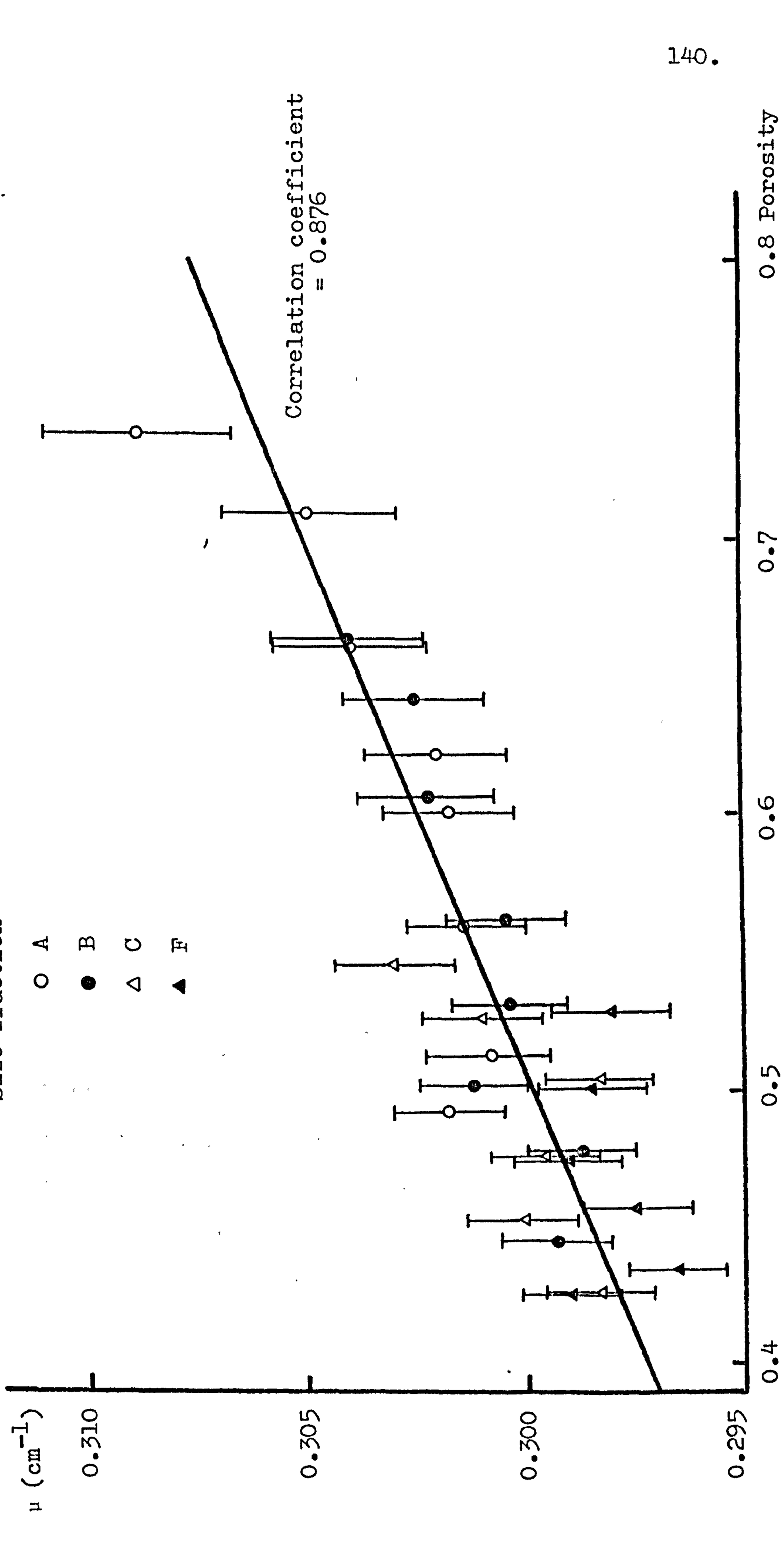

determinations, the following expression would appear to be acceptable:

$$\mu = (0.289 + 0.0215\varepsilon)\ cm^{-1} \qquad (5.12)$$

It is evident from this equation that measurement of local porosity values by the method of gamma-ray attenuation, in requiring a knowledge of μ, will also require a knowledge of ε itself. A means of overcoming this problem is discussed in Chapter 6.

It is interesting, though perhaps a coincidence, that the value of μ obtained by extrapolating to zero porosity is 0.289 cm^{-1}, which is effectively the same as the value of 0.288cm^{-1} calculated by the "mixture rule". The indication is that as porosity is introduced, more photons are removed from the primary beam, resulting in a higher observed value of μ. This effect may be tentatively explained either in terms of the apparatus or in terms of the sample material.

Coumoulos (1967) inferred that the effect was of a geometrical nature, in that as the voids ratio of his samples changed, their geometry with respect to the source, the detector and the collimators also altered. For example, by compressing a loosely-packed sample, most of the particles are effectively being moved nearer to either the source or the detector, depending on how the system is arranged. It is possible that some of the photons that

were initially scattered through small angles but still reached the detector, are now shielded out, or vice versa. In other words, the build-up factor, which consists of detected secondary photons, changes slightly, resulting in a different value of μ. This explanation doesn't appear to be relevant to experiment (ii), however, since by packing increasing quantities of powder into a constant volume, the sample, geometry is unaltered.

A completely different explanation can be proposed, based on the observation (Nakai and Fukuoka, 1978), that crystalline materials are prone to preferential orientation when compressed. If this occurs, the compressed packing will be ordered to some extent, and a high proportion of crystals may present a particular face to an incident gamma-ray beam. If the crystals have an anisotropic structure, it is feasible that the gamma-ray beam may encounter a different number of atomic electrons than it would if the packing were completely random. The implication here is that a single crystal of an anisotropic material would exhibit different linear attenuation coefficients when measured along different crystal axes. Thus, when a powder sample is progressively compressed to lower and lower porosity, the degree of preferential orientation increases, and the measured value of μ tends towards the value corresponding to that of a single crystal aligned accordingly.

5.5 Investigation into the porosity dependence of the attenuation coefficient of lactose

To test the validity of the above two theories, the geometry effect and the crystal orientation effect had to be separated and isolated.

It is possible to simulate powder samples of different porosity by preparing solutions of varying strength. The solute is then the,absorber in question, and a very dilute solution corresponds geometrically to a powder sample of high porosity. By studying the effect of solution strength and volume on the measured linear attenuation coefficient of the solute, the influence of geometry can be assessed in isolation, free from preferential packing effects.

The geometry effect may be eliminated by producing a single crystal of the absorber in question and measuring values of μ along each crystal axis. If these values differ significantly, and preferential orientation can be shown to result from compression of a powdered sample of the absorber, the second theory will have some experimental support.

5.5.1 The geometry effect

The use of aqueous solutions of lactose was considered initially for this experiment. Lactose, however, has an aqueous solubility of only about 17% at 20°C and has little more attenuating power than water, hence solutions

of different concentrations would show only minor variations in attenuation. Sodium bromide was considered to be a suitable alternative, having an aqueous solubility of 79.5% $^{w}/_{w}$ at $0^{o}C$ (Documenta Geigy, 1962), and a linear attenuation coefficient at 60keV estimated at $6.47cm^{-1}$ by the mixture rule (see Appendix 1).

(A) Theory

If a fixed mass of solute is dissolved in increasing volumes of water, and an attenuation coefficient for the solute is determined at each dilution, this simulates the situation in which the attenuation coefficient of a fixed mass of powder is determined at a number of overall porosities. Similarly, if the mass of dissolved solute in a fixed volume of solution is varied, and an attenuation coefficient is determined for the solute at each concentration, this simulates the situation in which a number of powder samples of the same bulk volume but varying overall porosity are studied.

A previous chapter has shown that to establish confidence limits, $\pm\Delta\mu$, for an attenuation coefficient, μ, of a sample of attenuating thickness, t_a, at the probability level p, a minimum blank count is necessary, $N_{o_{min}}$, such that:

$$\frac{N_{o_{min}}}{p^2} = \left[\frac{\exp\left[-\frac{1}{2}(\mu+\Delta\mu)t_a\right] + \exp\left[-\frac{1}{2}(\mu-\Delta\mu)t_a\right]}{\exp\left[-(\mu+\Delta\mu)t_a\right] - \exp\left[-(\mu-\Delta\mu)t_a\right]}\right]^2 \qquad (5.10)$$

For a given solution in a sample container:

weight of solute = W_s

particle density of solute = ρ_s

volume of solute = V_s = W_s/ρ_s

depth of container = d

volume of container = V_c

attenuating thickness of solute = t_s = d x V_s/V_c

The calculated value of $N_{o_{min}}$ will now be the minimum count required for a blank consisting of an identical container with exactly the same mass of water as the sample contained. This would be very difficult to carry out in practice, hence an "air blank" is taken instead of a "water blank". The air blank, which is obtained using an empty container, has to be of a minimum magnitude, denoted by $N'_{o_{min}}$, and is calculated as follows:

$$N'_{o_{min}} = N_{o_{min}} \exp(\mu_w t_w) \qquad (5.13)$$

where μ_w is the linear attenuation coefficient of water, and t_w is the attenuating thickness of water present in the solution sample. Hence the minimum "air blank", $N'_{o_{min}}$, is that count which is attenuated to the minimum "water blank", $N_{o_{min}}$, by an attenuating thickness, t_w, of water.

The quantity t_w is calculated in a similar manner to t_s:

weight of water, W_w = weight of solution - weight of solute, W_s

density of water = ρ_w

effective* volume of water = $V_w = W_w/\rho_w$

depth of container = d

volume of container = V_c

attenuating thickness of water = $t_w = d \times V_w/V_c$

*The effective volume of water, V_w, is calculated as the volume occupied by a weight, W_w, at a given temperature, in the absence of any dissolved solutes. Of course, when a solute is dissolved in water, there is usually a change in volume, but the assumption is made here that the attenuating thickness of the water is unaffected by such a change in volume.

Replacing t_a in equation 5.10 by t_s, and combining with equation (5.13):

$$N'_{o_{min}} = p^2 \cdot \left[\frac{\exp\left[-\frac{1}{2}(\mu+\Delta\mu)t_s\right] + \exp\left[-\frac{1}{2}(\mu-\Delta\mu)t_s\right]}{\exp\left[-(\mu+\Delta\mu)t_s\right] - \exp\left[-(\mu-\Delta\mu)t_s\right]} \right]^2 \times \exp(\mu_w t_w) \qquad (5.14)$$

(B) Experimental

The material used was sodium bromide (SLR Grade, Fison's Scientific Apparatus, Loughborough, Leics.).

A 200 mCi point source of Americium-241 (code No. AMC 26, The Radiochemical Centre, Amersham, Bucks.), having an active diameter of 5mm, now replaced the 14mCi

source, the net result being an approximate doubling of the count rate. Except for this change, the counting system used was as described in sections 5.1 and 5.3.

Two preliminary exercises were carried out before the sodium bromide solutions were investigated. First, the particle density of sodium bromide was determined using an Air Comparison Pycnometer (see Chapter 2).

Secondly, the linear attenuation coefficient of water at 60keV was determined. A known volume of distilled water was pipetted into an aluminium cylinder (described earlier), the sample was positioned in the path of the gamma-ray beam, and a "sample count", N, was recorded. A corresponding blank, N_o, (empty container) was taken and the sample thickness, t_w, was determined. The attenuation coefficient was calculated thus:

$$\mu_w = \frac{\ln \frac{N_o}{N}}{t_w}$$

This was in fact carried out on several occasions, and a mean value was therefore calculated.

The effect of dilution on the measured attenuation coefficient of sodium bromide was then studied

(i) at constant weight of solute

(ii) at constant sample volume

(i) A 60% $^{w}/_{v}$ aqueous solution of sodium bromide was prepared, and $5.0cm^3$ of this was pipetted into one of the aluminium sample containers described earlier. The required

counting time was calculated from the count rate and equation (5.14), then the sample was placed on the lower collimator and a "sample count", N, was recorded. A single count was adequate,since solute molecules are dispersed uniformly throughout a solution, and precise positioning of the sample was unimportant. An "air blank", N'_o, of the same duration was recorded using an empty, identical container.

Subsequent dilutions were prepared by adding $1.0cm^3$, $1.5cm^3$, $2.5cm^3$ and $2.0cm^3$ of water, giving 50%, 40%, 30% and 25%^{w}/v solutions respectively, and counts were recorded for each of these.

The experiment was carried out twice, first with a value of $\Delta\mu = 0.025cm^{-1}$, and secondly with $\Delta\mu = 0.015cm^{-1}$.

(ii) A sample volume of $10.0cm^3$ was chosen for this experiment. Solutions containing 20%, 25%, 30%, 35%, 40%, 45% and 50%^{w}/v of sodium bromide were prepared, and $10.0cm^3$ of each was pipetted in turn into a sample container. For each, a sample count and an air blank (N and N'_o) were taken. The value of $\Delta\mu$ chosen was $0.015cm^{-1}$.

In both experiments, a "water blank", N_o, was calculated from each air blank, N'_o by the following equation:

$$N_o = N'_o \exp-(\mu_w t_w) \qquad (5.15)$$

and N_o was then used in the calculation of the attenuation

coefficient of sodium bromide, thus:

$$\mu_s = \frac{\ln \frac{N_o}{N}}{t_s} \qquad (5.16)$$

(C) Results

Mean linear attenuation coefficient of water at 60keV = 0.2038 cm^{-1}

Particle density of sodium bromide = 3.13g cm^{-3}

Specific gravity of water at 20°C = 0.9982g cm^{-3}

(Documenta Geigy, 1962).

The results of experiment (i) appear in Tables 5.3(a) and 5.3(b), while Table 5.4 shows the results of experiment (ii). Attenuation coefficients are plotted as a function of solution concentration, at constant weight of solute (Figs. 5.12(a) and 5.12(b), and at constant sample volume (Fig. 5.13).

(D) Discussion

Figs. 5.12(a) and 5.12(b) suggest that as the volume of a solution containing a constant weight of sodium bromide increases, the attenuation coefficient of the sodium bromide increases. This trend corresponds with the increase in attenuation coefficient of a fixed weight of powder as its porosity increases, as was observed for lactose in Fig. 5.10. There is, however, no distinguishable trend in Fig. 5.13, so the observation, illustrated in Fig. 5.11, that the attenuation coefficient of lactose

Table 5.3(a)

The effect of dilution on the attenuation coefficient, μ_s, of a constant weight of sodium bromide in aqueous solution

($\Delta\mu$ = 0.025cm^{-1})

Volume of solution, (cm^3)	5	6	7.5	10	12
Concentration ($\%^w/v$)	60	50	40	30	25
t_w (cm)	1.473	1.827	2.339	3.206	3.896
$\mu_w t_w$	0.3001	0.3724	0.4767	0.6533	0.7939
Sample count, N	56719	52842	52911	55591	56430
Air blank, N_o'	638640	639051	714166	903759	107892
Water blank, N_o	473053	440353	443379	470235	581414
t_s (cm)	0.3345	0.3345	0.3345	0.3345	0.3345
μ_s(cm^{-1})	6.341	6.339	6.355	6.383	6.409

Table 5.3(b)

The effect of dilution on the attenuation coefficient, μ_s, of a constant weight of sodium bromide in aqueous solution

($\Delta\mu$ = 0.015cm^{-1})

Volume of solution (cm^3)	5	6	7.5	10	12
Concentration (%^{w}/v)	60	50	40	30	25
t_w (cm)	1.474	1.811	2.337	3.217	3.906
$\mu_w t_w$	0.3004	0.3691	0.4763	0.6557	0.7960
Sample count, N	151198	151629	145404	150960	153400
Air blank, N'_o	1720060	1845870	1969950	2466163	2880668
Water blank, N_o	1273755	1276119	1223485	1280132	1299587
t_s (cm)	0.3345	0.3345	0.3345	0.3345	0.3345
μ_s (cm^{-1})	6.371	6.368	6.368	6.391	6.388

Table 5.4

The effect of solute concentration on the attenuation coefficient, μ_s, of sodium bromide in aqueous solutions of constant volume

Volume of solution (cm^3)	10	10	10	10	10	10	10
Concentration (%w/v)	50	45	40	35	30	25	20
t_w (cm)	3.039	3.067	3.113	3.161	3.212	3.768	3.313
$\mu_w t_w$	0.619	0.625	0.634	0.644	0.655	0.666	0.675
Sample count, N	51385	66373	82978	110668	145260	219595	335658
Air blank, N_o'	3362802	3035537	2705694	2552676	2389666	2557241	2723264
Water blank, N_o	1810448	1624643	1434704	1340363	1241914	1313807	1386429
t_s (cm)	0.5575	0.5018	0.4460	0.3903	0.3345	0.2788	0.2230
μ_s (cm^{-1})	6.389	6.373	6.390	6.390	6.415	6.416	6.361

Fig. 5.12 Observed attenuation coefficient, μ_s, of a constant mass of sodium bromide in aqueous solution, as a function of concentration

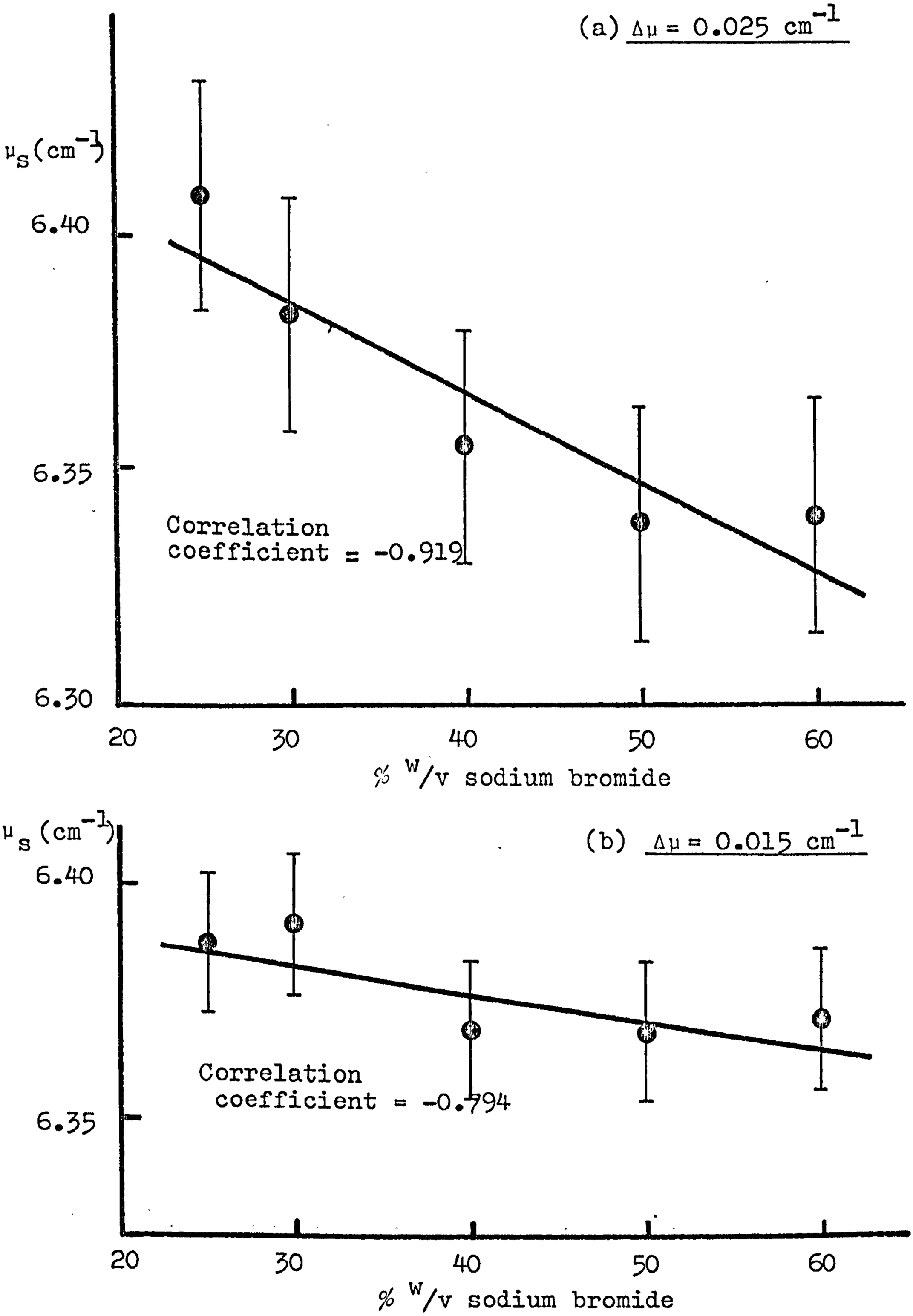

Fig. 5.13 Observed attenuation coefficient, μ_s, of sodium bromide in aqueous solutions of constant volume, as a function of concentration

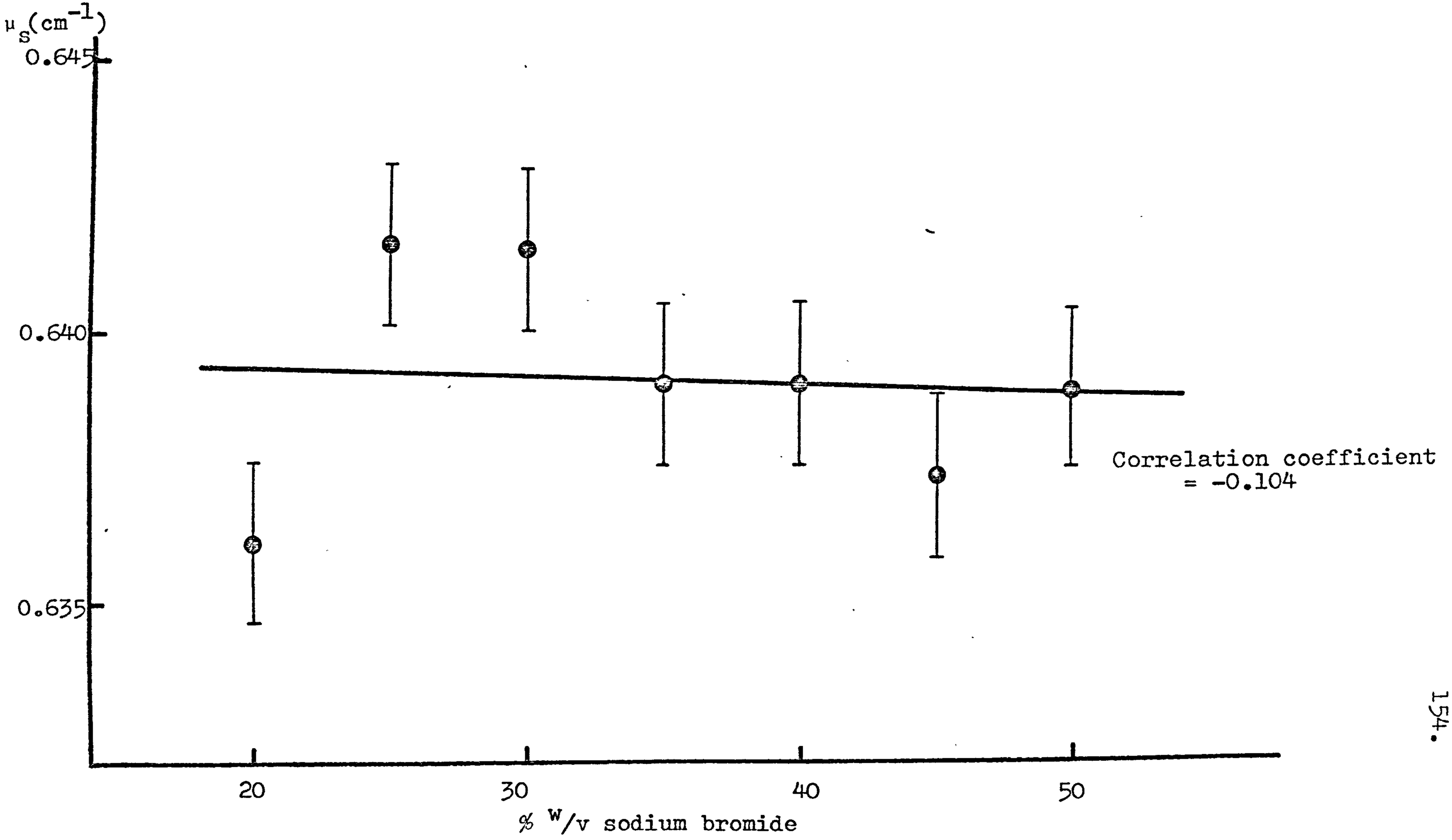

increases with porosity at constant volume, has no counterpart here.

There is, then, some evidence to suggest that the spatial arrangement, or geometry, of an absorber influences its attenuation coefficient, but it must be remembered that the range of μ-values recorded here for sodium bromide is really quite small, and the trends in Figs. 5.12(a) and 5.12(b) are barely significant, if at all. Also, quantities such as t_w and t_s have been quoted to four significant figures, whilst in practice, their accuracy is governed by the accuracy with which samples can be pipetted.

Furthermore, the behaviour of sodium bromide cannot be taken to be a perfect simulation of the behaviour of lactose. The former is a much denser material, contains elements of higher atomic number, and hence attenuates a gamma-ray beam to a much greater extent than lactose. More importantly, perhaps, elements of relatively high atomic number, such as bromine, interact with gamma photons of low energy, e.g. 60keV, largely by the photoelectric effect, whereas for low atomic number elements, such as carbon, hydrogen and oxygen, scattering is the predominant process at low energies. As a result, the detection of unwanted, scattered photons (i.e. the build-up factor) will be much less prevalent with sodium bromide than with lactose at 60keV, and any differences in attenuation coefficient caused by changes in absorber geometry, will be less marked.

5.5.2 The crystal orientation effect

Attempts were made to produce a sizeable single crystal of lactose, with a view to measuring attenuation coefficients along each crystal axis.

The method of fusion was tried first. A sample of powdered lactose (Analar grade, B.D.H. Chemicals Ltd., Poole, Dorset) was sealed under vacuum inside a glass crucible, melted in a crystallising furnace, then taken down a temperature gradient,with the intention of obtaining a single crystal. Unfortunately, however, lactose chars on melting, even under vacuum, so the method was unsuccessful.

Crystallisation from aqueous solution was also attempted. A saturated solution of Analar lactose was left to stand, enabling gradual evaporation to take place. The ensuing crystals were periodically removed and put into freshly prepared saturated solution, but on attaining a size of 2-3mm or more, they were seen to be generally quite opaque, due presumably to the presence of entrapped water. There was also a tendency for composite rather than single crystals to develop.

It was thought unlikely that a good quality, single crystal of lactose of adequate size would be produced, therefore a different crystalline material was sought which would present less difficulty.

(A) The choice of a model crystalline material

One substance from which large single crystals can

be produced with relative ease is potassium sodium tartrate, or Rochelle salt, $KNaC_4H_4O_6.4H_2O$. It has an orthorhombic structure, which means that all three crystal axes are perpendicular to each other, and the unit cell has the following dimensions:

a = 11.93 Å

b = 14,30 Å

c = 6.17 Å

(Beevers and Hughes, 1941)

Hence, to measure attenuation coefficients along each crystal axis, a single crystal was required from which a cube could be cut such that each face was parrallel to one of the axes.

The expected linear attenuation coefficient of potassium sodium tartrate was calculated by the mixture rule (see Appendix 1) to be $0.437cm^{-1}$. This indicated the size of crystal needed to provide a reasonable degree of attenuation.

(B) Experimental

Attenuation coefficients of potassium sodium tartrate were determined, using the apparatus described previously:

(i) Along each crystal axis of a cube cut from a single crystal.

(ii) On a size fraction of particulate material at various levels of overall porosity, both at constant

sample weight and at constant apparent thickness (cf. lactose experiments, section 5.4).

(i) A saturated aqueous solution of potassium sodium tartrate (Laboratory grade, BDH Chemicals Ltd., Poole, Dorset) was left to stand, allowing crystallisation to occur by evaporation. When a crystal of sufficient size had been obtained, it was cut down to an approximately cubic shape, which, measured (using a micrometer):

1.249cm in the a-direction

1.259cm in the b-direction

1.247cm in the c-direction

The crystal was positioned roughly centrally on the lower collimator of the gamma-ray apparatus, so that the radiation beam passed along one of the crystal axes, and a sample count was recorded, the duration of which was 20 minutes, as determined by a chosen $\Delta\mu$-value of 0.0020 cm^{-1}. A blank count was recorded with the crystal removed from the beam, and the procedure was repeated for the other two crystal axes. Attenuation coefficients were calculated from the attenuation equation as before.

(ii) A quantity of particulate potassium sodium tartrate was sieved to produce a sample of particle size +90-178 μm.

(a) An aluminium sample container was loosely filled with this size fraction, and the surface was scraped level with a spatula blade. The attenuation coefficient was determined, following the procedure described in section 5.4,

then the sample was compressed in stages and a new attenuation coefficient was determined at each new porosity. Attenuating thickness, t_a, remained constant. Count duration was governed by a chosen $\Delta\mu$-value of 0.0020cm^{-1}.

(b) Attenuation coefficients were determined for a number of samples of increasing mass but constant volume (i.e. the volume of the sample container). Thus, the apparent thickness of the samples, L, was constant, while the attenuating thickness, t_a, increased and overall porosity decreased. Again, $\Delta\mu$ was set at 0.0020cm^{-1}.

(C) Results

(i) Table 5.5 shows the results for the single crystal.

Table 5.5

The attenuation coefficient of potassium sodium tartrate, as measured along each axis of a cubic single crystal

Axis	Thickness, t (cm)	Blank count, N_o	Sample count, N	μ (cm^{-1})
a	1.249	1061649	617796	0.435
b	1.259	1062164	613964	0.436
c	1.247	1062063	619731	0.432

(ii) The results for the +90-178μm particle size fraction of potassium sodium tartrate are shown in Tables 5.6 and 5.7.

Table 5.6

The effect of overall porosity, ε, on the attenuation coefficient, μ, of potassium sodium tartrate, at constant attenuating thickness, t_a

Total blank count, N_o (4x150sec.)	Total sample count, N (60x10sec.)	L (cm)	t_a (cm)	ε	μ (cm^{-1})
495452	189468	4.447	2.166	0.513	0.4438
492992	188645	4.447	2.171	0.512	0.4425
493895	187463	4.224	2.171	0.486	0.4462
494545	189489	4.212	2.166	0.482	0.4429
491494	188127	4.092	2.171	0.470	0.4423
493876	189977	3.991	2.166	0.456	0.4411
491514	187852	3.873	2.171	0.440	0.4430
493564	189294	3.809	2.166	0.430	0.4437
491111	188102	3.671	2.171	0.409	0.4420
493310	188792	3.583	2.166	0.394	0.4434

Table 5.7

The effect of overall porosity, ε , on the attenuation coefficient, μ , of potassium sodium tartrate at constant apparent thickness, L.

Total blank count, N_o (4x150 sec.)	Total sample count, N (60x10sec.)	L (cm)	t_a (cm)	ε	μ (cm^{-1})
495748	189566	4.447	2.160	0.514	0.4451
496486	182477	4.447	2.255	0.493	0.4430
496486	174681	4.447	2.361	0.469	0.4424
496278	167750	4.447	2.448	0.450	0.4431
496267	161843	4.447	2.534	0.430	0.4422
494834	155010	4.447	2.620	0.411	0.4430
495623	151228	4.447	2.685	0.396	0.4421

The attenuation coefficients obtained in experiments (ii) (a) and (ii) (b) were plotted as a function of overall porosity (see Fig. 5.14).

(D) Discussion

The three values of attenuation coefficient obtained with the single crystal were all very similar, and if the 95% confidence intervals of $\pm$ 0.0020cm^{-1} are considered, no statistically significant difference can be established. The inference is that for potassium sodium tartrate, crystal orientation has no effect on attenuation coefficient, although firm conclusions cannot be drawn without also measuring attenuation coefficients in directions other than along the three crystal axes.

The results in Fig. 5.14 illustrate that porosity appears to have little or no effect on attenuation coefficient either. At overall porosities ranging from 0.394 to 0.514, no significant differences were established. It should be pointed out, though, that over a similar porosity range, the measured attenuation coefficients of lactose showed only marginal differences, a distinct trend becoming visible only when a much wider porosity range was considered.

It is interesting to note that for particulate potassium sodium tartrate, a consistently higher attenuation coefficient was observed than for the single crystal. This indicates that increasing porosity results in a

Fig. 5.14 Observed attenuation coefficient, μ, of potassium sodium tartrate, as a function of porosity

(a) Constant attenuating thickness t_a

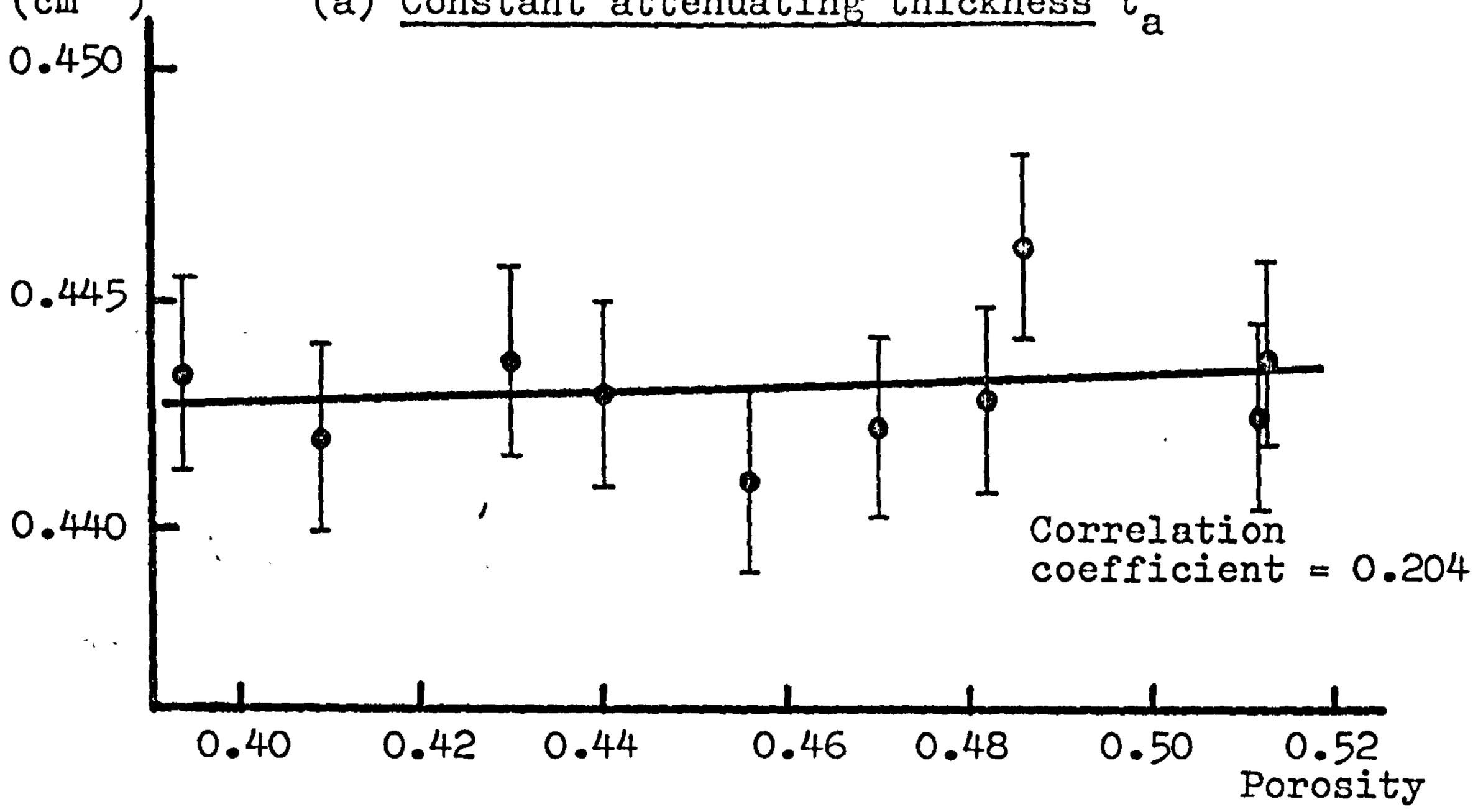

(b) Constant apparent thickness, L

higher attenuation coefficient, as was consistently illustrated with lactose.

It is clear, then, that reliable conclusions cannot be drawn on the significance of crystal orientation,on the basis of these results alone. An extension of the single crystal work to include measurements at oblique angles, plus a study of attenuation coefficients at a much wider porosity range with particulate potassium sodium tartrate could be worthwhile. Even then, there may not necessarily be parallel behaviour between potassium sodium tartrate and lactose. The former, as has already been mentioned, has an orthorhombic structure, i.e. three mutually perpendicular crystal axes. Lactose, on the other hand, has a monoclinic structure, which means it has three unequal crystal axes, of which one is perpendicular to the other two. Its unit cell dimensions are:

$a = 7.815$ Å

$b = 21.567$ Å

$c = 4.844$ Å

$\beta = 106.2^{\circ}$

(Beevers and Hansen, 1971)

where β is the angle between the a and c axes.

5.6 Conclusions

It has been demonstrated that, under the experimental

conditions described, the linear attenuation coefficient of particulate lactose at 60keV is not constant, but is dependent on the porosity of the sample studied. This porosity-dependence appears to be unaffected by particle size, and it occurs both with samples of constant weight and samples of constant bulk volume. Over the range of porosities studied, the relationship is approximately linear, according to the following equation:

$$\mu = (0.289 + 0.0215\varepsilon)\ cm^{-1} \qquad (5.12)$$

It is proposed that this expression should be used for local porosity determinations, rather than a fixed, average μ-value. A problem arises from the fact that there is a porosity term in equation (5.12), and yet it is the measurement of porosity that is being attempted. This is discussed in Chapter 6.

It has not been possible to determine the cause of the porosity-dependence of such attenuation coefficients.

Chapter 6

The Distribution Of Porosity Within Samples Of Lactose

When a dosator nozzle enters a powder bed, it penetrates virtually to the bottom, thus admitting powder from the whole depth of the bed. For this reason, if the porosity of a bed varies with depth, this alone will not affect capsule fill weights. On the other hand, lateral variation in porosity is bound to have an influence on the quantity of powder entering the nozzle, and attention has therefore been focussed on such variations. In practical terms, this involves directing the gamma-ray beam vertically downwards through a prepared sample at a number of defined positions, thus enabling local porosity measurements to be made.

6.1 Theory

It has been shown (Chapter 4) that the basic attenuation equation can be modified to take into account the porosity of particulate materials:

$$N = No \exp\left[-\mu(1-\varepsilon)L\right] \qquad (4.5)$$

This equation may be rearranged thus:

$$\varepsilon = 1 - \frac{\ln\frac{No}{N}}{\mu L} \qquad (6.1)$$

and this is the expression used to calculate local porosity values from attenuation measurements.

Chapter 5 described a means of establishing a statistically significant difference between two measured values of linear attenuation coefficient, by taking sufficiently high counts (see equation (5.9)). A similar treatment has been applied (Kurz, 1972) to derive the minimum counting interval required to establish a significant difference between two values of local porosity. For ease of reference, it is reproduced here.

Consider a powder bed of uniform apparent thickness, L_1 and overall porosity, ε . At two given counting positions, the porosities of those parts of the bed that are in the path of the gamma-ray beam are given by ε_1 and ε_2, and if a beam of intensity I_o is incident on these two positions in turn, the transmitted intensities will be I_1 and I_2 respectively (see Fig. 6.1). The attenuation at each position can be expressed thus:

$$N_1 = No \exp\left[-\mu(1-\varepsilon_1)L\right] \qquad (6.2)$$

$$N_2 = No \exp\left[-\mu(1-\varepsilon_2)L\right] \qquad (6.3)$$

where N_1 and N_2 are sample counts, No is a blank count of the same duration and μ is the linear attenuation coefficient of the sample material.

To establish a porosity difference $(\varepsilon_2-\varepsilon_1)$ at a level

Fig. 6.1 The attenuation of gamma rays by a non-homogeneous powder bed

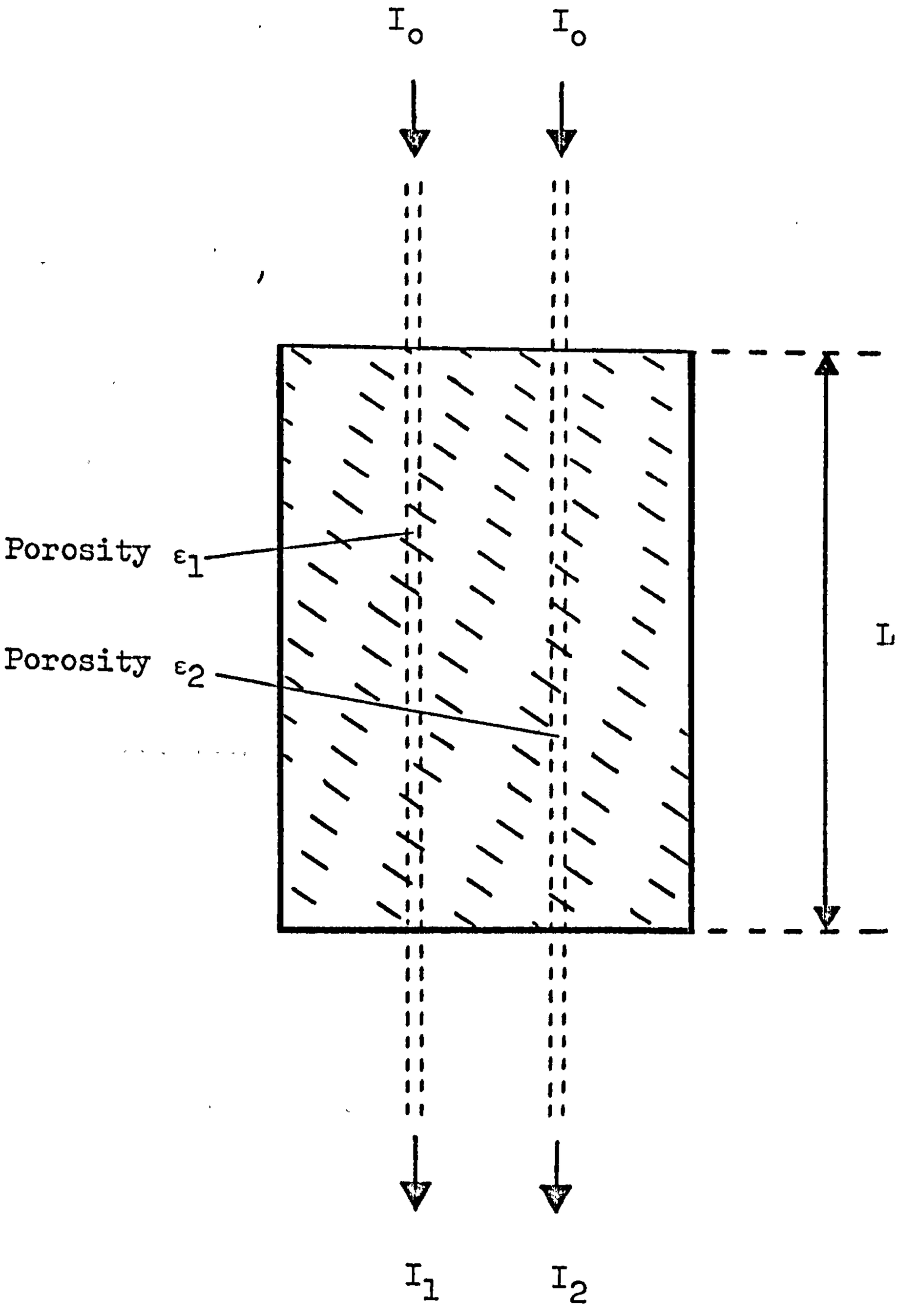

of confidence denoted by p, the following relationship must hold:

$$N_2 - N_1 \geqslant p.\sigma_1 + p.\sigma_2 \qquad (6.4)$$

where σ_1 and σ_2 are the standard deviations of counts N_1 and N_2 respectively. This situation is illustrated in Fig. 6.2.

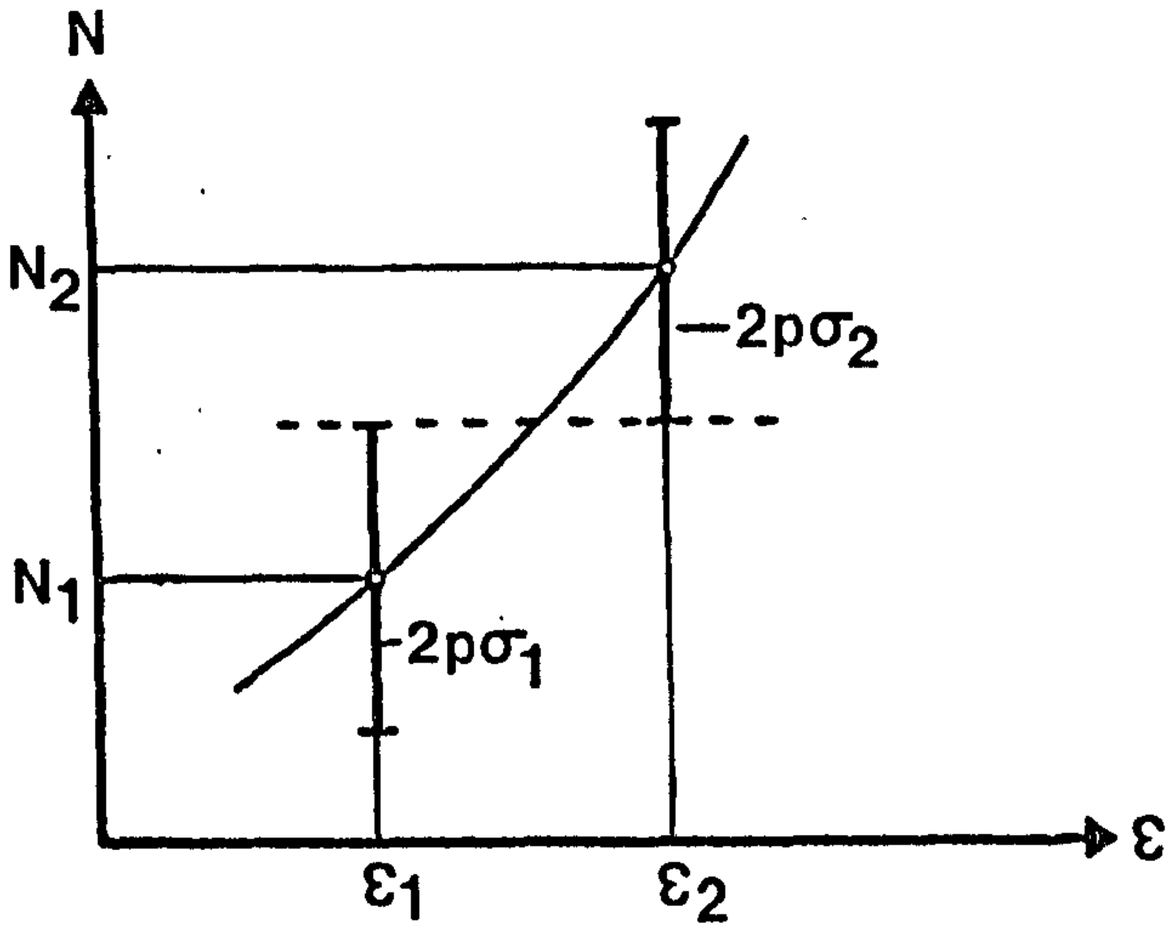

Fig. 6.2
Qualitative representation of equation (6.4)

Individual counts such as N_1 and N_2 are governed by the Poisson distribution, hence

$$\sigma_1 = \sqrt{N_1} \quad \text{and} \quad \sigma_2 = \sqrt{N_2}$$

and from equations (6.2) and (6.3):

$$\sigma_1 = No^{\frac{1}{2}} \exp\left[-\tfrac{1}{2}\mu(1-\varepsilon_1)L\right] \qquad (6.5)$$

$$\sigma_2 = No^{\frac{1}{2}} \exp\left[-\tfrac{1}{2}\mu(1-\varepsilon_2)L\right] \qquad (6.6)$$

Substituting (6.2), (6.3), (6.5) and (6.6) into (6.4):

$$\frac{N_{o_{min}}}{p^2} = \left[\frac{\exp\left[-\frac{1}{2}\mu(1-\varepsilon_2)L\right] + \exp\left[-\frac{1}{2}\mu(1-\varepsilon_1)L\right]}{\exp\left[-\mu(1-\varepsilon_2)L\right] - \exp\left[-\mu(1-\varepsilon_1)L\right]}\right]^2 \qquad (6.7)$$

(As in Chapter 5, p denotes the probability level, and for 95% confidence at ∞ degrees of freedom, p = 1.96.)

Similarly, if a local porosity value ε is to be measured with confidence limits of $\pm \Delta\varepsilon$, then equation (6.7) may be modified thus:

$$\frac{N_{o_{min}}}{p^2} = \left[\frac{\exp\left[-\frac{1}{2}\mu(1-\varepsilon-\Delta\varepsilon)L\right] + \exp\left[-\frac{1}{2}\mu(1-\varepsilon+\Delta\varepsilon)L\right]}{\exp\left[-\mu(1-\varepsilon-\Delta\varepsilon)L\right] - \exp\left[-\mu(1-\varepsilon+\Delta\varepsilon)L\right]}\right]^2 \qquad (6.8)$$

If $N_{o_{min}}/p^2$ is plotted against L on logarithmic scales at a number of levels of overall porosity ε, for a chosen porosity difference of $\varepsilon_2-\varepsilon_1 = 0.005$, the curves shown in Fig. 6.3 are obtained. The significance of the minimum in each curve is that for a powder of given porosity, there is an optimum value of the quantity L at which the blank count requirement, $N_{o_{min}}$, is at its lowest. This may be exploited such that by choosing a suitable gamma source, and using samples of the right apparent thickness, counting times can be minimised. In the present work, samples of lactose, of apparent thickness 4.4cm were irradiated with 60 keV photons from a source of Americium-241. The resulting value of L was approximately 1.3, which lies well to the left of the minima in Fig. 6.3. However, the required blank counts, denoted by

Fig. 6.3 The minimum blank count, $N_{o_{min}}$, necessary to establish a porosity difference of 0.005, as a function of various factors.

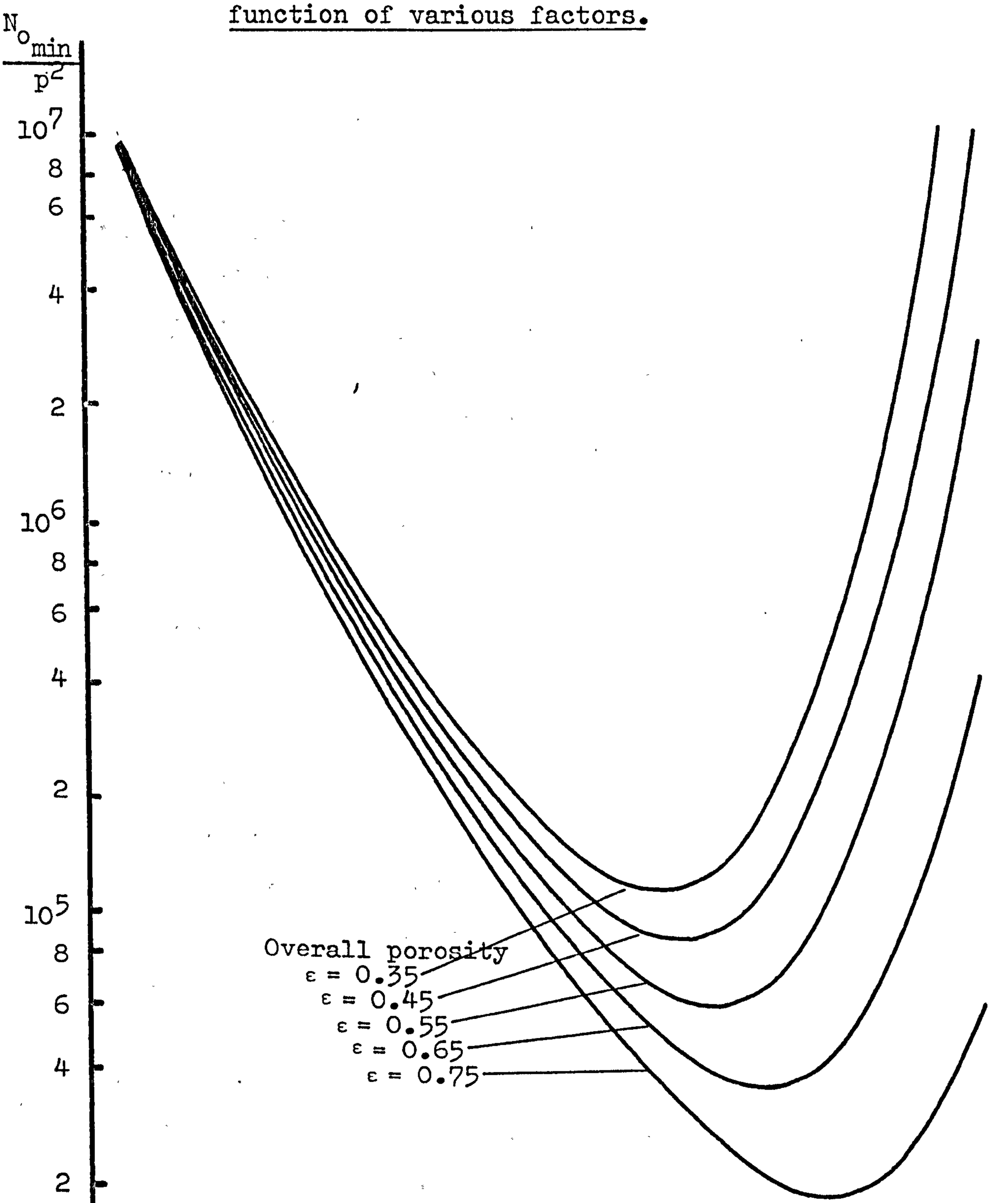

$N_{o_{min}}$, were still within manageable limits, and therefore, the decision was taken not to change the experimental conditions in order to optimise the system.

6.2 Non-vibrated powder samples

6.2.1 Experimental

(A) Apparatus and materials

In Chapter 5,, apparatus was described which enabled a well-collimated, cylindrical beam of gamma-radiation to be directed vertically downwards through a sample of powder held in a cylindrical aluminium container. Accurate positioning of the sample with respect to the beam was facilitated by means of a micromanipulator.

This same apparatus was used for local porosity determinations. The source activity was 200mCi, which provided a count rate of about 800 counts per second with no sample in the beam.

Three lactose particle size fractions were chosen for study, these being fraction B (+18.7-26.5μm), fraction D (+37.5-53μm) and fraction F (+75-105μm). These same size fractions were examined in Chapter 3 with regard to their overall packing density.

The range of systems described in Chapter 3 for producing different deposition methods was again available for use.

(B) Methods of preparing powder samples

Four deposition methods were employed for each of fractions B,D and F. These were: pouring directly from a jar, deposition from a vibrating chute via a funnel, deposition from a vibrating chute and perforated plate, and deposition from a vibrating chute into a container moving to and fro through the falling "curtain" of powder. These are methods (i), (iii), (iv) and (v) of Chapter 3. A fifth method, discharge from a vertical glass tube fitted with a circular orifice (method (ii)),was unsuitable for fraction B because of its poor flow properties, but the other two lactose fractions were deposited by this method, using a range of orifice sizes. For further details and diagrams, see Chapter 3.

In all cases, four sample containers were filled. The aluminium extension collar was attached, enabling containers to be overfilled, then after filling, the collar was removed and a spatula blade was used to scrape the upper surface of the sample level. The overall porosity of each sample was calculated from its weight, volume and apparent particle density.

(C) Method of obtaining a porosity distribution

Each sample, contained in a cylinder of known dimensions, was weighed and its overall porosity calculated. An approximate value of $0.3 cm^{-1}$ was assumed for the attenuation coefficient of lactose, and $\Delta\varepsilon$ was

set at 0.005. $N_{o_{min}}$ was then calculated from equation (6.8), taking p to be 1.96 (95% confidence). Having calculated a suitable counting interval, the sample container was attached to the micromanipulator by means of the steel ring and peg (see Chapter 5), and the position of the micromanipulator on its steel base-plate was adjusted until (x,y) coordinates of (75.0, 25.0) corresponded with the gamma-ray beam passing vertically down the centre of the sample. Counts of the calculated duration were then recorded with the sample in each of nineteen defined positions. These positions and their (x,y) coordinates are shown in Fig. 6.4. Blank counts of the same duration were recorded after every four sample counts, by positioning an identical, but empty container in the gamma-ray beam. In this way, attenuation due to the container base was cancelled out. For each sample count, N, the corresponding value of N_o was taken to be the average of the preceding and subsequent blank counts.

(D) Treatment of results

(i) Calculation of local porosity values

Having obtained values of N and N_o, and knowing L from the depth of the container, the calculation of local porosity, ε, requires a knowledge of the attenuation coefficient of lactose, μ. It has been observed that the value of μ is dependent on porosity. Therefore, a computer program was written to calculate μ by iteration,

Fig. 6.4 Array of counting positions for local porosity determinations, showing (x,y) coordinates

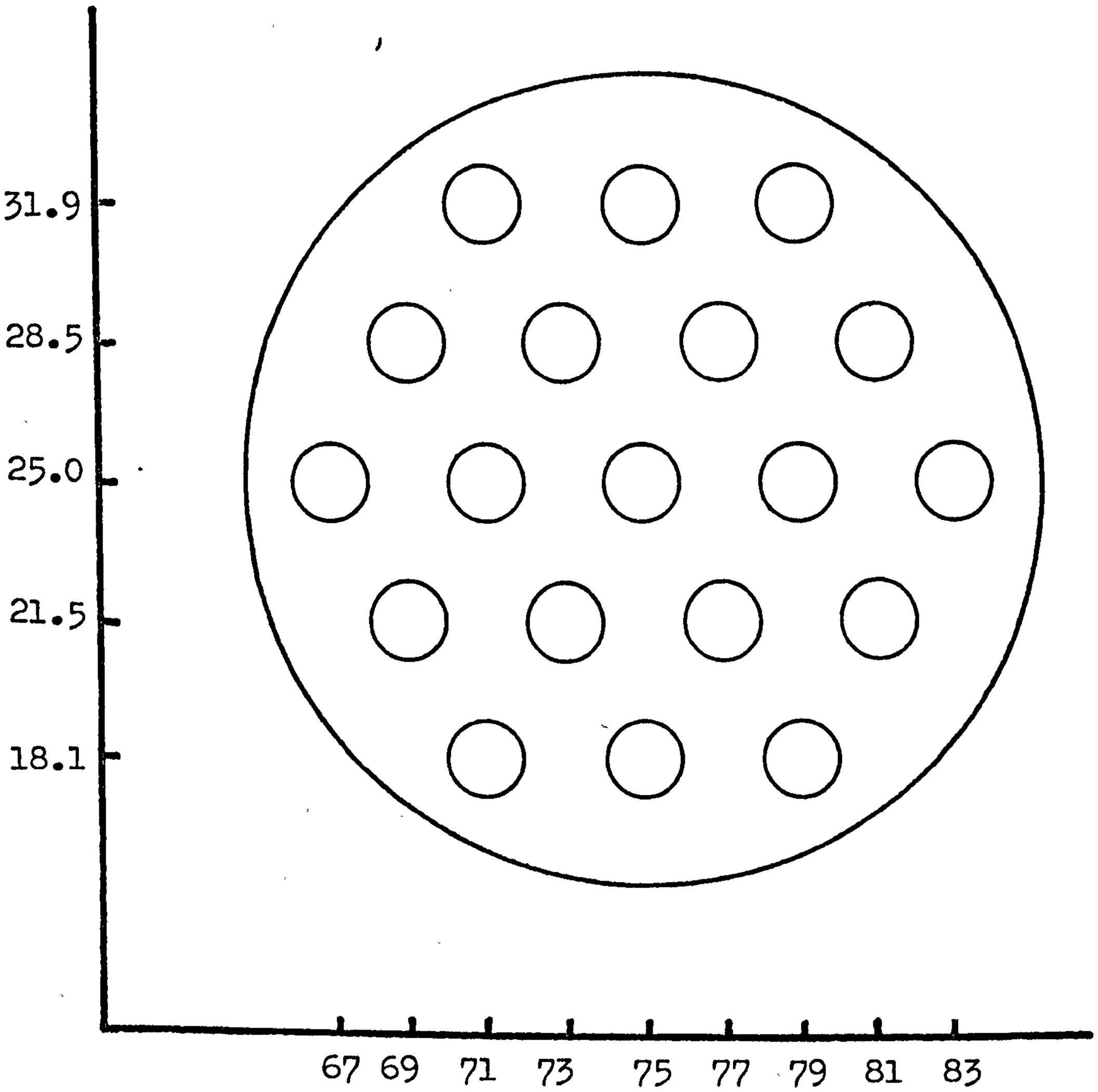

beginning with an approximation of $\mu = 0.3 cm^{-1}$. Local porosity was calculated, using this approximate value of μ, by the following equation:

$$\varepsilon = 1 - \frac{\ln \frac{N_o}{N}}{\mu L} \qquad (6.1)$$

then the result was substituted into the calibration expression for μ, which is:

$$\mu = (0.289 + 0.0215\,\varepsilon)\,cm^{-1} \qquad (5.12)$$

Thus a new value of μ was generated, which on substitution into equation (6.1) yielded a new value of ε. This procedure was continued until successive values of ε differed by less than 0.0001.

(ii) Calculation of confidence intervals

Having determined $N_{o_{min}}$ on the basis of confidence intervals of $\pm$ 0.005, then providing $N_{o_{min}}$ is satisfied, the stated confidence intervals should be guaranteed. However, since the value of μ in equation (6.8) was only an approximation, and ε was taken to be the overall porosity of the sample rather than individual local porosity values, confidence intervals were re-calculated for each individual porosity result using a trial and error method similar to that described in Chapter 5, for calculating confidence intervals for attenuation coefficients. Likely values of

$\Delta\varepsilon$ were substituted into equation (6.8), and when the calculated value of $N_{o_{min}}$ agreed closely with the recorded value of N_o, that value of $\Delta\varepsilon$ was accepted. This calculation was incorporated into the computer program described in (i) above. In practice, it was found that all of these confidence intervals fell within the range $\pm$ 0.0048 to $\pm$ 0.0052.

(iii) Analysis of variance

For each group of samples, 4 x 19 local porosity values were obtained, and for each set of nineteen, a mean and standard deviation were calculated. Comparison of the mean with the previously determined overall porosity served as an indication of the accuracy of the method, whilst the standard deviation was a measure of the uniformity of each sample.

In addition, an analysis of variance was performed on each set of 4 x 19 results. Of the 19 positions in the network, one was at the centre of the sample, and there were six each at distances of 4mm, 7mm and 8mm from the centre. By pooling results which were equidistant from the centre, the analysis was able to reveal any relationship between porosity and distance from the centre. The linear, quadratic and cubic fit of this relationship was also calculated. Between-samples variance, on the other hand, indicated whether any significant difference existed between the four samples. The analysis generated other

information, including the mean, minimum and maximum porosity in a set of 76 values, and the mean porosity at a given distance from the sample centre. Also, the total sum of squares was a useful measure of overall variability. All calculations were performed by computer, using a statistical package (Genstat V, Mark 4.01).

(iv) Visualisation of porosity distributions

A small computer (Model V76, Varian Associates Ltd., Walton-on-Thames, Surrey) was employed to produce grey-scale images of powder samples, thus illustrating local variations in porosity. A circular "frame" was divided up into nineteen square regions, corresponding to the nineteen counting positions illustrated in Fig. 6.4. For each set of 76 porosity values, obtained from a group of four samples, the mid-range porosity was assigned to the middle one of fifteen shades of grey, and a suitable porosity increment was chosen to correspond to successive shades, such that the range of local porosity present could be fully represented. An image of each individual sample was then constructed by assigning each local porosity value to the appropriate shade, such that regions of low porosity appeared dark grey, while high porosity regions were lighter. In this way, differences both within and between samples in a group of four could be revealed. Completed images were printed out electrostatically (Statos 33 printer/plotter).

An alternative method of visualisation was to create an image as described above, and display it on a colour television screen, using a suitable colour code. The image could then be photographed if a permanent record was required.

6.2.2 Results

Tables 6.2 to,6.7 summarise the results obtained.

In the analyses of variance, several variance ratios were calculated; reference to the appropriate statistical tables (Fisher and Yates, 1963) indicates whether these calculated values are significant at the 5% or 1% level. Table 6.1 lists minimum values of variance ratio at these two levels, taking into account the degrees of freedom possessed by each mean square.

Table 6.1

Minimum variance ratios at the 5% and 1% levels

	Degrees of freedom	5% level	1% level
Between samples	3,69	2.74	3.98
Distance from centre	3,69	2.74	3.98
Linear fit	1,69	4.08	7.01
Quadratic fit	1,69	4.08	7.01
Cubic fit	1,69	4.08	7.01

In Tables 6.3, 6.5, and 6.7, variance ratios significant at the 5% level are marked *, while those significant at

the 1% level are marked **. Radial distance from the sample centre is denoted by r.

Table 6.2

Porosity data for samples of lactose, fraction B.

Four containers filled by each method.

	Filling Method / Container	(i)	(iii)	(iv)	(v)
	1	0.672	0.687	0.674	0.632
Overall	2	0.667	0.690	0.676	0.630
porosity	3	0.673	0.687	0.669	0.623
	4	0.667	0.693	0.667	0.623
Mean local	1	0.672	0.688	0.666	0.629
porosity	2	0.664	0.690	0.669	0.628
	3	0.674	0.688	0.664	0.620
	4	0.669	0.693	0.663	0.622
Standard	1	0.0119	0.0341	0.0257	0.0096
deviation	2	0.0118	0.0304	0.0262	0.0074
of local	3	0.0089	0.0284	0.0243	0.0055
porosity	4	0.0087	0.0260	0.0268	0.0089

Table 6.3

Analyses of variance of local porosity in samples of lactose, fraction B, filled by different methods

Filling Method		(i)	(iii)	(iv)	(v)
Grand mean porosity		0.670	0.690	0.666	0.625
Minimum local value		0.650	0.628	0.631	0.606
Maximum local value		0.699	0.750	0.722	0.656
Mean local porosity	r = 0mm	0.662	0.652	0.682	0.616
	r = 4mm	0.665	0.673	0.640	0.621
	r = 7mm	0.671	0.697	0.668	0.624
	r = 8mm	0.675	0.706	0.686	0.631
Variance ratios:					
Distance from centre		4.903**	9.575**	29.271**	9.691**
Linear fit		14.258**	24.248**	61.932**	17.538**
Quadratic fit		0.414	4.169*	0.213	0.133
Cubic fit		0.038	0.309	25.666**	1.402
Between samples		4.150**	0.143	0.446	8.935**
Total sum of squares		0.00949	0.0685	0.0500	0.00618

Table 6.4

Porosity data for samples of lactose, fraction D.
Four containers filled by each method.

	Container \ Filling method	(i)	(iia)	(iib)	(iii)	(iv)	(v)
Overall porosity	1	0.574	0.546	0.528	0.544	0.544	0.510
	2	0.567	0.538	0.523	0.543	0.549	0.505
	3	0.564	0.531	0.530	0.536	0.555	0.510
	4	0.561	0.529	0.522	0.537	0.545	0.506
Mean local porosity	1	0.571	0.547	0.528	0.538	0.545	0.501
	2	0.567	0.544	0.524	0.541	0.551	0.496
	3	0.565	0.531	0.530	0.534	0.559	0.498
	4	0.558	0.528	0.523	0.538	0.545	0.500
Standard deviation of local porosity	1	0.0137	0.0078	0.0091	0.0273	0.0189	0.0082
	2	0.0168	0.0070	0.0105	0.0351	0.0106	0.0091
	3	0.0149	0.0128	0.0095	0.0389	0.0106	0.0065
	4	0.0111	0.0091	0.0098	0.0353	0.0161	0.0102

Table 6.5

Analyses of variance of local porosity in samples of lactose, fraction D, filled by different methods

Filling method		(i)	(iia)	(iib)	(iii)	(iv)	(v)
Grand mean porosity		0.565	0.538	0.526	0.536	0.550	0.499
Minimum local value		0.536	0.512	0.508	0.453	0.504	0.481
Maximum local value		0.592	0.561	0.549	0.586	0.581	0.522
Mean local porosity	r = 0mm	0.555	0.527	0.511	0.539	0.529	0.497
	r = 4mm	0.562	0.532	0.518	0.524	0.549	0.501
	r = 7mm	0.567	0.539	0.529	0.537	0.554	0.495
	r = 8mm	0.568	0.544	0.535	0.548	0.551	0.501
Variance ratios:							
Distance from centre		1.537	10.981**	39.207**	2.685	3.528*	2.750
Linear fit		3.348	30.387**	109.547**	7.086*	2.056	0.267
Quadratic fit		1.030	2.441	7.895**	0.111	4.672*	5.555*
Cubic fit		0.234	0.116	0.182	0.857	3.857	2.427
Between samples		2.764*	25.168**	5.956**	0.082	4.422**	1.356
Total sum of squares		0.0172	0.0118	0.00792	0.09	0.0186	0.00592

Table 6.6

Porosity data for samples of lactose, fraction F. Four containers filled by each method

	Filling method / Container	(i)	(iia)	(iib)	(iii)	(iv)	(v)
Overall porosity	1	0.528	0.517	0.529	0.481	0.474	0.460
	2	0.516	0.516	0.528	0.479	0.486	0.455
	3	0.521	0.513	0.528	0.479	0.474	0.447
	4	0.521	0.511	0.527	0.480	0.472	0.456
Mean local porosity	1	0.528	0.514	0.530	0.476	0.471	0.448
	2	0.517	0.516	0.530	0.478	0.480	0.446
	3	0.525	0.517	0.532	0.478	0.474	0.443
	4	0.521	0.512	0.528	0.479	0.470	0.446
Standard deviation of local porosity	1	0.0091	0.0092	0.0070	0.0255	0.0137	0.0130
	2	0.0054	0.0074	0.0074	0.0270	0.0238	0.0159
	3	0.0097	0.0077	0.0058	0.0249	0.0187	0.0101
	4	0.0106	0.0072	0.0065	0.0237	0.0174	0.0083

Table 6.7

Analyses of variance of local porosity in samples of lactose, fraction F, filled by different methods

Filling method		(i)	(iia)	(iib)	(iii)	(iv)	(v)
Grand mean porosity		0.523	0.515	0.530	0.478	0.474	0.446
Minimum local value		0.500	0.494	0.509	0.421	0.429	0.424
Maximum local value		0.543	0.530	0.545	0.512	0.513	0.478
Mean local porosity	r = 0mm	0.516	0.505	0.514	0.469	0.483	0.434
	r = 4mm	0.518	0.507	0.527	0.480	0.482	0.439
	r = 7mm	0.524	0.518	0.534	0.479	0.472	0.444
	r = 8mm	0.526	0.521	0.533	0.475	0.465	0.457
Variance ratios:							
Distance from centre		3.973*	45.342**	30.637**	0.279	3.832*	16.101**
Linear fit		10.122**	120.462**	49.536**	1.125	11.139**	47.255**
Quadratic fit		1.789	14.701**	31.437**	0.332	0.289	0.589
Cubic fit		0.008	0.864	10.939**	0.379	0.069	0.460
Between samples		4.984**	4.072*	2.567	0.025	1.189	1.011
Total sum of squares		0.00747	0.00505	0.00362	0.0486	0.0277	0.0116

6.2.3 Discussion

The technique has demonstrated that packing behaviour is dependent on deposition method. Fraction B was packed quite uniformly by method (v), the layering method, giving local porosity values ranging from 0.606 to 0.656. Pouring from a jar gave samples of higher porosity but which were only slightly less uniform. The other two deposition methods ((iii) and (iv)) gave samples having a high overall porosity and a much wider range of local porosity. This lack of uniformity can be explained by the observation that deposition took place in discrete streams which tended to form temporary heaps within the sample; these would periodically collapse, causing low kinetic energy secondary deposition, resulting in regions of high porosity. All four methods produced samples in which porosity was strongly dependent on radial position, being low near the centre of the samples, and increasing towards the periphery. A marked linear relationship was present in each case, and as an example, Fig. 6.5 shows grey-scale images of the group filled by method (iii).

The two methods producing the most uniform samples of fraction D were method (v), the layering method, and method (ii), in which powder was discharged from a vertical glass tube. Method (ii), having a high deposition intensity, produced samples of higher overall porosity, which showed a marked linear relationship between local porosity and radial position. Again, low

Fig. 6.5 Grey-scale images, illustrating radial porosity variations in samples of lactose, size fraction B, deposited from a vibrating chute and funnel.

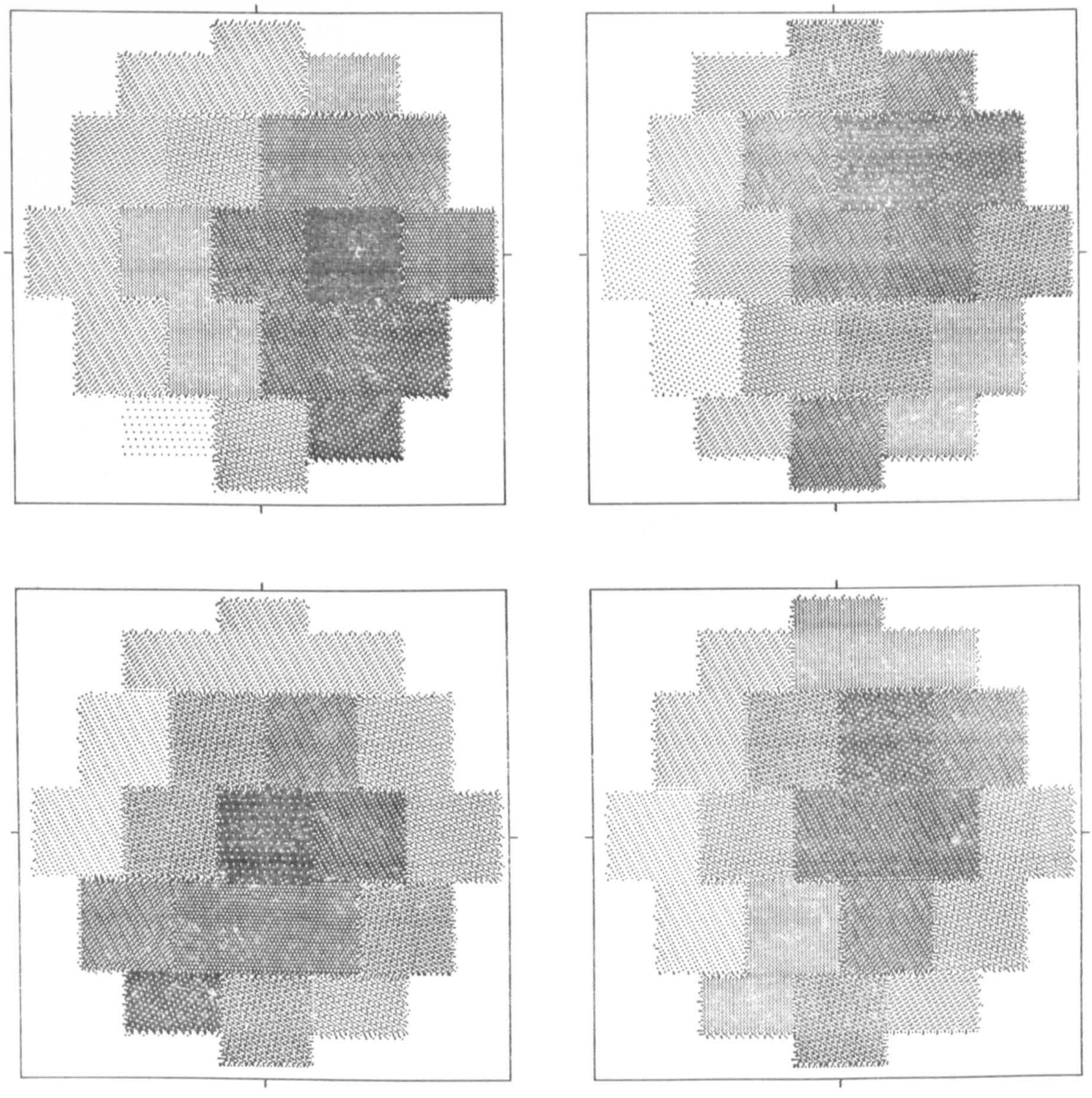

Mid-range porosity = 0.689

Porosity increment = 0.010

porosity occurred in central areas, and increased towards the periphery; this is illustrated in Fig. 6.6. Methods (i) and (iv) produced samples of moderate uniformity showing no marked trends, while method (iii), using the vibrating chute/funnel arrangement, gave samples of very high local porosity variation; in this example, low porosity regions could be readily located, as Fig. 6.7 illustrates. It is possible that the low porosity regions coincide with the positions in the containers at which the major streams of powder were deposited. Low kinetic energy secondary deposition would then lead to surrounding regions of high porosity.

With fraction F, the high intensity methods (i) and (ii) provided samples of high overall porosity and reasonable uniformity. Again, strong position-dependence was observed, porosity increasing with distance from the centre of the samples. Fig. 6.8 is an illustration of this trend. Method (iii) again gave high variability of local porosity, and in this case it appeared to be rather more random (see Fig. 6.9). Methods (iv) and (v) gave samples of moderate to poor uniformity, with porosity again tending to increase with distance from the centre.

On the basis of the above observations, the suitability of each filling method can be assessed to some extent. Method (i), pouring from a jar, was only included to serve as a comparison for other methods. Such a crude

Fig. 6.6 Grey-scale images, illustrating radial porosity variations in samples of lactose, size fraction D, deposited from a vertical glass tube fitted with a 15mm diameter orifice.

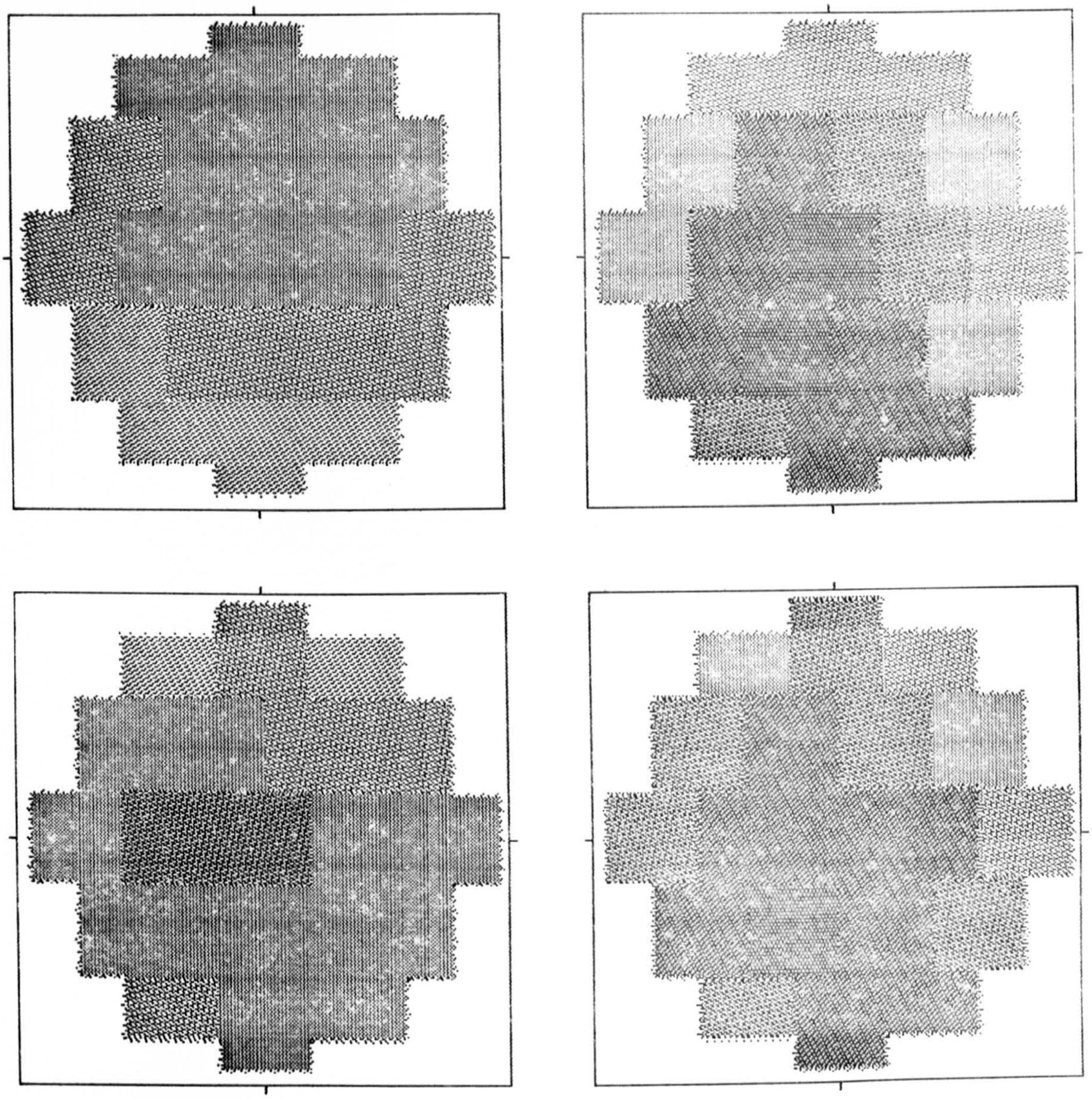

Mid-range porosity = 0.536

Porosity increment = 0.010

Fig. 6.7 Grey-scale images, illustrating radial porosity variations in samples of lactose, size fraction D, deposited from a vibrating chute and funnel.

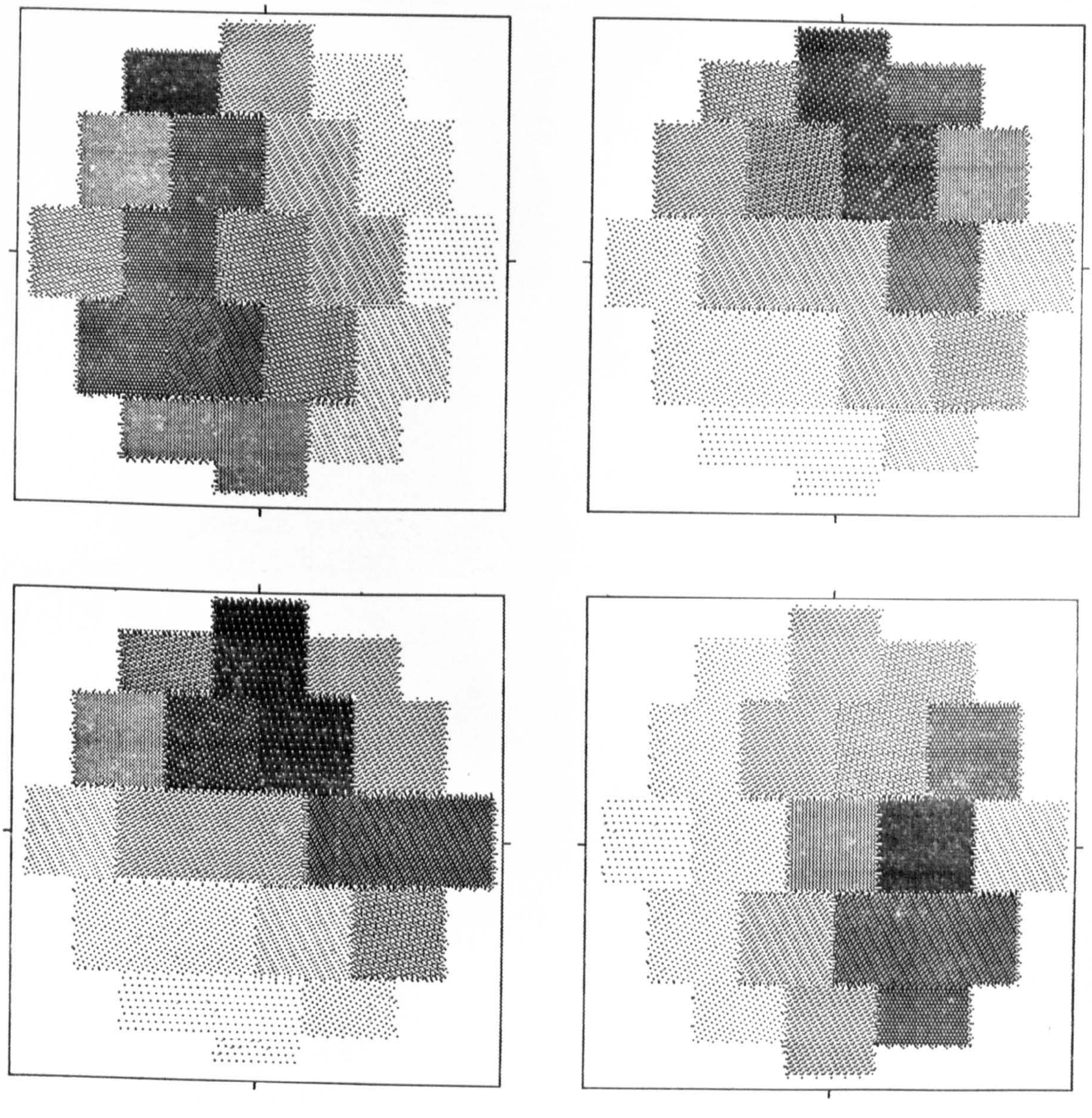

Mid-range porosity = 0.519

Porosity increment = 0.010

Fig. 6.8 Grey-scale images, illustrating radial porosity variations in samples of lactose, size fraction F, deposited from a vertical glass tube fitted with a 4mm diameter orifice.

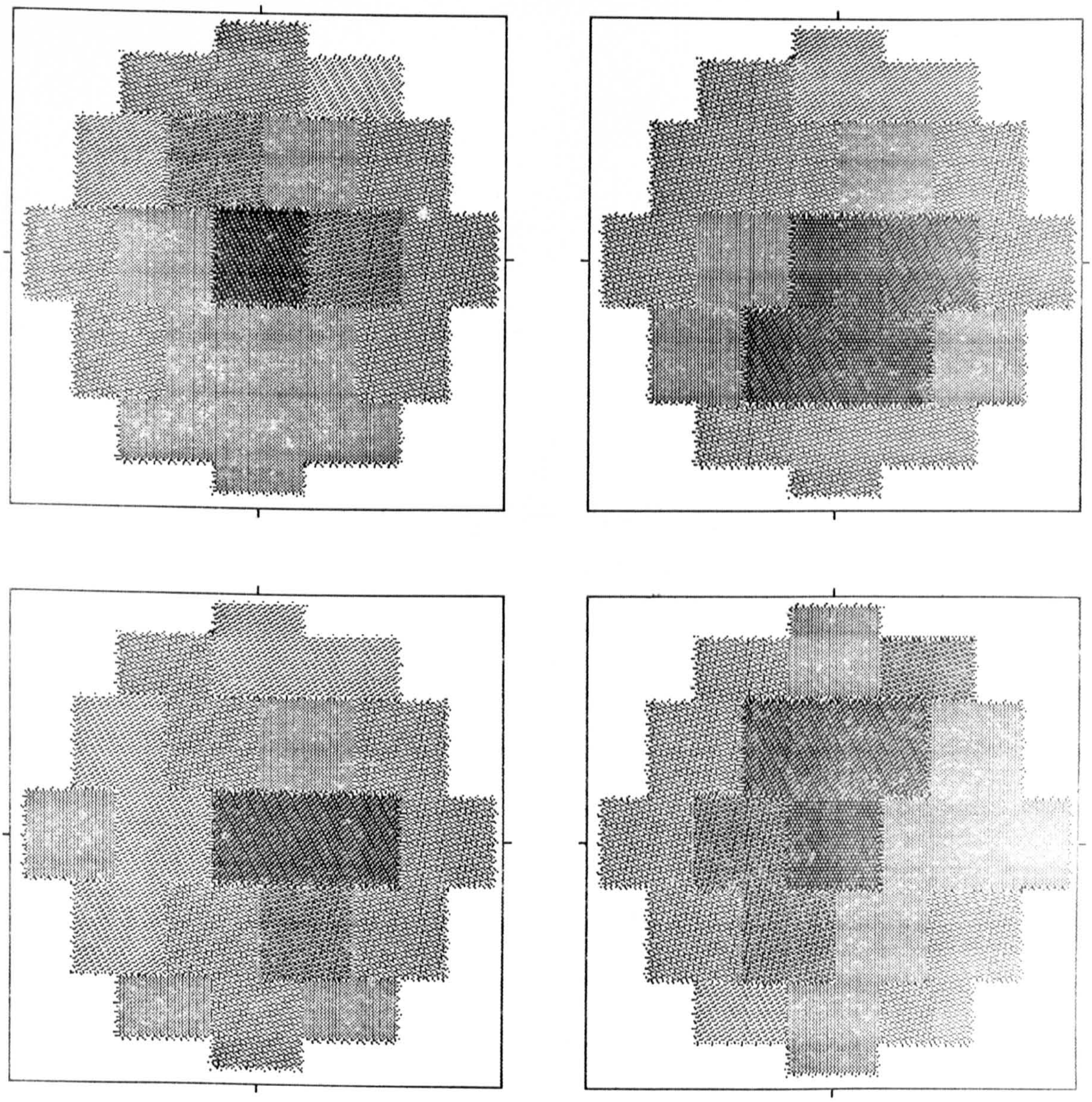

Mid-range porosity = 0.527

Porosity increment = 0.005

Fig. 6.9 Grey-scale images, illustrating radial porosity variations in samples of lactose, size fraction F, deposited from a vibrating chute and funnel.

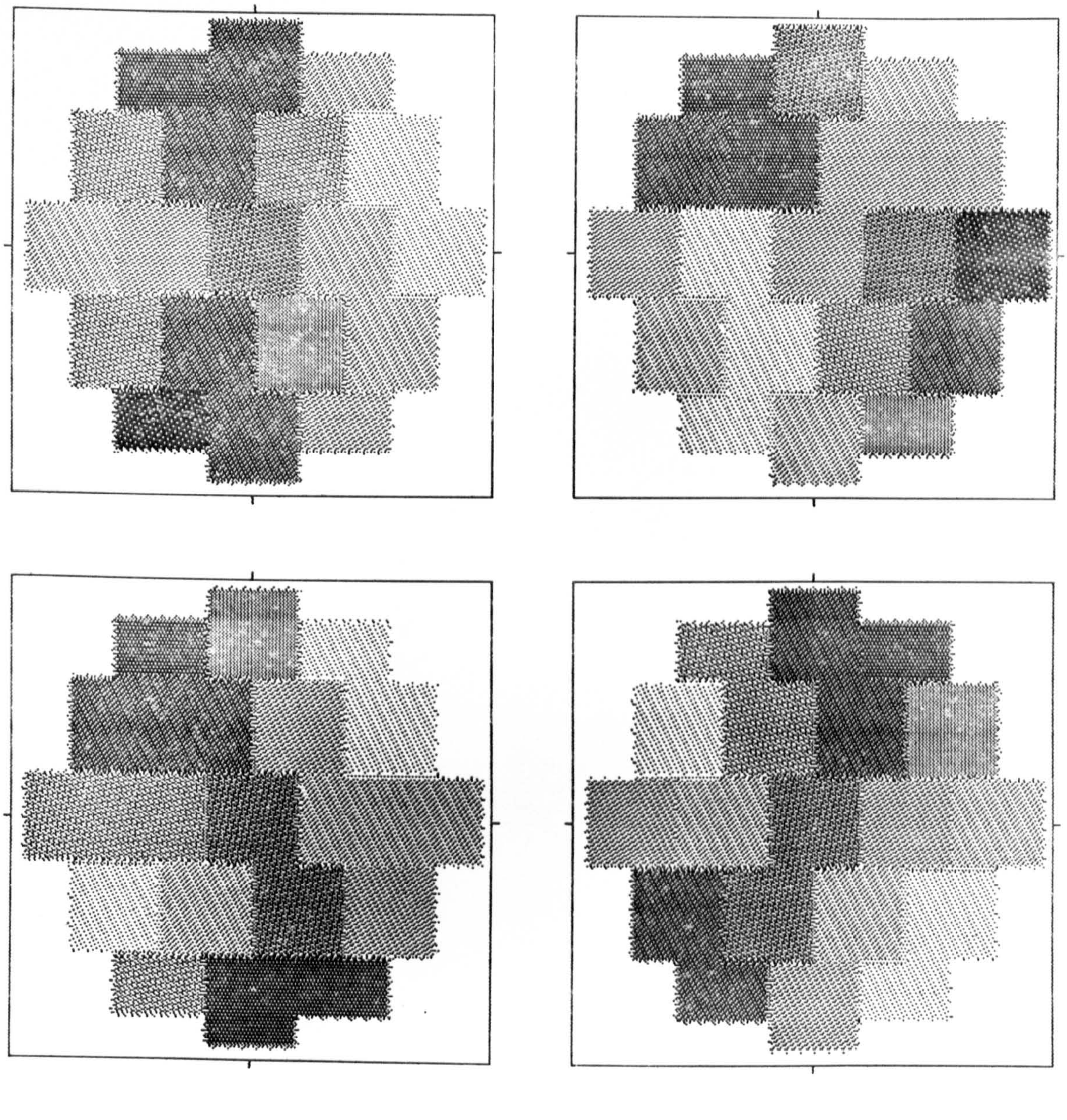

Mid-range porosity = 0.467

Porosity increment = 0.010

method would not be expected to give reproducible, uniform powder beds, but in fact, results have shown that moderately good uniformity can be achieved. Position-dependence can be observed in some cases for reasons which are not immediately obvious. Discharge from the vertical glass tube generally gives samples of quite good uniformity which have relatively dense central regions. This is presumably because the discharging stream is narrower in all cases than the sample container, hence the particles coming to rest near the periphery arrive by rolling outwards from the developing central region. Having less kinetic energy, they form a region of relatively high porosity. In method (iii), powder is discharged from the vibrating chute into a funnel, to emerge in several discrete jets or streams. Consequently, temporary heaps tend to build up and collapse periodically, giving rise to regions of relatively high porosity. Hence, a wide range of local porosity values can be observed. The variability becomes more random with powders of increasing flowability, perhaps because the discharging streams disperse more easily during descent. Method (iv), discharge from the vibrating chute/perforated plate assembly, results in samples of generally high local porosity variation, particularly with fraction B. It was hoped that the streams of powder descending from the plate would disperse and give rise to an even build up of the developing sample. The results suggest that

this does not occur, but that discrete heaps tend to form, as in method (iii). Dependence of porosity on position is present in some but not all cases, which is an indication that the method is generally inconsistent and difficult to reproduce. Method (v), the build-up of samples in layers, consistently produces samples of relatively low overall porosity, and uniformity is generally good. The trend of increasing porosity with increasing distance from the centre, seen with fractions B and F, is difficult to explain, however, since powder is deposited evenly over the whole cross-section of the developing sample.

6.3 Vibrated powder samples

6.3.1 Experimental

(A) Apparatus and materials

The counting system, collimator assembly and deposition apparatus described in earlier chapters were used for these experiments, together with the Derritron vibration system.

Again, lactose particle size fractions B, D and F were chosen for study.

(B) Method of preparing powder samples

The objective of this section of the work was to produce closely packed samples having highly uniform porosity distributions.

For each particle size fraction, a suitable frequency was selected from the findings of Chapter 3 at which to apply vertical vibration. Accelerations of 2g and 6g were evaluated at this frequency, on samples filled by pouring from a jar. A second frequency was chosen and applied at 6g to provide a comparison. Section 6.2 indicated that deposition by layering from a vibrating chute (method (v)), and deposition by discharge from a vertical glass tube (method (ii)), where applicable, generally gave samples of reasonably good uniformity. Therefore, these two methods were used to deposit powder into vibrating containers; it was hoped that simultaneous deposition and vibration would enhance close, uniform packing. Here again, a suitable frequency and an acceleration of 6g were applied. It proved impractical to move a vibrating sample container to and fro beneath a stream of powder falling from the vibrating chute, therefore the chute was hand-held approximately 10cm above the top of the vibrating container and moved manually slowly backwards and forwards, thus building up a powder sample in layers.

In addition to these vertical vibration conditions, a smaller number of experiments were carried out to examine the effect of horizontal vibration on packing uniformity, using a selected frequency, 6g acceleration, and the most promising deposition methods.

Samples were prepared in groups of four, and in each

case, vibration was applied to the container/collar assembly, with a nylon rod (see Chapter 3) resting on the upper surface of the sample. After vibration, the rod and collar were removed, and excess powder was scraped off in the usual way. In all cases, vibration was applied for ten minutes after deposition.

(C) Method of obtaining a porosity distribution } as in
(D) Treatment of results } Section 6.2

6.3.2 Results

The results are shown in Tables 6.8 to 6.13, to which the following key applies:

D/A: DA = vibration during and after deposition
A = vibration after deposition only

H/V: H = horizontal vibration
V = vertical vibration

r = distance from sample centre

* indicates a variance ratio significant at the 5% level

** indicates a variance ratio significant at the 1% level

(Filling methods are described in detail in Chapter 3)

Table 6.8

Porosity data for samples of lactose, fraction B, subjected to vibratory consolidation

	Filling method	(i)	(i)	(i)	(v)	(i)	(v)
	Frequency (Hz)	100	100	150	100	500	500
	Acceleration (g)	2	6	6	6	6	6
	D/A	A	A	A	DA	A	DA
	H/V	V	V	V	V	H	H
	Container						
Overall porosity	1	0.555	0.427	0.449	0.436	0.584	0.542
	2	0.564	0.432	0.479	0.446	0.557	0.531
	3	0.563	0.436	0.470	0.444	0.582	0.534
	4	0.551	0.437	0.490	0.446	0.576	0.534
Mean local porosity	1	0.562	0.419	0.445	0.429	0.487	0.540
	2	0.568	0.429	0.482	0.446	0.563	0.535
	3	0.566	0.433	0.473	0.442	0.589	0.536
	4	0.555	0.435	0.492	0.443	0.579	0.534
Standard deviation of local porosity	1	0.0036	0.0071	0.0039	0.0033	0.0097	0.0047
	2	0.0029	0.0038	0.0037	0.0058	0.0114	0.0068
	3	0.0042	0.0056	0.0038	0.0033	0.0077	0.0074
	4	0.0040	0.0048	0.0036	0.0040	0.0093	0.0059

Table 6.9

Analyses of variance of local porosity in vibratory consolidated samples of lactose, fraction B

Filling method	(i)	(i)	(i)	(v)	(i)	(v)
Frequency (Hz)	100	100	150	100	500	500
Acceleration (g)	2	6	6	6	6	6
D/A	A	A	A	DA	A	DA
H/V	V	V	V	V	H	H
Grand mean porosity	0.563	0.429	0.473	0.440	0.579	0.536
Minimum local value	0.548	0.404	0.438	0.423	0.531	0.525
Maximum local value	0.573	0.447	0.502	0.460	0.600	0.555
Mean local porosity r = 0mm	0.560	0.421	0.472	0.437	0.591	0.532
Mean local porosity r = 4mm	0.564	0.427	0.476	0.441	0.586	0.536
Mean local porosity r = 7mm	0.562	0.430	0.473	0.440	0.575	0.536
Mean local porosity r = 8mm	0.563	0.431	0.471	0.440	0.575	0.538
Variance ratios:						
Distance from centre	2.679	5.973**	4.570**	0.689	11.919**	0.964
Linear fit	0.311	12.917**	9.275**	0.049	26.292**	1.319
Quadratic fit	1.442	1.811	3.304	0.226	9.455**	0.044
Cubic fit	6.284*	3.191	1.132	1.792	0.010	1.528
Between samples	40.187**	36.875**	89.886**	36.994**	38.535**	3.459*
Total sum of squares	0.00266	0.00516	0.0241	0.00456	0.0148	0.00343

Table 6.10

Porosity data for samples of lactose, fraction D, subjected to vibratory consolidation

	Filling method	(i)	(i)	(i)	(iib)	(v)	(i)	(iib)	(v)
	Frequency (Hz)	200	200	100	100	100	100	100	100
	Acceleration (g)	2	6	6	6	6	6	6	6
	D/A	A	A	A	DA	DA	A	DA	DA
	H/V	V	V	V	V	V	H	H	H
	Container								
Overall porosity	1	0.503	0.406	0.393	0.400	0.403	0.461	0.461	0.425
	2	0.503	0.404	0.392	0.397	0.397	0.471	0.440	0.427
	3	0.498	0.409	0.389	0.397	0.396	0.481	0.454	0.424
	4	0.502	0.411	0.395	0.401	0.395	0.448	0.461	0.414
Mean local porosity	1	0.506	0.401	0.388	0.394	0.399	0.459	0.456	0.418
	2	0.506	0.403	0.391	0.393	0.394	0.475	0.438	0.424
	3	0.502	0.409	0.385	0.393	0.393	0.484	0.454	0.419
	4	0.501	0.406	0.393	0.396	0.392	0.451	0.462	0.409
Standard deviation of local porosity	1	0.0038	0.0042	0.0052	0.0030	0.0036	0.0119	0.0047	0.0064
	2	0.0051	0.0027	0.0039	0.0041	0.0040	0.0170	0.0041	0.0056
	3	0.0019	0.0032	0.0038	0.0039	0.0046	0.0042	0.0044	0.0051
	4	0.0035	0.0049	0.0039	0.0037	0.0034	0.0084	0.0040	0.0045

Table 6.11

Analyses of variance of local porosity in vibratory consolidated samples of lactose, fraction D

Filling method	(i)	(i)	(i)	(iib)	(v)	(i)	(iib)	(v)
Frequency (Hz)	200	200	100	100	100	100	100	100
Acceleration (g)	2	6	6	6	6	6	6	6
D/A	A	A	A	DA	DA	A	DA	DA
H/V	V	V	V	V	V	H	H	H
Grand mean porosity	0.504	0.405	0.389	0.394	0.395	0.467	0.453	0.418
Minimum local value	0.493	0.393	0.375	0.385	0.386	0.438	0.431	0.402
Maximum local value	0.517	0.417	0.400	0.405	0.407	0.497	0.470	0.437
Mean local porosity r = 0mm	0.499	0.406	0.388	0.396	0.395	0.467	0.453	0.418
Mean local porosity r = 4mm	0.502	0.406	0.391	0.395	0.396	0.470	0.453	0.421
Mean local porosity r = 7mm	0.505	0.404	0.388	0.392	0.394	0.467	0.451	0.417
Mean local porosity r = 8mm	0.505	0.404	0.389	0.394	0.395	0.466	0.455	0.415
Variance ratios:								
Distance from centre	5.241**	1.570	3.241*	3.635*	0.901	0.429	2.764*	21.297**
Linear fit	7.334**	4.045*	3.425	2.596	0.579	0.881	2.248	53.057**
Quadratic fit	7.937**	0.627	1.763	7.755**	1.741	0.100	5.592*	9.710**
Cubic fit	0.451	0.038	4.535*	0.556	0.382	0.306	0.451	1.123
Between samples	9.737**	14.667**	12.382**	2.806*	10.506**	31.202**	99.438**	41.374**
Total sum of squares	0.00145	0.00180	0.00202	0.00131	0.00167	0.0230	0.00752	0.00440

Table 6.12

Porosity data for samples of lactose, fraction F, subjected to vibratory consolidation

	Filling method	(i)	(i)	(i)	(iib)	(v)	(iib)	(v)
	Frequency (Hz)	150	150	200	150	150	120	120
	Acceleration (g)	2	6	6	6	6	6	6
	D/A	A	A	A	DA	DA	DA	DA
	H/V	V	V	V	V	V	H	H
	Container							
Overall porosity	1	0.496	0.404	0.411	0.406	0.402	0.436	0.421
	2	0.508	0.405	0.474	0.397	0.400	0.432	0.414
	3	0.506	0.418	0.416	0.406	0.410	0.434	0.414
	4	0.512	0.409	0.422	0.409	0.404	0.434	0.418
Mean local porosity	1	0.496	0.398	0.407	0.401	0.396	0.430	0.414
	2	0.511	0.403	0.426	0.395	0.399	0.429	0.408
	3	0.509	0.418	0.417	0.405	0.410	0.430	0.409
	4	0.516	0.408	0.421	0.406	0.404	0.429	0.412
Standard deviation of local porosity	1	0.0048	0.0035	0.0037	0.0026	0.0025	0.0057	0.0087
	2	0.0074	0.0031	0.0057	0.0029	0.0030	0.0061	0.0090
	3	0.0033	0.0028	0.0043	0.0031	0.0020	0.0053	0.0096
	4	0.0036	0.0023	0.0047	0.0034	0.0042	0.0054	0.0083

Table 6.13

Analyses of variance of local porosity in vibratory consolidated samples of lactose, fraction F

Filling method		(i)	(i)	(i)	(iib)	(v)	(iib)	(v)
Frequency (Hz)		150	150	200	150	150	120	120
Acceleration (g)		2	6	6	6	6	6	6
D/A		A	A	A	DA	DA	DA	DA
H/V		V	V	V	V	V	H	H
Grand mean porosity		0.508	0.407	0.418	0.402	0.402	0.429	0.411
Minimum local value		0.487	0.391	0.402	0.388	0.391	0.419	0.397
Maximum local value		0.521	0.422	0.437	0.413	0.414	0.444	0.450
Mean local porosity	r = 0mm	0.507	0.408	0.418	0.401	0.404	0.434	0.403
	r = 4mm	0.508	0.408	0.421	0.402	0.404	0.430	0.406
	r = 7mm	0.508	0.406	0.417	0.402	0.401	0.425	0.409
	r = 8mm	0.508	0.407	0.415	0.401	0.401	0.433	0.421
Variance ratios:								
Distance from centre		0.102	2.898*	6.263**	0.575	4.570**	13.602**	18.664**
Linear fit		0.109	3.737	15.254**	0.853	9.275**	5.359*	52.576**
Quadratic fit		0.011	4.689*	0.712	0.040	3.304	35.394**	3.023
Cubic fit		0.187	0.267	2.823	0.831	1.132	0.052	0.393
Between samples		97.465**	155.854**	69.724**	43.804**	89.886**	0.591	1.122
Total sum of squares		0.00520	0.00469	0.00555	0.00197	0.00313	0.00244	0.00759

6.3.3 Discussion

The first impression gained from this series of results, is that vibratory consolidation, as well as reducing the overall porosity of a powder sample, also improves the uniformity of packing. However, some conditions of vibration are more successful than others in reducing local porosity variations.

Fraction B, being considerably more cohesive than the other two, is rather less susceptible to vibratory consolidation; the overall porosities obtained are not as low as those achieved with fractions D and F. However, a good degree of uniformity is achieved within individual samples, particularly using vertical vibration. For example, deposition method (v), coupled with vibration at 100 Hz/6g gave a set of four samples showing a range of local porosity of 0.423 to 0.460. If this is compared with the range observed with deposition method (iii) in section 6.2, which was 0.628 to 0.750, it is clear that a marked improvement in uniformity can readily be achieved. An acceleration of 2g resulted in a higher overall porosity, but a low level of local variation, comparable to that attained with 6g. With all the vertically vibrated samples of fraction B, the majority of the variability occurred between individual samples in a set, as reflected in the very high between-samples variance ratios, and as exemplified by Fig. 6.10. Horizontal vibration was not only less effective in

Fig. 6.10 Grey-scale images, illustrating radial porosity variations in samples of lactose, size fraction B, deposited by pouring from a jar, followed by vertical vibration at 150Hz and 6g.

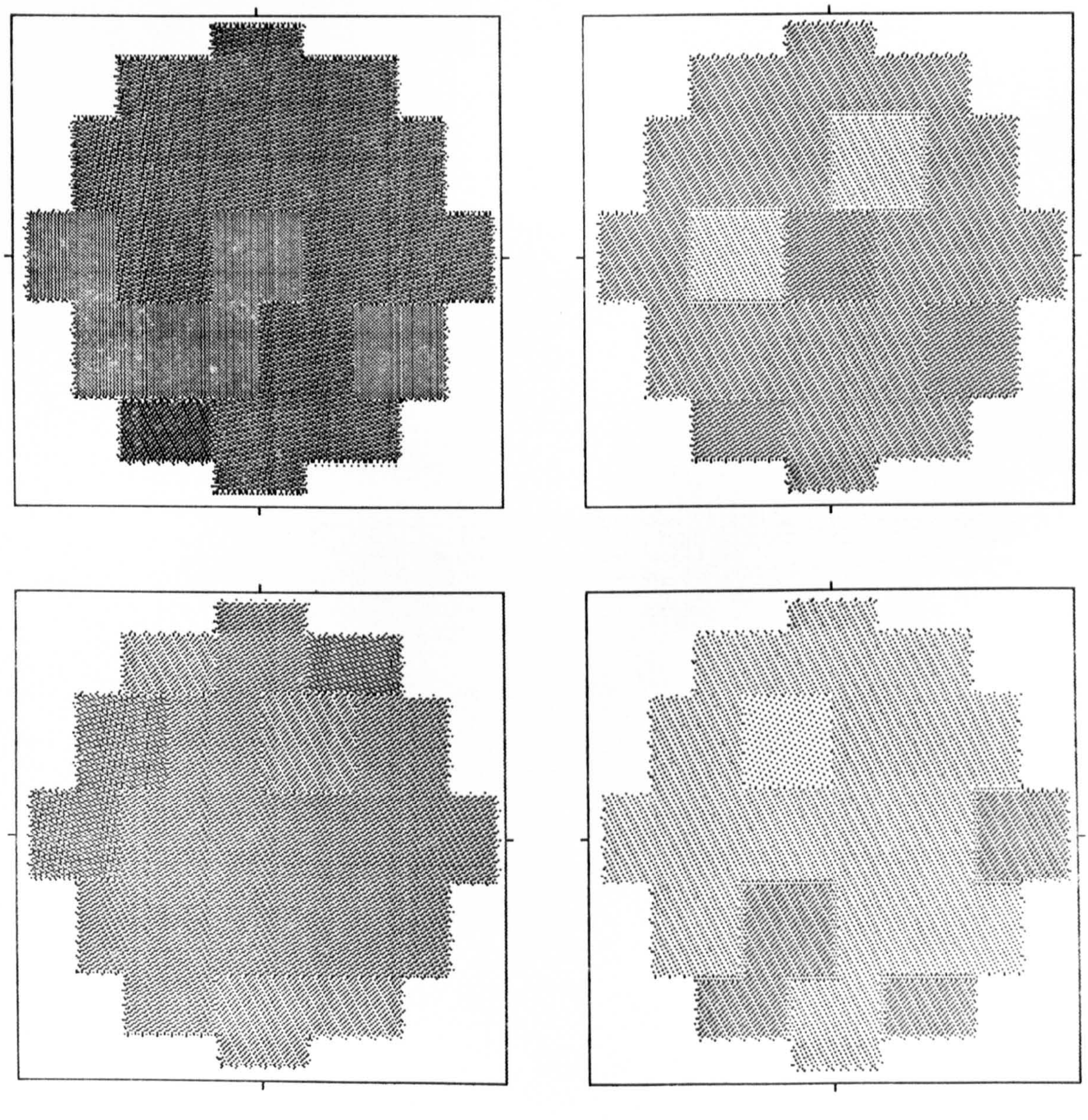

Mid-range porosity = 0.449

Porosity increment = 0.010

reducing porosity than vertical vibration, but individual samples also tended to pack less uniformly. It should be noted, however, that deposition method (v), with horizontal vibration at 500 Hz and 6g, gave four samples of moderately low within-samples porosity variation. When added to the fact that the overall porosities of the four samples were very similar, the total variability, as reflected by the range of local porosity, was in fact very low. Fig. 6.11 contains images of these four samples.

With fraction D, an overall porosity of about 0.4 could be achieved under various conditions, providing a vertical vibration of 6g acceleration was included. Low variability within individual samples was a consistent result of such experiments. Between-samples variance, although the dominant component in most instances, was low enough to maintain a narrow range of local porosity values. Application of 2 g acceleration yielded similar results, but at a higher overall level of porosity. An example of vibrated samples of fraction D is illustrated by the images in Fig. 6.12, which are those of samples deposited from the glass tube and 12mm orifice, into containers vibrating at 100Hz and 6g. Once again, horizontal vibration gave samples of somewhat higher porosity, and deposition from a jar followed by vibration at 100Hz and 6g produced a set of samples of rather high variability, the majority of

Fig. 6.11 Grey-scale images, illustrating radial porosity variations in samples of lactose, size fraction B, deposited by layering from a vibrating chute into containers vibrating horizontally at 500Hz and 6g.

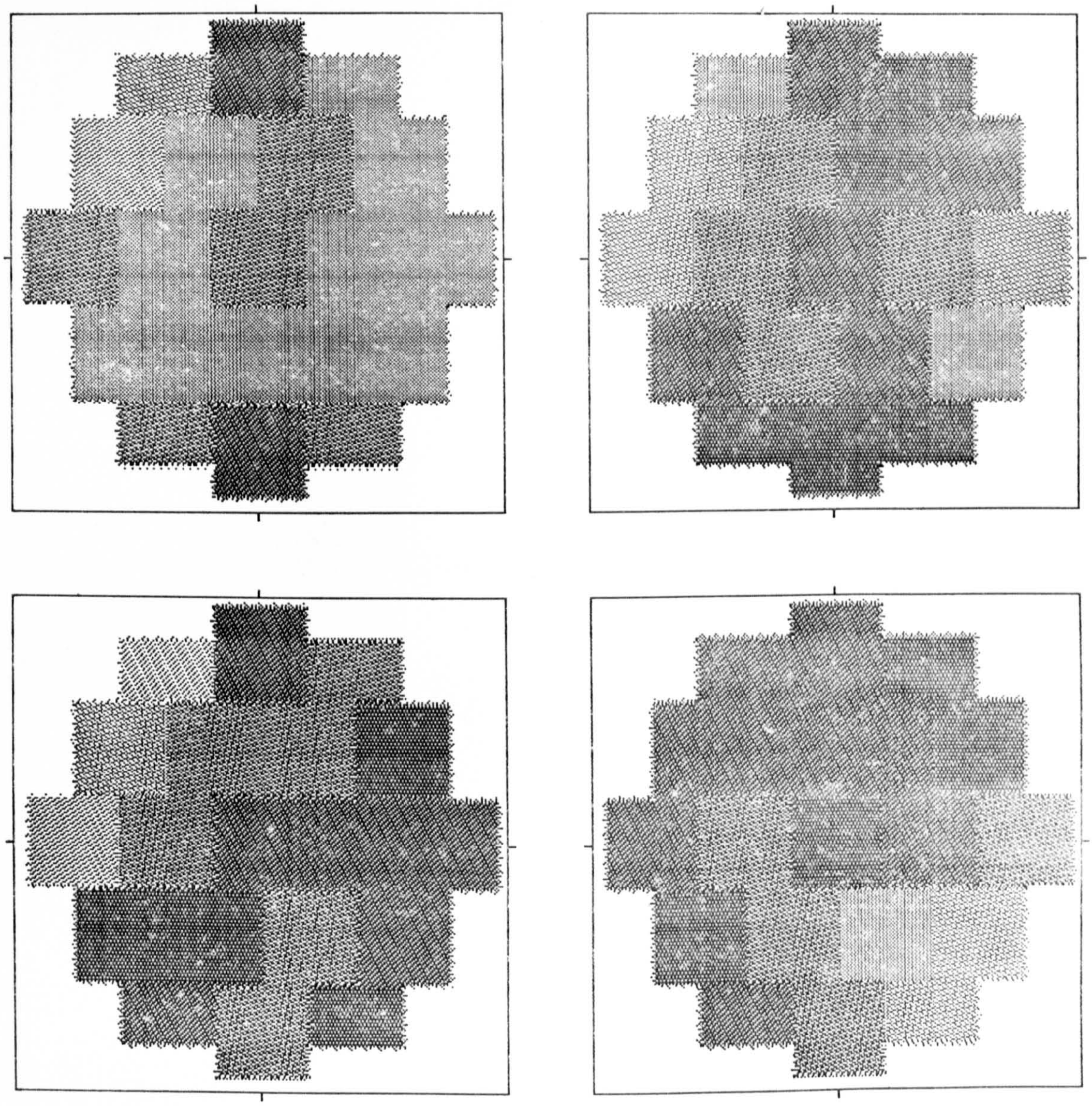

Mid-range porosity = 0.540

Porosity increment = 0.005

Fig. 6.12 Grey scale images, illustrating radial porosity variations in samples of lactose, size fraction D, deposited from a vertical glass tube, fitted with a 12mm orifice, into containers vibrating vertically at 100Hz and 6g.

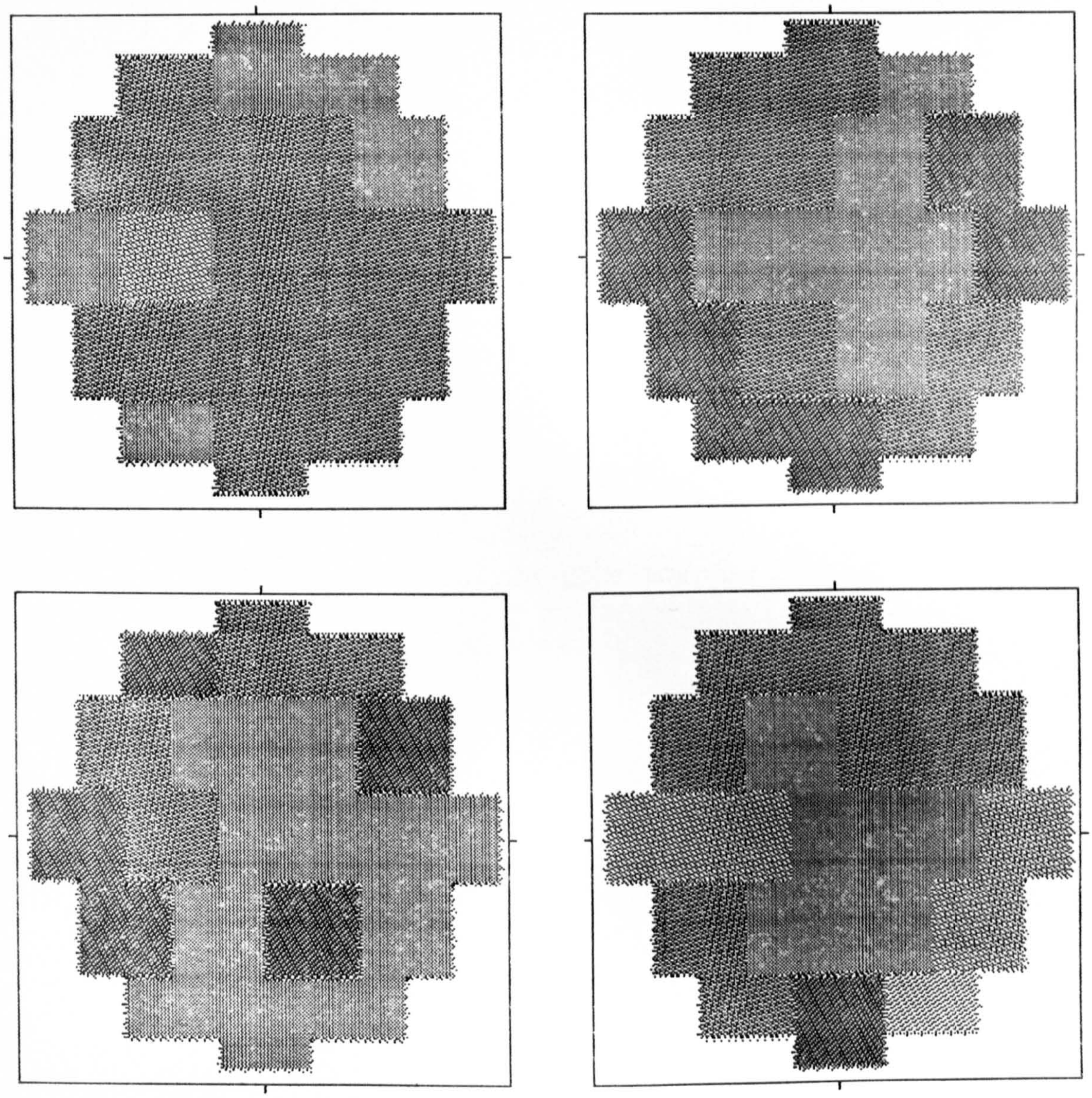

Mid-range porosity = 0.395

Porosity increment = 0.005

which occurred between samples (see Fig. 6.13). Interestingly, the total variability could be reduced by employing either of deposition methods (ii) and (v), with the same horizontal vibration conditions, although highly significant between-samples variance ratios were still obtained (see Table 6.11).

Vertically vibrated samples of fraction F all possessed low within-samples porosity variation, and relatively low overall variability. In all cases, between-samples variance ratios were highly significant, but as Fig. 6.14 illustrates, the physical effect of this is not necessarily very marked, and in this example, a reasonably narrow range of local porosity of 0.388 to 0.413 was recorded. The effect of horizontal vibration on the packing uniformity of fraction F was interesting. Deposition from a jar followed by vibration at 120Hz and 6g gave samples of such widely differing and irreproducible overall porosities that local porosities were not measured. However, on changing to deposition methods (ii) and (v), very low between-samples variance was achieved, and strong position-dependence appeared. Method (v), layering into containers vibrating horizontally at 120Hz and 6g, gave samples in which there was a strongly linear relationship between local porosity and distance from the sample centre (see Fig. 6.15). A similar effect was seen using fraction D (see Tables 6.11 and 6.13).

Fig. 6.13 Grey-scale images, illustrating radial porosity variations in samples of lactose, size fraction D, deposited by pouring from a jar, followed by horizontal vibration at 100Hz and 6g.

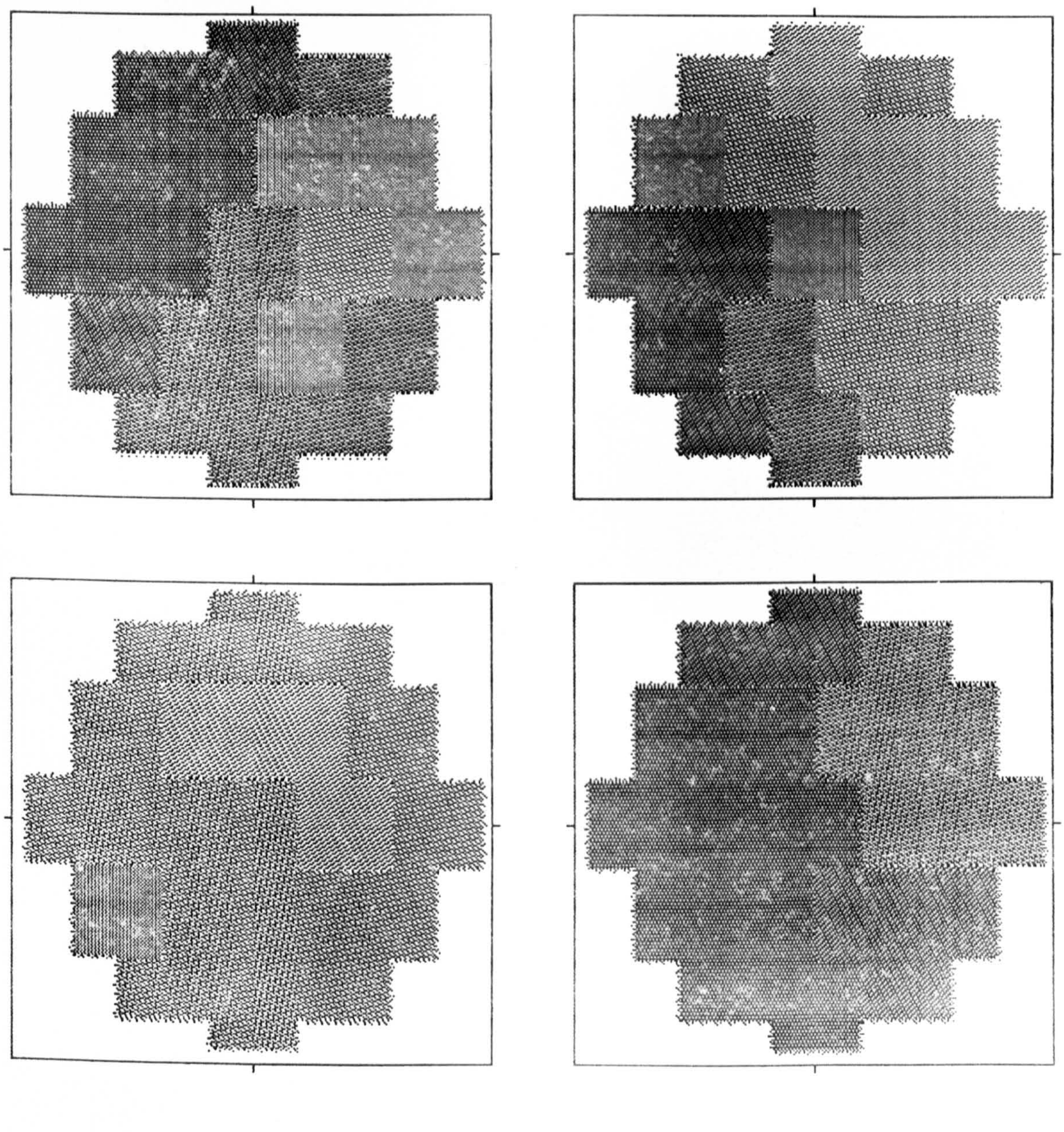

Mid-range porosity = 0.468

Porosity increment = 0.010

Fig. 6.14 Grey-scale images, illustrating radial porosity variations in samples of lactose, size fraction F, deposited from a vertical glass tube, fitted with a 4mm orifice, into containers vibrating vertically at 150Hz and 6g.

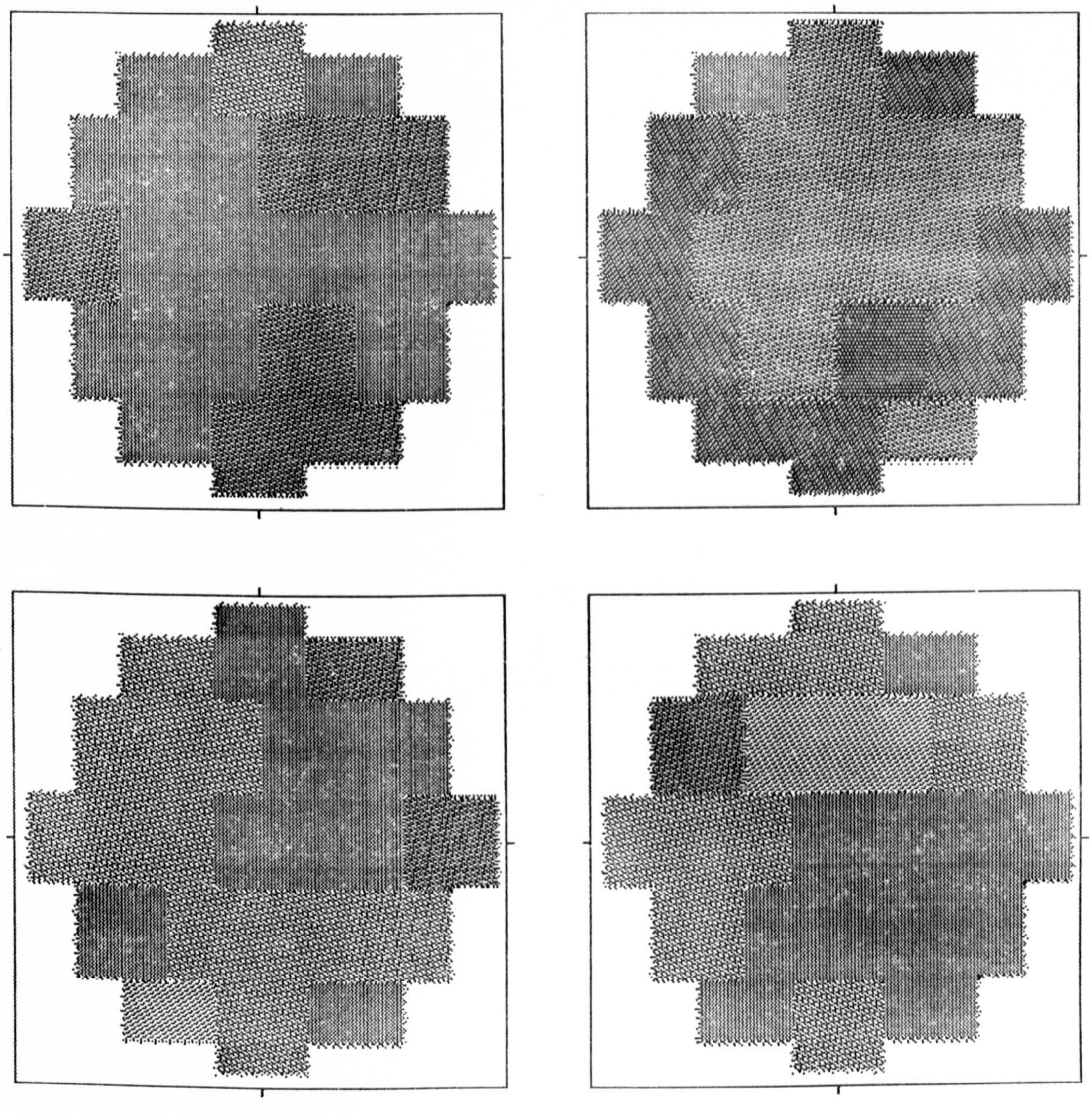

Mid-range porosity = 0.401

Porosity increment = 0.005

Fig. 6.15 Grey-scale images, illustrating radial porosity variations in samples of lactose, size fraction F, deposited by layering from a vibrating chute into containers vibrating horizontally at 120Hz and 6g.

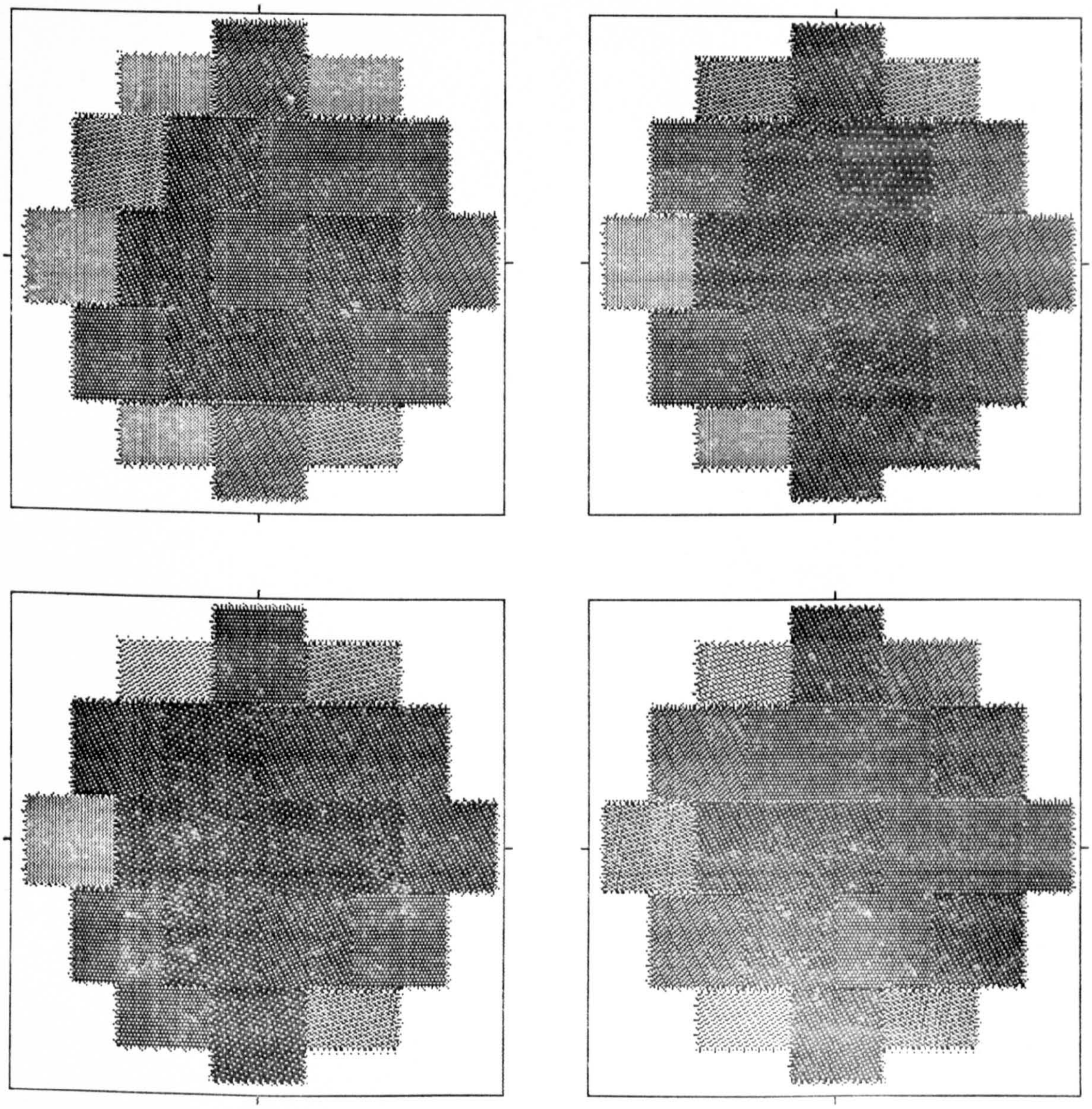

Mid-range porosity = 0.423

Porosity increment = 0.005

It may be that this effect is caused by particles striking the rim of the container and bouncing onto the developing sample surface at a lower velocity than intended. If such particles were to deposit near the periphery of the sample, a relatively high porosity could result in that region.

6.4 The effect of light compression

In Chapter 1, it was noted that compression can be shown to improve the uniformity of packing of particulate materials (Stanley-Wood, 1978), although Train (1957) found that the application of a uniaxial stress to a mass of powder gave rise to a definite stress destribution within the mass, resulting in a similarly non-uniform distribution of density.

Experiments were therefore carried out to investigate the effect of light compression on the distribution of porosity within samples of lactose.

6.4.1 Experimental

(A) Apparatus and materials

The gamma-counting system described previously was used, together with lactose particle size fractions B,D and F.

Dead weight loads of between 100g and 1kg were applied vertically to samples contained in aluminium cylinders.

(B) Method of preparing compressed samples

Four sample containers were filled with lactose by pouring from a jar as described in Chapter 3. After removing excess powder with a spatula blade, each sample was weighed, then a nylon rod (also described in Chapter 3) was carefully positioned on the surface of the sample, and a weight was placed on top of the rod. A travelling microscope was used to measure the depression of the rod and hence the compression of the sample, enabling the resulting overall porosity of the sample to be calculated. The weight and the nylon rod were then removed. The four samples were loaded with weights of 100g, 200g, 500g and 1000 g respectively, plus the weight of the nylon rod in each case (12g). The applied compressive stress was calculated by dividing the load by the cross-sectional area of the sample.

(C) Method of obtaining a porosity distribution

For each sample, a value of $N_{o_{min}}$ was calculated, using equation (6.8). Overall porosity, ε , and apparent thickness of sample, L, were determined from the observed compression of the sample, whilst the attenuation coefficient of lactose, μ , was taken to be $0.3cm^{-1}$. The probability level, p, was set at 1.96 and as before, confidence limits of $\Delta\varepsilon = \pm 0.005$ were chosen.

Having calculated suitable counting intervals, the distribution of porosity in each sample was determined by the method described in section 6.2(C).

(D) Treatment of results

The calculation of local proosity values at each counting position, together with corresponding confidence intervals, were calculated using the computer program described in section 6.2(D).

For each sample, nineteen local porosity values were obtained, and from each set of values, a mean and standard deviation were calculated.

6.4.2 Results and discussion

The results of applying relatively small compressive stresses to samples of lactose fractions B, D and F are illustrated in Table 6.14, where:

ε_1 = overall porosity of sample before compression

ε_2 = overall porosity of sample after compression

$\bar{\varepsilon}$ = mean local porosity after compression

σ_ε = standard deviation of local porosity after compression

The effect of light compression is, of course, to reduce overall porosity. Samples of free-flowing powders tend to be less porous initially than more cohesive materials, hence these samples are more stable and less susceptible to compression. Thus, while a stress of $35 kNm^{-2}$ reduced the porosity of a sample of fraction B from 0.67 to 0.54, the same stress, applied

Table 6.14

The effect of light compression on the distribution of porosity in lactose samples

Size Fraction		Compressive stress (kNm^{-2}) 3.88	7.34	17.72	35.02
B	ε_1	0.672	0.667	0.673	0.667
	ε_2	0.603	0.579	0.561	0.538
	$\bar{\varepsilon}$	0.607	0.582	0.567	0.541
	σ_ε	0.0055	0.0051	0.0036	0.0043
D	ε_1	0.568	0.568	0.560	0.565
	ε_2	0.514	0.509	0.496	0.495
	$\bar{\varepsilon}$	0.517	0.511	0.498	0.497
	σ_ε	0.0060	0.0070	0.0050	0.0034
F	ε_1	0.520	0.517	0.519	0.513
	ε_2	0.502	0.496	0.494	0.489
	$\bar{\varepsilon}$	0.502	0.496	0.495	0.489
	σ_ε	0.0089	0.0116	0.0078	0.0053

to a sample of fraction F, only reduced its porosity from 0.51 to 0.49.

Light compression also resulted in increased uniformity of local porosity,as can be seen by comparing the σ_ε values in Table 6.14 with corresponding data in Tables 6.2, 6.4, and 6.6. This effect was much less marked in the case of fraction F than with the other two more cohesive, materials, again indicating that such relatively small compression stresses can cause only slight changes in an existing packing of this free-flowing material.

6.5 Variation of porosity with depth in vibrated samples

Van Brakel and Heertjes (1974) used an X-ray attenuation technique to measure porosity variations down the depth of samples of particulate materials, and used their measurements to assess various methods of deposition and vibration. They concluded that deposition from a certain height, and with a certain intensity, into containers undergoing horizontal vibration, was most successful in obtaining homogeneous packings. The use of vertical vibration resulted in less homogeneity, with porosity being dependent on depth.

Therefore, a short experiment was carried out to test whether similar observations could be obtained using lactose.

6.5.1 Experimental

(A) Apparatus and materials

The source, collimators, detector and counting system described previously were again used, but now, in order to direct the gamma-ray beam horizontally through a sample, the apparatus was arranged as shown in Fig. 6.16. The micromanipulator was mounted on a second steel plate, so that accurate positioning of the sample could still be carried out. An aluminium cylinder and the extension collar were again used to contain the samples, and the Derritron vibration system was again utilised.

Particle size fraction F was chosen for this experiment.

(B) Method of preparing powder samples

One sample was prepared by pouring powder into the container/collar assembly until full, and vibrating it vertically at 150Hz and 6g for ten minutes, using the nylon rod to maintain a level sample surface. A second sample was prepared similarly, except that horizontal vibration of 120Hz and 6g was employed. In both cases, the collar was left in position after vibration, resulting in a sample 5-6cm deep.

(C) Method of obtaining local porosity values

The attenuating thickness of powder across a diameter of the container was now only about 1.9cm;

Fig. 6.16 Experimental arrangement for horizontal irradiation of powder samples

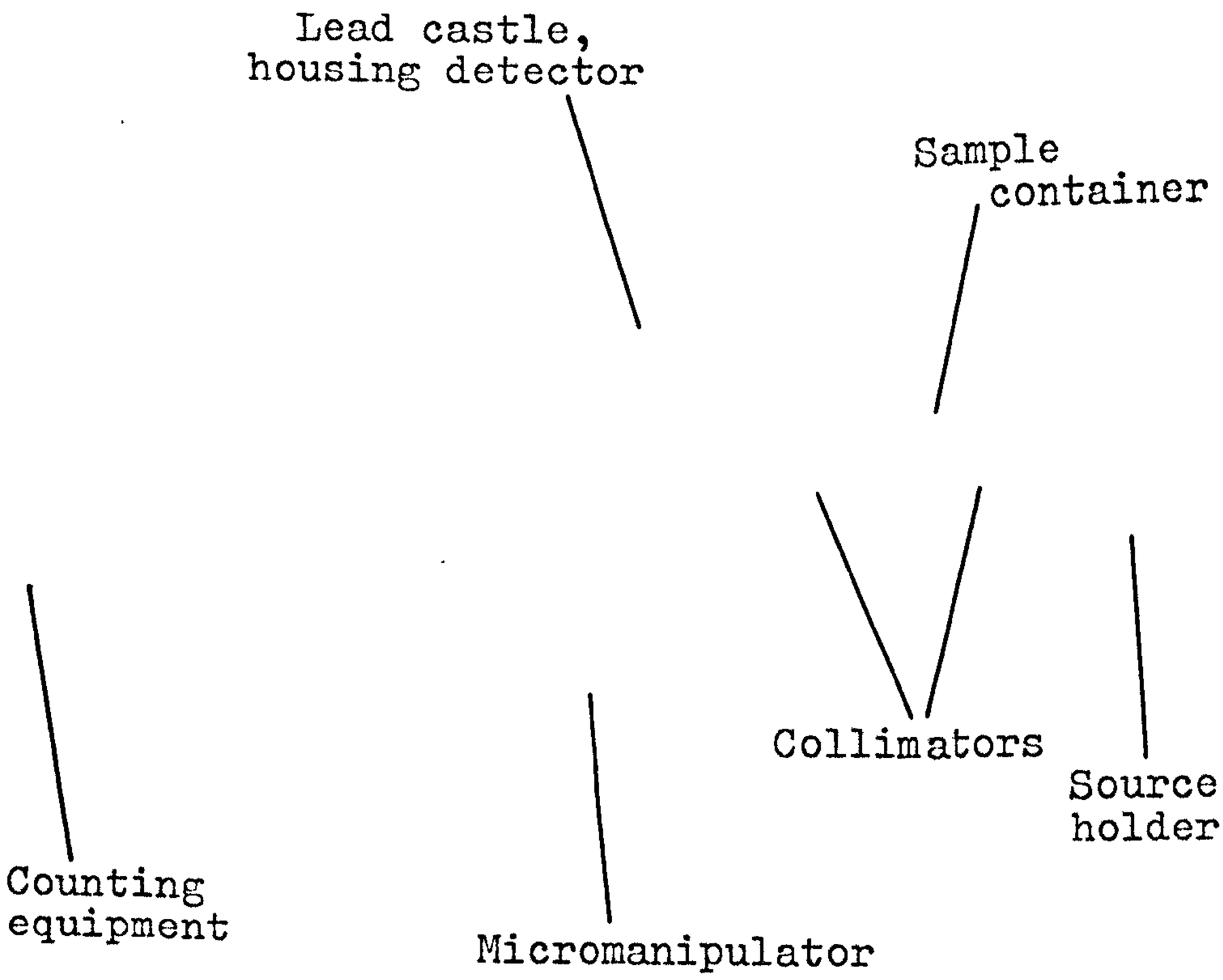

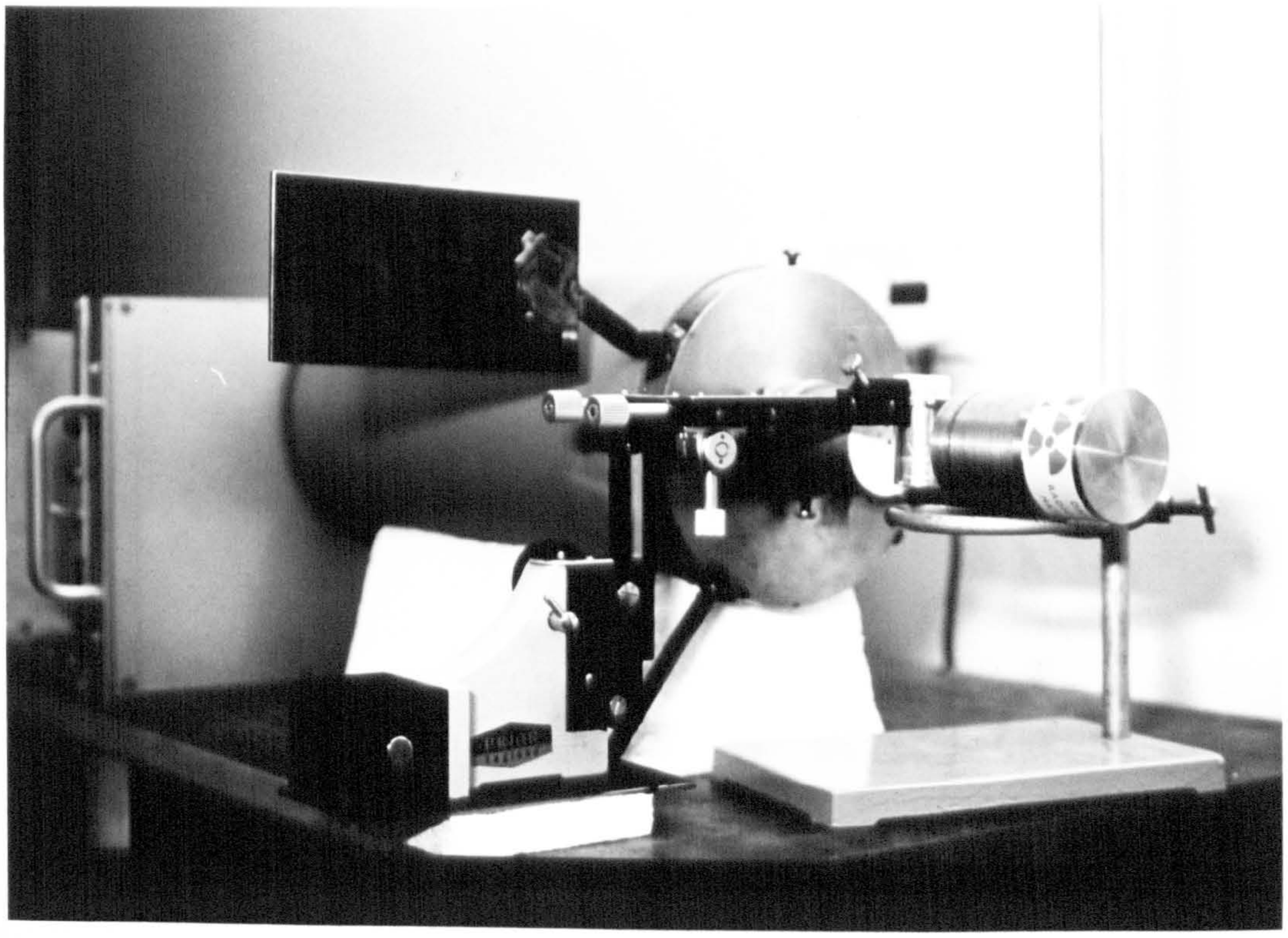

this resulted in a much higher value of $N_{o_{min}}$ than was necessary for making vertical measurements. Despite this, $\Delta\varepsilon$ was again set at 0.005 and p at 1.96.

Having calculated $N_{o_{min}}$, the sample was clamped to the micromanipulator using the steel ring and peg described earlier. A travelling microscope aided positioning of the container so that the beam passed across a diameter, in each vertical position of the sample, and the lateral position of the container was adjusted so that it was roughly central between the two collimators. Alternate "sample" and "blank" counts of the required duration were then recorded. Sample counts were taken at six positions down the depth of the sample; blanks consisted of counts recorded through an empty container.

(D) Treatment of results

Local porosities were calculated using the following equation:

$$\varepsilon = 1 - \frac{\ln \frac{N_o}{N}}{\mu L} \qquad (6.1)$$

combined with the calibration expression for μ:

$$\mu = (0.289 + 0.0215\varepsilon)\,cm^{-1} \qquad (5.12)$$

The iterative method for calculating ε is described in

section 6.2, as is the method for re-calculating the 95% confidence intervals.

6.5.2 Results and discussion

The local porosities obtained for the vertically vibrated and horizontally vibrated samples are shown in Figs. 6.17 and 6.18.

From the limited amount of data available, it can be seen that the porosity of the horizontally vibrated sample varied little in the lower half, but decreased sharply towards the top. The vertically vibrated sample, on the other hand, exhibited a gradual increase in porosity from the centre downwards. On the whole, less variation was observed in the vertically vibrated sample.

If horizontally vibrated samples always pack in this manner, it is easy to see why the procedure adopted in earlier experiments results in samples of relatively high porosity; the low porosity upper region of the sample is scraped off after removing the collar, and the remaining sample is of considerably higher porosity. This effect is much less marked in the case of vertically vibrated samples.

6.6 Conclusions

The results of the work described in this chapter give an indication of how best to deposit powders in order to achieve uniform packing, and also show that

Fig. 6.17 The variation of porosity with depth in a vertically vibrated sample of lactose, size fraction F

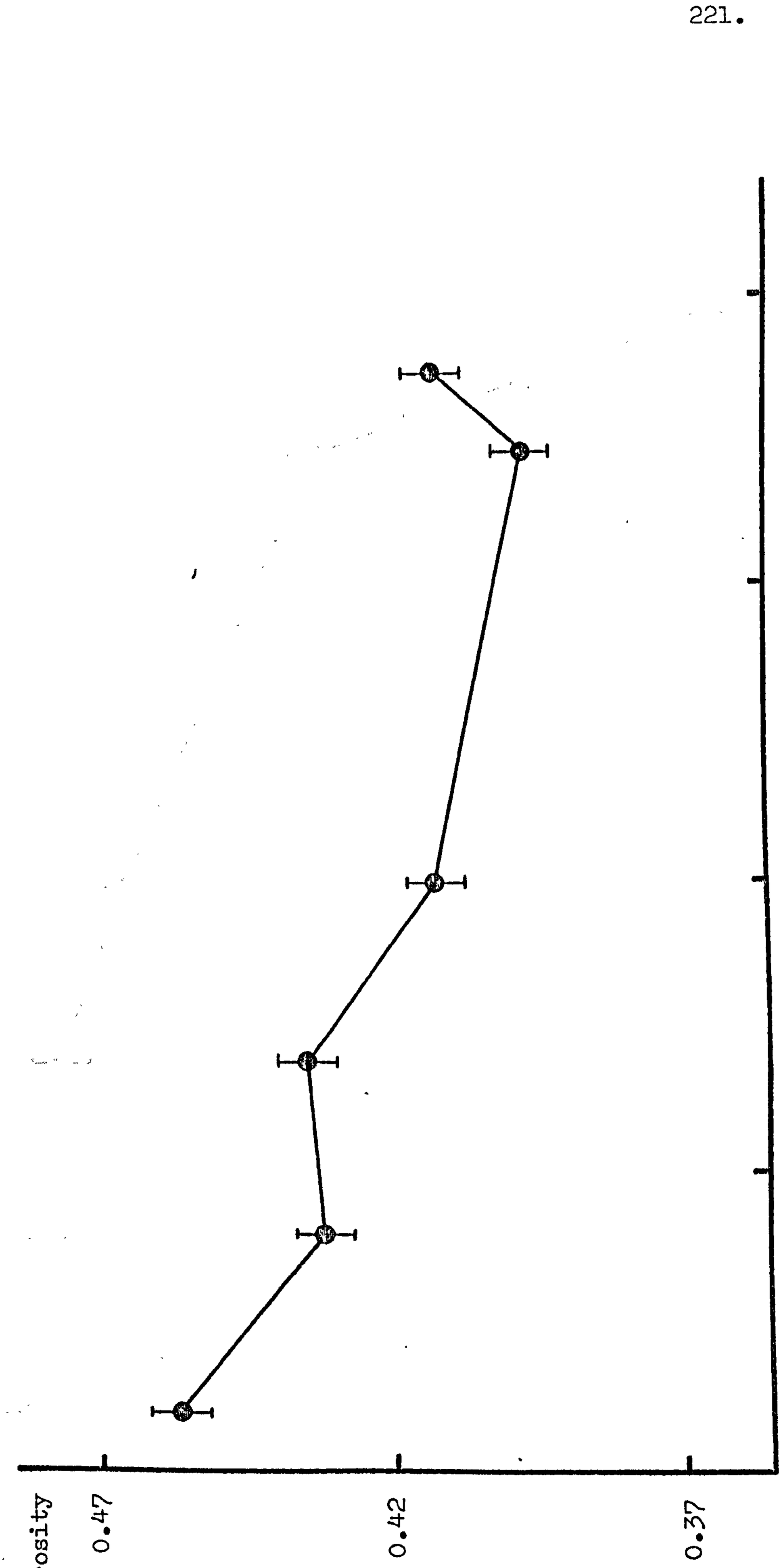

Fig. 6.18 The variation of porosity with depth in a horizontally vibrated sample of lactose, size fraction F

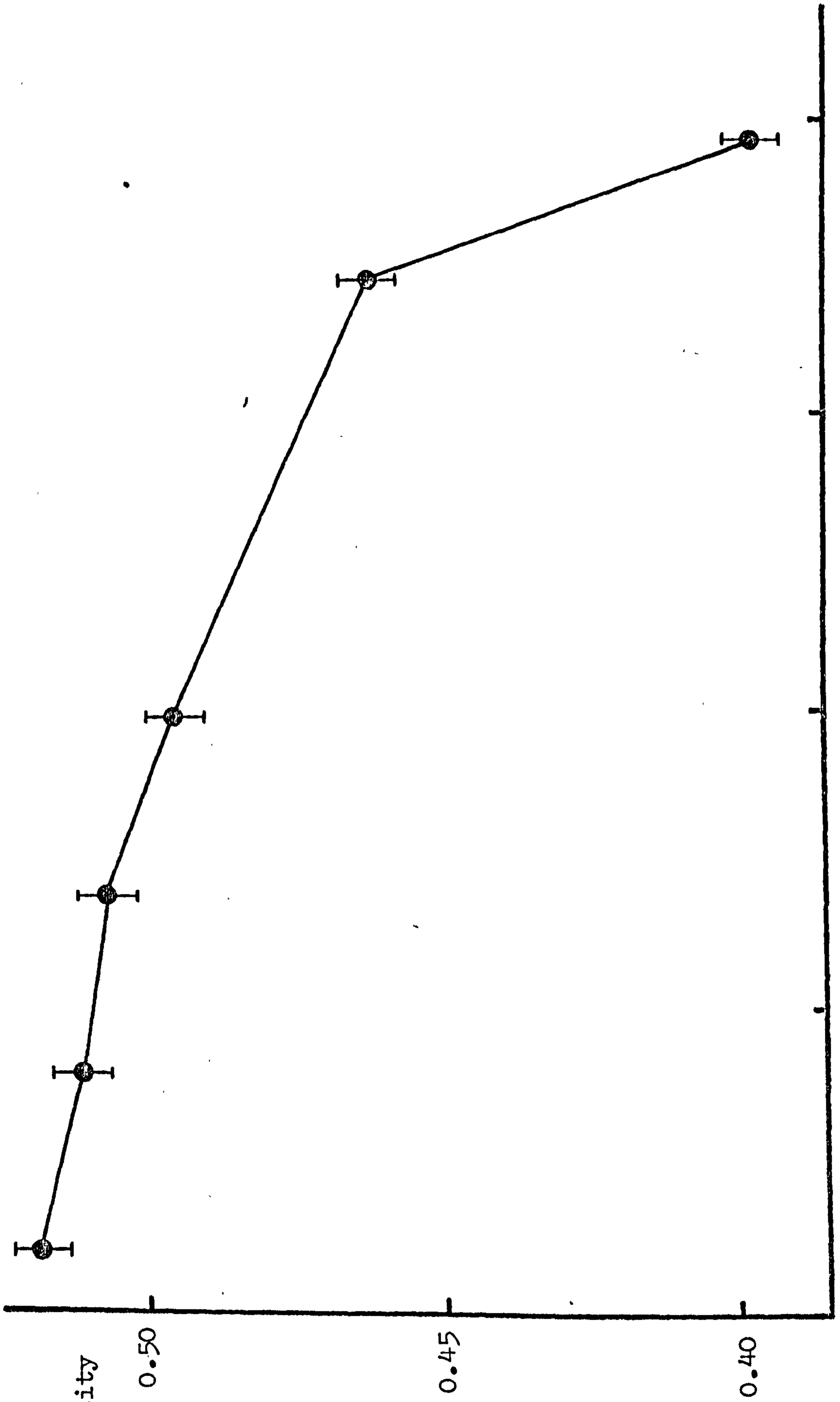

methods suitable for one type of particulate solid may not be suitable for another.

Low overall porosity does not necessarily guarantee that uniform packing exists. Similarly, good flow properties do not always ensure low local porosity variations.

Vibration reduces the porosity and improves the packing uniformity of powder samples, particularly if applied vertically. Also, simultaneous vibration and deposition can be advantageous in producing uniformly packed samples. However, vibration often results in a disappointing lack of reproducibility of overall porosity between successive samples prepared under the same conditions. The reasons for this are unclear.

The application of relatively small compressive forces also lowers the porosity and improves the uniformity of packings, although free-flowing materials are much less susceptible than cohesive ones.

Porosity is likely to vary with depth to some extent in vibrated powder samples. The extent of this variation will presumably depend on vibration conditions and particle properties.

Chapter 7

A Model Dosator System For Studying The Capsule Filling Process

The work described in Chapter 6 provided some useful information concerning the factors affecting the uniformity of porosity of powder beds. Local porosity variations in powder beds are likely to have some effect on the fill weights of capsules produced on a dosator-type machine, and therefore, to establish how significant this influence is in practice, a model dosator system was required.

7.1 Description of filling machine

(A) General

All subsequent capsule filling studies employed a purpose-built, semi-automatic, lab-scale filling rig (Technical Services Capsule Division, Eli Lilly & Co. Ltd., Basingstoke, Hants.), which was designed to simulate the Zanasi type of dosator system by featuring intermittent motion of the capsule-filling components. The rig carried one dosator, and was capable of filling at a rate of about one capsule per two seconds. The design enabled instrumentation to be incorporated, for the purpose of measuring various forces and displacements arising during the filling process. Fig. 7.1 is a general view of the rig, while Fig. 7.2 shows the filling area in more detail.

Fig. 7.1 The Lilly instrumented capsule filling machine

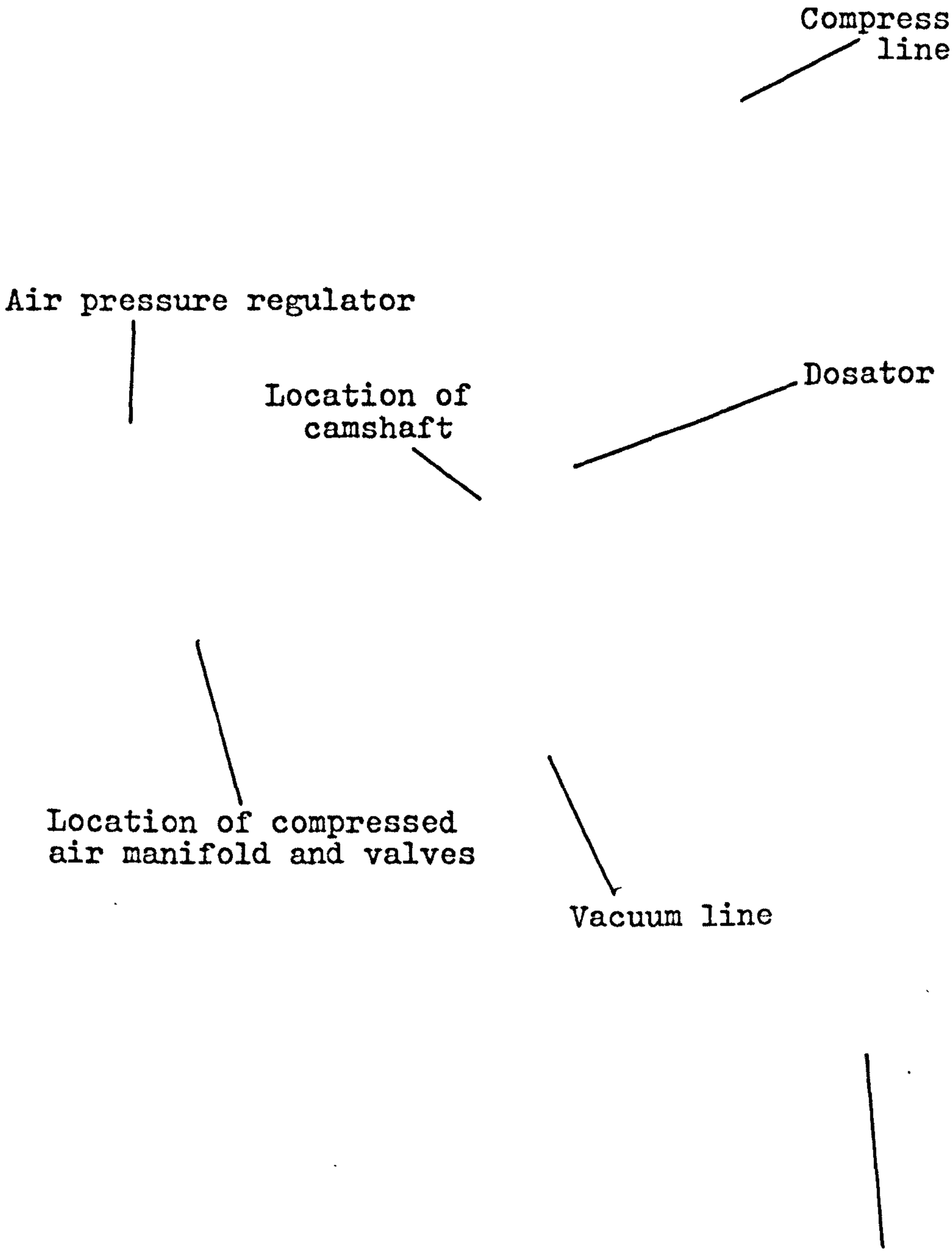

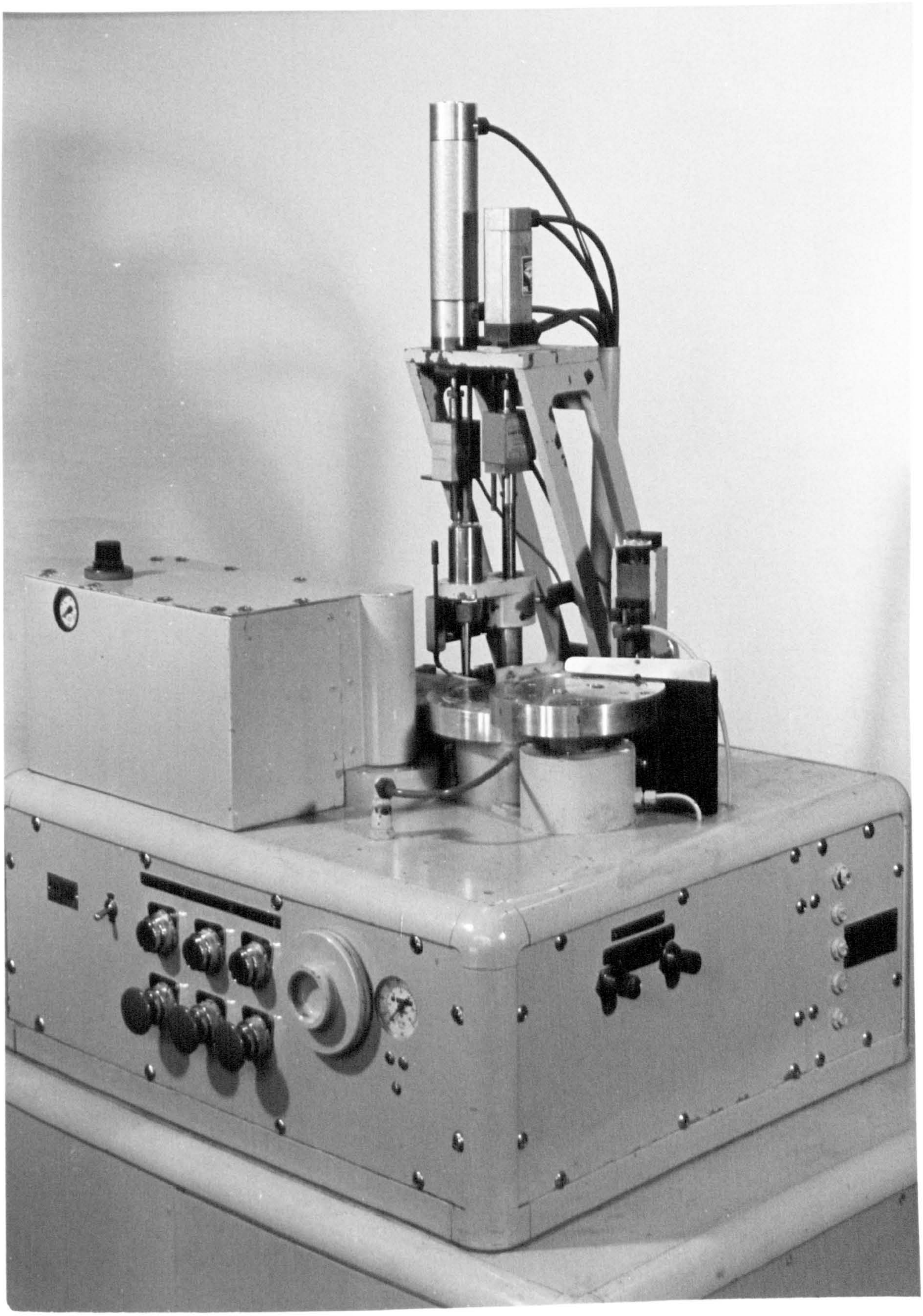

Fig. 7.1 The Lilly instrumented capsule filling machine

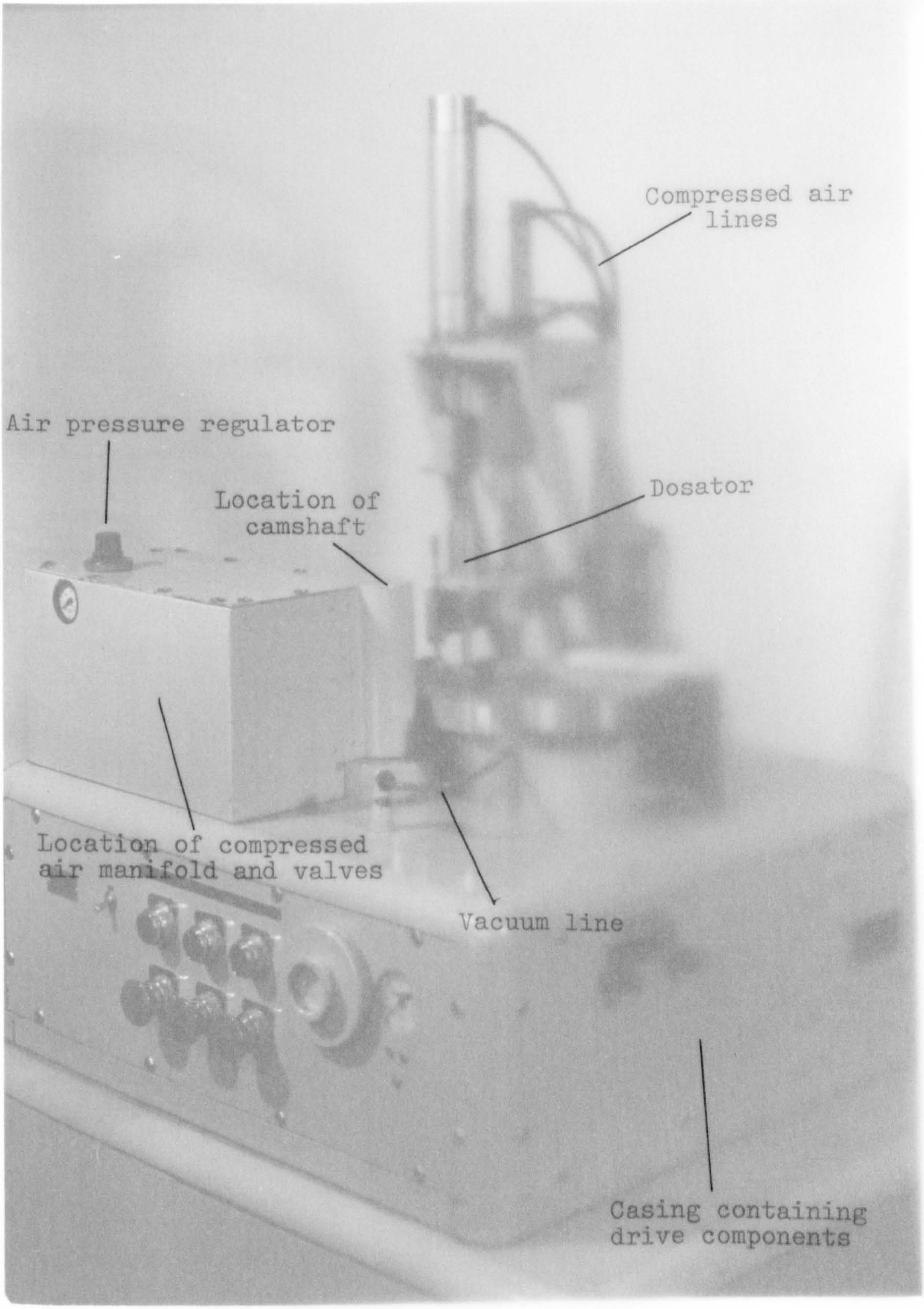

Fig. 7.2 The capsule filling components and instrumentation of the Lilly machine

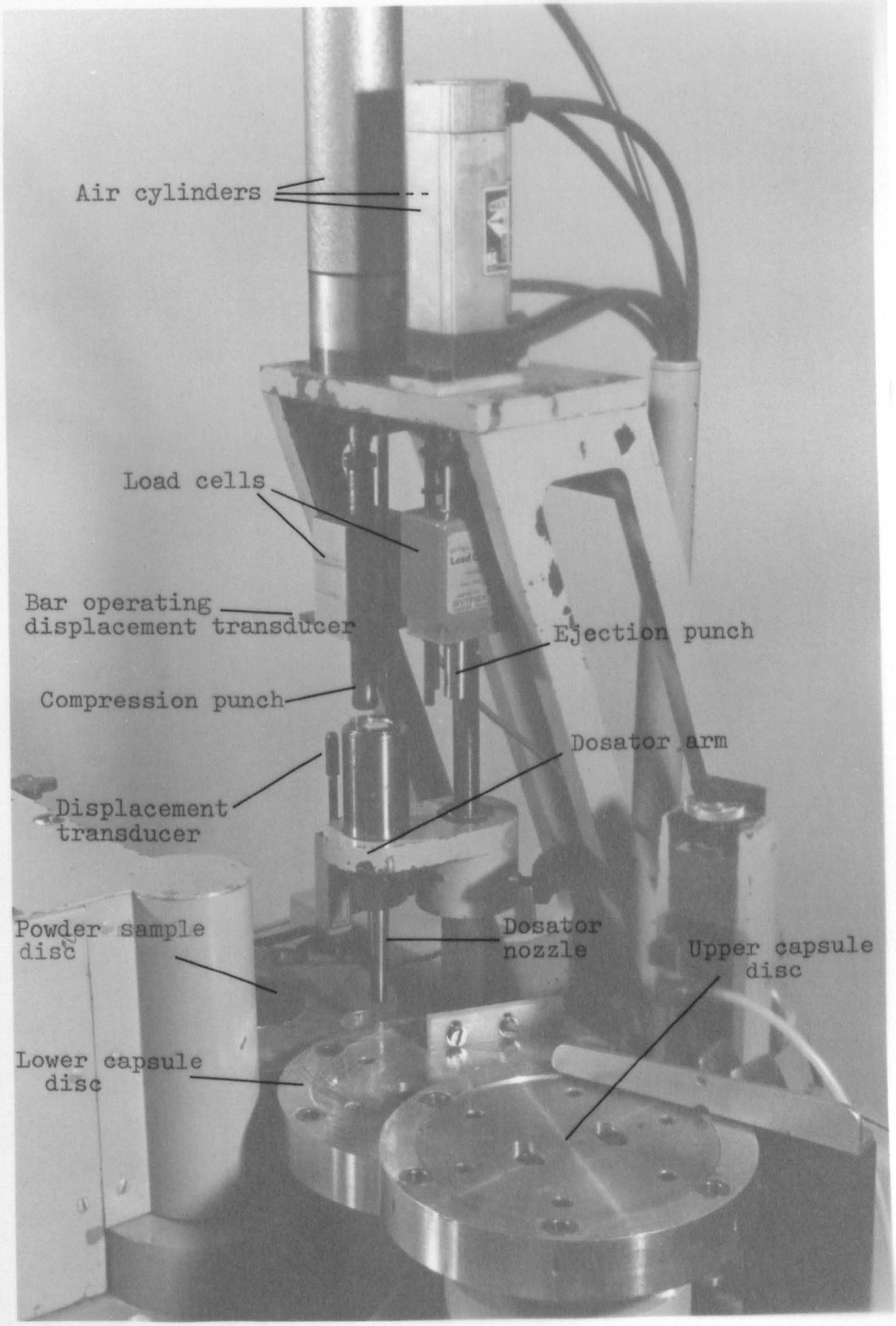

(B) Drive

An electric motor provided drive via a magnetic clutch to a reduction gear box. The output shaft from the gearbox transmitted drive via a belt to a "Geneva star", which translated continuous motion into intermittent motion. Connected to this, by various linkages, were the upper and lower capsule discs, the powder sample disc and the dosator shaft; each of these components underwent intermittent rotation during normal operation of the machine.

A low-geared handwheel was provided to enable the machine to be operated manually at a very slow speed. This facilitated the adjustment or alignment of the various moving parts.

(C) Upper and lower capsule discs

These discs, made out of light alloy, each carried six interchangeable bushes at regular intervals around their periphery. The bushes in the upper disc were designed to retain a capsule cap whilst allowing the capsule body to pass through, whereas the bushes in the lower disc were designed to hold a capsule body such that its top edge was flush with the top of the bush. When in position on the machine and correctly adjusted, two adjacent bushes on each disc were vertically aligned. Beneath one of these stations, a vacuum line provided suction so that by placing a closed, empty capsule shell

in the upper bush, separation of cap and body would take place. At the other of these aligned stations, re-closing of capsules took place. A small circular aperture in the bottom of the lower bush enabled a brass rod to push the capsule body upwards and into a waiting cap, which was itself prevented from moving vertically by a retaining plate positioned over the upper bush. At each stepwise movement, both discs rotated clockwise through 60°, thus a cap having just been separated from an empty body would be transferred to the closing station to mate with a full body. The empty body meanwhile moved towards the filling station. After closing, the full capsule moved to the capsule ejection station; ejection was effected by a second brass rod which pushed the capsule out of the upper bush and down a chute into a suitable receptacle.

Upper and lower bushes were available in capsule sizes 0, 1, 2, 3 and 4.

(D) Powder sample disc

This disc, also made out of light alloy, featured four vertical wells, spaced regularly around its periphery. Each well was of a suitable diameter to hold an aluminium cylinder containing a powder sample, and at each stepwise movement, the disc rotated clockwise through 90°, taking a powder sample into a position at which the dosator nozzle could then enter the powder.

In this way, each capsule was filled from a specific powder sample, which was subsequently discarded.

(E) Compressed air system

Compressed air was supplied by an external generator via a manifold located inside the casing of the machine, to eight air lines, two of which were connected to each of four air cylinders. On each cylinder, one line supplied air for the downstroke and the other controlled the upstroke.

One of these cylinders drove a stage carrying the capsule closing and ejecting rods (see earlier); the other three cylinders were all mounted on a rigid platform directly above the filling area. Attached to the piston of one of these cylinders, via a 12.7mm diameter upper vertical shaft of variable length, was the dosator arm. This consisted of a short horizontal arm, mounted on a 25.4mm diameter lower vertical shaft which was free to move up and down, under the action of the air piston. The extent of downward travel of the dosator arm and shaft was limited by a stop, while its upward travel was limited by the fixed stroke of the air piston. The dosator itself consisted of an upper chamber, housing the plunger and return spring, and beneath this, a nozzle, which was held in position by a retaining nut (see Fig.7.3). The dosator arm and shaft were driven mechanically backwards and forwards between

Fig. 7.3 The dosator of the Lilly instrumented capsule filling machine

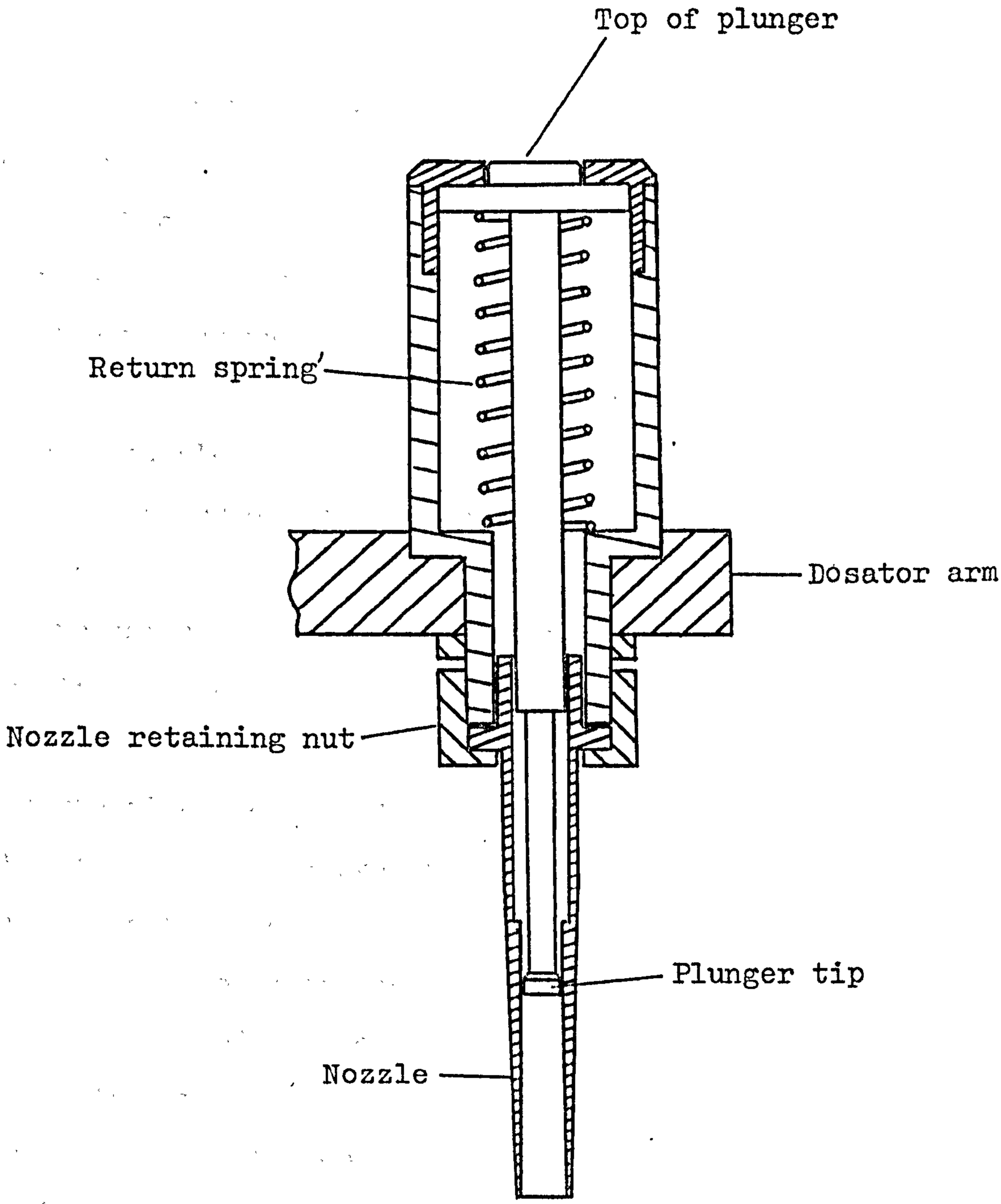

two positions at an angle of 90°, in order to pick up powder plugs and transfer them to empty capsule bodies.

The other two air cylinders drove the compression and ejection punches. These punches consisted of shafts of adjustable length, 12.7mm in diameter, the middle section of which could be replaced by load cells (see later). The compression punch was positioned above the filling station of the powder sample disc, so that when the dosator nozzle had swung into position and descended into a powder sample, the compression punch descended into the upper chamber of the dosator, depressed the plunger, and compressed the powder in the nozzle. On raising the compression punch, the plunger returned to its former position under the action of the spring. The dosator was then retracted from the powder sample and swung across to the plug ejection station of the lower capsule disc. Mounted directly above this station was the ejection punch; actuation of the appropriate air piston caused this punch to enter the dosator chamber, depress the plunger and eject the plug into a waiting capsule body.

The operation of these four air cylinders was controlled by the opening and closing of a series of valves. The valve timing was governed by a vertical camshaft, driven by the machine's gearbox. Speed controls were incorporated into each air line so that the speed of each vertical movement could be adjusted without altering the air pressure.

During normal operation of the machine, the valve sequence and mechanical drive were synchronised such that one cycle consisted of the sequence of events shown in Table 7.1.

A minimum working air pressure of about 350kNm^{-2} was necessary in order to operate an air-pressure switch in the clutch circuit; below this pressure, the clutch had no electrical, supply, and hence could not engage. A typical working pressure, therefore, was 490kNm^{-2}; this pressure was supplied to all cylinders except the one operating the compression punch. Provision had been made for this cylinder to operate at lower pressures by fitting a regulator in the line; in this way, relatively small compression forces could be applied while considerably larger forces were available for ejection.

Each piston would travel the full length of its fixed stroke unless (a) the component it was driving met a resistance greater than the available air pressure, or (b) the stroke had been slowed down to such an extent that before it could be completed, the return stroke began.

(F) Sample containers

The aluminium cylinders used as powder sample containers in previous chapters, were approximately 44mm deep. Rough calculations suggested that to fill size 0 capsules with lactose, powder beds of about 20mm depth

Table 7.1

Sequence of events in one cycle of operation of the Lilly model dosator system

Horizontal movements	Vertical movements
Dosator swings into position above a powder sample	Closing and ejecting rods descend
	Dosator descends, and nozzle enters powder sample
Upper and lower capsule discs rotate through 60°	Compression punch descends
	Compression punch rises
	Dosator rises, and nozzle exits powder sample
Dosator swings across to ejection position; meanwhile, powder sample disc rotates through 90°	Closing and ejecting rods rise
	Ejection punch descends
	Ejection punch rises
Dosator swings back towards compression position	

Time

would be suitable. The decision was taken to use containers of this latter depth, rather than to attempt to part-fill the original ones. Hence, ten similar aluminium cylindrical containers were made, having a depth of 20mm, an internal diameter of approximately 19mm, and a base thickness of about 2mm. These new containers, having an external diameter of 25mm, were a comfortable fit in the wells of the powder sample disc.

7.2 Instrumentation

In any study of mechanical processes, a knowledge of some of the forces and displacements that arise can help to account for observations relating to machine performance and efficiency. Thus, in a capsule-filling process such as the one described here, instrumentation can provide useful data. Three quantities were regarded as being particularly important in this respect. These were compression stress, which is the force per unit area applied vertically to a powder plug inside the dosator nozzle to aid retention, ejection stress, which is the force per unit area applied vertically to a powder plug for the purpose of ejecting it from the dosator nozzle, and compression displacement, which is the reduction in length of a powder plug on compression.

A limited amount of work has been published on the instrumentation of dosator-type capsule filling machines. Cole and May (1975), Small and Augsburger (1977), and

Jolliffe (1980) all described systems in which strain gauges were mounted on flats machined on the shaft of a dosator plunger. In this way, vertical stresses applied to the powder plugs inside the dosator nozzle were translated into electrical signals which could be recorded and measured quantitatively. Mony et al (1976) were able to make similar measurements using a quartz load washer, operating on the piezo-electric principle. This was mounted towards the top of a Zanasi dosator plunger.

An alternative method of stress measurement had been incorporated into the design of the Lilly rig. Load cells of the JP type (Schaevitz Bytrex, Waltham, Mass., U.S.A.) were built in to the compression and ejection punches as shown in Fig. 7.4. These load cells have a central, vertical diaphragm which deforms under load; semiconductor strain gauges mounted on the diaphragm provide an electrical signal proportional to the applied load. Hence, recording this signal enables stress measurements to be made. One disadvantage of this arrangement is that the stresses are measured at a point some distance from the powder itself, and the assumption has to be made that the load on the diaphragm equals the load on the powder plug.

Measurement of compression displacement was carried out using a displacement transducer (Type DR68, Intersonde Ltd., Watford, Herts.). This was mounted in such a way

Fig. 7.4 Attachment of the JP load cells

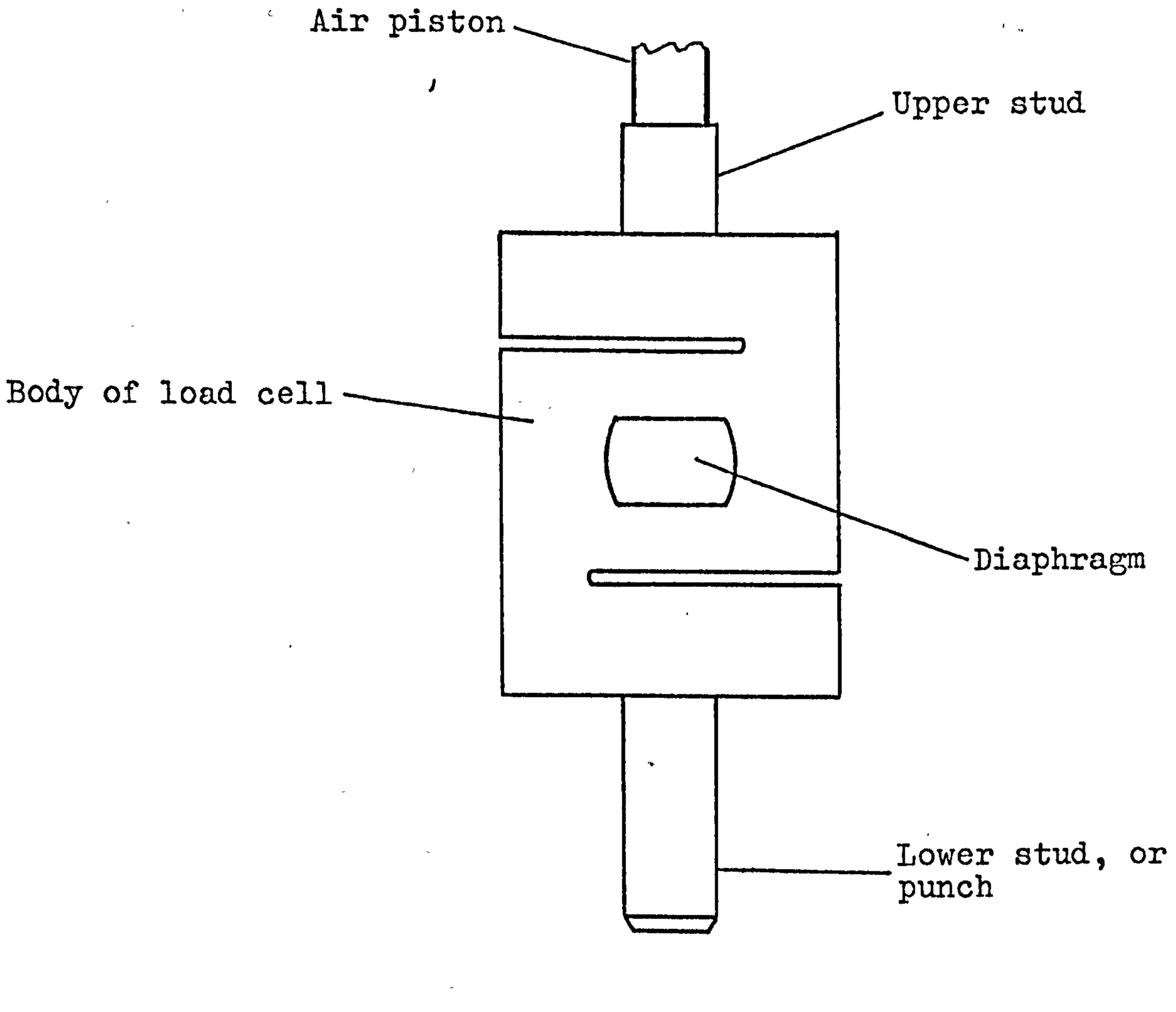

that a horizontal bar attached to the compression punch contacted the piston of the transducer just as the plunger tip reached the surface of the powder in the dosator nozzle. Thus, a given reduction in the length of the powder plug was accompanied by depression of the transducer piston through the same distance. The transducer generated an electrical signal directly proportional to the displacement of its piston.

The load cell attached to the compression punch was of approximately 45kg (100lb) capacity and power input was supplied to it from a constant voltage supply (Type L30B, Farnell Instruments Ltd., Wetherby, Yorks.). Output from the transducer was fed directly to a mirror galvanometer of appropriate sensitivity, housed in an ultraviolet recorder (Series 40,000, Bryans Southern Instruments, Mitcham, Surrey).

The load cell attached to the ejection punch was of approximately 230kg (500lb) capacity, and a constant input voltage was supplied to it by a bridge-amplifier (Model FE-154-ABSYC, Fylde Electronic Labs., Preston, Lancs.), which also provided amplification of the output signals if and when required. These signals were then transmitted to a suitable mirror galvanometer in the ultra-violet recorder.

The displacement transducer was connected to a combined power supply and preamplifier (Electronic Workshop, Nottingham University), which provided a constant

input voltage, and converted output signals into a form suitable for measurement using the ultra violet recorder and a mirror galvanometer.

Mirror galvanometers of three nominal sensitivities were available (Bryans Southern Instruments):

Type SMI/S, natural frequency 160Hz, sensitivity 0.375mV/cm

Type SMI/P, natural frequency 300Hz, sensitivity 2.2 mV/cm

Type SMI/M, natural frequency 1000Hz, sensitivity 16.0mV/cm

Their suitability for the proposed measurements is discussed later.

7.3 Setting-up

Capsule bushes, nozzles and plungers were available in sizes 0, 1, 2, 3 and 4. Size 0 was chosen for all capsule-filling experiments, and components of that size were therefore fitted.

The length of the upper dosator shaft was adjustable by means of a threaded upper stud which screwed on to the end of the air piston. The position of this stud was firmly secured by a locknut. With the shaft adjusted to its shortest length, the dosator nozzle in its lowered position was several millimetres above the base of a sample container in the powder sample disc. By gradually

lengthening the shaft, the position was reached at which the compressed air piston just completed its full down stroke as the dosator arm reached its stop. At this point, the tip of the nozzle came within 1mm of the sample container base. In its raised position, however, it cleared the lower capsule disc by an excessive margin on the way to the plug ejection station; such a gap could cause powder loss, on ejection. Further lengthening of the shaft was able to reduce this gap to a suitable magnitude of about ¼mm, and this had no effect on the lowered position of the nozzle, since the full stroke of the compressed air piston was now prevented by the dosator stop.

The length of the compression and ejection punches could also be altered by means of adjustable upper studs and locknuts. The upper position of the compression punch was fixed such that the clearance between the punch tip and the top of the dosator (in its raised position) was 2-3mm. The air piston driving this punch had a sufficiently long stroke to cause adequate depression of the plunger with the dosator in its lowered position. The length of the ejection punch was adjusted so that at the bottom of the downstroke, the tip of the dosator plunger just reached the nozzle outlet, thus ensuring complete plug ejection.

After making the necessary adjustments, the machine was started up and allowed to run without either powder

or empty capsules, to ensure that all moving parts were operating satisfactorily. Such a "dry run" was carried out routinely before experimentation, with the intention of revealing any maladjustments.

7.4 Preliminary experiments

7.4.1 Suitability of galvanometers

When using mirror galvanometers of the type employed with the ultra-violet recorder, two important points must be considered:

(i) The galvanometer chosen must have a sufficiently high natural frequency to be able to produce a satisfactory response to the signal in question. If the signal is of a higher frequency than approximately 60% of the galvanometer's natural frequency, the trace obtained from the recorder is likely to be incorrect.

(ii) The resistance of the source whose output is to be measured must be compatible with the damping resistance of the galvanometer. Otherwise, the recorded signal will be either overdamped or underdamped, resulting in an unsatisfactory trace.

(A) Experimental

(i) Lactose, fraction D, was poured into a number of sample cups and samples were levelled with a spatula blade. Size 0 capsules were filled from these samples using the instrumented Lilly rig, with the air pressure

at 490kNm^{-2} and the compression cylinder operating at 70kNm^{-2}. Compression stress was recorded directly by a type SMI/S galvanometer, while ejection stress and compression displacement signals underwent suitable amplification before being recorded by type SMI/M galvanometers. By running the U.V. recorder at a high paper speed, the time taken for signals to reach their maxima could be estimated. It soon became clear that in each case, signal frequency was well within the limits imposed by the natural frequencies of the galvanometers.

(ii) The compatibility of source resistance and galvanometer damping resistance was investigated, for each transducer/ galvanometer combination likely to be used. This was carried out by recording the "step function response" of each combination. A given transducer was subjected to a typical load, with the output disconnected from the galvanometer. By suddenly bringing the galvanometer into the circuit, a response was recorded, which stabilised at a level corresponding to the applied load. Fig. 7.5 illustrates underdamped, satisfactory and overdamped step function responses. All combinations tested proved to be satisfactory.

(B) Discussion

These experiments indicated that the galvanometers available would be suitable for use with the instrumented rig.

Fig. 7.5 Possible step function responses of mirror galvanometers

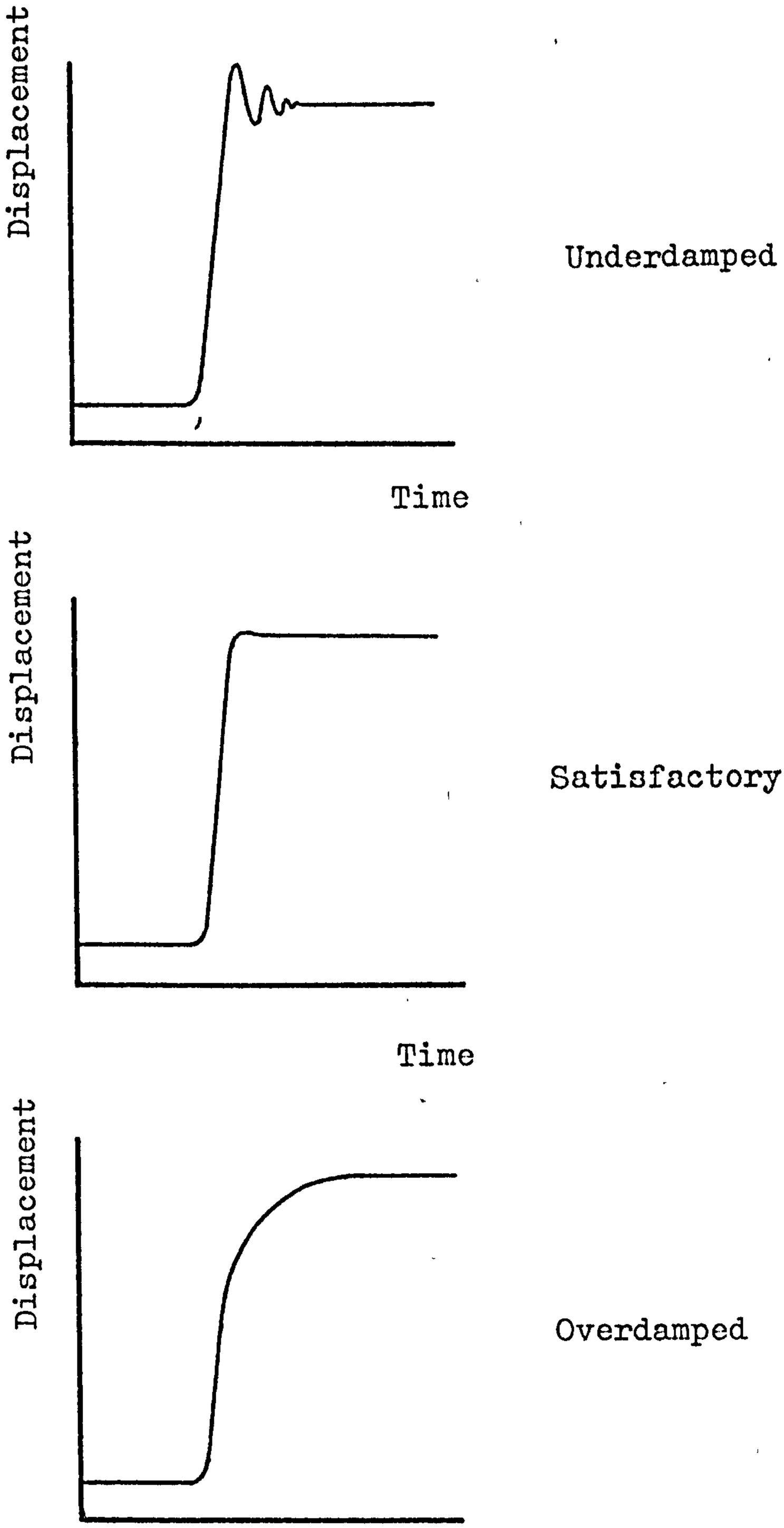

It became apparent in experiment (i) that ejection stress was the signal of highest frequency. The reason is that at ejection, a powder plug is only restrained by the nozzle walls, and if this resistance is overcome very quickly, the build-up of ejection force may occur over a very short time interval. It therefore seemed sensible to record these signals with the highest frequency galvanometer available.

The other two signals, compression stress and compression displacement, were characterised by a much slower build up, due to the presence of the sample container base preventing the plug from leaving the dosator nozzle. Assuming that frequency considerations can be met, it is generally advantageous to use the most sensitive galvanometer possible, to ensure a high signal to noise ratio and thus facilitate the measurement of small signals. For this reason, type SMI/S was chosen to record compression stress. Signals from the displacement transducer/preamplifier arrangement, on the other hand, were of much higher magnitude, hence type SMI/M was suitable for recording these.

7.4.2 Calibration of instrumentation

(A) Experimental

Each load cell/galvanometer combination to be used was calibrated by hanging a series of weights on the cell and measuring the deflection obtained on the U.V. recorder.

The displacement transducer was calibrated by depressing its piston through a given distance, measuring that distance with a travelling microscope, and measuring the resulting deflection on the recorder.

It was also necessary to calibrate the dosator spring. During depression of the plunger, part of the applied load was supported by the spring and did not therefore act on the powder plug. Hence, a correction had to be subtracted from all measured forces, and the magnitude of the correction was dependent on the extent of depression of the spring. The calibration involved loading the plunger and spring with a series of weights, and measuring the resulting depression, using a travelling microscope.

(B) Results

All calibration graphs are included in Appendix 3.

Chapter 8

The Influence of Method Of Powder Bed Preparation On Capsule Fill Weight Variation

The instrumented capsule filling machine described in Chapter 7 is characterised by the provision of a number of individual powder sample cups, from each of which just one hard gelatin capsule is filled. By determining the weight and volume of these individual powder samples, and knowing the apparent particle density of the powder, overall porosity can be calculated for each sample. Variations in overall porosity between successive samples, occurring during the filling of a batch of capsules,may then be related to the weight variation of the filled capsules.

In addition, local porosity variations may be present within individual powder samples. Chapter 6 illustrated this, and showed that the extent of such variation is dependent on the properties of the powder, the method of deposition used in preparing the samples, and on whether the samples are subjected to compression or vibration.

The objective of this section of the work was to evaluate the influence of powder porosity variations,

both between-samples and within-samples, on the fill weight variation of hard gelatin capsules.

8.1 Experimental

(A) Apparatus and materials

All capsule filling experiments were carried out using the instrumented filling machine described in Chapter 7.

Lactose size fractions B (+ 18.7-26.5μm), D (+ 37.5-53μm) and F (+75-105μm), whose packing behaviour had been investigated in Chapters 3 and 6, were chosen for filling into size 0 hard gelatin capsules.

By considering the results of Chapter 6, it was possible to select three methods of powder sample preparation which could be expected to produce beds of differing degrees of local porosity variation, for all three particle size fractions. These were:

(i) Pouring from a jar, giving samples of moderate variability.

(ii) Deposition from a vibrating chute through a funnel, giving samples of high variability.

(iii) The application of vertical vibration at selected conditions to samples deposited by pouring from a jar, giving low variability of local porosity.

A more detailed account of these methods can be found in Chapter 3, together with a description of the

apparatus employed. All capsules were filled from samples contained in cylinders of 20mm depth. The containers described in earlier chapters were 44mm deep; otherwise, the details remained the same. No attempt was made to determine the local porosity distribution within these samples.

(B) General method

The following method of filling capsules was used throughout. The dosator nozzle and plunger were cleaned with tap water and a nozzle brush, then dried. They were then rinsed with carbon tetrachloride, and left to dry in an air stream. In this way, any adherent powder, dirt or grease was removed before the nozzle and plunger were attached to the dosator arm. Samples were prepared in lots of ten, weighed, and loaded into the sample disc as required. A suitable compression air pressure was set, and the air pressure to the three other cylinders was fixed at $490 kNm^{-2}$. An empty capsule body was placed in the bush preceeding the plug ejection station in the lower capsule disc. The output from the instrumentation was adjusted as required, and the paper feed on the ultra violet recorder was switched on at a suitable speed. The filling machine was then run just long enough for a plug of powder to be picked up by the dosator nozzle and deposited in the empty capsule body. In this time, three traces were obtained on the recorder,

corresponding to compression stress, compression displacement and ejection stress (see Chapter 7). The filling machine and recorder paper feed were then switched off, and the full capsule body was removed from the lower capsule disc. The sample cup from which the plug was removed was reweighed, and the powder ejected into the capsule body was also weighed.

Ten capsules, were filled in this manner, one from each sample cup. If the filling conditions were regarded as satisfactory at this point, a further number of capsules were filled as required. Cleaning of the nozzle and plunger was carried out only at the start of an experiment, thus any effects due to the build-up of a powder coating on the nozzle bore could be observed.

(C) Treatment of results

From the weight of each sample, the volume of the container, and the apparent particle density of lactose, a value of overall porosity was calculated. Then, by considering the dimensions of the nozzle and the depth of the sample, an estimate of expected fill weight was made, for a given set of conditions. This could be compared with observed fill weights.

For each capsule filled, compression force, ejection force and compression displacement were determined from the traces obtained, using the relevant calibration data. The measured forces were corrected to account for

the reaction of the dosator spring and were then divided by the internal cross-sectional area of the nozzle to give corresponding stresses. The compression displacement was used, together with initial sample porosity, to calculate the resulting porosity of the plug.

When suitable filling conditions had been achieved for a given size fraction, using samples prepared by a given method, fifty capsules were filled. The mean values and coefficients of variation of sample porosity, capsule fill weight, and weight removed from samples, were calculated.

8.2 Results and discussion

8.2.1 Fraction D

(A) Experiments with the size 0 nozzle and size 0 plunger

Ten sample cups were filled by pouring from a jar. Mean sample weight, cup dimensions and nozzle dimensions were used to calculate an expected fill weight. The compression air pressure was adjusted to 70kNm^{-2} and the size 0 nozzle and plunger were fitted to the dosator arm. Capsules were then filled from these samples.

Fill weights began at about $\frac{2}{3}$ of the expected value and decreased quite markedly (Fig. 8.1). The same graph shows that compression displacements increased as filling proceeded. Indeed, the plunger was being depressed to such an extent that it would be impossible for the

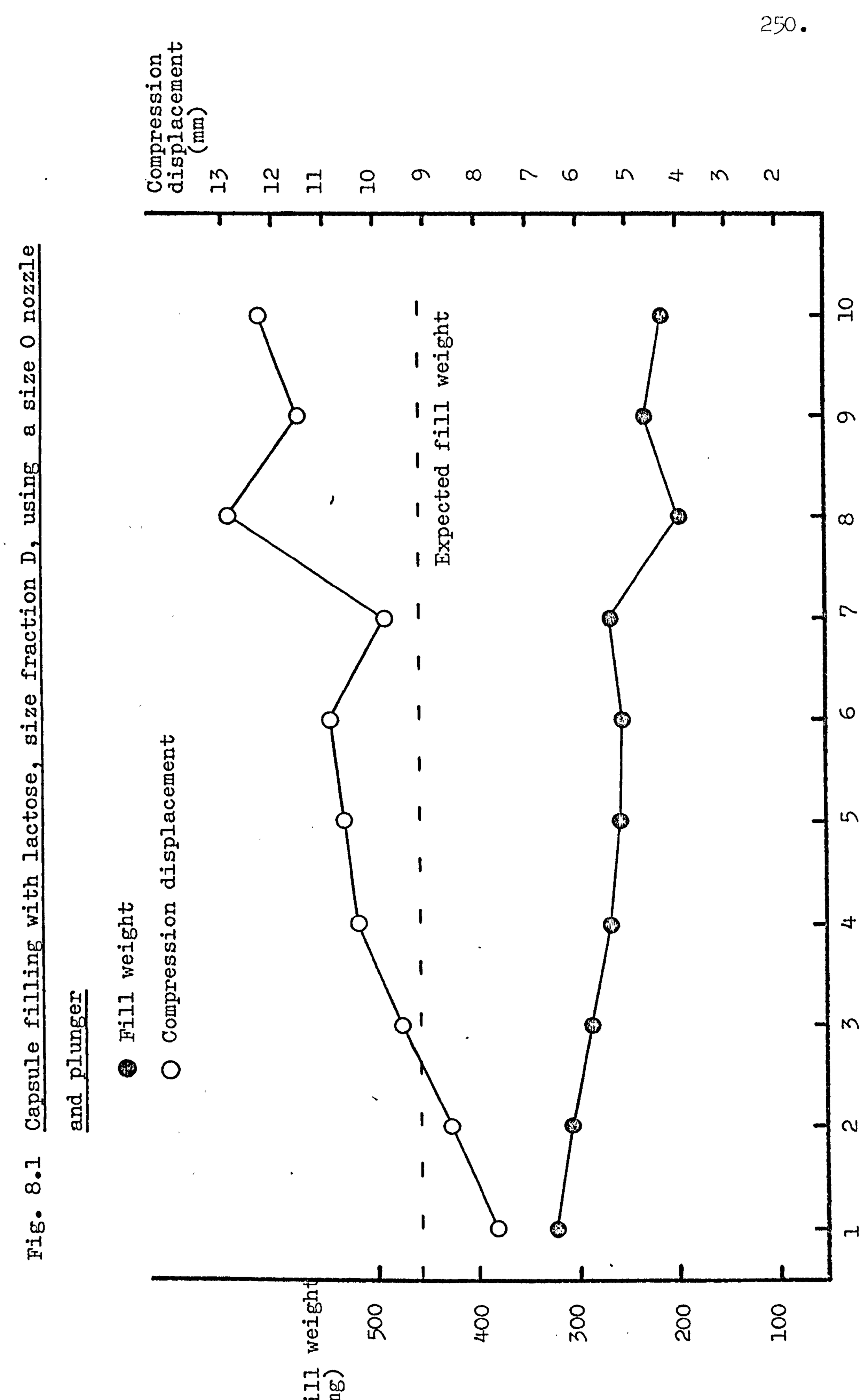
Fig. 8.1 Capsule filling with lactose, size 0 nozzle and round plunger
Fill weight
Compression displacement
Expected fill weight
Fill weight (mg)
500
400
300
200
100
Compression displacement (mm)
13
12
11
10
9
8
7
6
5
4
3
2
1
Capsule number
3
4
5
1
2
6
7
8
9
10

expected fill weight to pack inside the remaining available volume in the nozzle. This indicated that during the process of lowering the nozzle,then depressing the plunger, a considerable quantity of powder was escaping from within the nozzle. It seemed unlikely that such a large quantity could be forced out fromthe nozzle through the gap between the nozzle outlet and the cup base, under the action of the plunger. An alternative explanation was that as the nozzle entered the sample, the air inside the nozzle and beneath the plunger failed to escape through the vent hole in the nozzle and was not completely displaced by powder before the nozzle reached the bottom of its travel. In this way, the descending "air front" inside the nozzle pushed some of the powder which was intended to enter the nozzle, out of its path, and a low fill weight resulted. Poor venting such as this could be caused by insufficient clearance between plunger tip and nozzle bore, and would be aggravated by any build-up of powder coating inside the nozzle. This might explain why the fill weights were initially low and then decreased even further. Two experiments were performed to investigate whether lack of venting was in fact the cause of the low fill weights.

(i) The speed of descent of the dosator arm was reduced to the minimum possible to give the air below the plunger time to escape through the vent hole.

The machine was operated manually until the nozzle had descended into the powder sample, then normal motor drive was supplied, a compression air pressure of 70kNm^{-2} was applied,and the powder plug was collected and weighed as normal. Five samples, poured from a jar, were used, and the nozzle and plunger were cleaned between cycles. (It should be noted that such cleaning between cycles is a departure from the "General method" described above.)

(ii) In this experiment, the machine was motor driven and the dosator arm descent was returned to a typical working speed. However, the plunger was removed until the nozzle had entered the powder sample, thus providing no obstacle to venting. At this point, the cycle was interrupted and the plunger was replaced. The filling cycle was then continued and the plug was collected and weighed. Again, five hand-poured samples were used, and the nozzle and plunger were cleaned between cycles.

The fill weights obtained in these two experiments are shown in Table 8.1. A significant improvement on the fill weights seen in Fig. 8.1 was observed, particularly in experiment (ii), in which recorded fill weights fell short of the expected value by only approximately 40mg. This remaining discrepancy was probably due to powderloss at the plug ejection stage, where some of the powder invariably missed the capsule body despite the fact that the nozzle outlet and the lower

Table 8.1

Fill weights obtained with fraction D using a size 0 nozzle and plunger, with enhanced venting during descent of dosator.

(i) Very slow dosator descent	(ii) Plunger absent during dosator descent
365mg	414mg
335mg	403mg
320mg	400mg
341mg	415mg
372mg	416mg

capsule bush were correctly aligned. This was because the powder was not ejected as a complete coherent plug.

It was clear that inadequate venting was the cause of the very low fill weights shown in Fig. 8.1. Rather than modifying the nozzle, by, for example, drilling further vent holes, the use of a smaller diameter plunger was considered. A size 1 plunger was readily available, and as a further alternative, a plunger of intermediate diameter was made; this will be referred to as size 01. The tip diameters of size 0, 01 and 1 plungers were measured using a micrometer, and are given in Table 8.2, together with the resulting clearance inside the size 0 nozzle, which has an internal diameter of 6.40mm.

Table 8.2

Dosator plunger tip diameters and clearance inside a size 0 nozzle

	Diameter (mm)	Clearance (mm)
Size 0	6.28	0.06
Size 01	5.83	0.285
Size 1	5.38	0.51

(B) The influence of compression air pressure

The effect of compression air pressure on filling performance was studied, using a size 1 plunger and a size 0 nozzle. Two lots of ten capsules were filled at compression air pressures of 70 and 140kNm^{-2}, from samples of fraction D prepared by pouring from a jar. Mean values of initial sample porosity, fill weight, and weight removed from sample, were compared (see Table 8.3), together with calculated values of expected fill weight.

Fill weights were slightly higher at 140kNm^{-2} compression air pressure than at 70kNm^{-2}, while the mean weight removed from the samples was very similar at each pressure, indicating that at the lower pressure, more powder loss occurred in transit from the sample cup to the capsule body, due to less efficient retention in the nozzle. At both compression pressures, there was still a

Table 8.3

Influence of compression air pressure on filling performance of lactose, fraction D

	$70kNm^{-2}$	$140kNm^{-2}$
Mean initial sample porosity	0.540	0.539
Expected fill weight	459mg	460mg
Mean recorded fill weight	395mg	410mg
Mean weight removed from sample	478mg	475mg

considerable loss of powder on ejection. Increasing the compression air pressure to $210kNm^{-2}$ did not prove to be advantageous, since an air pressure of $490kNm^{-2}$ was not always capable of effecting plug ejection. It therefore appeared that $140kNm^{-2}$ was a suitable compression air pressure for samples of fraction D having a porosity of approximately 0.54.

(C) The influence of nozzle/plunger clearance

The size 0 nozzle and size 1 plunger were thoroughly cleaned, then five lots of ten capsules were filled from hand-poured samples, employing a compression air pressure of $140kNm^{-2}$. For each capsule filled, six quantities were calculated, these being overall sample porosity, compression stress, ejection stress, plug porosity, fill weight and weight removed from the sample.

These quantities were plotted as a function of capsule production number (Fig. 8.2).

The experiment was then repeated using the size 01 plunger. The results are shown in Fig. 8.3.

With both size plungers, fill weight followed a similar pattern to weight removed from sample. In the case of the size 1 plunger, both quantities fluctuated around an average, value, while weights obtained with the size 01 plunger decreased gradually during the course of the run. If this latter trend were due to a powder coat building up on the nozzle walls and reducing its effective capacity, it would be expected to occur with the size 1 plunger also, since a larger clearance would presumably allow a thicker coat to develop. This, however, was not the case.

The overall porosities of the samples varied to some extent, but with no apparent trend. In neither experiment did variations in sample porosity appear to influence fill weights. There are two possible explanations for this lack of correlation. It may be that overall sample porosity is not a good approximation to the local porosity in the region where the dosator nozzle enters the sample, and in Chapter 6, it was seen that samples of fraction D filled by the method used here exhibit a considerable and largely random variation in local porosity. On the other hand, it is possible that the effect of reasonably small porosity variations on capsule

Fig. 8.2 Capsule filling data: Lactose, size fraction D, deposited by pouring from a jar. Nozzle size 0, plunger size 1.

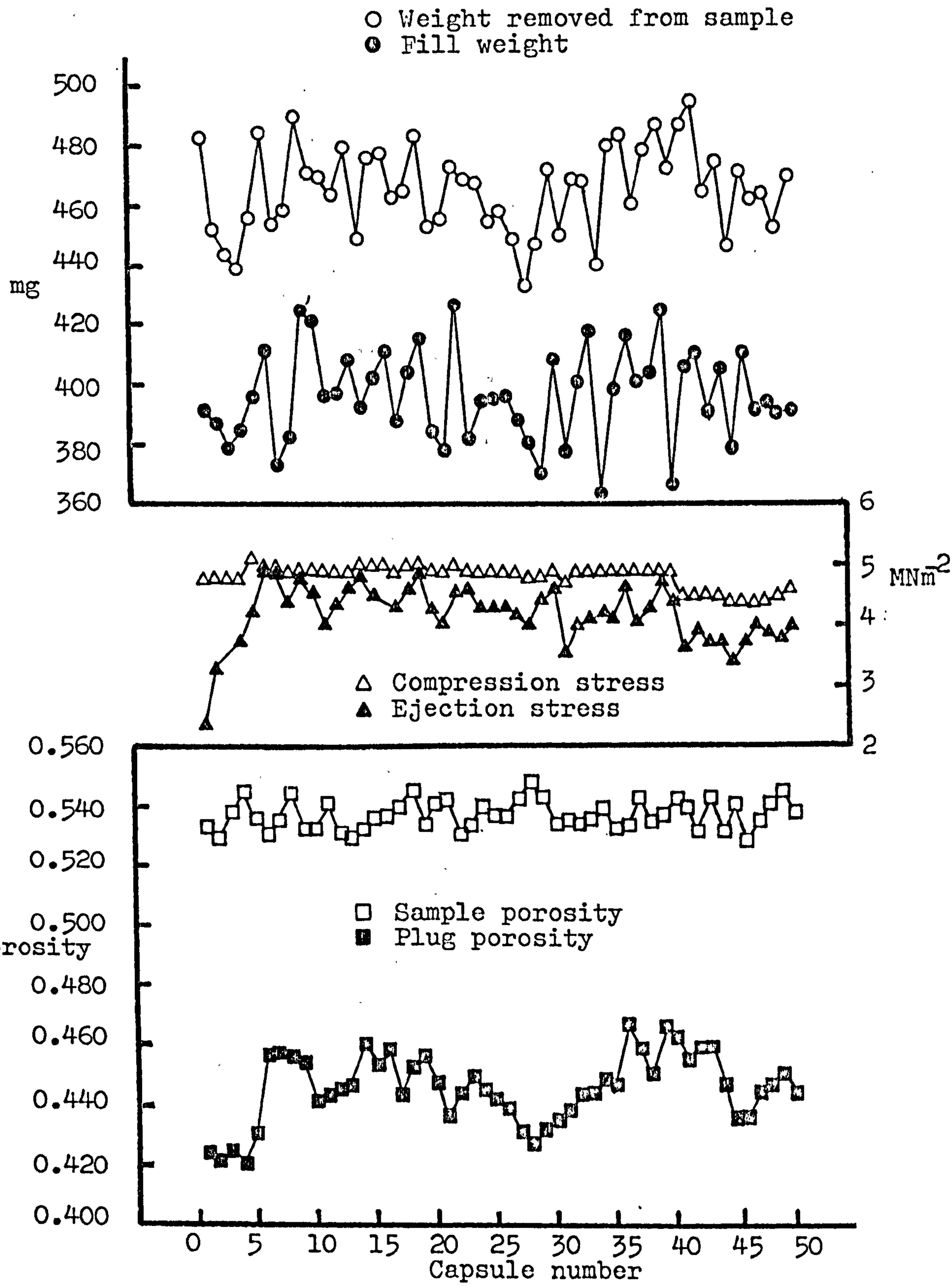

Fig. 8.3 Capsule filling data : Lactose, size fraction D, deposited by pouring from a jar. Nozzle size 0, plunger size 01

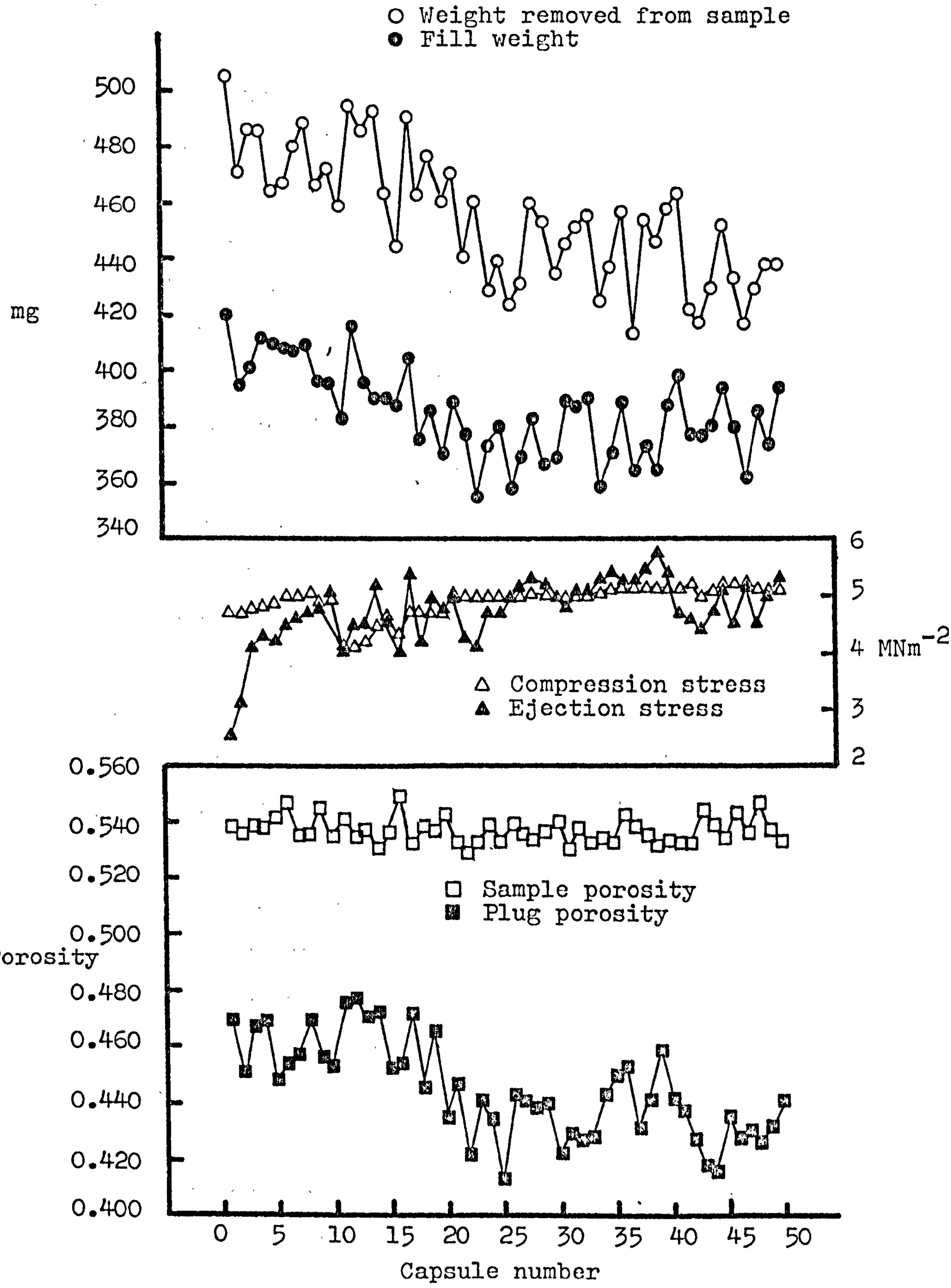

fill weight is masked by other factors, such as the extent of any powder coating inside the nozzle; this may vary during a capsule-filling run and affect plug retention ability.

Plug porosities were rather more variable than sample porosities, and the two quantities bore little relation to each other, except that in all cases, the plug was naturally of lower porosity than the sample it was taken from. A sample of relatively low porosity, for example, did not necessarily give a plug of relatively low porosity. With the size 1 plunger, plug porosity showed a similar pattern of variation to ejection stress. This was rather surprising; one might expect a low porosity plug to require a relatively large ejection stress, since powder-wall interactions increase with compression. The significance of this observation is not clear.

Ejection stress began at a relatively low level, and increased steadily for a few cycles, while a powder coating presumably developed on the nozzle walls. It then fluctuated around an average value of about 4 to 5 MNm^{-2}. Compression stress, on the other hand, was reasonably constant, and any variations that occurred were due mainly to pressure fluctuations in the air supply. In addition, variations in compression displacement affected the compression stress to some degree, since the correction applied to account for the reaction of the dosator spring was dependent on the extent to which

it was depressed. With both plunger sizes, any change in compression stress tended to result in a similar but more marked variation in ejection stress.

On the whole, the size 1 dosator plunger gave slightly higher fill weights, with no tendency to decrease during a run of fifty capsules.

(D) The effect of different methods of sample preparation

In accordance with section 8.1(A), two methods were investigated in addition to the method of pouring from a jar, the results of which have already been discussed.

Five lots of ten samples were prepared using the vibrating chute and funnel, and as before, one capsule was filled from each sample cup, with the compression air pressure again set at $140kNm^{-2}$. In this and all other experiments, the nozzle and plunger were thoroughly cleaned before filling began, and were allowed to become coated with powder as the run proceeded. The size 1 plunger was used, together with the size 0 nozzle. The results are given in Fig. 8.4.

Capsule filling from vibrated samples of fraction D was then investigated. Each sample was prepared by pouring powder from a jar into a sample cup and collar, and vibrating vertically at 100Hz. The duration and acceleration of vibration were chosen to give appreciable consolidation, without producing a sample of such density that it could not be fully penetrated by the nozzle. By

Fig. 8.4 Capsule filling data : Lactose, size fraction D, deposited from a vibrating chute and funnel.

Nozzle size 0, plunger size 1

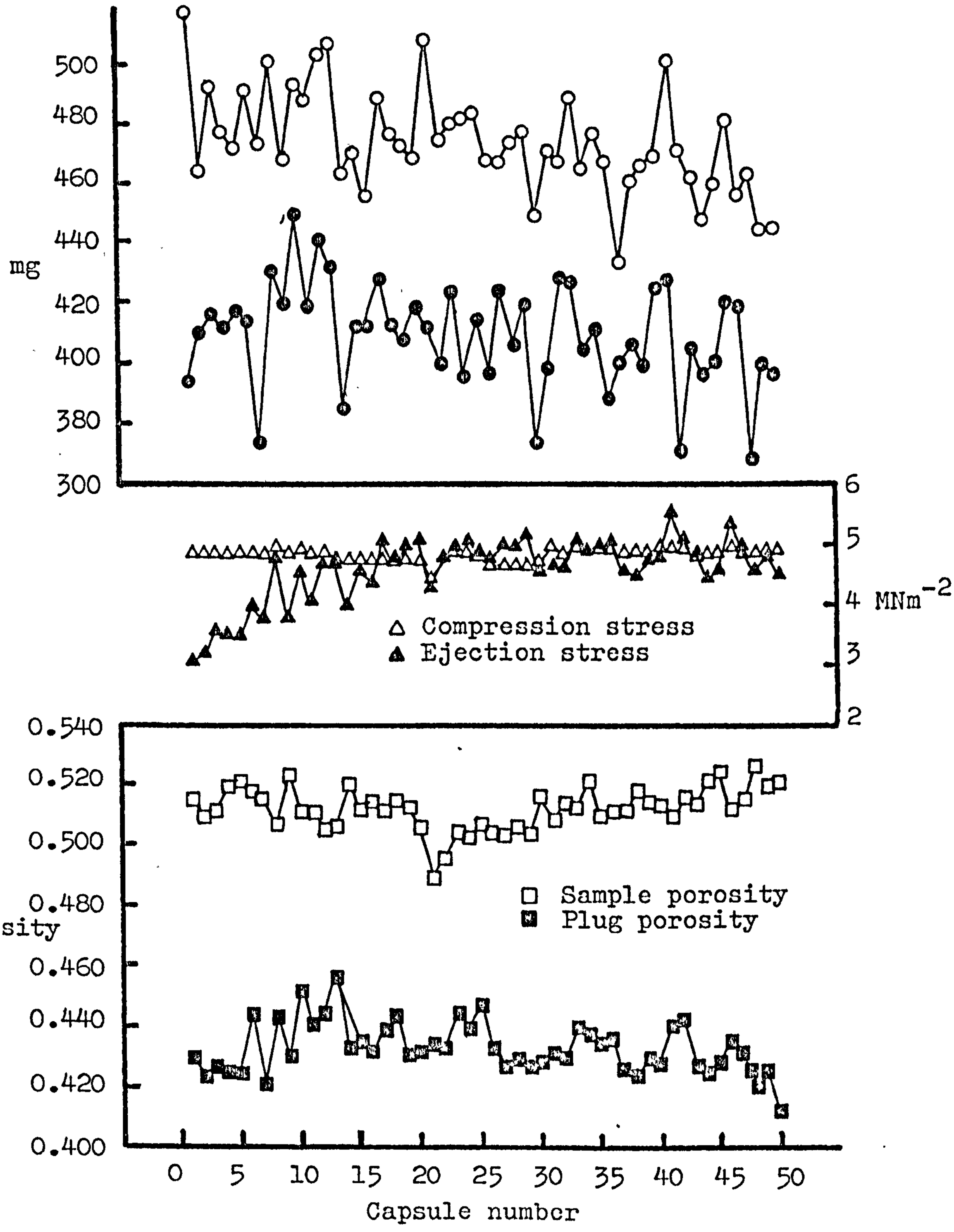

trial and error, two minutes at 2g acceleration were found to be suitable conditions. The samples produced were of rather lower porosity than in previous experiments, hence a compression air pressure of 70kNm^{-2} proved to be adequate. Again, the size 1 plunger was used. The results are given in Fig. 8.5.

The overall porosities of samples filled from the vibrating chute and funnel showed considerable variation, but this appeared to have little effect on capsule fill weight, or on the weight of powder removed from the samples (see Fig. 8.4).

Plug porosities were significantly lower than sample porosities, as expected, but as in the previous experiments (Figs. 8.2 and 8.3), the patterns of variation of the two quantities were not alike. In fact, the observed fluctuations in plug porosity bore some resemblance to the variations in ejection stress (cf. Fig. 8.2).

Ejection stress increased during the first few cycles, after which it fluctuated around an average value of about 4.5 to 5MNm^{-2}. Compression stress was much steadier, at a similar level; small changes usually led to similar but greater variations in ejection stress.

Reference to Fig. 8.5 shows that the overall porosity of the vibrated samples varied rather less than that of samples prepared by other methods. However, capsule fill weights and weights removed from samples were highly variable, much more so than could be attributed solely to sample porosity variations.

Fig. 8.5 Capsule filling data : Lactose size fraction D, deposited from a jar then vibrated. Nozzle size 0, plunger size 1

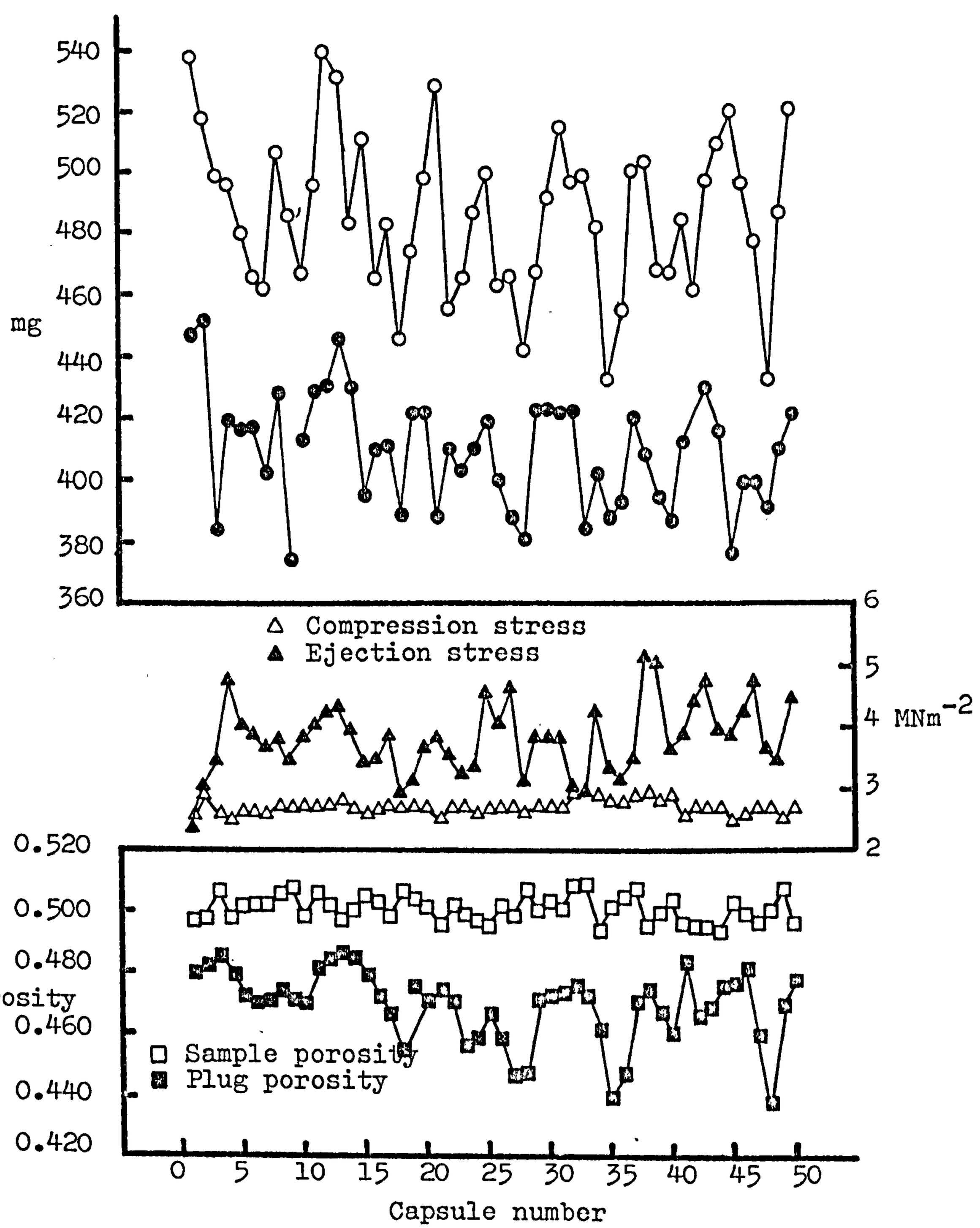

Plug porosity was only a little lower than sample porosity. This was because sample porosity had already been reduced to a relatively low level by vibration, and also because a compression air pressure of only 70kNm^{-2} was applied. The pattern of variation of plug porosity bore some resemblance to that of the weight removed from the samples, suggesting that the greater the mass of a plug, the higher its porosity at a given compression air pressure. Such a trend was less apparent in earlier results, except perhaps in Fig. 8.2, where the two quantities show similar behaviour.

Ejection stress was rather more variable than observed in previous experiments, and showed less correspondence to changes in compression stress. It fluctuated around an average of about 4MNm^{-2}, which was only slightly lower than the ejection stresses shown in Figs. 8.2, 8.3 and 8.4, even though compression stresses of under 3MNm^{-2} were applied, compared to previous values of approximately 5MNm^{-2}.

Table 8.4 presents means and coefficients of variation of sample porosity, fill weight, and weight removed from samples, for each of the three methods of sample preparation, using a size 1 plunger.

In all cases, the mean weight removed from samples was in close agreement with the calculated value of expected fill weight. The actual fill weight was invariably rather less, due to loss of powder either in

Table 8.4

The effect of method of powder sample preparation on capsule filling performance. Lactose, fraction D; size 1 plunger

		Method of sample preparation		
		Pouring from a jar	Discharge from vibrating chute and funnel	Vertical vibration 100Hz/2g/2 min.
Sample porosity	Mean	0.537	0.512	0.501
	C. of V.	1.04%	1.50%	0.88%
Fill weight (mg)	Mean	395	409	411
	C. of V.	3.86%	4.17%	4.41%
Wt. removed from sample (mg)	Mean	465	474	486
	C. of V.	3.13%	3.70%	5.46%
Expected fill weight* (mg)		462	487	498

*Based on mean sample porosity, and the dimensions of dosator nozzle and sample cups.

transit to the plug ejection station, or during ejection itself, when some of the powder fell outside the empty capsule body.

The variability of both fill weight and weight removed was consistently and markedly greater than the variability of sample porosity, indicating that plug retention is influenced by other factors which mask the effect of sample porosity. The coefficients of variation of fill weight and weight removed were expected to be lowest for vibrated samples, since they showed the most consistent overall porosities, and also because the results of Chapter 6 indicated that vibration generally produces uniform packings. However, the opposite was observed; the vibrated samples gave the highest fill weight variability. This again implies that variations in sample porosity of the order of magnitude recorded in these experiments, have no significant effect on fill weights. It may have been preferable to employ a compression air pressure of $140kNm^{-2}$ for the vibrated samples. $70kNm^{-2}$ was chosen at the time because it gave rise to ejection stresses comparable to those recorded in the other experiments, but the possibility exists that this lower compression air pressure was insufficient to ensure consistent retention of entire plugs.

8.2.2 Fraction B

(A) Experiments with the size 0 nozzle and size 0 plunger

Ten sample cups were filled with lactose fraction B

by pouring from a jar then levelling with a spatula blade. Mean sample weight, cup dimensions and nozzle dimensions were used to calculate an expected fill weight. Capsules were filled from these samples using a compression air pressure of $140kNm^{-2}$.

Measured fill weights were totally unsatisfactory, and excessive compression displacements were recorded (see Fig. 8.6). Filling was discontinued after five cycles. It was clear that much of the powder which should have been picked up by the nozzle was being pushed out of its path by the advancing "air front", thus allowing an excessively large travel of the plunger on the compression stroke, and resulting in very low, erratic fill weights.

(B) The influence of compression air pressure

Ten capsules were filled using the size 1 plunger at a compression air pressure of $70kNm^{-2}$, twenty were filled using the size 01 plunger, again at $70kNm^{-2}$, then a further twenty were filled using the size 01 plunger and a compression air pressure of $140kNm^{-2}$. In each case, samples were prepared by pouring from a jar. Mean values of overall sample porosity, fill weight and weight removed from the sample were calculated, and are shown in Table 8.5, together with values of expected fill weight.

In all cases, fill weights and weights removed from samples were much lower than expected fill weights. If anything, a compression air pressure of $70kNm^{-2}$ gave

Fig. 8.6 Capsule filling with lactose, size fraction B, using a size 0 nozzle and plunger

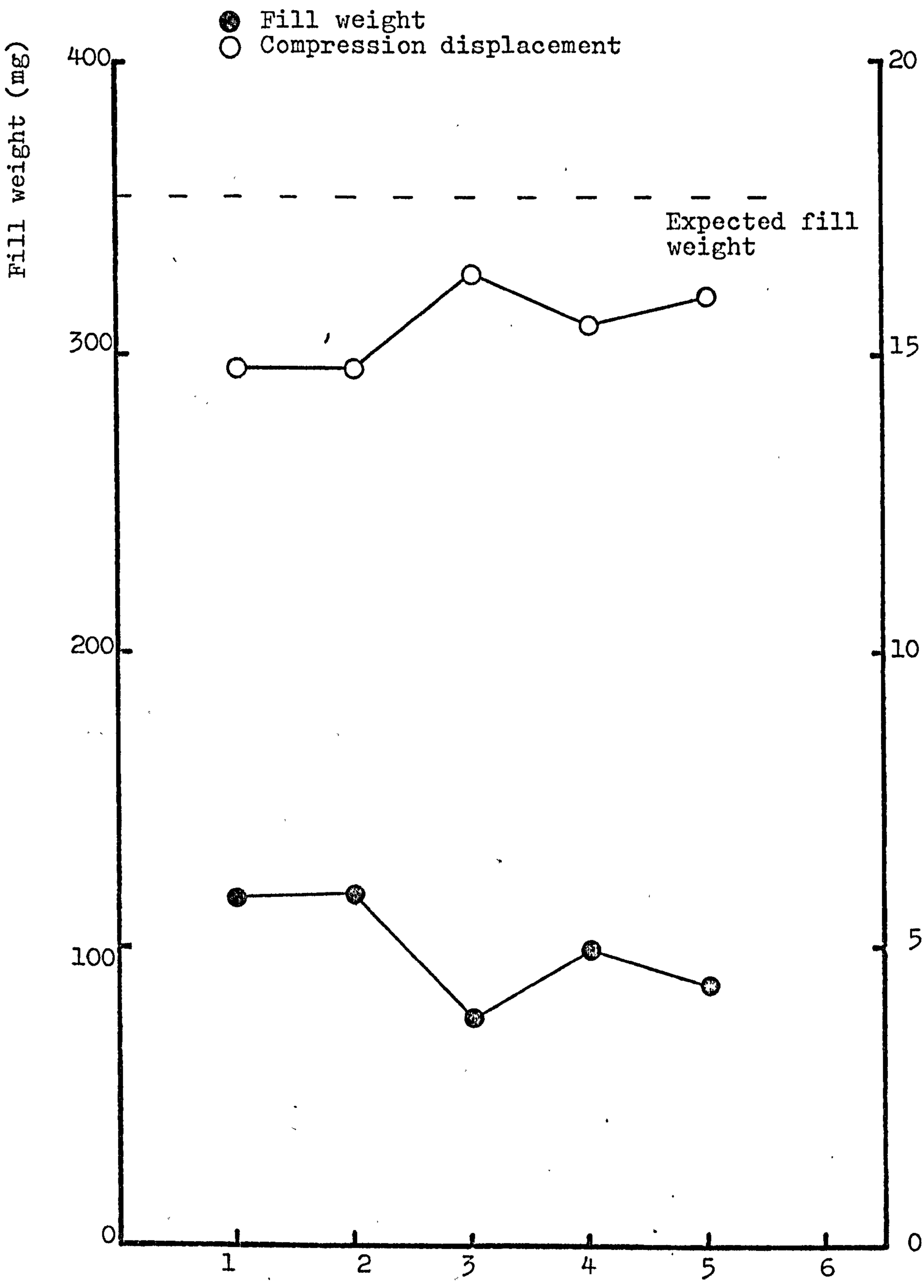

higher fill weights than 140kNm^{-2}.

Table 8.5

Influence of compression air pressure on filling performance of lactose fraction B

	Size 1 plunger 70kNm^{-2}	Size 01 plunger 70kNm^{-2}	Size 01 plunger 140kNm^{-2}
Mean initial sample porosity	0.644	0.639	0.650
Expected fill weight	356mg	361mg	350mg
Mean recorded fill weight	238mg	244mg	232mg
Mean weight removed from sample	275mg	289mg	249mg

(C) The influence of nozzle/plunger clearance

From the results shown in Table 8.5, it would appear that when a dosator nozzle enters a bed of lactose fraction B, inadequate venting occurs even when there is an undersize plunger fitted, thus resulting in low fill weights. To test the validity of this assumption, the plunger was removed during that part of the filling cycle up to and including the descent of the nozzle into a powder sample. The plunger was then replaced and the cycle was continued. Capsules were filled from five hand-poured samples, using a compression air pressure of 140kNm^{-2}, and the resulting fill weights were recorded. This experiment was carried

out with both size 1 and size 01 plungers. The results are shown in Table 8.6.

Table 8.6

Fill weights obtained with fraction B using the size 0 nozzle with size 1 and size 01 plungers. (Plunger absent during dosator descent.)

Size 1 plunger	Size 01 plunger
250mg	317mg
242mg	290mg
262mg	297mg
238mg	340mg
234mg	340mg

These results suggest that impaired venting is the cause of low fill weights with the size 01 plunger, but not with the size 1 plunger. In the latter case, removal of the plunger during dosator descent failed to produce any appreciable increase in fill weight. It therefore seems likely that the size 1 plunger only ejects the central core of a retained powder plug, leaving a thick coating adhering to the bore of the nozzle. If this coating is reasonably stable, the effective capacity of the nozzle is reduced, and low fill weights ensue. The clearance between the size 01 plunger and the size 0 nozzle

is rather less, and a greater tendency for impaired venting might therefore be expected. On the other hand, the clearance is sufficient to allow some build-up of powder coating on the nozzle bore, hence low fill weights are probably due to a combination of the two effects.

(D) The influence of the gap between the nozzle outlet and the sample container base

It can be seen from Table 8.5 that fill weights were slightly lower at 140kNm^{-2} compression air pressure than at 70kNm^{-2}, when filling capsules using the size 01 plunger. A possible explanation for this is that on the compression stroke, some of the powder is pushed out of the nozzle, through the gap between the outlet and the container base. This gap had been set at approximately 0.6mm, and was apparently small enough to prevent the escape of fraction D (cf. expected fill weights with weights removed from samples in Table 8.4). To reduce the gap to less than 0.6mm, the nozzle had to be lengthened in some way, since the dosator arm was prevented from descending any further by a stop. A 1.5mm thick fibre washer was inserted above the flange on the nozzle, and the length of the upper dosator shaft was adjusted so that the nozzle outlet, when in its lowered position, came as close as possible to the sample container base without actually making contact. In this way, escape of powder on the compression stroke could be virtually eliminated.

Ten capsules were filled, using the size 01 plunger and a compression air pressure of 140kNm^{-2}. Recorded fill weights were appreciably higher, having minimised the gap between the nozzle outlet and the container base, and therefore a further forty capsules were filled under these conditions. The results are shown in Fig. 8.7.

(Although at this stage there was no definite indication that the size 01 plunger would give higher and more consistent fill weights than the size 1 plunger, the former was retained for further experiments with fraction B. It was thought that the relatively thick powder coating which tended to build up between the size 1 plunger and the nozzle bore, might be dislodged periodically, giving rise to occasional high fill weights.)

It can be seen from Fig. 8.7 that fill weight and weight removed from samples varied to a much greater extent than sample porosity, and both quantities fell short of the expected fill weight of approximately 355mg. The average weight loss from the nozzle during pick up and ejection was 25mg, considerably less than was recorded when filling fraction D. This improvement was due to the greater tendency for fraction B to form coherent plugs which could be ejected intact.

The first value recorded for weight removed from the sample was considerably higher than subsequent values. This was because the nozzle was initially clean, and as filling proceeded, the formation of a powder coating on the nozzle bore tended to reduce the effective capacity

Fig. 8.7 Capsule filling data : Lactose, size fraction B, deposited by pouring from a jar. Nozzle size 0, plunger size 01

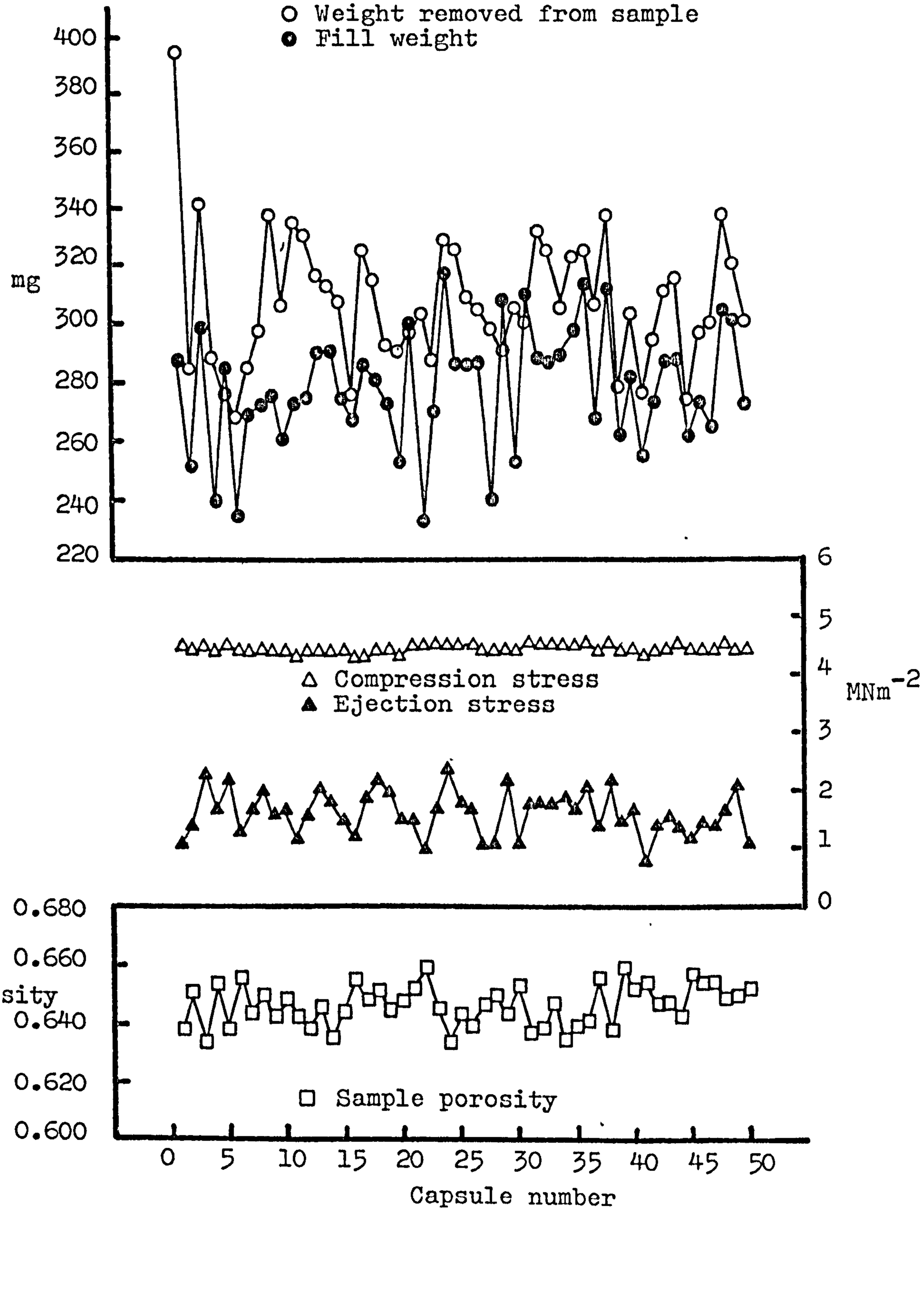

of the nozzle. Given the formation of a reasonably stable coating, the weight removed and the fill weight would be expected to show a similar pattern of variation. In practice, such similarity was only slight, indicating that the quantity of powder adhering to the nozzle bore during such experiments is variable.

Compression stress showed only minor variations, while ejection stress underwent considerable fluctuation. The initial upward trend in ejection stress during the first few filling cycles was less noticeable in this experiment than in the results for fraction D, and the overall level of ejection stress was appreciably lower, despite the application of the same compression air pressure.

Recorded values of compression displacement were found to be excessively high, and on calculating plug porosity, the values obtained were lower than could reasonably be achieved in practice. The results were therefore regarded as unreliable and were not included in Fig. 8.7. A feasible explanation for such misleading values of compression displacement is that as the undersize plunger descends, powder is able to pass between the plunger tip and the nozzle bore, and this displacement of powder enables the plunger to descend further before encountering sufficient reaction to arrest its travel.

Some degree of correlation between sample porosity and capsule fill weight can be observed (see Fig. 8.8). Low porosity samples tended to give relatively high fill

Fig. 8.8 Capsule fill weight as a function of initial sample porosity.

Lactose, size fraction B, deposited by pouring from a jar

Nozzle size O, plunger size O1

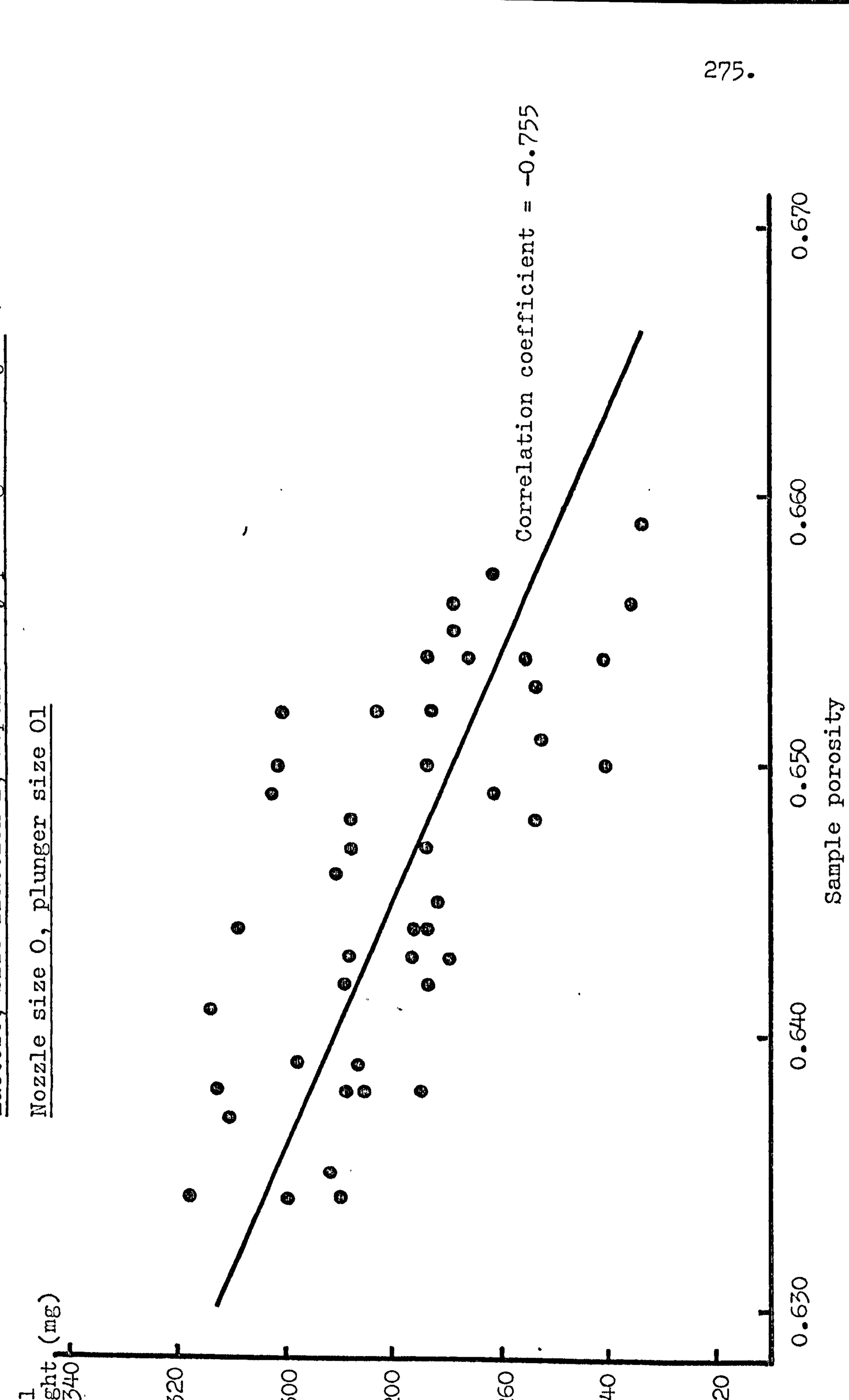

weights, though fill weight variation was too large to be attributed solely to sample porosity variations.

(E) The effect of different methods of sample preparation

Capsules were filled from samples of fraction B prepared by discharge from the vibrating chute and funnel, using a size 0 nozzle, size 01 plunger and a compression air pressure of $140kNm^{-2}$. Five lots of ten samples were prepared, and as before, one capsule was filled from each sample.

Similarly, fifty capsules were filled from samples which had been subjected to vertical vibration. By trial and error, vibration conditions of 100Hz, 2g acceleration and two minutes duration were found to be suitable, and again, a compression air pressure of $140kNm^{-2}$ was employed.

In both cases, the nozzle and plunger were cleaned before filling commenced, and throughout each filling run, sample porosity, plug porosity, compression stress, ejection stress, fill weight and weight removed from the sample were recorded as before. The results are shown in Figs. 8.9 and 8.10.

For samples filled from the vibrating chute and funnel, overall sample porosity showed considerable variation,but had little obvious influence on either capsule fill weight or weight removed from samples. Both these latter quantities were again noticeably more variable

Fig. 8.9 - Capsule filling data: Lactose, size fraction B, deposited from a vibrating chute and funnel. Nozzle size 0, plunger size 01

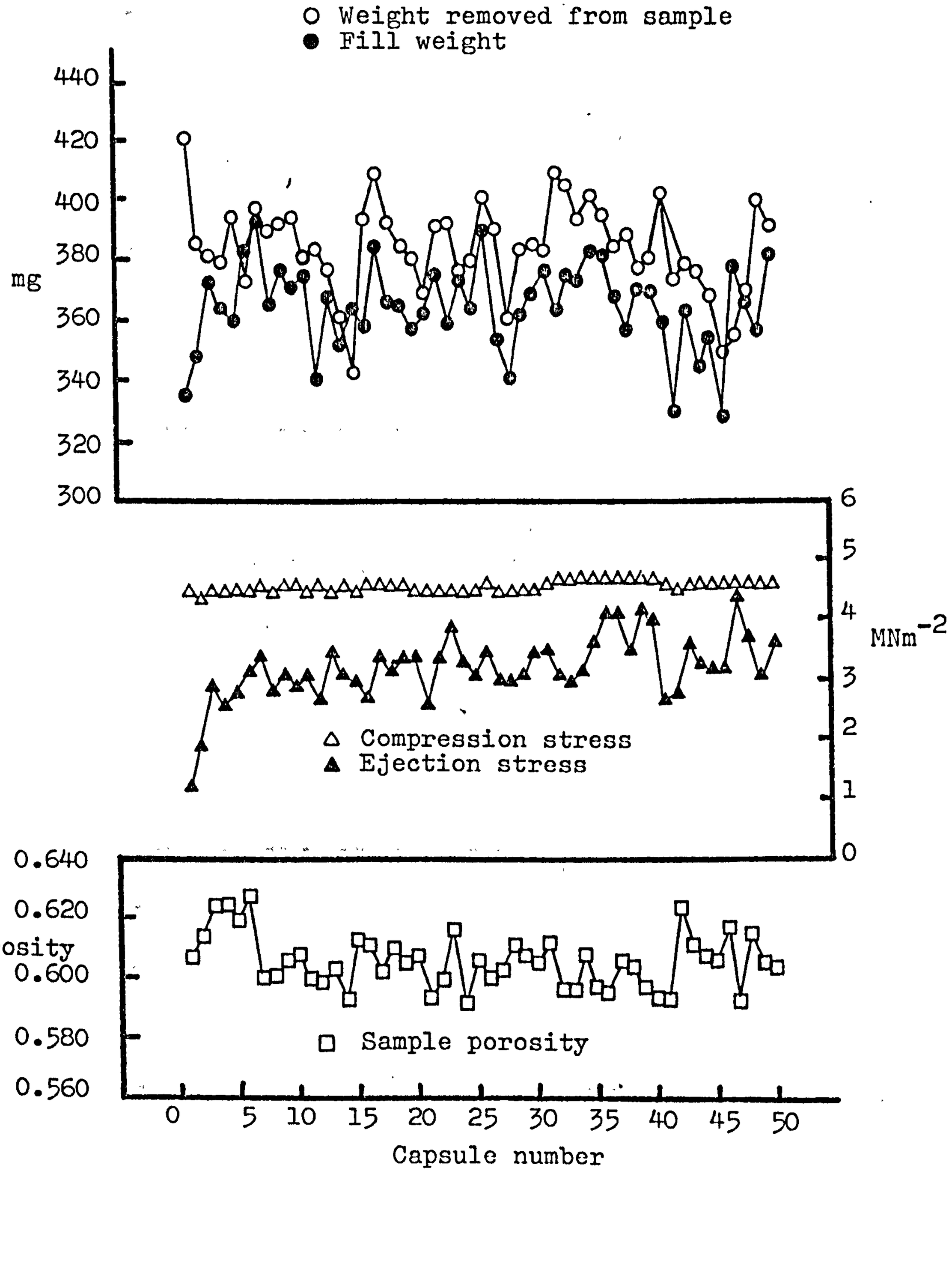

Fig. 8.10 Capsule filling data: Lactose, size fraction B, deposited from a jar then vibrated.

Nozzle size 0, plunger size 01.

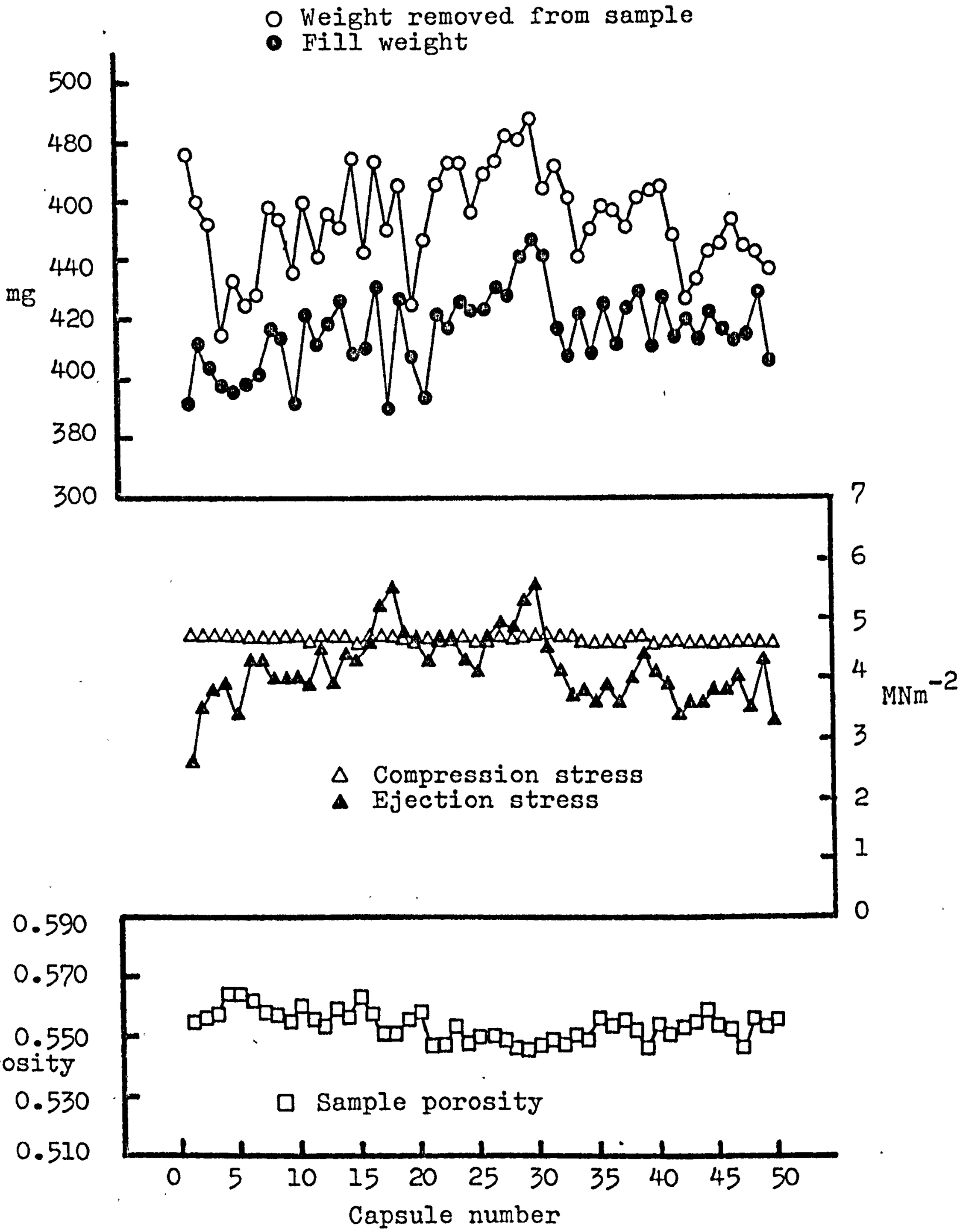

than sample porosity. On average, fill weight was found to be about 20mg less than weight removed from samples, although on a few occasions, fill weight actually exceeded weight removed. This is a further indication of the variable and unstable nature of the powder coating on the bore of the nozzle. The weight removed from samples began at a high value, for reasons discussed earlier, then fluctuated around a level very close to the expected fill weight of 386mg, which implies that there is little reduction of nozzle capacity due to powder coating. However, it was seen in chapter 6 that samples of fraction B prepared by this method tend to be considerably denser in the central region (see Table 6.3). Since plugs were also removed from the centre of each sample, a quantity corresponding to the value of expected fill weight (based on overall porosity) could still be picked up by the nozzle despite the presence of a coating on the bore.

As in all previous experiments, ejection stress was much more variable than compression stress. The general behaviour of ejection stress was rather different to that illustrated in Fig. 8.7. A definite upward trend was observed during the first few filling cycles, and by the time fifty capsules had been filled, the magnitude of ejection stress was approaching that of compression stress. The fact that the level of ejection stress shown in Fig. 8.9 is considerably higher than that seen in Fig. 8.7 can be attributed to the low level of sample

porosity achieved by filling from the vibrating chute and funnel, coupled with the application of the same compression air pressure in both experiments.

Values of plug porosity were calculated but were again found to be ~~unrealistic~~ misleading, and were therefore not included in Fig. 8.9.

Ejection stress showed a similar pattern of variation to that of fill weight. This does not seem unreasonable, since a small plug is likely to have a lower area of contact with the nozzle bore than a large plug, and ejection might be expected to be easier for this reason.

Reference to Fig. 8.10 shows that the overall porosity of samples of fraction B subjected to vibration varies rather less than that of samples prepared by other methods. However, both capsule fill weight and weight removed from samples were still much more inconsistent than sample porosity. On this occasion, some similarity could be observed between the patterns of variation of the two weights, indicating a relatively stable powder coating, with the discrepancy between the two (averaging about 40mg), being lost either in transit or during ejection. The weight removed from samples fluctuated around a level of about 450mg, which is very close to the expected fill weight of 445mg. In this case, the findings of Chapter 6 (see Table 6.9) do not predict a denser central region in the vibrated samples, so the weight removed from samples would appear to be a little high,

bearing in mind that a powder coating is presumed to have been present on the nozzle bore. Once again, the initial value of weight removed was rather high, due to the clean condition of the nozzle at the outset, but it is interesting to note that similarly high values were recorded on several subsequent occasions, perhaps indicating that coating was less extensive in this experiment than in others.

Sample porosity was lower in this experiment than in either of the previous two, and in addition to the resultant higher fill weights, the level of ejection stress was also increased, exceeding compression stress on several occasions. An initial upward trend was followed by variation around an average level of about 4 to 4.5MNm^{-2}. Calculated values of plug porosity were again regarded as unrealistic.

Table 8.7 lists the means and coefficients of variation of sample porosity, fill weight, and weight removed from samples, for each of the three methods of sample preparation studied.

Comparison of the mean values of weight removed from samples with corresponding values of expected fill weight, indicates that the tendency for a powder coating to adhere to the nozzle bore, thus reducing its effective capacity, increases with the porosity of the samples from which plugs are taken. It is possible that when a dosator plunger enters a low density sample, an appreciable

Table 8.7

The effect of method of powder sample preparation on capsule filling performance. Lactose, fraction B; size 01 plunger

		Method of sample preparation		
		Pouring from a jar	Discharge from vibrating chute and funnel	Vertical vibration 150Hz/2g/2min
Sample porosity	Mean	0.646	0.606	0.554
	C. of V.	1.09%	2.28%	1.07%
Fill weight (mg)	Mean	279	364	416
	C. of V.	7.23%	4.02%	3.08%
Wt. removed from sample (mg)	Mean	309	384	454
	C. of V.	7.26%	3.97%	3.62%
Expected fill weight (mg)*		353	393	445

*Based on mean sample porosity and the dimensions of dosator nozzle and sample cups.

quantity of powder passes between the descending plunger tip and the nozzle bore, and does not become part of the compressed plug, but stays in the nozzle during the ejection stage. Samples of greater density (lower porosity) are more likely to behave as a coherent mass, with less powder remaining in the nozzle on ejection.

In these experiments, the discrepancy between fill weight and weight removed was markedly less than was observed using fraction D. The reason for this reduction in powder loss was the greater tendency of fraction B to be ejected as a coherent plug, which could enter the waiting empty capsule body intact.

The variabilities of fill weight and weight removed were significantly greater than the variability of sample porosity, suggesting, as was the case with fraction D, that any effect on capsule fill weight variation due to changes in sample porosity is masked by other factors governing plug retention.

Fill weight variation appeared to be less dependent on the variability of sample porosity than on its actual magnitude. The lower the mean sample porosity, the lower was the resulting coefficient of variation of capsule fill weight. From a different point of view, it could be said that fill weight variation decreased as average ejection stress increased, although it would be unwise to assume that such a trend could continue indefinitely.

8.2.3 Fraction F

(A) Experiments with the size 0 nozzle and size 0 plunger

Ten sample cups were filled with fraction F, by pouring from a jar then scraping the surface level with a spatula blade. The size 0 nozzle and plunger were cleaned and fitted to the dosator arm, and the compression air pressure was fixed at 140kNm^{-2}. Capsules were then filled from these ten samples.

Fill weights and compression displacements were recorded and are shown in Fig. 8.11. It can readily be seen that fill weights were very low, averaging only approximately half of the expected value of 461mg. This observation, coupled with recorded compression displacements ranging from 7.7mm to 10.3mm, indicates quite clearly that a significant proprotion of the powder expected to occupy the dosator nozzle was in practice pushed out of the path of the nozzle by the descending air front. Thus, immediately prior to the depression of the plunger, a depth of powder much less than the intended 20mm was present inside the nozzle. This "air-front" effect is aggravated by any build up of powder coating on the nozzle bore; hence, as seen in Fig. 8.11, fill weights began at a low level and decreased further as the filling cycle was repeated. This was accompanied by a simultaneous rise in compression displacements.

(B) The influence of nozzle/plunger clearance

Having established that the size 0 nozzle and size 0

Fig. 8.11 Capsule filling with lactose, size fraction F, using a size 0 nozzle and plunger

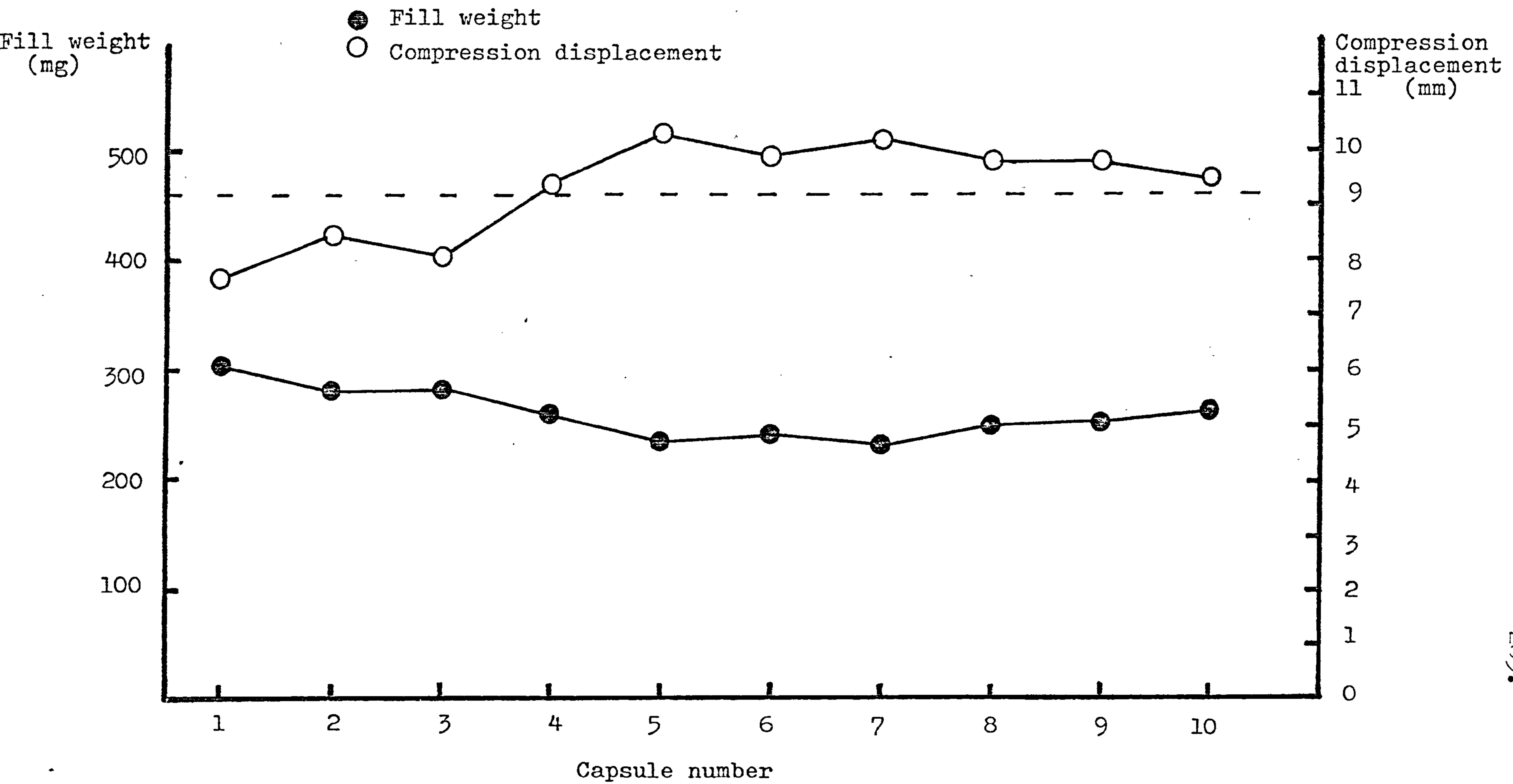

plunger were an unsatisfactory combination, experiments were carried out to compare the performance of the size 1 and size 01 plungers, when used with the size 0 nozzle.

For each nozzle/plunger combination, five lots of ten sample cups were filled with fraction F, by pouring from a jar. One capsule was filled from each sample in the usual way, employing a compression air pressure of $140kNm^{-2}$. This pressure was selected on the basis of experience with fraction D, and the resulting satisfactory plug retention and ejection suggested it was suitable for samples of fraction F having overall porosities of approximately 0.54.

Data were recorded as before, and are shown in Figs. 8.12 and 8.13.

In both experiments, sample porosity varied about a mean of approximately 0.54, whilst the variabilities of both fill weight and weight removed were noticeably greater. Sample porosity variations appeared to have little direct effect on these weights. The discrepancy between fill weight and weight removed was approximately 60mg in each case, and was due mainly to loss on ejection (see section 8.2.1). The weight variabilities were less marked using the size 1 plunger, and the average weight removed (458mg) was closer to the expected fill weight (462mg) than was the case using the size 01 plunger, where the corresponding values were 440mg and 460mg respectively.

Compression stress was relatively steady at a little

Fig. 8.12 Capsule filling data: lactose, size fraction F, deposited by pouring from a jar. Nozzle size 0, plunger size 1.

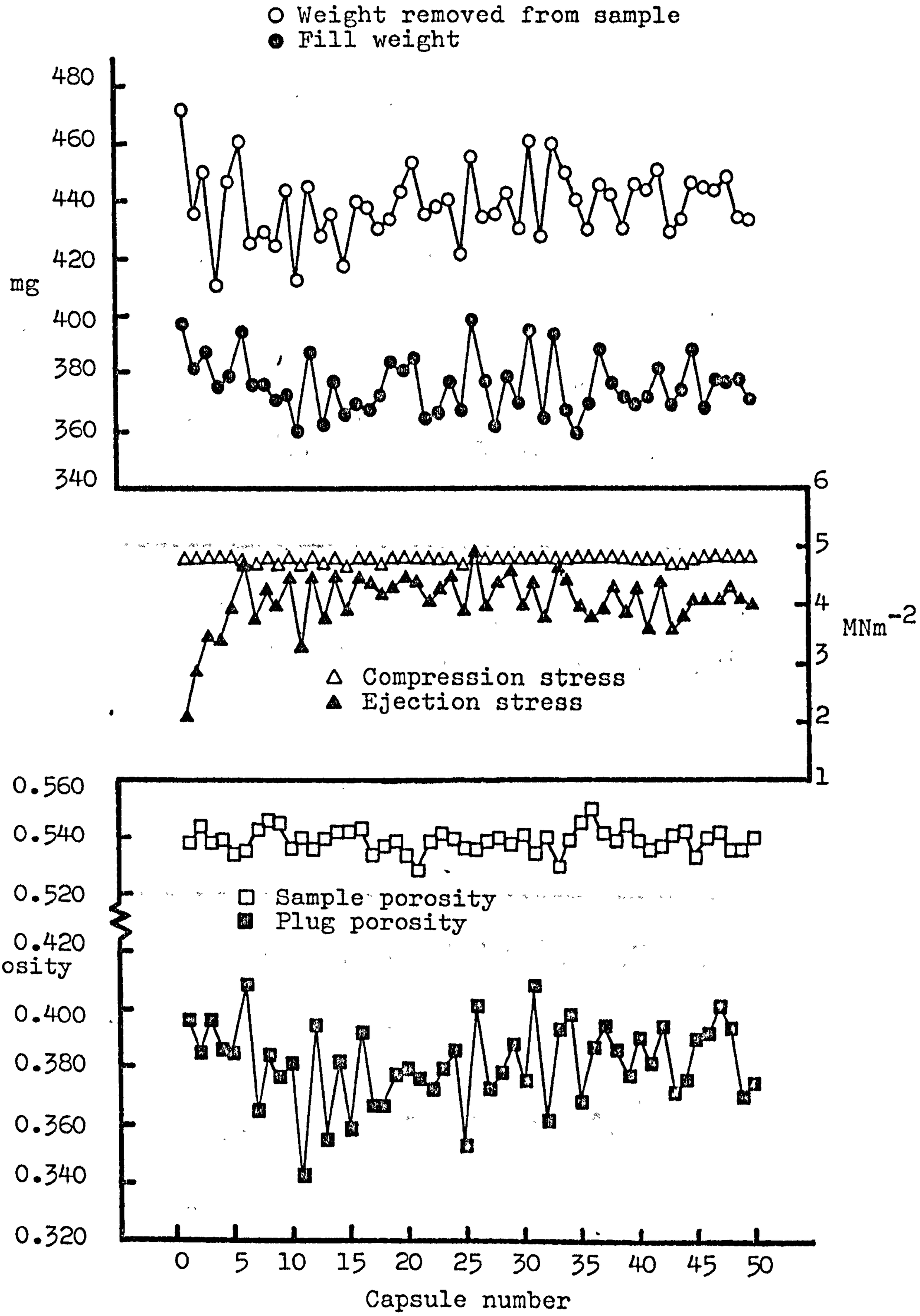

Fig. 8.13 Capsule filling data: Lactose, size fraction F, deposited by pouring from a jar. Nozzle size 0, plunger size 01.

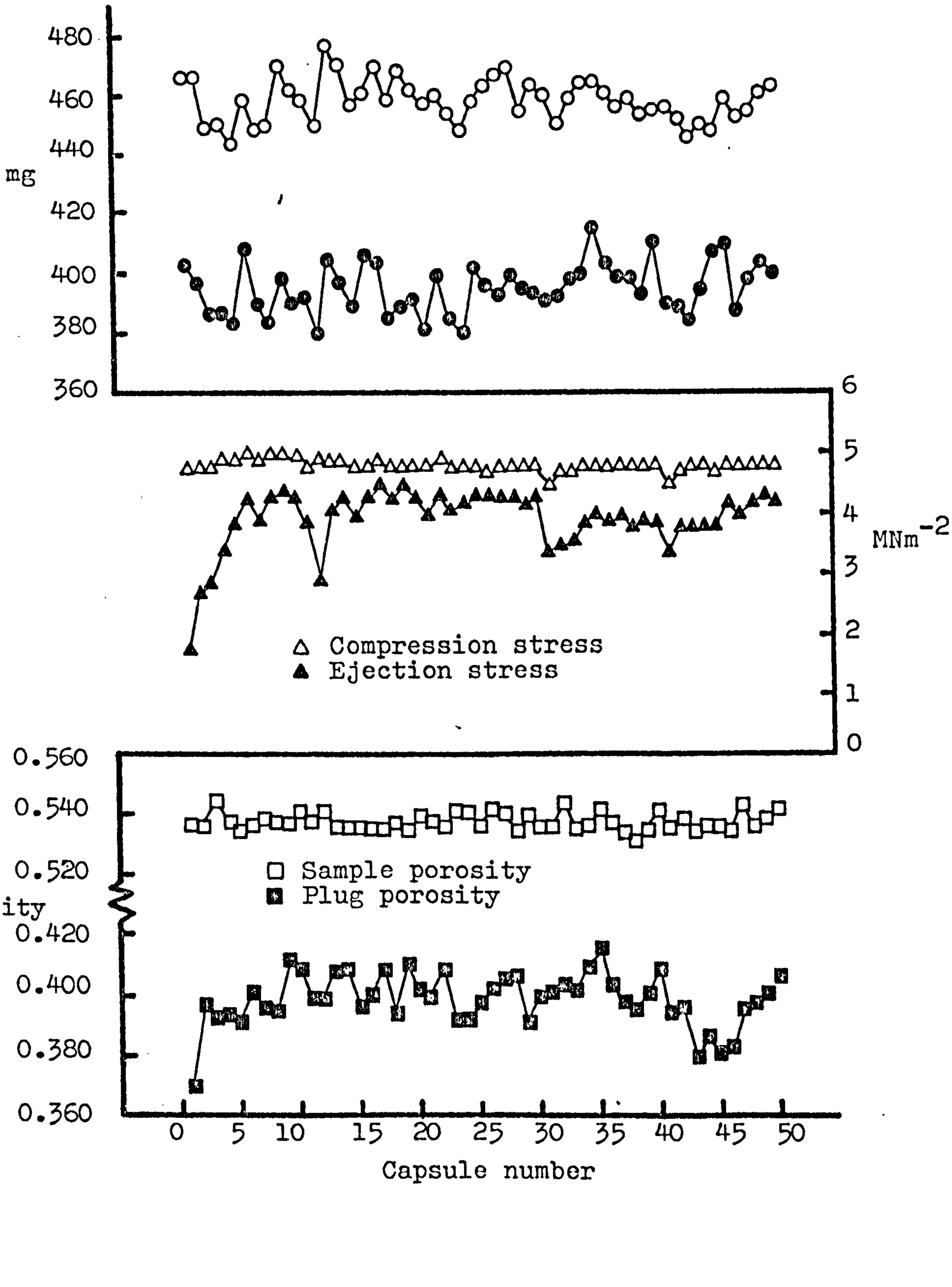

under $5MNm^{-2}$, while ejection stress, initially about $2MNm^{-2}$, rose during the first few filling cycles, and levelled off at approximately $4MNm^{-2}$. Small changes in compression stress tended to result in larger variations in ejection stress.

Plug porosity values were rather more variable than sample porosities, particularly when using the size Ol plunger, and there did not appear to be much correlation between the two quantities. Plug porosity was found to be slightly higher using the size 1 plunger than with the size Ol plunger, indicating that the larger plunger produced a greater compression displacement at the same compression stress. The reason for this is not clear.

The size 1 plunger was thought to be the more suitable of the two, mainly because recorded fill weights were both slightly greater and less variable. A possible explanation is that the size 1 plunger allows more efficient venting, there being, perhaps, a slight "air front" effect with the size Ol plunger. The mean particle volume diameter of fraction F is 80.8µm, whilst a mean clearance of 285µm exists between the tip of the size Ol plunger and the bore of the size O nozzle. Thus a coating approximately three or four particles diameters thick might seriously restrict the escape of air during dosator descent.

It was observed during this experiment that the coherent part of a typical plug after ejection tended to be roughly conical in shape, and the diameter

of the top of the plug appeared to be the same as the diameter of the plunger being used. Thus, narrower plugs were obtained with the size 1 plunger than with the size 01, whilst more loose accompanying powder was ejected (see Fig. 8.14). Despite this, the ejection stresses recorded were very similar.

(C) The effect of different methods of sample preparation

In accordance with the scheme set out at the beginning of this chapter, five lots of ten samples were filled using the vibrating chute and funnel, and a further five lots were prepared by pouring from a jar, followed by the application of vertical vibration at 150Hz, and 2g acceleration for two minutes.

One capsule was filled from each sample, using a size 0 nozzle and size 1 plunger. Sample porosities were somewhat lower than in section 8.2(B), hence a lower compression air pressure of $105 kNm^{-2}$ was employed.

The usual data were recorded and are shown in Figs. 8.15 and 8.16.

The overall porosity of samples prepared by deposition from the vibrating chute and funnel varied around an average of about 0.495. Both fill weight and weight removed showed wider variation than sample porosity, and both decreased from a high initial level as filling proceeded. By the time the run of 50 capsules had been completed, the two weights appeared to be increasing again.

Fig. 8.14 The influence of plunger size on the coherence of a plug of lactose, size fraction F, ejected from a size 0 nozzle

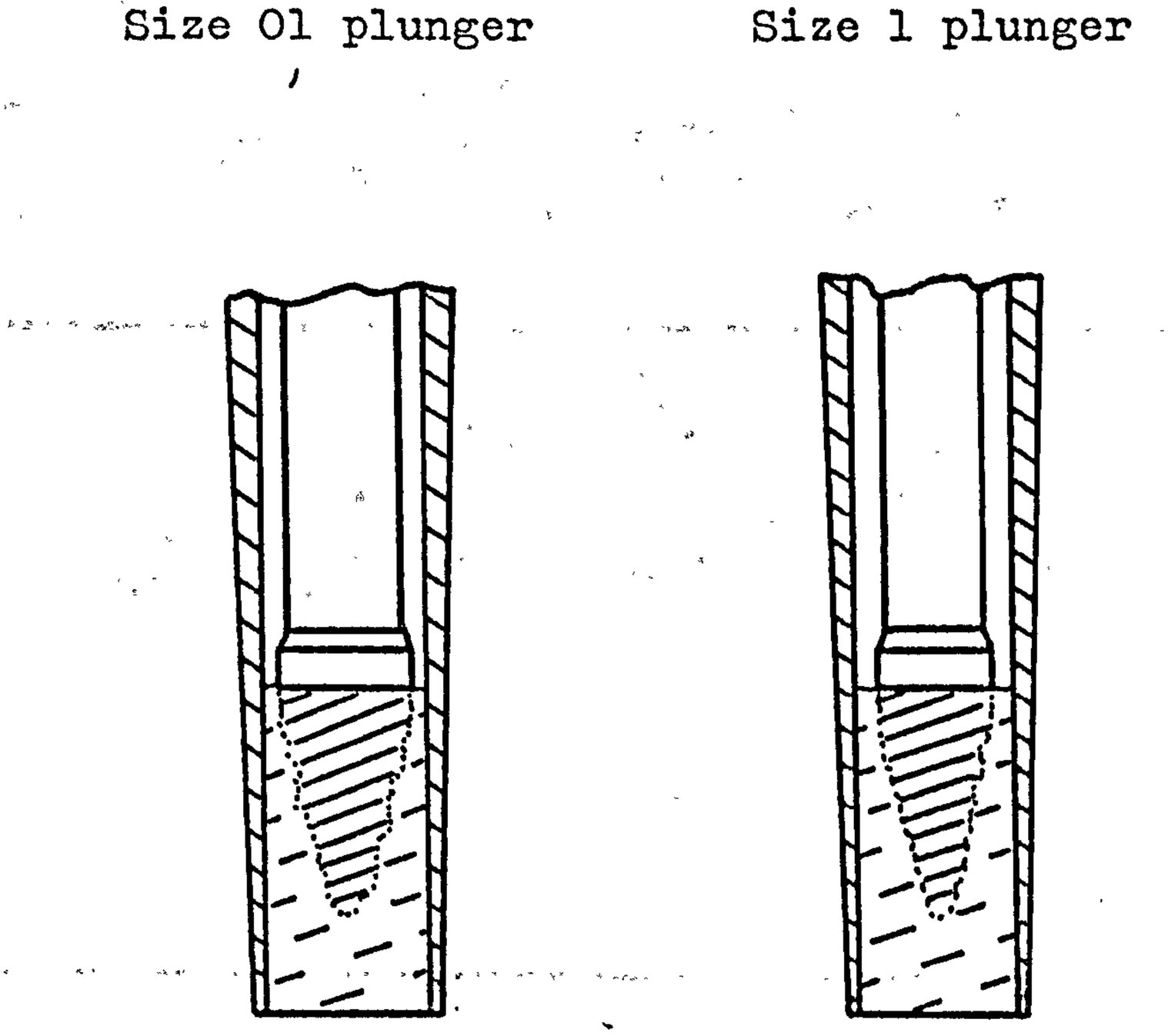

Fig. 8.15 Capsule filling data: Lactose, size fraction F, deposited from a vibrating chute and funnel.
Nozzle size 0, plunger size 1.

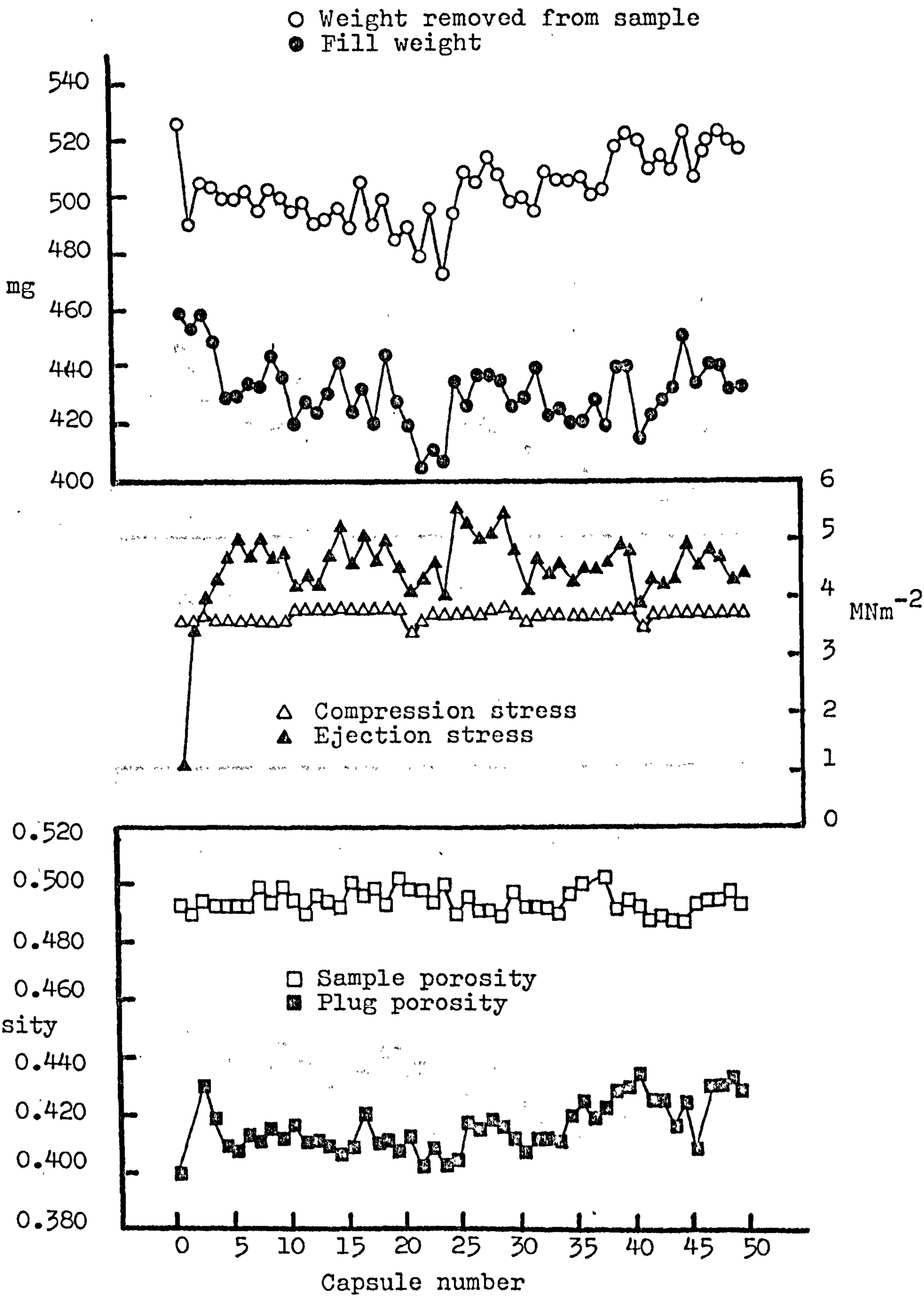

Fig. 8.16 Capsule filling data: Lactose, size fraction F, deposited from a jar then vibrated. Nozzle size 0, plunger size 1.

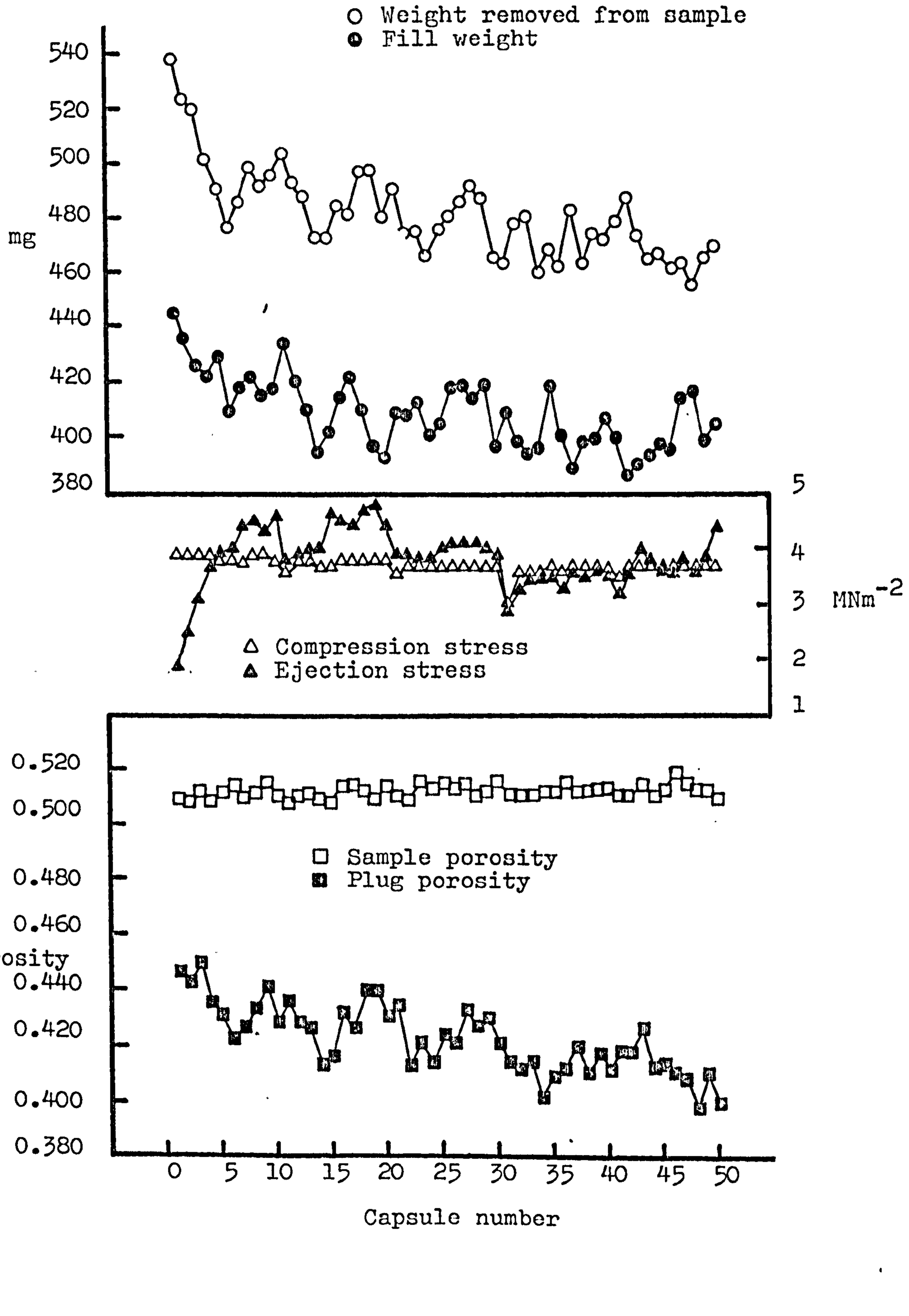

These trends were unlikely to be due entirely to variations in porosity between different samples.

The mean weight removed from samples was 503mg while the expected fill weight was calculated to be 504mg. The mean actual fill weight was some 70mg less, due as before to loss of powder at the ejection stage.

Ejection stress rose sharply, levelling off after about six cycles at a level slightly higher than that of compression stress. Relatively low sample porosity was the cause of such comparatively high ejection stresses. For example, the ejection stresses shown in Fig. 8.13 are no higher than those shown in Fig. 8.15, despite the fact that a greater compression stress was in operation in the former case. The samples represented in Fig. 8.15, however, were more dense initially, thus aiding retention in the nozzle.

Plug porosity, once again, proved to be rather more variable than sample porosity, and appeared to be on the increase towards the end of the run, for no obvious reason.

Ejection stress and fill weight showed a similar pattern of variation apart from during the first ten cycles or so, when the development of a coating on the nozzle was accompanied by an increase in ejection stress and a decrease in fill weight. A high fill weight may reasonably be expected to require a high ejection stress, due to the increased area of contact between nozzle and powder.

Vibrated samples were of a marginally higher overall porosity than those filled from the vibrating chute and funnel. This was due to the fact that pouring from a jar gives rise to relatively high porosity, which is only slightly decreased by the application of vibration of the specified characteristics.

Fill weight and weight removed underwent variations much too great to be caused solely by sample porosity variations. Both weights appeared to decrease during the course of the run, although a general levelling off can probably be assumed to have taken place after about twenty cycles. The expected fill weight of 487mg was almost attained by the mean weight removed from samples (482mg), while the mean actual fill weight was again approximately 70mg less, for reasons given previously.

Ejection stress again showed a rapid increase during the first few filling cycles then stabilised at a level similar to that of compression stress. As before, small fluctuations in compression stress generally gave rise to more exaggerated variations in ejection stress.

Plug porosity was rather more variable than sample porosity, and underwent a gradual decrease as the run proceeded, showing a similar pattern of variation to that of weight removed from samples.

The mean values and coefficients of variation of sample porosity, fill weight, and weight removed from samples, for each method of sample preparation, are shown in Table 8.8.

Table 8.8

The effect of method of powder sample preparation on capsule filling performance. Lactose, fraction F; size 1 plunger

		Method of sample preparation		
		Pouring from a jar	Discharge from vibrating chute and funnel	Vertical vibration 150Hz/2g/2min
Sample porosity	Mean	0.537	0.495	0.512
	C. of V.	0.64%	0.79%	0.49%
Fill weight (mg)	Mean	395	431	409
	C. of V.	2.11%	2.72%	3.13%
Wt. removed from sample (mg)	Mean	458	503	482
	C. of V.	1.57%	2.32%	3.47%
Expected fill weight (mg)*		462	504	487

*Based on mean sample porosity and the dimensions of dosator nozzle and sample cups.

In each case, mean weight removed was very similar to expected fill weight. Loss of powder in transit to the ejection station, and, more particularly, during ejection, resulted in actual recorded fill weights being generally about 70mg lower. This discrepancy is very similar to that observed with fraction D, and observation of the plug ejection process showed that powder was going astray in the same manner (see earlier).

In common with the results for both fraction D and fraction B, the variations in fill weight and weight removed from samples were consistently higher than the variation in overall porosity between successive samples, implying once again that the effects of porosity variations of the order of magnitude encountered in these experiments, are masked by other, more significant aspects of plug retention.

The vibrated samples showed the least between-samples porosity variation, and the results of chapter 6 suggest that they would also possess the least within-samples variation. Despite this, the capsules filled from these samples displayed the highest variation in fill weight and weight removed.

In discussing the results for fraction D, it was suggested that the use of different compression air pressures may make a comparison of different sets of results more complicated. This problem recurs with these results for fraction F. However, the choice of compression

air pressure is dictated to some extent by the initial porosity of the samples from which plugs are to be taken, and since this porosity is dependent on the method of sample preparation, it is not always feasible to maintain the same compression air pressure for different sets of samples. If ejection stress were taken to be a criterion for characterising the degree or "strength" of retention, then the choice of a compression air pressure giving rise to a certain pre-selected ejection stress might be a reasonable basis for comparing capsule filling performance from samples of different initial porosity.

8.2.4 Correlation between sample porosity and capsule fill weight

Previous discussion has noted the apparent lack of correlation between the overall porosity of the powder samples and the fill weights of capsules filled from them. To quantify this observation, linear regressions were performed on the results contained in Tables 8.4, 8.7 and 8.8, yielding a number of values of correlation coefficient for the relationship between the two quantities (see Table 8.9).

In each linear regression, there were fifty data points, giving 48 degrees of freedom. At fifty degrees of freedom, minimum values of correlation coefficient are as follow:

For 95% significance : 0.273

For 99% significance : 0.354

Table 8.9

Values of correlation coefficient for the relationship between overall sample porosity and capsule fill weight

Size fraction	Method of sample preparation		
	Pouring from a jar	Discharge from vibrating chute and funnel	Vertical vibration at specified condations
B	0.768	0.268	0.513
D	0.427	0.340	0.306
F	0.201	0.414	0.302

(Fisher and Yates, 1963). Of the nine values in Table 8.9, four are significant at the 99% level of probability, three others are significant at the 95% level, and the remaining two are not significant at the 95% level.

The inference from Table 8.9 is that in most cases, there is a significant linear relationship between sample porosity and fill weight, despite the fact that in all cases, fill weight variation was considerably greater than sample porosity variation. The highest correlation coefficient (0.768), obtained for samples of fraction B prepared by pouring from a jar, corresponds to the graph shown in Fig. 8.8. This particular set of results was the only one in which a relationship between sample porosity and fill weight was readily visible.

8.3 Conclusions

Throughout all the results in this chapter, capsule fill weight variation greatly exceeded variations in overall porosity between successive powder samples. However, in most cases, a significant linear relationship could be established between these two quantities, indicating that the influence of overall sample porosity can be detected, despite the existence of other factors governing fill weight variation.

The significance of within-samples variations in porosity has not been successfully determined. Uniform samples would be expected to facilitate the prediction,

based on overall porosity, of capsule fill weight. There is, however, no evidence in this chapter that highly uniform samples have a more predictable effect on fill weight than samples possessing large local porosity variations. The physical size of the dosator nozzle may reduce the effect of such local variations by averaging them out to some extent.

Certain other, trends and correlations were observed in isolated experiments, but none were repeated consistently enough to be regarded as significant.

An alternative approach to capsule filling would have been to select a suitable quantity, for example ejection stress, which could be kept approximately constant, enabling a more meaningful comparison to be made between different sets of results. The aim of the work was not to study the effect of overall porosity on plug retention ability at a given compression stress, but to monitor the quantity of powder actually entering the dosator nozzle, and to ensure efficient retention of that powder. Since ejection stress can be regarded as a measure of the "strength" of retention, then by adjusting to a suitable level the compression stress applied to a given set of powder samples, the level of ejection stress could be controlled, thus providing a reproducible degree of retention.

The use of a size 0 plunger in combination with a size 0 nozzle proved to be unsatisfactory with all three

particle size fractions of lactose studied. It was illustrated conclusively that inadequate venting occurs, reducing fill weights to little over half the expected values, due to the "air front" effect. Although the production machines employed in the pharmaceutical industry carry dosators of different design to the one used in this work, similarly low fill weights could presumably be encountered. The cause of this poor venting was shown to be insufficient clearance between plunger tip and nozzle bore, and the problem was aggravated by any build-up of powder coating on the nozzle bore. The incorporation of lubricants into commercial formulations might alleviate the problem to some degree. The difficulty was successfully overcome by employing undersize plungers.

The gap between the nozzle outlet, when in its lowered position, and the base of the sample container, was found to be significant, although no relationship between particle size and maximum allowable gap size was established. A gap of 0.6mm proved small enough to prevent the escape of an appreciable quantity of fraction D (+36.5-53μm) during compression, but the same gap was found to be too great for fraction B(+18.7-26.5μm), allowing a detectable amount of powder to be pushed out of the nozzle during the compression stroke. The gap was therefore reduced to a minimum and was maintained thus during all experiments with fractions B and F.

In terms of capsule filling performance, fractions

D and F behaved very similarly. A considerable quantity of powder failed to be directed into the empty capsule body on ejection; the tendency for this "spraying" effect was due partly to the lack of coherence of the plugs. With both size fractions, the same rank order of fill weight variation was observed for the methods of sample preparation studied; pouring from a jar produced least fill weight variation, followed by deposition from the vibrating chute and funnel, while vibrated samples gave the highest variability of fill weight. Furthermore, the size 1 plunger was found to be more suitable than the intermediate size (01), possible because of a slight "air-front" effect with the latter.

The capsule filling characteristics of fraction B were rather different, due to its cohesive nature. Retention and ejection posed few problems, plugs were much more coherent than with either of fractions D and F, and little powder was lost at the plug ejection stage. The rank order of fill weight variation for the methods of sample preparation employed was the opposite to that observed for fractions D and F. Vibrated samples gave the lowest fill weight variations, followed by deposition from the vibrating chute and funnel, while hand-poured samples produced the highest variability of fill weight. The intermediate size (01) plunger appeared to be preferable to the size 1, for filling fraction B, due to the tendency for the latter to allow excessive powder

coating to develop on the nozzle walls.

Each capsule filling run began with a clean dosator nozzle and plunger, and initial values of ejection stress were generally relatively low. Subsequent values showed a gradual increase, until, after the completion of several filling cycles, a plateau was reached, about which further recorded values of ejection stress fluctuated. This observed increase was due to the development of a powder coating on the walls of the nozzle. Jolliffe (1980), using lactose, showed that the force required to cause powder to slide over a metal surface depends on the angle of wall friction. If the process is carried out repeatedly, some particles stick in the surface irregularities of the wall, and some of the powder-wall friction is replaced by powder-powder friction. Since the effective angle of internal friction of lactose is always greater than the angle of wall friction, irrespective of the roughness of the wall, the result is an increase in the force required for motion to occur. Thus, as a nozzle becomes coated, the ejection stress, which is a measure of the force required to cause the plug to slide out of the nozzle, must increase. Similarly, the considerable variations in ejection stress, observed even after the initial increase was complete, indicate that the area of nozzle wall covered by a powder coating varied from one cycle to the next. This might have a significant influence on capsule fill weight variation.

The model dosator system employed for these experiments possessed a number of advantages. Capsules were filled one at a time, and the cycle could be started and stopped easily and at any point. All filling components were easily accessible and adjustable, and the attachment of the load cells to the air pistons enabled the capsule size to be changed without affecting the instrumentation. The provision of individual powder sample cups facilitated both the control of sample depth and the calculation of expected fill weight for each individual capsule filled. The use of an air cylinder for operating the compression punch ensured that a fixed compression stress could be applied to each plug, irrespective of initial sample porosity. Plug compression on production machines is characterised by a fixed displacement, and thus if a nozzle dips into a low porosity region, a relatively high compression stress is applied, and this will result in an increase in ejection stress.

The model system also had a number of disadvantages. The load cell diaphragms were positioned approximately 17cm above the powder plugs at the time of stress application; the effect of this distance on the accuracy of measurements was unknown. In addition, there was no compensation for any acceleration effects which might contribute to the traces obtained. The use of an air cylinder to effect plug ejection was found to have limitations. The air pressure tended to build up as the

plunger encountered the plug, then the plug would be ejected very suddenly. In the case of fractions D and F, this sudden ejection resulted in the break-up of the plug,and the failure of some of the powder to be directed into the empty capsule body. Furthermore, the maximum air pressure available for ejection was only about $490kNm^{-2}$, and hence it was quite possible for strongly-retained plugs not to be ejected at all. Mechanical methods of ejection generally provide a smoother and more reproducible action. The use of individual sample cups made capsule filling a slow and laborious procedure, and the filling of large batches proved impracticable.

Chapter 9

Concluding Discussion

The work contained in the previous chapters has investigated the influence of the packing behaviour of a model powder system (lactose) on the weight variation of hard gelatin capsules filled by a model dosator system. The purpose of this chapter is to consider the findings of each section and to draw overall conclusions.

By choosing to work with a number of particle size fractions of a single particulate material, a considerable range of flow and packing properties was encompassed. In chapter 3, it was found that generally, as particle size increases, over the range studied, the porosity of a loose packing decreases, since the absence of cohesive forces enables particles to find positions of high stability and close packing. However, the porosity is dependent on the method of deposition. For free-flowing materials, the effect of deposition method followed existing theories, in that low intensity and high velocity of deposition tended to give relatively low porosity packings. More cohesive material behaved in a more complicated manner, due to the tendency for powder to be deposited as loose aggregates rather than as individual particles. Cohesive forces also allowed the intermittent build-up and collapse of temporary structures in a developing sample, resulting in the production and

maintenance of high porosity regions. For this reason, a need was observed for preparing samples in even layers, if low porosity was to be achieved.

Overall porosity could be significantly reduced by the application of controlled vibration. For the particle size fractions of lactose studied, a frequency range of about 100-200Hz appeared to be most useful. Free-flowing materials were more susceptible to vibratory consolidation than cohesive materials, hence the latter required greater vibration accelerations to achieve a similar porosity. This is due to the fact that with cohesive powder,there are stronger interparticulate forces to be overcome to effect particle rearrangement. Vertical vibration was found to be consistently more effective than horizontal vibration in producing consolidation. For the size of samples used, there appeared to be no advantage in employing accelerations in excess of 12g.

Chapters 4, 5 and 6 were concerned with the application of the technique of gamma-ray attenuation for assessing local porosity variations within individual powder samples, and for this purpose, a narrow beam of 60keV gamma-radiation from an Americium-241 point source was used. Convincing evidence was obtained to suggest that the experimentally determined attenuation coefficient of particulate lactose increases with porosity, and for the range of porosity encountered, a linear relationship was suggested. This relationship appeared to be

independent of both particle size and apparent sample thickness. Attempts were made to discover the reason for the variation in observed attenuation coefficient, and two alternative theories were investigated. The first suggested that by compressing a powder sample (i.e. reducing its porosity), the geometry of the absorber was being altered, and the angular distribution of scattered photons would inevitably change. In any practical system, even those employing narrow-beam conditions, a certain small proportion of scattered photons actually reach the detector, resulting in a falsely high count, and it is likely that the extent to which this detection of unwanted radiation occurs is affected by changes in absorber geometry. However, the theory underlying the detection of such secondary photons is highly complex, and no attempt was made to predict quantitatively the effect of changes in sample porosity on the detection of secondary radiation. An experiment was carried out in which powder porosity changes were simulated by altering the solute concentration in aqueous solutions of sodium bromide, and determining a series of attenuation coefficients. There was some evidence that attenuation coefficient is dependent on sample geometry, but the results were inconclusive. The second theory suggested that crystalline materials such as lactose may exhibit different attenuation coefficients, depending on the direction of measurement in relation to

the crystal axes. Thus, if any preferential orientation of the crystals were to result from the compression of a sample, a change in attenuation coefficient might be observed. Attempts were made to produce a sufficiently large single crystal of lactose for the purpose of determining values of attenuation coefficient along each crystal axis. When this proved unsuccessful, a similar experiment was performed using a single cubic crystal of potassium sodium tartrate. No significant difference was observed between the three values obtained, but all were appreciably lower than the corresponding results for samples of particulate potassium sodium tartrate. This supported the previous conclusion that the introduction of porosity into an absorbing system results in an increase in observed attenuation coefficient. However, no evidence was obtained to suggest that attenuation coefficient is dependent on crystal orientation.

The linear relationship between attenuation coefficient and porosity (see above), although unlikely to hold over the entire porosity range from 0 to 1, was thought to be an adequate description of the experimental results, over the range of porosity studied. The proposed expression for attenuation coefficient was then utilised for the determination of local porosity variations within lactose samples. Measurements were confined almost entirely to cylindrical samples, in which the radial distribution of porosity was assessed

by directing the collimated beam of radiation axially through a number of specified points in the sample. The objective was to investigate the influence of deposition method, and in some cases vibration, on the distribution of porosity. For each set of conditions studied, four samples were assessed, yielding 4 x 19 porosity values, which were subjected to an analysis of variance to compare the relative significance of within-samples and between-samples variability. A method was also developed for converting such local porosity data into grey-scale images, thus providing a visual representation of the distribution of porosity. The above techniques were employed to investigate the packing behaviour of a relatively free-flowing particle size fraction of lactose, a much more cohesive one, and a third, having flow properties intermediate between the other two. The results showed that the extent of local porosity variation is certainly dependent on the method of deposition, and that by building up samples in even layers, this variability can be minimised. Deposition methods which produced uneven sample build-up, by, for example, depositing powder in a number of discrete streams, tended to result in very high local porosity variations, particularly with the more cohesive materials. This was thought to be due to low-velocity secondary deposition, which occurs when temporary heaps collapse, leading to the formation of regions of relatively high

porosity. It would appear, then, that methods producing low overall porosity (see earlier) also result in low local variability. However, samples poured from a jar also gave samples of moderate to low local porosity variation, despite the fact that the high intensity and relatively low velocity of deposition resulted in a high overall level of porosity.

The application of controlled vibration to powder samples invariably improved their uniformity of packing, with vertical vibration being more effective than horizontal vibration. Much of the reduction in porosity variation could be achieved using an acceleration as low as 2g, suggesting that large voids are less stable and more susceptible to vibration than smaller voids. Although vibration was very successful in reducing the level of porosity variation within individual samples,the difference between the overall porosities of successive samples prepared under the same conditions was often disappointingly large, for no obvious reason.

Using the knowledge gained in Chapters 3 and 6, it was possible to prepare batches of samples possessing different degrees of porosity variation. By filling hard gelatin capsules from such samples, the influence of local porosity variations on capsule fill weight variation was investigated. An instrumented capsule filling machine, simulating the intermittent type of dosator system, was described in Chapter 7, and used for all

capsule filling studies, the results of which appear in Chapter 8. The three particle size fractions that were studied in Chapter 6 were used again, and a significant relationship between overall sample porosity and capsule fill weight could not be established consistently, although significant correlation coefficients were obtained in some cases. Furthermore, it was not possible to demonstrate that uniformly packed samples give rise to better correlation between sample porosity and fill weight, than less uniform samples. It was therefore concluded that other factors, such as the presence and stability of a powder coating on the bore of the dosator nozzle, have a greater influence on plug retention, and tend to mask the effects of porosity variations of the order of magnitude that were encountered.

Attempts to fill capsules with any of the three chosen size fractions of lactose, using a size 0 nozzle and size 0 plunger, proved unsatisfactory. Low and erratic fill weights resulted, due to inadequate venting of air from the nozzle during descent into the powder samples. This problem was overcome by using one of two undersize plungers, which allowed the passage of air up beyond the plunger tip and out of the space to be occupied by powder, much more freely than the size 0 plunger. One disadvantage in using an undersize plunger was that a thicker powder coating was able to develop on the nozzle bore, particularly when using cohesive powder.

The use of an air cylinder for providing plug compression was regarded as a very good feature of the filling machine. This ensured that a fixed compression stress could be applied to each plug, irrespective of the mass or porosity of the plug. It is more usual for the compression stroke to be of a fixed displacement, in which case the stress applied depends largely on the initial porosity of the plug, and variations in the latter can cause large variations in compression stress. However, the provision of a second air cylinder for effecting plug ejection was not considered advantageous. The ejection process itself was characterised by a build-up of pressure in the cylinder followed by a sudden release of the piston as the frictional forces retaining the plug in the nozzle were overcome. With non-cohesive powder, this resulted in disintegration of the plug, and failure of some of the powder to enter the capsule body. A mechanical ejection mechanism would have been more efficient, having a smoother and more reproducible action.

Suggestions for further work

The technique of gamma-ray attenuation has been shown to be useful for detecting local porosity variations within powder samples, and could conceivably be employed to study powder beds contained in the feed trays of different types of capsule filling machine. Small-scale detectors, connected by flexible fibre optic

tubing to the required counting equipment, are already commercially available, and such systems would facilitate the use of the technique in cases where access of a conventional size detector to the site of measurement might be prevented.

Gamma-ray attenuation might also be usefully employed in the tabletting field, where a knowledge of density distributions within hoppers, dies and compacts may be required.

The capsule filling process, as carried out by existing dosator systems, successfully produces millions of hard gelatin capsules every year. Despite this fact, not all of the factors affecting filling efficiency have been identified and fully understood. The findings of this work indicate that, even though plug retention can be consistently achieved, the actual weight of powder ejected into capsules may be dependent on the extent of powder coating on the bore of the dosator nozzle. A more extensive study of this coating, its stability and variability, would be justified.

Appendix 1

Estimation Of Mass Attenuation Coefficients Using The "Mixture Rule"

If an absorber is a chemical compound or a mixture, its mass attenuation coefficient, μ/ρ, can be approximately evaluated from the coefficients μ_i/ρ_i for the constituent elements, according to the weighted average:

$$\mu/\rho = \sum_i w_i(\mu_i/\rho_i)$$

where w_i is the proportion by weight of the ith constituent. Values of μ_i/ρ_i are obtainable from tables (Hubbell, 1969).

(a) Lactose, $C_{12}H_{22}O_{11}.H_2O$

Molecular weight = 12(12.011) + 24(1.008) + 12(15.999)

= 360.312

$$\left(\frac{\mu}{\rho}\right)_{\text{lactose}} = \frac{12(12.011)}{360.312}\left(\frac{\mu}{\rho}\right)_C + \frac{24(1.008)}{360.312}\left(\frac{\mu}{\rho}\right)_H + \frac{12(15.999)}{360.312}\left(\frac{\mu}{\rho}\right)_O$$

(i) At 30 keV :

$\left(\frac{\mu}{\rho}\right)_C = 0.230$, $\left(\frac{\mu}{\rho}\right)_H = 0.357$, $\left(\frac{\mu}{\rho}\right)_O = 0.335$ cm^2/g

Hence $\left(\frac{\mu}{\rho}\right)_{\text{lactose}} = 0.294$ cm^2/g

(ii) At 60 keV:

$\left(\frac{\mu}{\rho}\right)_C = 0.170$, $\left(\frac{\mu}{\rho}\right)_H = 0.326$, $\left(\frac{\mu}{\rho}\right)_O = 0.181$ cm^2/g

Hence $\left(\frac{\mu}{\rho}\right)_{lactose} = 0.186$ cm^2/g

Apparent particle density of lactose = 1.55g cm^{-3}

Hence, at 30keV, $\mu_{lactose} = 0.456$ cm^{-1}

at 60keV, $\mu_{lactose} = 0.288$ cm^{-1}

(b) Sodium bromide, NaBr

Molecular weight = 22.990 + 79.904

= 102.894

$$\left(\frac{\mu}{\rho}\right)_{NaBr} = \frac{22.990}{102.894}\left(\frac{\mu}{\rho}\right)_{Na} + \frac{79.904}{102.894}\left(\frac{\mu}{\rho}\right)_{Br}$$

At 60keV:

$\left(\frac{\mu}{\rho}\right)_{Na} = 0.209$, $\left(\frac{\mu}{\rho}\right)_{Br} = 2.60$ cm^2/g*

Hence $\left(\frac{\mu}{\rho}\right)_{NaBr} = 2.07$ cm^2/g

Apparent particle density of sodium bromide = 3.13g cm^{-3}

Hence, at 60keV, $\mu_{NaBr} = 6.47$ cm^{-1}

(*By interpolation from Hubbell's data)

(c) Potassium sodium tartrate, $KNaC_4H_4O_6.4H_2O$

Molecular weight = 39.102 + 22.990 + 4(12.011) +
12(1.008) + 7(15.999)
= 234.225

$$\left(\frac{\mu}{\rho}\right)_{KNa\ tartrate} = \frac{39.102}{234.225}\left(\frac{\mu}{\rho}\right)_K + \frac{22.990}{234.225}\left(\frac{\mu}{\rho}\right)_{Na} + \frac{4(12.011)}{234.225}\left(\frac{\mu}{\rho}\right)_C$$

$$+ \frac{12(1.008)}{234.225}\left(\frac{\mu}{\rho}\right)_H + \frac{7(15.999)}{234.225}\left(\frac{\mu}{\rho}\right)_O$$

At 60keV:

$\left(\frac{\mu}{\rho}\right)_K = 0.512\ cm^2/g$ (values for Na, C, H and O appear above)

Hence $\left(\frac{\mu}{\rho}\right)_{KNa\ tartrate} = 0.244\ cm^2/g$

Specific gravity of potassium sodium tartrate = 1.790 g cm^{-3}
(Handbook of Chemistry and Physics, 1973-1974)

Hence, at 60keV, $\mu_{KNa\ tartrate} = 0.437\ cm^{-1}$

Appendix 2

Determination Of The "Dead Time" of the Gamma Counting System

A2.1 Theory

The decrease in activity of a radio isotope in time, t, is given by the following equation:

$$A_t = A_o\, e^{-\lambda t} \quad , \qquad \text{(A2.1)}$$

where A_o is the initial activity

A_t is the activity at time t and λ, the disintegration constant, is given by:

$$\lambda = \frac{\ln 2}{t_{\frac{1}{2}}} \qquad \text{(A2.2)}$$

where $t_{\frac{1}{2}}$ is the half life of the isotope.

Therefore, a plot of log. count rate as a function of time will produce a straight line, providing the count rate is not so high that the detector dead time prevents some of the incident photons from being counted. If this upper limit of count rate is exceeded, the observed count rate will give a low estimate of activity, and a correction must be made.

If an experiment is carried out in which the count rate of a radioactive source initially exceeds the upper limit, but decreases to a level below the limit during the course of the experiment, a plot of log. count rate

as a function of time will produce a straight line in the later stages, but departure from a straight line in the early part of the experiment. Then, by taking a point on the straight line portion as a true representation of the activity of the source, a plot of log. activity as a function of time can be produced by applying equation (A2.1) at suitable values of t. This will be a straight line, coinciding with the extrapolation of the straight line portion of the plot of log. count rate versus time.

If observed count rate is then plotted against calculated activity at each time value, the point at which the resulting curve deviates from a straight line denotes the upper limit of count rate for practical purposes. This graph can also be used to estimate the actual dead time of the detector, according to the following equation (Sorenson, 1975):

$$R_o = R_t \exp(-R_t \tau) \qquad (A2.3)$$

where R_t is the true count rate (activity)

R_o is the observed count rate

τ is the dead time

A2.2 Experimental

Indium-113m was chosen as a suitable isotope, having a half-life of 1.75 hours. A sample, in the form

of indium chloride in dilute hydrochloric acid, and with an initial activity of approximately 2 mCi, was clamped at a suitable distance above the detector, and the controls of the counting system were adjusted to detect the 392keV energy peak.

Counts of ten seconds duration were taken at suitable time intervals over a period of six hours. The recorded count rate was plotted as a function of time (see Fig. A2.1).

The recorded count rate at t = 6 hours was taken to be a true representation of activity, and A_o, the activity at t = 0, was calculated using equation (A2.1) as follows:

Activity at t = 6 hours, A_6 = 3852 c.p.s.

Therefore, $3852 = A_o \exp(-6\lambda)$

$$\lambda = \frac{\ln 2}{1.75} = 0.396$$

$$\text{Hence } A_o = \frac{3852}{0.0929} = 41454 \text{ c.p.s.}$$

A_o was then substituted back into equation (A2.1) to yield further values of A_t, which are shown in Table A2.1 together with corresponding values of observed count rate.

Fig. A2.1 Recorded count rate as a function of time for a sample of Indium-113m (half-life 1.75 hours).

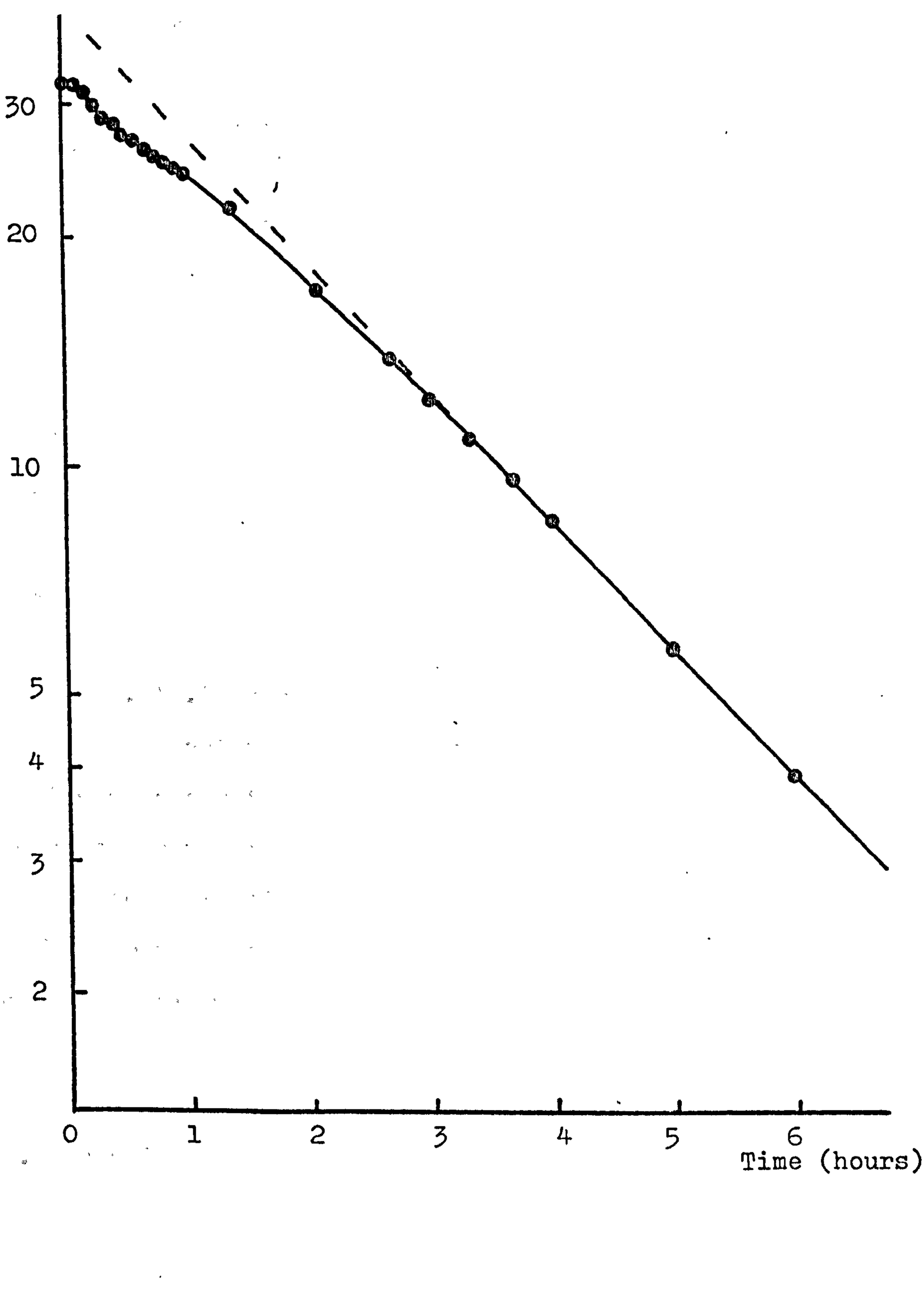

Table A2.1

Comparison of calculated values of activity with recorded values of count rate over a period of six hours.

Source: Indium - 113m

Time, t (hours)	Recorded count rate (c.p.s.)	Calculated activity, A_t (c.p.s.)
6	3852	3852
5	5686	5724
4	8410	8505
3	12213	12638
2.08	17030	18169
1.38	21634	23972
1	24241	27902
0.5	27337	34011

Fig. A2.2 is a graph of recorded count rate as a function of activity. Departure from a straight line begins at a count rate of about 10^4 c.p.s., and this denotes the upper limit of count rate, above which a dead time correction must be made.

A point on the curve in Fig. A2.2, having coordinates: recorded count rate = 2.33×10^4 c.p.s.

activity = 2.67×10^4 c.p.s.

was chosen arbitrarily for the calculation of dead time, τ. Equation (A2.3) can be rearranged thus:

Fig. A2.2 Recorded count rate as a function of activity, for a sample of Indium-113m.

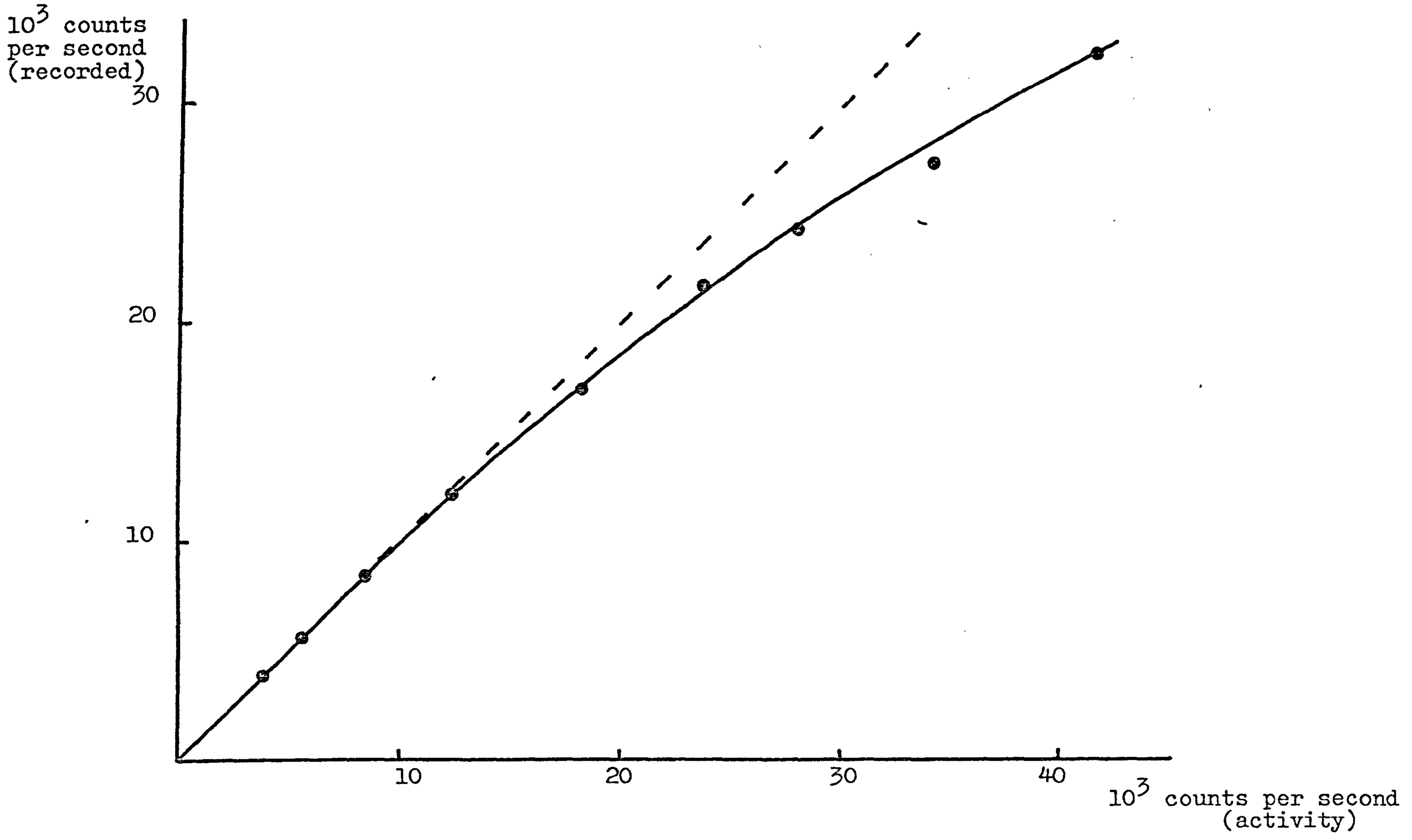

$$\tau = -\left[\frac{\ln \frac{R_o}{R_t}}{R_t}\right]$$

Substituting $R_t = 2.67 \times 10^4$ c.p.s.

$R_o = 2.33 \times 10^4$ c.p.s.

$\tau = 5.01 \times 10^{-6}$ sec.

This value of dead time can be used to correct recorded count rates in excess of 10^4 c.p.s.

Appendix 3

Calibration Of Instrumentation For The Model Dosator System

The graphs on the following pages, Figs. A3.1, A3.2, A3.3 and A3.4 show calibration data for the two load cells (compression and ejection arms), the displacement transducer, and the dosator spring.

The three transducers were connected to the same input and output devices during calibration as they were during capsule-filling experiments (see Chapter 7).

N.B. A dead-weight load of 1kg corresponds to a compressive stress of 0.305 MNm^{-2}, acting vertically on a powder plug in a size 0 dosator nozzle.

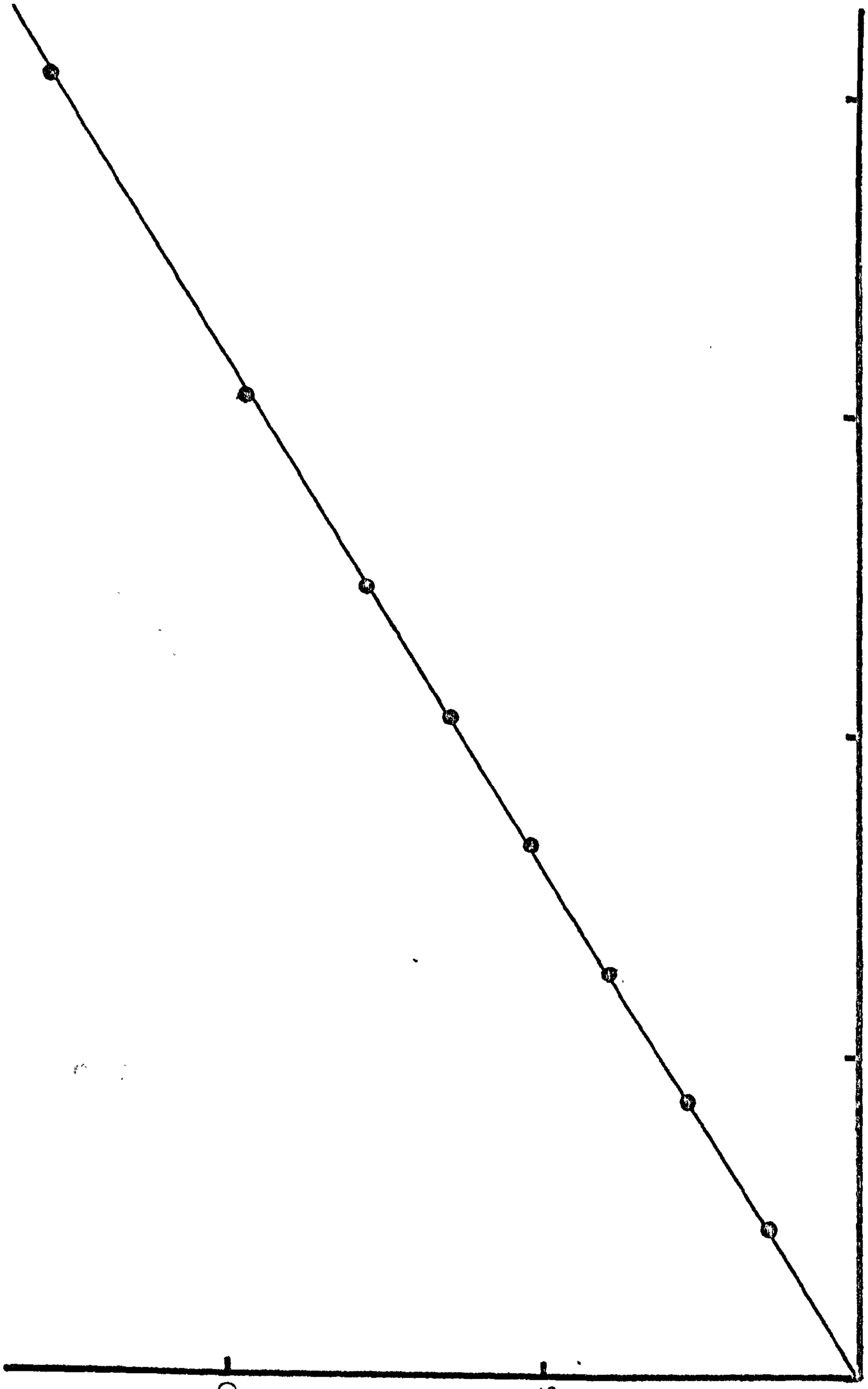

Fig. A3.1 Calibration curve for JP100 load cell

Fig. A3.2 Calibration curves for the JP500 load cell

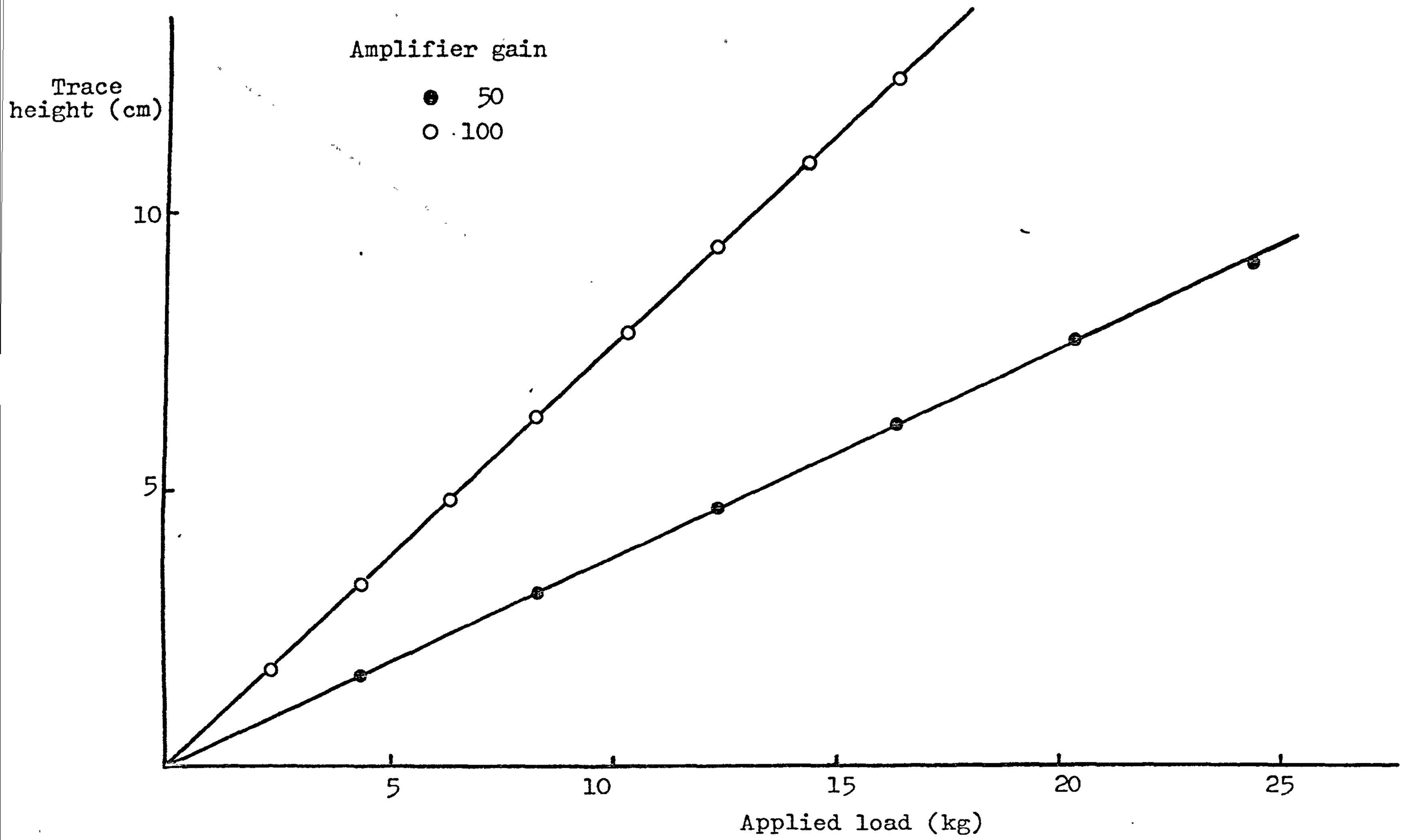

Fig. A3.3 Calibration curve for the displacement transducer

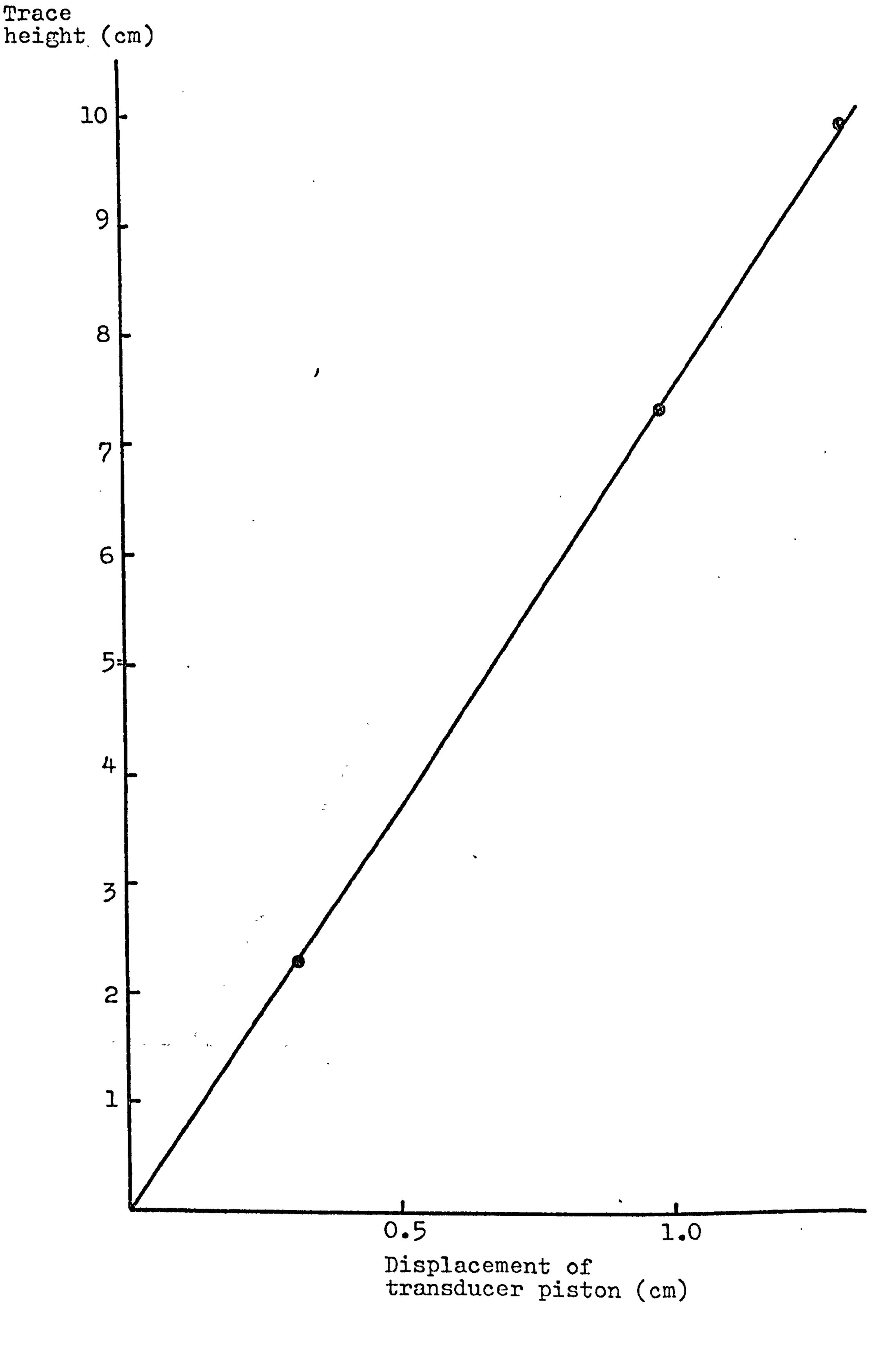

Fig. A3.4 Calibration curve for the dosator spring

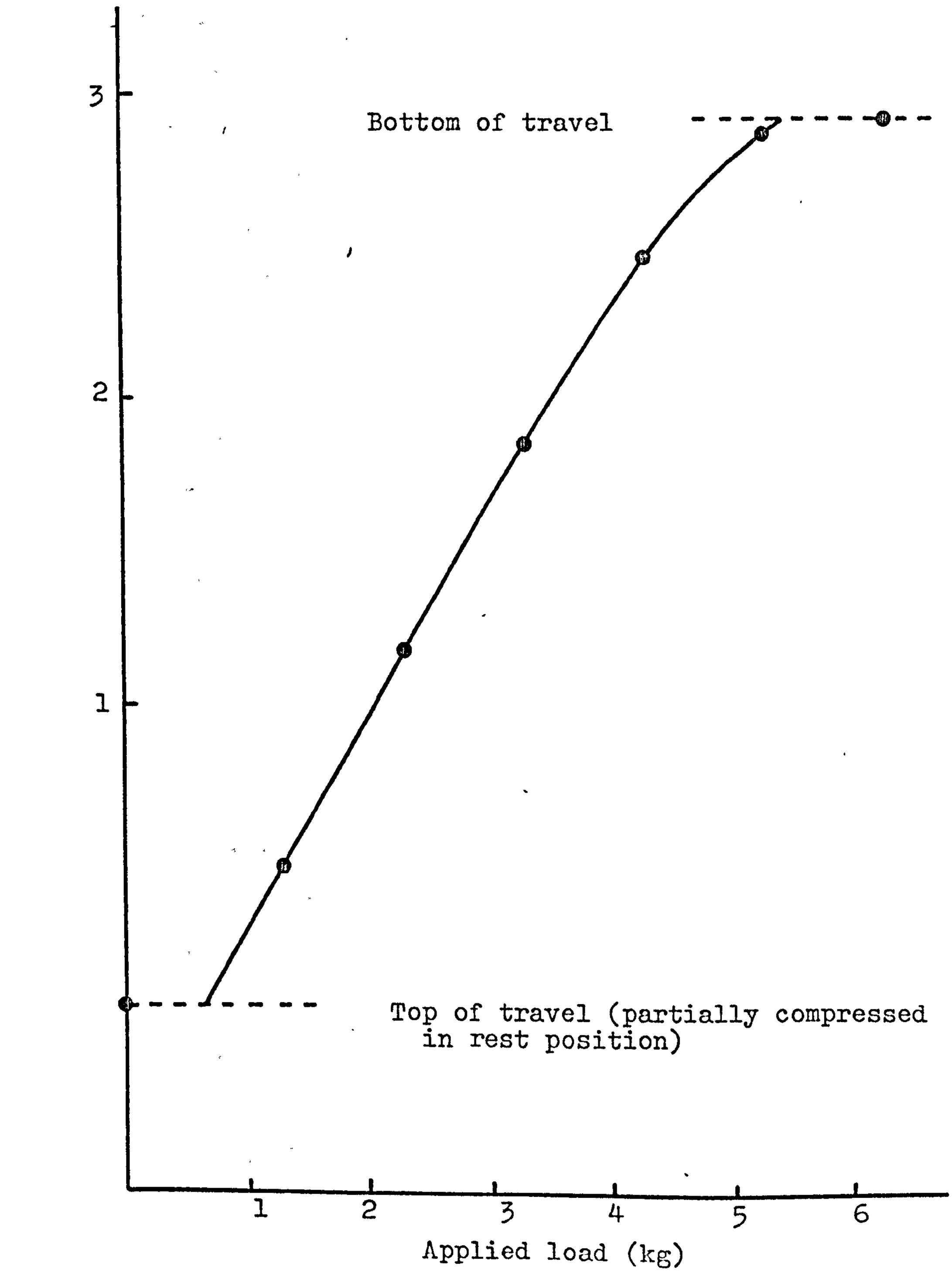

References

Anon (1977) Mfg. Chem. 48 (7) 19-20.

Ahmad, K. and Smalley, I.J. (1973) Powder Technol., 8 69-75.

Arthur, J.R.F. and Dunstan, T. (1969) Nature, Lond., 223 464-468.

Arthur, J.R.F. and Dunstan, T. (1969-70) Powder Technol., 3 195-207.

A.S.T.M. (1960) 'Symposium on nuclear methods for measuring soil density and moisture.' Sp. Publ. No. 293. Philadelphia.

Ayer, J.E. and Soppet, F.E. (1965) J. Am. Ceram. Soc. 48 (4) 180-183.

Ayer, J.E. and Soppet, F.E. (1966) J. Am. Ceram. Soc. 49 (4) 207-210.

B.S. 1460 (1967) 'Method for determination of the apparent density after compaction of precipitated calcium carbonate.'

Beevers, C.A. and Hansen, H.N. (1971) Acta crystallogr., B27 1323-1325.

Beevers, C.A. and Hughes, W. (1941) Proc. R. Soc., A177 251-259.

Bell, W.C. (1958) in Kingery, W.D. (ed). 'Ceramic fabrication processes.' pp. 74-77. Cambridge, Mass.: MIT Technology Press.

Benenati, R.F. and Brosilow, C.B. (1962) A.I.Ch.E. Journal, 8 (3) 359-361.

Bernhard, R.K. and Chasek, M. (1955) Proc. Am. Soc. Test. Mater., 55 1199-1215.

Bernhard, R.K., Chasek, M. and Griggs, P. (1956) Proc. Am. Soc. Test. Mater., 56 1288-1299.

Bo, M.K., Freshwater, D.C. and Scarlett, B. (1965) Trans. Instn. chem. Engrs., 43 T228-T232.

van Brakel, J. and Heertjes, P.M. (1974) Powder Technol., 9 263-271.

Bransby, P.L. (1973) University of Cambridge Report, CUED/C-Soils/TR14. 'The use of X-rays and γ-rays to measure the density of particulate solids.'

Brown, R.L. and Richards, J.C. (1970). 'Principles of powder mechanics.' Oxford: Pergamon Press.

Cameron, J.R., Mazess, R.B. and Sorenson, J.A. (1968) Invest. Radiol., 3 141-150.

Carlson, D., Lewis, G., and McIntyre, C. (1977) Int. Conf. Powder & Bulk Solids Handling & Processing, Proceedings of the Technical Program. Rosemont, Illinois, pp. 97-104.

Carmichael, J., Duncan, D., and Crompton, G.K. (1978) Br. med. J., 2 657-658.

Carr, R.L. (1970) Br. chem. Engng., 15 (12) 1541-1549.

Carstensen, J.T., Puisieux, F., Mehta, A. and Zoglio, M.A. (1978) Powder Technol., 20 249-255.

Casteel, J.L., Pringle, O.A., Lin, J.S., Schmidt, P.W., Slocum, D.H., McGinnes, E.A. and Beall, F.C. (1978) Wood and Fiber, 10 (1) 6-18.

Cole, G.C. and May, G. (1975) J. Pharm. Pharmac., 27 353-358.

Compton, A.H. and Allison, S.K. (1935). 'X-rays in theory and experiment.' 2nd ed. London: MacMillan.

Coumoulos, D.G. (1967) Ph.D. Thesis, University of Cambridge. 'A radiographic study of soils.'

Derjaguin, B.V. (1961) in 'Powders in industry', S.C.I. Monograph No. 14, pp. 102-114. London: S.C.I.

Documenta Geigy (1962). 6th ed. Manchester: Geigy Pharmaceutical Co. Ltd.

Dollimore, D., Horridge, T.A. and Robinson, R. (1973) Powder Technol., 7 39-43.

Eastwood, J., Matzen, E.J.P., Young, M.J. and Epstein, N. (1969) Br. chem. Engng, 14 (11) 1542-1545.

Evans, P.E. and Millman, R.S. (1964) Powder Metall., 7 (13) 50-63.

Ewell, G.J. (1979) Am. Ceram. Soc. Bull., 58 (3) 317.

Faires, R.A. and Parks B.H. (1973). 'Radioisotope laboratory techniques.' 3rd ed. London: Butterworths.

Fano, U. (1953a) Necleonics, 11 (8) 8-12.

Fano, U. (1953b) Nucleonics, 11 (9) 55-61.

Faust, R.N., Vanderwalk, W. and Warrick, R. (1976) Chem. Engng Prog., 72 (6) 84-87.

Fell, J.T. (1972) Ph.D. Thesis, University of Manchester. 'A comparative study of the properties of spray-dried and crystalline lactose, with special reference to their tabletting characteristics.'

Filipczynski, L., Pawlowski, Z. and Wehr, J. (1966). 'Ultrasonic methods of testing materials.' London: Butterworths.

Fisher, R.A. and Yates, F. (1970). 'Statistical tables' 6th ed. Edinburgh: Oliver and Boyd.

Fisher, T.P. and Coleman, D.S. (1974) Powder Metall. 17 (34) 302-318.

Furnas, C.C. (1931) Ind. Engng Chem. ind. Edn, 23 (9) 1052-1058.

Gold, G., Durall, R.N. and Palermo, B.T. (1966) J. Pharm. Sci., 55 1133-1136.

Gotoh, K., Jodrey, W.S. and Tory, E.M. (1978) Powder Technol., 20 257-260.

Graton, L.C. and Fraser, H.J. (1935) J. Geol., 43 785-909.

Gray, W.A. (1968). 'The packing of solid particles.' London: Chapman and Hall.

Handbook of Chemistry and Physics (1973). 54th ed. Cleveland, Ohio: CRC Press.

Harwood, C.F. (1977) Powder Technol., 16 51-57.

Hauth, J.J. (1967) in Hausner, H.H. (ed). 'Perspectives in powder metallurgy. Vol. 2: Vibratory compacting.' pp. 253-274. New York: Plenum Press.

Heertjes, P.M., Khoe, G.K. and Kuster, D. (1978) Powder Technol., 21 63-71.

Homilius, J. and Lorch, S. (1957) Geophys. Prospect., 5 449-468.

Hostetler, V.B. and Bellard, J.Q. (1976) in Lachman, L., Leiberman, H. and Kanig, J. (ed). 'The theory and practice of industrial pharmacy.' 2nd ed. pp. 389-404, Philadelphia: Lea and Febiger.

Hubbell, J.H. (1969) National Bureau of Standards Report, NSRDS-NBS29. 'Photon cross sections.'

Irwin, G.M., Dodson, G.J. and Ravin, L.J. (1970) J. Pharm. Sci., 59 (4) 547-550.

Ito, K., Hitomi, M., Kaga, S.-I. and Takeya, Y. (1969) Chem. pharm. Bull., Tokyo, 17 (6) 1138-1145.

Jolliffe, I.J. (1980) Ph.D. Thesis, University of Nottingham. 'The filling of hard gelatin capsules.'

Jones, B.E. and Turner, T.D. (1974) Pharm. J., 213 614-617.

Jones, T.M. (1979) Drug Cosmet. Ind., 124 (3) 40-56.

Kennett, T.J., Prestwich, W.V. and Robertson, A. (1976) Int. J. appl. Radiat. Isotopes, 27 (9) 529-532.

Kolbuszewski, J. (1950) Research, Lond., 3 478-483.

Krautwasser, P. and Nickel, H. (1977) Nucl. Technol. 35 (2) 310-319.

Kurihara, K. and Ichikawa, I. (1978) Chem. pharm. Bull., Tokyo, 26 (4) 1250-1256.

Kurz, H.P. (1972) Powder Technol., 6 167-170.

Kurz, H.P. and Schwedes, J. (1976) Chemie-Ingr-Tech., 48 (6) 555.

Lawrence, L.R. and Beddow, J.K. (1968-9) Powder Technol., 2 125-130.

Mackenzie, C.D. and Armitage, B.H. (1976) Nucl. Instrum. Meth., 133 (3) 489-493.

Macrae, J.C. and Gray, W.A. (1961) Br. J. appl. Phys., 12 164-172.,

Marquardt, H.G. and Clement, H. (1970) Drugs Germ., 13 21-23.

Marquardt, H.G. and Pfeiffer, W. (1977) Parke-Davis Capsule Division News Sheet.

McGeary, R.K. (1967) in Hausner, H.H. (ed). 'Perspectives in powder metallurgy. Vol. 2: Vibratory compacting.' pp. 209-236. New York: Plenum Press.

Meigh, A.C. and Skipp, B.O. (1960) Géotechnique, 10 110-126.

Messing, G.L. and Onada, G.Y. (1978a) J. Am. Ceram. Soc., 67 (1-2) 1-5.

Messing, G.L. and Onada, G.Y. (1978b) J. Am. Ceram. Soc., 67 (7-8) 363-366.

Mony, C., Sambeat, C. and Cousin, G. (1976) Parke-Davis Capsule Division News Sheet.

Nakai, Y. and Fukuoka, E. (1978) J. pharm. Soc. Japan, 98 (1) 23-30.

Nakajima, Y., Whiten, W.J. and White, M.E. (1978) Trans. Inst. Min. metall. Sect. C , 87 C194-C203.

Newton, J.M. (1978) Pharm. J., 221 78.

Pekarskii, G.S., Katsman, Y.Y., Kucher, G.A., Chislov, N.N. and Pirtskhalava, D.A. (1978) Ind. Lab., 94 (8) 1105-1107.

Petrov, L.K., Rimkevich, I.M. and Benzar, V.K. (1974) J. Eng. Phys. (USA), 26 (5) 595-598.

Pilpel, N. (1971) Adv. Pharm. Sci., 3 173-219.

Powell, M.J. (1980) Powder Technol., 25 45-52.

Propster, M. and Szekely, J. (1977) Powder Technol., 17 123-138.

Reier, G., Cohn, R., Rock, S. and Wagenblast, F. (1968) J. Pharm. Sci., 57 (4) 660-666.

Ridgway, K. and Callow, J.A.B. (1973) Pharm. J., 211 281-285.

Ridgway, K. and Scotton, J.B. (1973) Harold Heywood Memorial Symposium, Preprints. Loughborough University.

Ridgway, K. and Tarbuck, K.J. (1966) J. Pharm. Pharmac., 18 168S-175S.

Ripple, C.D., James, R.V. and Rubin, J. (1973) Powder Technol., 8 165-175.

Roberts, A.W. and Scott, O.J. (1978) Powder Technol., 21 45-53.

Roscoe, K.H. (1968) Proc. THTR Symp. on Problems of the Pebble Bed and Granular Materials. Julich, pp. 79-115.

Scott, G.D. (1962) Nature, Lond., 194 956-958.

Shatalova, I.G., Gorbunov, N.S. and Likhtman, V.I. (1967) in Hausner, H.H. (ed). 'Perspectives in powder metallurgy. Vol. 2: Vibratory compacting.' pp. 1-206. New York: Plenum Press.

Shergold, F.A. (1953) Mag. Concr. Res., 5 (13) 3-10.

Shotton, E. and Harb, N. (1966) J. Pharm. Pharmac., 18 175-178.

Siegbahn, K. (1955) (ed). 'Beta- and gamma-ray spectroscopy.' Amsterdam: North-Holland.

Singhal, A.K. and Dranchuk, P.M. (1973) Can. J. chem. Engng, 51 503-506.

Skopek, J. (1957) Proc. 4th Int. Conf. Soil Mech., London, 1 107-110.

Skorokhod, V.V. and Tuchinskii, L.I. (1978) Sov. Powder Met. & Metal Ceram., 17 (9) 668-671.

Small, L.E. and Augsburger, L.L. (1977) J. Pharm. Sci., 66 504-509.

Sorenson, J.A. (1975) J. nucl. Med., 4 284-288.

Sowka, J. and Schubert, H. (1978) Aufbereitungs-Tech., 19 (12) 593-598.

Spasski, M.R. (1977) Colloid J. USSR, 39 (3) 429-436.

Standish, N. and McGregor, G. (1977) Chem. Engng Sci., 33 (5) 618-619.

Stanek, V. and Eckert, V. (1979a) Arch. EisenhüttWes., 50 19-24.

Stanek, V. and Eckert, V. (1979b) Chem. Engng Sci. 34 933-940.

Stanley-Wood, N.G. (1978) in Groves, M.J. (ed). 'Particle size analysis.' pp. 278-288. London: Heyden.

Stewart, D.A. (1962). 'High quality concrete.' 2nd ed. London: Spon.

Stone, D.E.W. and Clarke, B. (1975) Non-destruct. Test. 8 (3) 137-145.

Train, D. (1957) Trans. Instn chem. Engrs., 35 258-266.

Train, D. and Lewis, C.J. (1962) Trans. Instn chem. Engrs , 40 235-240.

Wakeman, R.J. (1975) Powder Technol., 11 (3) 297-299.

Williams, J.C. and Shields, G. (1967) Powder Technol., 1 134-142.

Symbols

$\Delta\varepsilon$	confidence interval of measured porosity value
$\Delta\mu$	confidence interval of measured linear attenuation coefficient
ε	porosity
$\bar{\varepsilon}$	mean local porosity
λ	radioactive disintegration constant
μ	linear attenuation coefficient
μ/ρ	mass attenuation coefficient
ρ	apparent particle density, or specific gravity
σ	standard deviation
τ	dead time of gamma counting system
A_o	activity of radioactive source at zero time
A_t	activity of radioactive source at time t
d	depth of container
I_o	intensity of incident radiation
I	intensity of transmitted radiation
L	apparent thickness of absorber
N	"sample" count
N_o	"blank" count
$N_{o_{min}}$	minimum blank count required to ensure specified confidence level
p	probability level
r	radial distance from the centre of a cylindrical powder sample
R_o	observed count rate

R_t	true count rate
t	thickness of absorber
t_a	attenuating thickness of particulate absorber
V	volume
W	weight
w_i	proportion by weight of the ith constituent in a mixture or compound